2019

Regulation of Protein Degradation by ADP-Ribosylation

Yetis Gultekin

REGULATION OF PROTEIN DEGRADATION BY ADP-RIBOSYLATION

A Thesis Presented to the Faculty of

The Rockefeller University

in Partial Fulfillment of the Requirements for

the degree of Doctor of Philosophy

by

Yetis Gultekin

June 2019

REGULATION OF PROTEIN DEGRADATION BY ADP-RIBOSYLATION

Yetis Gultekin, Ph.D.

The Rockefeller University 2019

Protein quality control is essential for cellular homeostasis. The Ubiquitin-Proteasome System (UPS) is responsible for the regulated breakdown of intracellular proteins. All proteins are not degraded at the same rate in the cell. For instance, global protein turnover rates in mammals change with an average time between 1-2 days. On the other hand, a handful of proteins such as myelin exhibits limited turnover for months or even years. The UPS recycles most of the short-lived proteins in a time range from minutes to days depending on their localization and post-translational modifications. The post-translational modification, poly-ADP-ribosylation has an estimated half-life of only 1-6 min.

My thesis research aimed to reveal how the substrates of Tankyrase are degraded rapidly. Using *Drosophila melanogaster,* I described the role of Iduna E3 ubiquitin ligase in the regulation of Axin and Tankyrase proteolysis. I found that Iduna controls the proliferation of stem cells in the *Drosophila* midgut. Using a MS-based approach, I identified lysine 598 as an ADP-ribose acceptor site in *Drosophila* Tankyrase and showed that $Tnks^{K598A}$ adult flies live significantly shorter than control flies. $Tnks^{K598A}$ adult flies also reduce their flight, climbing abilities, global protein poly-ADP-ribosylation, and the activation of JNK signaling with age. Furthermore, I demonstrated that the ubcD1 ubiquitin-conjugating enzyme enhances the ubiquitin ligase activity of Iduna. Finally, I proposed a model by which poly-ADP-ribosylation brings together Tankyrase, target proteins, E2 ubiquitin-conjugating enzymes, E3 ubiquitin ligases and 26S proteasomes to accelerate the breakdown of target proteins.

My work addresses the general question of how proteins can be rapidly turned over, focusing on the role of Tankyrase-mediated poly-ADP-ribosylation. This work provides novel mechanistic insights into the regulation of protein quality control. Ultimately, these results may be useful to guide the development of new therapies.

Dedicated to lovely my family (Sevgili Aileme)

ACKNOWLEDGMENTS

I would like to first thank my advisor, Dr. Hermann Steller, for welcoming me into the lab and providing guidance and support for both personal and scientific growth throughout my Ph.D. Your guidance and advice on how to communicate, think, and challenge new ideas always help me to improve myself. I would like to thank my committee members Dr. Cori Bargmann, Dr. Shai Shaham and Dr. David Allis, who have provided support, guidance as well as thoughtful advice during my studies that have expanded my knowledge on approaching scientific questions. I would also like to thank my external examiner Dr. Erika Bach from NYU Medical School for accepting my invitation, imparting her time and knowledge to provide feedback on my thesis.

I am so grateful for the Dean's office and all its members- Sid, Emily, Kristen, Cris, Marta, and Stephanie here at The Rockefeller University, who have been supporting us with all aspects of graduate school.

All the Steller lab members, past and present, who have made the lab a great place to work and each contributed to my growth as a scientist: Drs. Ainhoa Perez, Junko Shimazu, Joe Rodriguez, Sigi-Benjamin-Hong, Dolors Ferres Marco, Adi Minis, Irit Shachrai, Cristinel Sandu, Anshuman Kelkar, Park Cho Park, Kai Liu, Sandra Jones, Tommy Hsiao. Special thanks to the two high school summer students I had the privilege of mentoring: Richard and Onur, who were very outstanding, intelligent, fun, and eager to learn.

Furthermore, I owe my passion and pursuit of science to my previous mentors: Dr. David M. Sabatini, Dr. Omer Yilmaz, Dr. Kivanc Birsoy, and Dr. Nesrin Ozoren, my high school biology teachers Hulya Caylaksevdi and Nurser Gurses, who introduced me to

research, nominated me for countless fellowships, and continue to support and encourage me all these years later.

Special thanks go to The Rockefeller University proteomics core facility staff Dr. Milica Tesic Mark and its director Dr. Henrik Molina for their time, help, and guidance during my thesis project.

Last but not the least, I would like to thank to my friends especially Ali, Caner, Erman, Pinar, and Arman for all the laughs, motivation, support, guidance, patience, and updates on the outside world. My biggest thanks go to my lovely family in Turkey, my mom Vildan, my dad Cemal and my brother Yasin, for as long as I could remember, who have pushed me to take on challenges and supported me in everything I've ever pursued.

LIST OF FIGURES

LIST OF TABLES

LIST OF ABBREVIATIONS

AD — Alzheimer`s Disease

hNUDT16 —human Nudix type motif 16

AIF — apoptosis inducing factor

APC — *adenomatous polyposis coli*

DUB — deubiquitinating enzyme

pH3 — phospho-Histone 3

si-RNA — small- RNA

SDS-PAGE — sodium dodecyl sulfate polyacrylamide gel electrophoresis

r-RNA — ribosomal Ribonucleic acid

ARC — akyrin repeat clusters

ALS — amyotrophic lateral sclerosis

cADPR — cyclic ADP-ribose

ADP-r — ADP ribose

CRISPR — clustered regularly interspaced short palindromic repeats CKI

— Casein Kinase I

E1 — ubiquitin-activating enzymes

E2 — ubiquitin-conjugating enzymes

E3 — ubiquitin ligases

EC — enterocyte

EE — enteroendocrine

EB — enteroblast

FTD — frontotemporal dementia

GPCR — G-protein-coupled receptors

hnRNP A1 — heterogeneous nuclear riboprotein A1

ISC — intestinal stem cell

Na — nicotinic acid

Nam — nicotinamide

NAD+ — Nicotinamide adenine dinucleotide

NMDA — *N*-methyl-D-aspartate receptor

NMNAT — Nicotinamide mononucleotide adenylyltransferase

MAR — mono-ADP-ribose

MS — mass spectrophotometry

PAR — Poly-ADP-ribose

PARG — Poly-ADP-ribose glycohydrolase

PARP — Poly-ADP-ribose polymerase

PARsylate — to poly-ADP-ribosylate

PARsylation — poly-ADP-ribosylation

PI31 — Proteasome inhibitor 31 kDA

PBM — PAR-binding motif

PTRE1 — Proteasome regulator 1

GSK3β — glycogen synthase kinase 3β

RNF146 — Ring finger protein 146

RFLP — restriction fragment length polymorphism

SAM — a sterile-alpha motif

TNKS — Tankyrase

TDP-43 — TAR DNA binding 43kDA

TGA— Triglycerides

TARG1— Terminal ADP-ribose glycohydrolase 1

TBM — Tankyrase-binding motif

UPS — Ubiquitin-Proteasome System

1 INTRODUCTION

1.1 Protein quality control and the Ubiquitin-Proteasome System

Proteins are essential to execute the diverse cellular functions to maintain cell and organismal viability. The proper balance between protein biogenesis and protein degradation is crucial for normal cellular function. All living cells must carry out a rigorous quality control process in which both nascent and newly synthesized proteins are examined to maintain proper cellular functions. Thus, this process is crucial to protect cells against the pathological accumulation of unfolded, misfolded and damaged proteins (Narayan et al., 2014).

Protein quality control can deliver damaged proteins to the lysosomal proteolysis pathway or the ubiquitin–proteasome system (UPS) for their degradation in eukaryotic cells (Murata et al., 2009; Xie et al., 2010; Glickman and Ciechanover, 2002). Lysosome-mediated protein degradation is a bulk process that involves the uptake of extracellular proteins, cytoplasmic organelles, or cytoplasmic proteins in the membrane-bound vesicles fusing with the lysosome. Eventually, engulfed proteins are exposed to digestive enzymes inside these membrane-bound vesicles (Rousseau and Bertolotti, 2018; Narayan et al., 2014). On the other hand, the UPS is highly selective for individual proteins tagged for destruction, and it mediates the degradation of most short-lived proteins that control cell cycle, cell survival, cellular metabolism, transcription, DNA repair, and apoptosis (Rousseau and Bertolotti, 2018; Narayan et al., 2014). The proteasome is also essential for amino acid homeostasis (Rousseau and Bertolotti, 2018). Finally, the proteasome particles in the immune system generate major histocompatibility complex class I- presented peptides by breaking down the proteins derived from intracellular pathogens (Murata et al., 2009; Xie et al., 2010; Glickman and Ciechanover, 2002). Not only the diversity but also the complexity of the proteasome functions may explain

why aberrant proteasome function is often linked to the pathogenesis of human diseases, such as cancer, auto-inflammatory disorders and neurodegenerative diseases (Xie et al., 2010; Glickman and Ciechanover, 2002).

1.1.1 The composition of the UPS and the ubiquitin pathway

There are two types of signals for the proteasome-mediated protein turnover. The first one is ubiquitylation, which most commonly is in the form of lysine 48-linked poly-ubiquitin chains. The second is the presence of unstructured regions in proteins that can act as initiators for their degradation (de Bie and Ciechanover, 2011).

The UPS contains enzymes to modify target proteins by attaching multiple ubiquitin chains for their degradation. Ubiquitin (Ub) is a highly conserved 76 amino acid polypeptide that is usually attached to lysine residues on target proteins (Glickman and Ciechanover, 2002; de Bie and Ciechanover, 2011; Hershko and Ciechanover, 1998). Conjugation of target proteins with poly-Ub chains is a multi-step reaction that is catalyzed by distinct enzymes. These include the ubiquitin activating enzymes (E1s), ubiquitin conjugating enzymes (E2s), and ubiquitin ligases (E3s). After poly-ubiquitylation, target proteins are destructed by a multi-subunit protease termed the 26S proteasome (Murata et al., 2009; Xie et al., 2010; Glickman and Ciechanover, 2002).

Figure 1.1 The Ubiquitin-Proteasome system-mediated protein degradation. Ubiquitylation is a crucial step to tag substrates for degradation by the 26S proteasome. Conjugating substrates with poly-ubiquitin involves three distinct classes of enzymes, E1, E2, and E3s that work in concert to attach distinct ubiquitin chains. The ubiquitin-activating enzyme, E1, uses ATP to activate ubiquitin to transfer to the E2, ubiquitin-conjugating enzyme. The last step catalyzed by the E3 ubiquitin-ligase taking ubiquitin to link it to a lysine residue on the substrate protein. The specificity of degradation is largely mediated by E3 ubiquitin-ligases, which are abundant and recognize one or a few specific proteins. Following the ubiquitylation, the substrate is degraded by the 26S proteasome. The figure was adapted from (Vilchez et al., 2014).

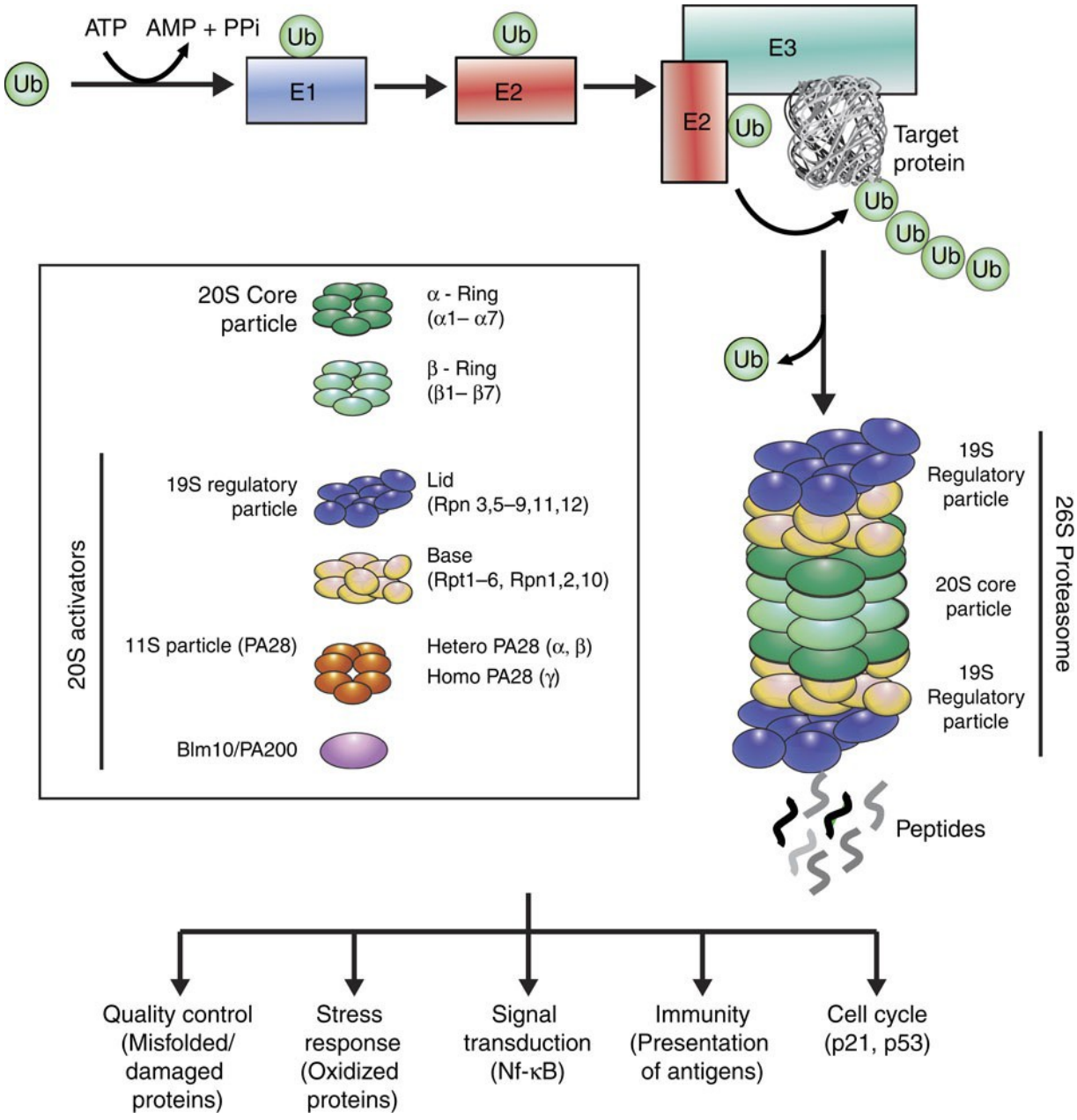
ATP
AMP + PPi
Ub
E1
E2
E3
Target protein
20S Core particle
α - Ring (α1– α7)
β - Ring (β1– β7)
19S regulatory particle
Lid (Rpn 3,5–9,11,12)
Base (Rpt1–6, Rpn1,2,10)
11S particle (PA28)
Hetero PA28 (α, β)
Homo PA28 (γ)
Blm10/PA200
20S activators
19S Regulatory particle
20S core particle
26S Proteasome
Peptides
Quality control (Misfolded/ damaged proteins)
Stress response (Oxidized proteins)
Signal transduction (Nf-κB)
Immunity (Presentation of antigens)
Cell cycle (p21, p53)

In the first step of ubiquitylation, one of the E1's activates ubiquitin in an ATP-dependent manner that generates a high-energy thiol-ester intermediate. Next, one of the E2s receives the activated ubiquitin from the E1 and forms a similar thiol-ester ubiquitin intermediate before binding to one of the E3s. Finally, the E3 ubiquitin ligase binds to a specific substrate and takes the activated ubiquitin from the E2 to transfer that to the target protein (Finley, 2009). Therefore, E3 ubiquitin ligases are key to substrate specificity in the UPS. The subsequent additional ubiquitin to lysine residues on previously conjugated enzyme forms the poly-ubiquitin chain that is recognized by the 26S proteasome.

The 26S proteasome is the major non-lysosomal protease devoted to protein breakdown in eukaryotic cells. This is a sophisticated 2.5 MDa multimeric self-compartementalized protease complex. It contains two sub-complexes, the 20S proteasome, which forms the proteolytic core particle, and the 19S regulatory particle, which recognizes poly-Ub targets and delivers them in an ATP-dependent manner to the core particle (Murata et al., 2009; Xie et al., 2010; Glickman and Ciechanover, 2002). The 20S is a cylindrical particle that is formed by axial stacking of four hetero-heptameric rings: Two outer α-rings and two inner β-rings, each comprising seven structurally similar α- and β- subunits, respectively. β-rings form a proteolytic chamber and α-rings serve as a gate for entry into the chamber (Murata et al., 2009; Xie et al., 2010; Glickman and Ciechanover, 2002). The 19S proteasome contains six ATPase subunits (Rpt1-6) that are organized in a hexameric ring and facilitate gate-opening and substrate unfolding by using ATP (Murata et al., 2009; Xie et al., 2010; Glickman and Ciechanover, 2002).

1.1.2 The regulation of the UPS

Protein breakdown by the UPS is controlled at different levels. It involves both substrate ubiquitylation as well as regulation of proteasome assembly and activity. The attachment of ubiquitin to lysine residues allows for branched poly-ubiquitin chains. This branching is tightly regulated and results in different biological processes, such as protein degradation by the 26S proteasome when ubiquitinylation takes place in lysine 48, and modification of signaling cascades when lysine 63 is ubiquitylated (de Bie and Ciechanover, 2011).

Alternative activators, various interacting proteins and post-translational modifications (PTMs) can regulate the assembly and the activity of the 26S proteasome (Rousseau and Bertolotti, 2018). While the majority of proteasomes in eukaryotic cells are composed of 20S and 19S core particles to form the 26S proteasome, populations of proteasomes can be heterogeneous in a tissue (Förster et al., 2005).

PTMs of the proteasome can regulate protein degradation. Protein phosphorylation by various kinases and phosphatases can promote or repress the activity of the proteasome (Guo et al., 2017; Rousseau and Bertolotti, 2018). Serine 120 of Rpt6 was first demonstrated to be phosphorylated by cAMP-dependent protein kinase A (PKA) and dephosphorylated by protein phosphatase 1-gamma (Satoh et al., 2001; Pereira and Milk, 1990; Asai et al., 2009; Rousseau and Bertolotti, 2018). PKA-mediated phosphorylation of Rpt6 regulates the 26S proteasome, possibly by promoting the binding Rpt6 to α-2 subunit of the 20S (Satoh et al., 2001).

Tankyrase (TNKS)-mediated ADP-ribosylation is another PTM that regulates 26S proteasome assembly and activity. PI31 (Proteasome inhibitor 31 kDA) was initially identified based on its ability to inhibit 20S proteasome activity *in vitro* (Chu-Ping et al., 1992; Zaiss et al., 1999). TNKS ADP-ribosylates PI31, which in turn alters the binding-affinity of PI31 for 20S

proteasome alpha subunits and 19S assembly chaperons. As a consequence, PI31-ADP ribosylation stimulates 26S proteasome assembly and activity (Park and Steller, 2013). *In vivo* studies of PI31 in *Drosophila* demonstrated that PI31 is an activator of the 26S proteasome (Bader et al., 2011). Loss of *PI31* causes accumulation of poly-ubiquitylated proteins in *Drosophila* (Bader et al., 2011).

Moreover, orthologs of PI31 in yeast and plants have been shown to stimulate proteasome activity and protein breakdown (Yashiroda et al., 2015; Yang et al., 2016). Our lab has recently found that PI31 plays a role in proteasome transport and is required for synaptic structure and function (Liu et al., 2019). PI31 directly couples proteasomes to dynein light chain proteins (DYNLL1/2). Depletion of *PI31* inhibits proteasome motility in axons and disrupts synaptic protein homeostasis, structure, and function (Liu et al., 2019).

The proteasome can be specialized in certain tissues through the incorporation of specific subunits. For example, the immune-proteasome has four additional β-subunits, and the thymoproteasome contains a thymus-specific β5-t subunit (Kloetzel, 2004; Tanaka and Kasahara, 1998; Murata et al., 2009). These alternative proteasomes have important roles in adaptive immunity to present antigens. On the other hand, mammalian and *Drosophila* testis have specific isoforms of 20S proteasome subunits (Belote et al., 1998; Ma et al., 2002; Zhong and Belote, 2007).

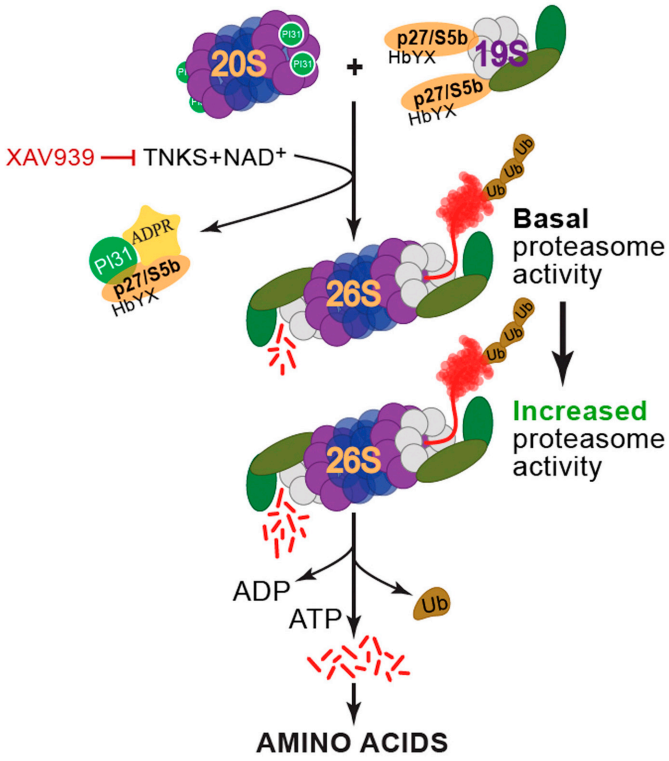

Figure 1.2 Model for increased proteasome assembly upon TNKS-mediated ADP-ribosylation of PI31. PI31 is regulated by TNKS-mediated ADP-ribosylation, which alters the binding affinity of PI31 for 20S proteasome alpha subunits and 19S assembly chaperones. As a consequence, PI31-ADP-ribosylation promotes the 26S proteasome assembly and activity. The figure was adapted from (Park and Steller, 2013).

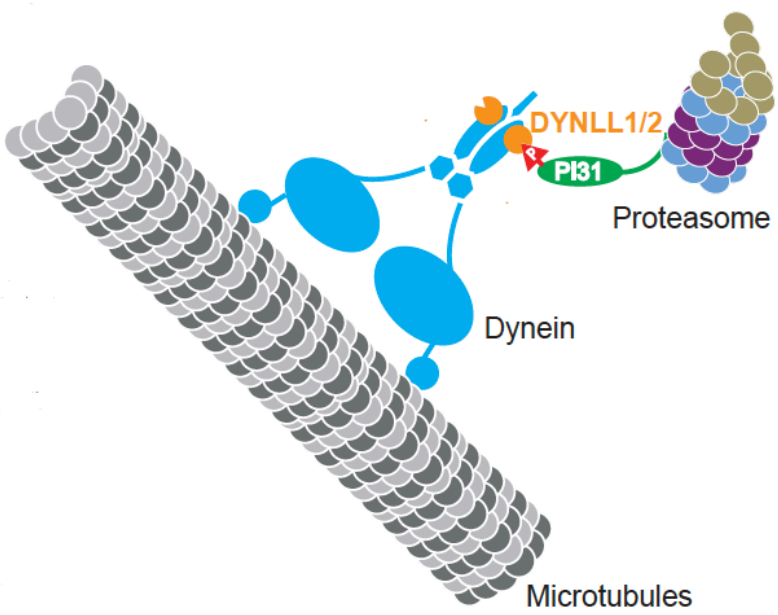

Figure 1.3 Model for PI31-mediated transport of proteasomes in axons. Proteasomes can move rapidly along microtubules to fulfill dynamic local demands for protein degradation in different cellular compartments. PI31 is an adaptor protein for proteasome transport in *Drosophila* axons. PI31 directly binds to proteasomes with dynein light chain proteins (DYNLL1/2). p38-MAP kinase-mediated PI31 phosphorylation enhances binding of PI31 to DYNLL1/2. The figure was adapted from (Liu et al., 2019).

1.2 ADP-ribosylation as a post-translational modification

ADP-ribosylation is a strikingly dynamic and reversible PTM, in which ADP ribose (ADP-r) units are attached to acceptor proteins by ADP-r transferases. The first ADP-ribose transferase was discovered as a bacterial toxin (Schreiber et al., 2006). Cholera and diphtheria toxins are ADP-ribose transferases, inhibiting or enhancing the protein synthesis or GPCR signaling in the host cells, respectively (Ruf et al., 1996; Oliver et al., 2004; Hassa et al., 2006; Perina et al., 2014). In eukaryotes, ADP-ribosylation affects many cellular processes. Therefore, aberrant regulation of ADP-ribosylation causes human diseases including acute central nervous system disorders, inflammatory diseases, and cancer (Palazzo et al., 2015; Schreiber et al., 2006).

Poly-ADP-ribosylation (PARsylation), on the other hand, is an endogenous reversible PTM of proteins that is mediated by poly-ADP-ribose polymerases (PARPs). PARPs generate negatively charged large polymers by adding ADP-r units to the acceptor proteins. Glu, Asp, Lys, Arg, Cys, Thr, or phosphorylated Ser are the amino acid residues that can accept the poly-ADP-ribose moieties (Daniels et al., 2014; DaRosa et al., 2018; Martello et al., 2016; Zhang et al., 2013).

Nicotinamide adenine dinucleotide (NAD+) is a co-substrate of PARPs to generate ADP-r polymers on protein acceptors. PARPs transfer multiple ADP-r units to their substrates forming both elongated and also branched poly-ADP-ribose modifications (Schreiber, 2006; Ame, 2004). Therefore, in contrast to several other PTMs, covalently attached PAR molecules on an acceptor protein differ greatly in size up to several hundred ADP-ribose residues with branching and large negative charges (Miwa and Masutani, 2007; Miwa et al., 1979; Hayashi et al., 1983). PARsylation can influence protein fate through several mechanisms, including a direct effect on

protein activity, recruitment of binding partners that recognize PAR or by affecting protein turn over (Guettler et al., 2011).

1.2.1 The roles of poly-ADP-ribose polymerases

At this time, 17 PARP members have been identified from genome sequencing (Schreiber et al., 2006). PARP1 is the first investigated PARP, that is involved in DNA repair following by its activation in response to single and double strand DNA breaks (Schreiber et al., 2006). PARP1 activity undergoes an over 500-fold increase upon its binding to DNA strand breaks (Eustermann et al., 2015; Nottbohn et al., 2007; Fan et al., 2018). During DNA damage repair, PARP1-induced auto-PARsylation acts as a molecular scaffold to recruit DNA damage repair proteins to the close proximity of the DNA strand breaks. PARP1 also poly-ADP-ribosylates histone tails, causing chromatin relaxation. This allows the recruitment of several chromatin remodelers through their binding to PAR, which further relax chromatin to facilitate DNA repair (Chaudhuri and Nussenzweig, 2017). As a result, DNA damage is repaired within several minutes. Hence, *Parp1* mutant animals have different vulnerability spectrum to the genotoxic mutagens (Menissier et al., 2003; Miwa and Masutani, 2007).

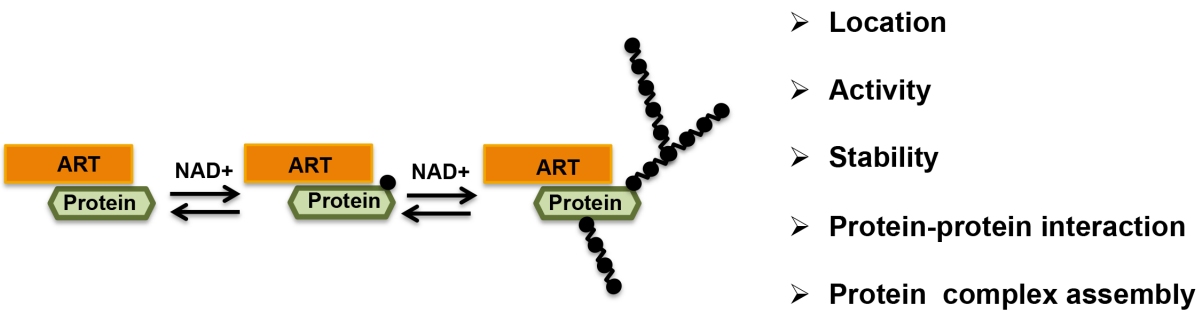

Figure 1.4 ADP-ribose transferases (ARTs) use NAD+ to modify their target proteins. ADP-ribosylation is a very dynamic and reversible post-translational modification. Target proteins can be mono-ADP-ribosylated or poly-ADP-ribosylated by ARTs. ADP-ribosylation has an impact on protein fate through several mechanisms including changing localization, activity, stability, protein interactions and complex assembly.

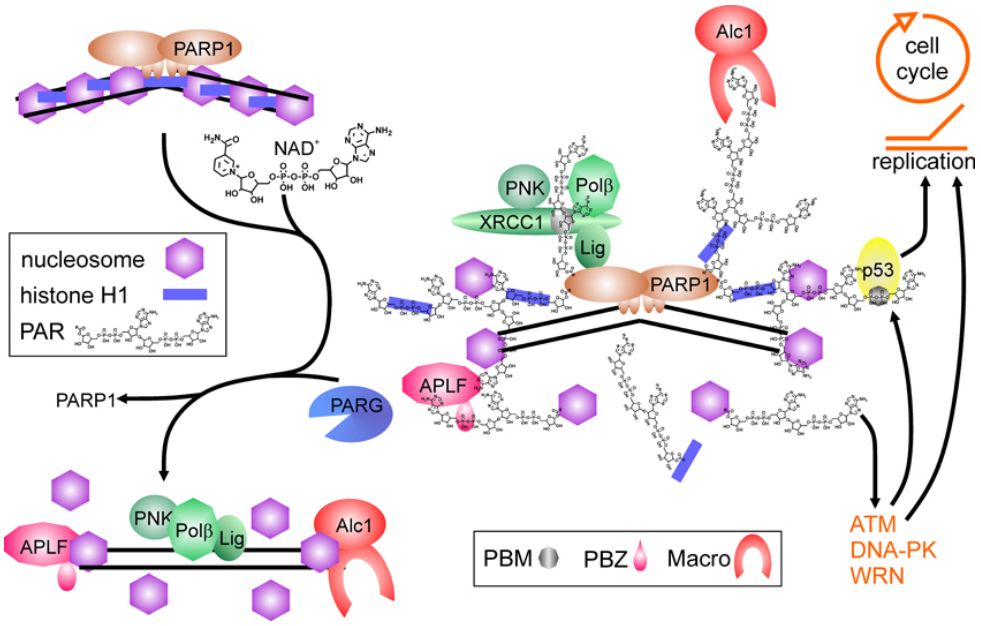

Figure 1.5 ADP-ribosylation generates a scaffold for DNA damage repair proteins. PARP1-induced auto-PARsylation acts as a molecular scaffold to recruit DNA damage repair proteins to the close proximity of the DNA strand breaks. Furthermore, PARP1 PARylates histone tails, which causes chromatin relaxation. This allows the recruitment of several chromatin remodelers through their binding to PAR, which further relax chromatin to facilitate DNA repair. The figure is adapted from (Beneke et al., 2012).

PARP1-dependent PARsylation also controls the nuclear localization of several proteins such as pyruvate kinase isoform M2, a glycolytic enzyme that converts phosphoenolpyruvate to pyruvate, in EGFR-mutant cancer cells (Li et al., 2016). PKM2 is not a PARsylation target of PARP1, however, PKM2 has a canonical PAR-binding motif. PAR binding is required for PKM2 nuclear retention. That is crucial for glycolysis and tumor growth. It is also shown that PAR level correlates with nuclear localization of PKM2 in EGFR mutant cells (Li et al., 2016). Therefore, inhibition of PARP1-dependent PAR generation suppresses the growth of EGFR mutant cancers.

Nuclear PARP1 also facilitates ribosomal biogenesis in *Drosophila* (Boamah et al., 2012). PARP1 becomes auto-PARsylated upon each act of transcription start within r-DNA gene. Auto-PARsylated PARP1 serves as a chaperoning machine during whole cycle of ribosome maturation in nucleus. The dynamic PARP1-mediated PAR scaffold brings a subset of nucleolar proteins to the proximity of precursor r-RNA and coordinates the order of events including r-RNA processing, modification and loading of subsets of ribosomal proteins to mature pre-ribosome in *Drosophila* (Boamah et al., 2012). Depletion of *Parp1* leads to the loss of PAR-binding proteins from nucleoli, which disrupt processing, modification and folding of ribosomal RNA in *Drosophila* (Boamah et al., 2012).

Tnks (Parp5) has two isoforms in mammals. Tnks proteins contain a PARP domain at the C-terminus, and dimerization of the catalytic domain is required for TNKS activity (Fan et al., 2018). Immediately upstream of its catalytic domain, there is a SAM, a sterile-alpha motif, domain required for the oligomerization of TNKS (Smith et al., 1998; De Rycker and Price, 2004). The basal activity of the isolated TNKS catalytic domain is extremely low, approximately 1000-fold lower than PARP1 (Nottbohm et al., 2007). The activity is dramatically elevated by

the SAM domain-dependent polymerization (Nottbohm et al., 2007; Fan et al., 2018). The stimulation of Wnt signaling by TNKS1/2 is dependent on SAM domain-mediated oligomerization, which is important for both TNKS localization and substrate recruitment (Marino-Echarri et al., 2016; Fan et al., 2018). The polymerization of TNKS1/2 is inhibited by auto-PARsylation (De Rycker and Price, 2004). Finally, there is a large ankyrin repeat domain, containing conserved ankyrin repeat clusters (ARCs), which are known for substrate recognition and binding (Lehtio et al., 2013). For instance, ARC5 appears essential for TRF1 PARsylation, the release of TRF1 from telomeres and telomere elongation (Seimiya et al., 2004). Each substrate has a TNKS binding motif (TBM) with an RxxxxG consensus, which mediates binding to the ARC domain (DaRosa et al., 2018; Guettler et al., 2011).

TNKS1/2 play important roles in cellular pathways that are critical for cancer cell growth, including telomere cohesion and length maintenance, GLUT-4-mediated vesicle transport, the Wnt/β-catenin pathway, as well as apoptosis (Daniels et al., 2014). Studies on human *Tnks1/2* knock out cell lines indicate that they are necessary to maintain telomere cohesion and mitotic spindle integrity (Bhardwaj et al., 2014). The quantitative proteome analysis of human TNKS double knockout cells demonstrates Notch1, 2, 3 receptors are the targets of TNKS (Bhardwaj et al., 2014).

Mutations in the immune adaptor protein 3BP2 that impair interaction with TNKS cause Cherubism, characterized by progressive, painless, bilateral swelling of the jaw during childhood. Loss of TNKS-mediated destruction of 3BP2 through Iduna is the underlying mechanism of the disease (Levaot et al., 2011; Guettler et al., 2011 Ueki et al., 2007).

In contrast to mammals, *Drosophila* has only a single *Tnks* gene. The overall similarity between *Drosophila* and human TNKS1/2 proteins is 79% (Wang et al., 2016). While double

knockout of *Tnks1 and 2* lead to lethality in mice, *Drosophila Tnks* is not required for viability (Feng et al., 2014). TNKS is essential for Axin degradation *in vivo* but loss-of *Tnks* does not lead to obvious morphological defect in *Drosophila* (Feng et al., 2014; Yang et al., 2016; Wang et al., 2016). TNKS antagonizes the β-catenin destruction complex through ADP-ribosylation of Axin and APC2 (Kroy et al., 2016). Therefore, the Wnt pathway is regulated by ADP-ribosylation.

Genetic depletion of *Tnks* causes Axin elevation that blocks Wingless signaling in enterocytes and activates JAK-STAT signaling to promote intestinal stem cell proliferation in the *Drosophila* midgut (Wang et al., 2016). Conditional genetic inactivation of *Tnks1/2* in mice results in a rapid decrease of Lgr5+ intestinal stem cells and promotes cell death in small intestinal crypts. As a result of intestine degeneration, increased mice mortality is indicated (Ye et al., 2018). On the other hand, TNKS can stimulate apoptosis in the *Drosophila* eye and wing by activating JNK signaling (Feng et al., 2018).

TNKS also has other PTMs but their impacts on TNKS are not well understood. Mitogen-activated protein kinase phosphorylates TNKS1 on its serine residues by after insulin or growth factor stimulation (Chi and Lodish, 2000). TNKS can be hydroxylated by hypoxia-inducible factor asparagine hydroxylase (FIH), although precise functions of these PTMs are not clear (Cockman et al., 2009). Finally, auto-PARsylation of TNKS provides a recognition signal for ubiquitylation and 26S-proteasome-mediated degradation through the Iduna (RNF146) (Gultekin and Steller, 2019; Callow et al., 2011; Zhang et al., 2011).

1.2.2 Regulation of ADP-ribosylation

As a highly dynamic and reversible PTM, poly-ADP-ribosylation has an estimated half live of only 1-6 min (Alvarez-Gonzales et. al., 1989). PAR glycohydrolase (PARG), Nudix type

motif 16 (NUDIX16) and NUDIX9 can remove PARsylation (Slade et al., 2011; Lin et al. 1997; Slade et al., 2011; Palazzo et al., 2015).

The opposing effects of PARPs and PARG in regulating protein PARsylation are important in a variety of cellular processes, including chromatin modeling, DNA repair, transcription regulation and cell death (Ahel et al, 2008; Andrabi et al., 2006; Frizzell et al., 2009; Sing et al., 2017). Impairments in the hydrolysis of PAR chains, therefore, involve in various human disorders such as cancer, neurodegeneration, oxidative stress, neural injury, and regeneration (Deng, 2009; Hanai et al., 2004; Martire et al., 2015; Brochier et al., 2015). Interestingly, PAR, some PARPs as well as PARG can be found in cytoplasmic stress granules and may regulate micro-RNA-dependent translational repression and mRNA cleavage (Gagne et al, 2008; Kotova et al., 2009; Leung et al., 2011). Mutations on RNA-binding proteins such as heterogeneous nuclear riboprotein A1 and TAR DNA binding 43kDA (TDP-43) enhance protein aggregation in mouse and fly models of familial amyotrophic lateral sclerosis (ALS) and frontotemporal dementia (FTD) (Kim et al., 2013; Neumann et al., 2006). TNKS-mediated PARsylation modulates stress granule assembly, phase separation and neurotoxicity of ALS-related RNA binding proteins hnRNP A1 and TDP43 (McGurk et al., 2018; Duan et al., 2018).

There are also other enzymes that cleave mono-ADP-ribose moieties on target proteins. For instance, Terminal ADP-ribose glycohydrolase (TARG1) can remove mono-ADP-ribose on glutamate residues (Sharifi et al., 2013). Homozygous mutations of TARG1 are associated with severe neurodegeneration in human patients (Sharifi et al., 2013). The source of ADP-ribose units is NAD+, which has been shown in a variety of systems to be neuroprotective and increases health-span (Lehmann et al., 2016; Ocampo et al., 2013; Verdin, 2015; Wang et al., 2008; Zhang et al., 2016).

Figure 1.6 TNKS-mediated ADP-ribosylation largely stimulates ubiquitinylation and substrate degradation by the 26S proteasome. TNKS is conserved from flies to human. Fly genome encodes a single *Tnks* gene. In contrast, mammalian cells have two TNKS isoforms. Both structure and amino acid composition of fly TNKS are similar to mammalian TNKSs. Ankyrin repeat clusters (ARCs) are responsible for recognizing and binding to the substrate proteins. α-sterile-alpha motif is required for TNKS oligomerization. Poly-ADP-ribose polymerase domain is the catalytic region of TNKS. TNKS makes a complex with Iduna E3 ubiquitin ligase. Then, TNKS binds to its target protein and ADP-ribosylates that by using NAD+. When the modification in the target protein is iso-or poly-ADP-ribose, Iduna E3 ubiquitin ligase is activated and ubiquitinylates the target protein. Finally, the poly-ubiquitinylated target protein is degraded by 26S proteasomes. The functional domain image of TNKSs is adapted from (Wang et al., 2016).

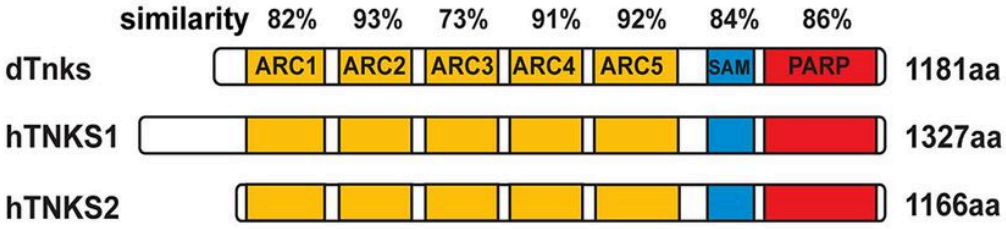
similarity
82%
93%
73%
91%
92%
84%
86%
dTnks
ARC1
ARC2
ARC3
ARC4
ARC5
SAM
PARP
1181aa
hTNKS1
1327aa
hTNKS2
1166aa

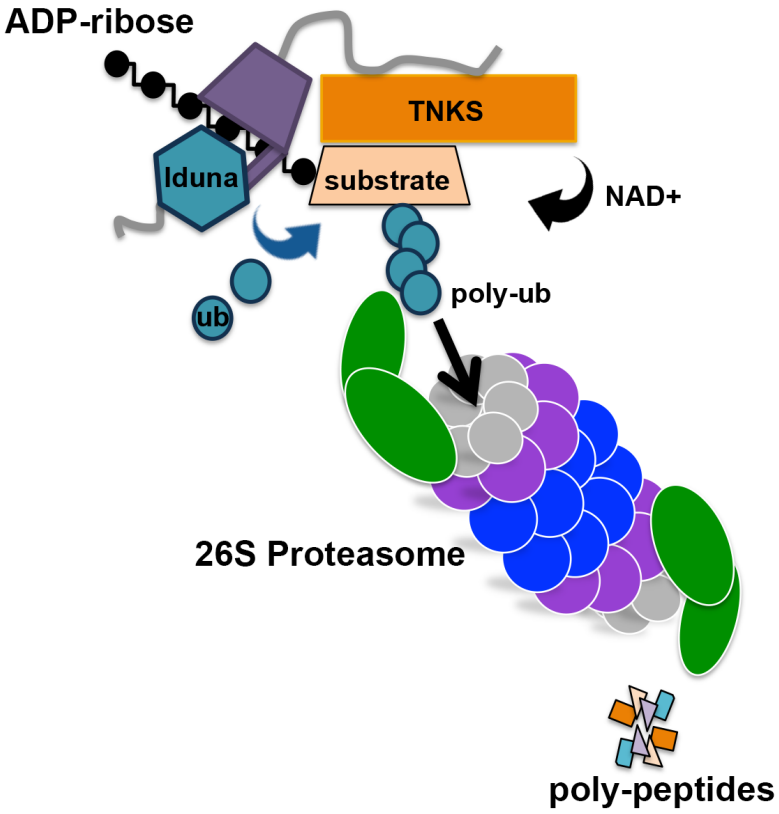
ADP-ribose
TNKS
Iduna
substrate
NAD+
poly-ub
ub
26S Proteasome
poly-peptides

Depletion of NAD+ leads to failure to generate ATP, a major requirement for many cellular processes. Therefore, recycling and production of NAD+ is crucial.

NAD+ producing pathways include *de novo* synthesis from tryptophan, and a salvage pathway, which recycles nicotinamide and nicotinic acid from the diet. PARPs, c-ADP-ribose synthases and Sirtuins are general NAD+ consumers (Cantó et al., 2013). For instance, CD157 or Bst-1 is an ectoenzyme on Paneth cells in the mouse small intestine. Caloric restriction increases NAD+ levels (Guarente and Picard, 2005). Upon caloric restriction, elevated Bst1 is thought to promote stem cell proliferation through converting NAD+ to cyclic ADP-ribose (cADRP) (Yilmaz et al., 2012; Igarashi and Guarente, 2016).

Dietary nicotinic acid (Na) and nicotinamide (Nam) intake significantly alters NAD+ levels in organisms (Belenky et al., 2007; Elhassan et al., 2017). The salvage pathway is crucial to metabolize the dietary NAD+ precursors, Na and Nam. Nicotinamide mononucleotide adenylyltransferase (NMNAT) is an essential enzyme, participating in the synthesis of NAD+ from Na or Nam. Genetic depletion of *nmnat* results in lethality in *Drosophila*. Interestingly, the salvage pathway-mediated NAD+ boost increases longevity in various model systems (Lin et al., 2000; McClure et al., 2012; Ocampo et al., 2013). Therefore, NAD+ metabolism is important for poly-ADP-ribosylation.

1.2.3 RNF146/Iduna E3 ubiquitin ligase

Iduna, an evolutionarily conserved protein, is a unique E3 ubiquitin ligase that specifically promotes the degradation of PARsylated proteins (Zhou et al., 2011; Wang et al., 2012; He et al., 2012; DaRosa et al., 2014; Zhang et al., 2011; Callow et al., 2011).

Under normal physiological conditions, Iduna is found as an inactive enzyme. Binding to TNKS mediated iso- or poly-ADP-ribosylated proteins is an allosteric activation signal of Iduna-dependent ubiquitylation and the 26S proteasome-mediated degradation (DaRosa et al., 2014). Iduna is a positive regulator of Wnt signaling since it promotes Axin poly-ubiquitylation and degradation. Depletion of zygotic *Rnf146* with a translational blocking morpholino in *Xenopus* causes anteriorized development (Zhu et al., 2017). Conditional inactivation of *Iduna* promotes osteoclast activity and inflammation in mouse bone (Matsumoto et al., 2017a). On the other hand, *Iduna* depletion reduces proliferation of osteoblasts and promotes adipogenesis in the mouse skeleton (Matsumoto et al., 2017b).

TNKS and Iduna have received considerable attention as potential targets for cancer therapy. Overexpression of Iduna in non-small cell lung cancer enhances proliferation and invasion of tumors through the Wnt/β-catenin pathway (Gao et al., 2014). Furthermore, knock down of *Tnks1/2* stabilizes the tumor suppressor PTEN, reduces AKT phosphorylation and inhibits cell proliferation and glycolysis *in vitro* and tumor growth *in vivo*. TNKS1/2 are upregulated and negatively correlated with PTEN expression in human colon carcinomas (Li et al., 2015). Finally, TNKS and Iduna are positive regulators of Hippo-YAP signaling identified through a CRISPR screen (Wang et al., 2016). YAP is an oncoprotein whose expression is elevated in several human cancers. Small molecule inhibitors of TNKS suppress the oncogenic of YAP through stabilizing angiomotin family proteins via TNKS-Iduna axis (Wang et al., 2015; Wang et al., 2016).

On the other hand, Iduna protects mice against glutamate excitotoxicity and stroke (Andrabi et al., 2011). It also preserves cells from environmental stress-induced cell death by scavenging PARs (Zhou et al., 2011; Andrabi et al., 2011; Gerö et al., 2014; Kang et al., 2011;

Wang et al., 2011; Xu et al., 2013). Iduna has a neuroprotective role against NMDA toxin induced cell death. NMDA induces PAR polymers in the nucleus. Accumulated PAR diffuses into cytoplasm that interacts with apoptosis inducing factor (AIF). That leads to AIF release from mitochondria outer membrane. AIF then enters to nucleus and causes DNA fragmentation and cell death. Over-expression of Iduna in the mouse brain prevents the interaction of PARs with AIF. This abrogates AIF-release and blocks neuronal cell death in mice (Andrabi et al., 2011). Iduna is also highly expressed in the brain of patients that suffers from Alzheimer's Disease (AD) (von Rotz et al., 2005). Hence, Iduna may play a role for protection against stress-induced cell death and neurodegeneration.

1.3 The Wnt/β-catenin (Wingless) signaling pathway

Wnt/β–catenin (Wingless) signaling is an evolutionarily conserved pathway from invertebrates to vertebrates. This pathway has critical functions during embryonic development, stem cell self-renewal and differentiation, adipogenesis, neural maturation, as well as tissue and animal regeneration (Nusse and Clevers, 2017).

The key process in the canonical pathway is to control of β-catenin concentration by a destruction complex, which is composed of Axin/GSK3, APC and Casein Kinase I (Kimelman and Xu, 2006; Nakamura et al., 1998; Hart et al., 1998; Ikeda et al., 1998). When there is no Wnt ligand, the destruction complex associates with β-catenin and enhances the degradation of phosphorylated and poly-ubiquitylated β–catenin through the 26S proteasome (Zeng et al., 1997). On the other hand, if there is a Wnt ligand, it binds to Frizzled and LRP receptors on the cell membrane. β-catenin is then stabilized with its degradation complex on the cell membrane,

accumulates in the cytoplasm and finally trans-locates into the nucleus to induce expression of the pathway-associated genes (Lee et al., 2003; Zeng et al., 1997).

Axin is the central scaffold protein in the destruction complex. It binds the components of the complex through its different domains (Nakamura et al., 1998; Hart et al., 1998; Ikeda et al., 1998; Zeng et al., 1997). Axin is present at a lower level than the other components of the complex and over-expression of Axin in cultured cells promotes the degradation of β-catenin (Lee et al., 2003). Hence, Axin is a rate-limiting factor of the pathway and its level is tightly controlled (Lee et al., 2003; Zeng et al., 1997). There is an Axin threshold in a time and tissue-dependent manner in *Drosophila.* To observe functional alterations in Wingless activity in the developing embryo of *Drosophila*, there should be Axin elevation more than its endogenous protein level. This threshold is 3-6 fold of endogenous Axin level to observe abnormal wing development. On the other hand, adult *Drosophila* midgut is more sensitive tissue to reduced Wingless signaling (Feng et al., 2014; Wang et al., 2016; Yang et al., 2016). It is therefore required to degrade the rate-limiting protein Axin through the UPS to prevent the attenuation of Wnt signaling (Li et al., 2012).

Axin degradation depends on the combined actions of TNKS poly-ADP-ribose polymerase and Iduna (Zhang et al., 2011). UPS-dependent degradation of Axin occurs in a specific temporal order. As an initial step, Iduna binds to TNKS but Iduna initially exists in an inactive state in the complex. Once Axin binds to the Iduna-TNKS complex through its TBM, TNKS ADP-ribosylates Axin by using NAD+. After Axin has iso- or poly-ADP-ribose, Iduna changes its confirmation to recognize and bind to Axin through its WWE domain and poly-ubiquitylates Axin. After the ADP-ribosylation and ubiquitylation, post-translationally modified Axin is rapidly degraded by the 26S proteasome (DaRosa et al., 2014; Wang et al., 2016a and

2016b; Croy et al., 2016; Callow et al., 2011). This tight control suggests an important function for Iduna to regulate the Wnt/β-catenin pathway.

1.4 Intestinal stem cells in the adult *Drosophila* midgut

Adult stem cells are essential for maintaining basal tissue integrity and are a resource for tissue regeneration upon injury. Tissue homeostasis requires a tight control to coordinate the actions between the removal of old or damaged cells, and the production of new cells. The intestinal epithelium has a remarkable regeneration potential. The small intestinal epithelium of the mouse completely renews itself every 3-5 days (Barker et al., 2007; Barker et al., 2012).

The *Drosophila* adult midgut has similar structure and function with the mammalian small intestine (Micchelli and Perrimon, 2006; Ohlstein and Spradling, 2006; Barker et al., 2007). Similar to the mammalian intestine, the fly midgut provides essential physiological functions, including food digestion, nutrient absorption and solid waste elimination, and displaying key endocrine, immune and metabolic roles (Perochon et al., 2018).

The *Drosophila* midgut has intestinal stem cells (ISCs) (Micchelli and Perrimon, 2006; Ohlstein and Spradling, 2006). Paracrine Wingless signaling controls self-renewal of *Drosophila* midgut stem cells (Perochon et al., 2018; Herr et al., 2012; Lin and Xi, 2008).

Under homeostatic conditions, reduced Wingless signaling causes over-proliferation of ISC in *Drosophila*. (Kramps et al., 2002; Wang et al., 2016 a, b; Tian et al., 2016; Gultekin and Steller, 2019). Non-cell autonomous mechanisms also orchestrate tissue remodeling in the *Drosophila* midgut, highlighting the importance of the stem cell niche as a sensor of organismal physiology. The JAK-STAT pathway can be non-cell autonomously activated to promote proliferation of stem cells in the *Drosophila* midgut (Gultekin and Steller, 2019; Herrera and

Bach, 2019; Zeidler et al., 2000; Zoranovic et al., 2013; Markstein et al., 2014; Zhou et al., 2013; Tian et al., 2016).

In response to genetically or pharmacologically induced stress, bacterial infection, and apoptosis, enterocytes and enteroblasts have been shown to express and secrete Unpaired (UPD) cytokines. Secreted UPDs then bind to the Domeless receptor on enteroblasts or intestinal stem cells to activate the JAK-STAT pathway in stem cells (Herrera and Bach, 2019; Ghiglione et al., 2002; Zhou et al., 2013; Xu et al., 2011). Moreover, other conserved signaling pathways including JNK, Hippo, EGRF, Hh, Dpp/BMP signaling have been shown to mediate damage or stress-induced intestinal regeneration in *Drosophila* (Jiang and Edgar, 2011; Naszai et al., 2015; Apidianakis et al., 2009; Jiang et al., 2009; Buchon et al., 2009; Shaw et al., 2010).

Figure 1.7 ADP-ribosylation activates the Wnt/β−catenin signaling pathway. When Wnt is ``off``, the destruction complex, composed of Axin/GSK3, APC and Casein Kinase I associates with β−catenin and enhances the degradation of phosphorylated and poly-ubiquitylated β−catenin through the 26S proteasome (1). On the other hand, if Wnt is ``on``, WNT ligand binds to Frizzled and LRP receptors on the cell membrane (2). β−catenin is then stabilized with its degradation complex on the cell membrane, accumulates in the cytoplasm and finally translocates into the nucleus to induce expression of the pathway-associated genes (3). On the other side, TNKS PARsylates Axin, the rate limiting protein of the Wnt pathway. Finally, PARsylated-Axin is poly-ubiquitylated by RNF146/Iduna for its turnover (4). The figure is adapted from (McCubrey et al., 2014).

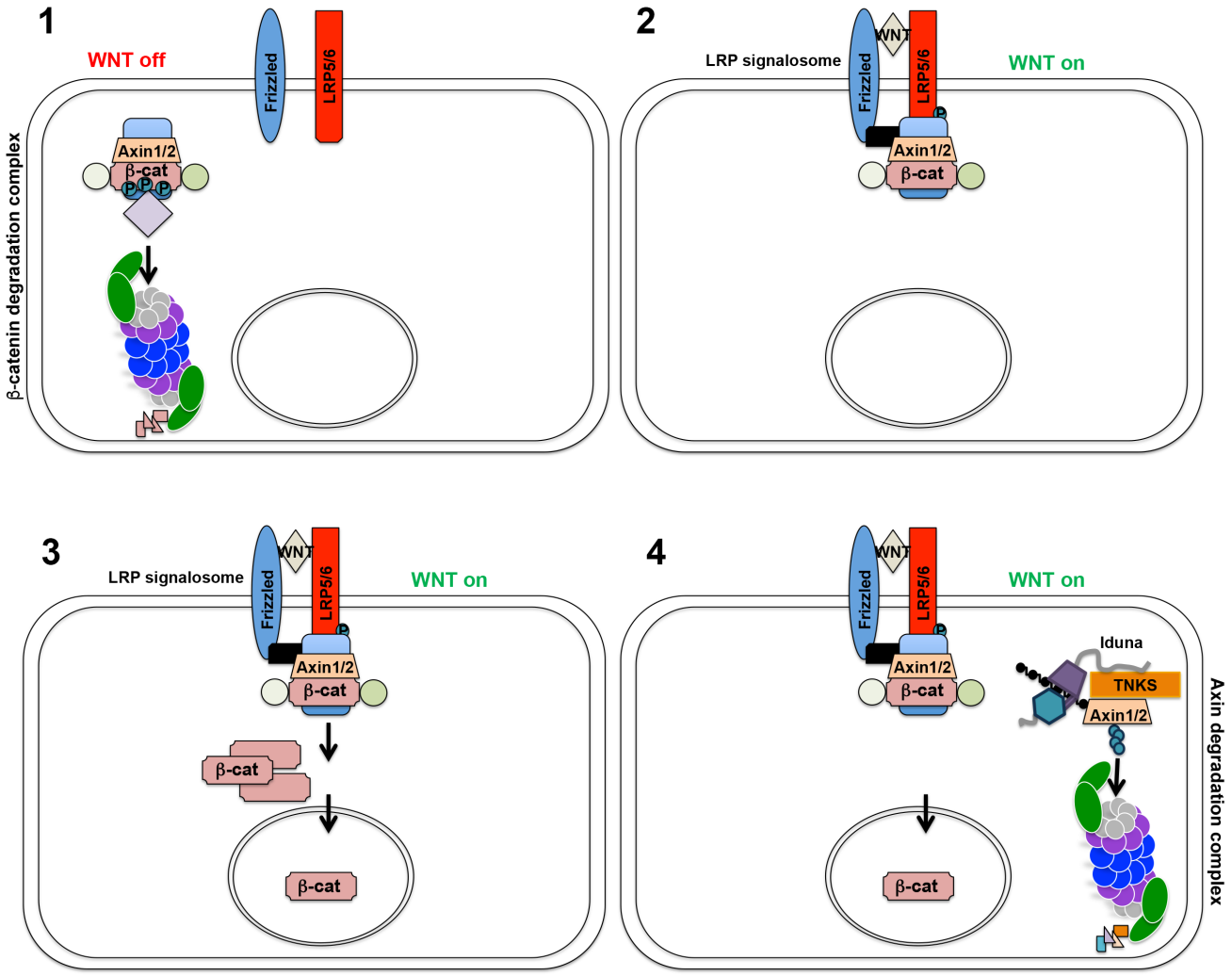
1
WNT off
Frizzled
LRP5/6
Axin1/2
β-cat
β-catenin degradation complex
2
LRP signalosome
WNT on
WNT
3
LRP signalosome
WNT on
4
WNT on
Iduna
TNKS
Axin1/2
Axin degradation complex

Figure 1.8 Intestinal stem cells reside in the *Drosophila* midgut epithelium. A- Just as the mammalian intestine, the *Drosophila* midgut has several intestinal regions including the foregut, anterior midgut, the posterior midgut, and the hindgut. **B-** *Drosophila* intestine has stem cells (ISCs), which give rise to all intestinal compartments. ISCs give rise to daughter cells: undifferentiated enteroblasts (EBs) and terminally differentiated enterocytes (ECs) and enteroendocrine (EEs) cells. **C-** The Wingless pathway is necessary to maintain midgut homeostasis in *Drosophila*. Axin is a rate-limiting factor in the Wingless pathway. There is an Axin threshold to observe functional consequences of altered Wingless signaling in a time and tissue-dependent manner in *Drosophila.* Adult *Drosophila* midgut is more sensitive tissue to reduced Wingless signaling.

A

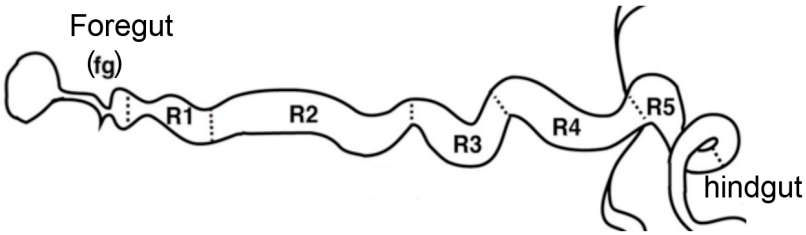

B

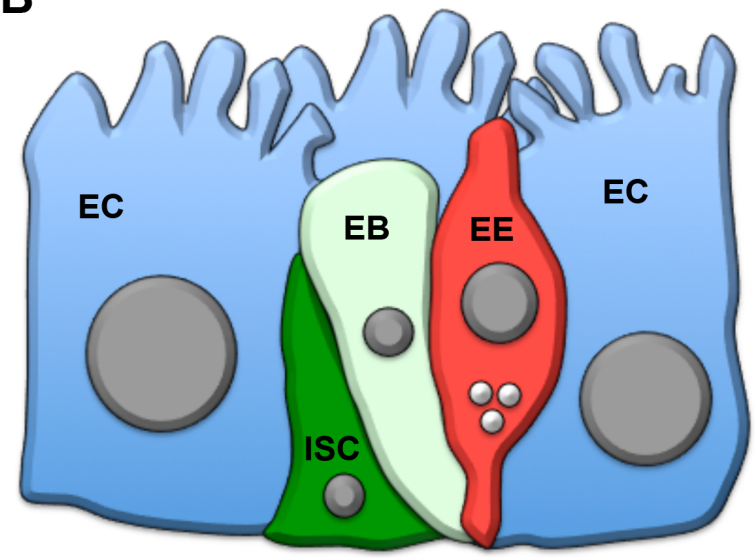

C

***Drosophila* tissue**	**Axin threshold (fold)**
• Embryo	> 3
• Wing imaginal discs	3-9
• Adult midgut	≥ 2

1.5 Relevance to this thesis

The UPS degrades most of the short-lived proteins in the cell. The rates of proteolysis often correlate with cellular functions, cellular localization as well as post-translational modifications (PTM) of a protein. Poly-ADP-ribosylation is a highly dynamic and reversible PTM, affecting protein activity and stability. For instance, poly-ADP-ribosylated TRF1, a negative regulator of telomere length localized on the telomeres, has not been detected *in vivo*, owing to its rapid degradation (Ye and de Lange, 2004).

My graduate thesis has aimed to address the questions on why target proteins of TNKS have short half-lives and how they are degraded rapidly. I am interested in understanding the mechanism that allows for very fast and efficient degradation of labile proteins. I have hypothesized that PTM of proteins by ADP-ribosylation provides a molecular scaffold to assemble them together with a specific E3 ubiquitin ligase and proteasomes, thereby locally concentrating all "players" and causing accelerated degradation of target proteins (Fig 1.6).

I have proposed that TNKS forms a complex with Iduna, which is inactive when bound to non-PARylated TNKS in the cell. After substrate binding to TNKS and subsequent PARylation, Iduna binds an internal unit of PAR. This binding causes a conformational change in the RING domain of Iduna, activating its ubiquitin ligase activity and enabling the poly-ubiquitylation of the substrate. As a consequence, TNKS may be promoted for its PARsylation activity to assemble PARsylation scaffold. Finally, I suggest that PI31 may play a role in proteasome recruitment. 26S proteasomes, therefore, can be recruited to the scaffold and concentrating them in the local environment for the rapid breakdown of the target proteins (Fig 1.6).

The overarching goal of this thesis is to understand the mechanisms that allow for rapid and efficient protein degradation. I combined the power of fly genetics with that of molecular

and cellular tools to investigate the regulatory functions of PARsylation and Iduna on TNKS-coupled protein degradation. I, therefore, i) determined the physiological role(s) of Iduna by generating loss-of-function mutants, ii) understood the role of Iduna for TNKS-coupled PARsylation and proteolysis, iii) investigated whether ADP-ribosylation served as a molecular scaffold to accelerate the proteolysis of TNKS target proteins by mapping ADP-ribose acceptor site(s) of TNKS and its possible substrates, and finally iv) identified the possible regulatory proteins that have an impact on PARsylation-mediated protein breakdown.

This thesis addresses the role of PARsylation in TNKS-mediated rapid protein degradation. This work, therefore, provides novel mechanistic insights into the regulation of protein quality control. Ultimately, these results may also provide a conceptual basis to guide the development of new therapies.

Figure 1.9 Hypothetical working model. ADP-ribosylation provides a molecular scaffold to assemble them together with the specific E3 ubiquitin ligase and proteasomes, thereby locally concentrating all "players" and causing accelerated degradation of target proteins. We propose that TNKS forms a complex with Iduna, which is inactive when bound to non-PARylated TNKS in the cell. After substrate binding to TNKS and subsequent PARylation, Iduna binds an internal unit of PAR. This binding causes a conformational change in the RING domain of Iduna, which activates its ubiquitin ligase activity, enabling the poly-ubiquitinylation of the substrate. As a consequence, TNKS may be promoted for its ribosylation activity to assemble poly-ADP-ribose scaffold. Finally, we suggest that PI31 may have a role in proteasome recruitment. 26S proteasomes, therefore, can be recruited to the scaffold and concentrated in a local environment for rapid break down of the target protein.

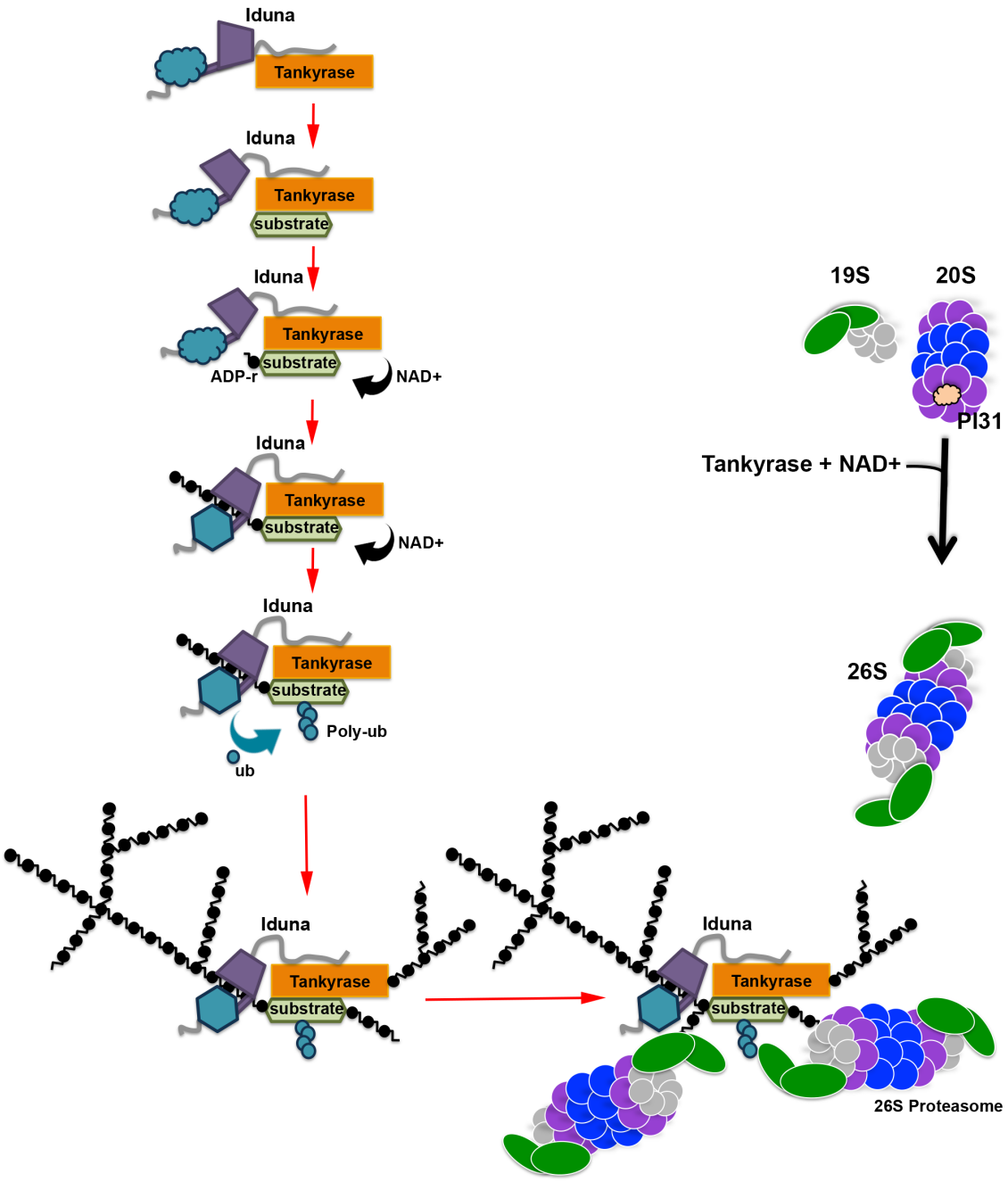
Iduna
Tankyrase
Iduna
Tankyrase
substrate
Iduna
Tankyrase
substrate
ADP-r
NAD+
Iduna
Tankyrase
substrate
NAD+
Iduna
Tankyrase
substrate
Poly-ub
ub
19S
20S
PI31
Tankyrase + NAD+
26S
Iduna
Tankyrase
substrate
Iduna
Tankyrase
substrate
26S Proteasome

2 Axin proteolysis by Iduna is required for the regulation of stem cell proliferation and intestinal homeostasis in *Drosophila*

2.1 Summary

The self-renewal of intestinal stem cell is controlled by Wingless/Wnt-β catenin signaling in both *Drosophila* and mammals. Since Axin is a rate-limiting factor in Wingless signaling its regulation is essential. Iduna is an evolutionarily conserved ubiquitin E3 ligase that has been identified as a critical regulator for degradation of ADP-ribosylated Axin and thus of Wnt/β-catenin signaling. However, its physiological significance remains to be demonstrated. Here, I generated loss-of-function mutants of *Iduna* to investigate its physiological role in *Drosophila*. I show genetic depletion of *Iduna* causes the accumulation of both TNKS and Axin. Increase of Axin protein in enterocytes non-autonomously enhanced stem cell divisions in the *Drosophila* midgut. Enterocytes secreted Unpaired and thereby stimulated the activity of the JAK-STAT pathway in intestinal stem cells. A decrease in *Axin* gene expression suppressed both the over-proliferation of stem cells and restored their numbers to normal levels in *Iduna* mutants. These findings suggest that Iduna-mediated regulation of Axin proteolysis is essential to maintain tissue homeostasis in the *Drosophila* midgut.

2.2 Introduction

The evolutionarily conserved Wnt/β-catenin signaling pathway is a main regulator of animal development. It controls proliferation, differentiation and regeneration of adult tissues (Herr et al., 2012; Nusse and Clevers, 2017). The Wingless pathway is also involved in adult tissue self-renewal in *Drosophila* (Lin et al., 2008). Genetic depletion of proteins in the Wingless pathway, such as *Tcf*, *arr, dsh* and *pygo,* leads to inhibition of Wingless signaling activation which in turn causes over-proliferation of stem cells in the *Drosophila* midgut (Kramps et al., 2002; Wang et al., 2016 a, b; Tian et al., 2016). However, inactivation of Wnt signaling in the mouse small intestine decreases the proliferative potential of stem cells (Fevr et al., 2007; Korinek et al., 1998). On the other hand, mutations resulting in the over-activation of the Wnt/β-catenin pathway promote tumorigenesis (Clevers and Nusse, 2012; Andreu et al., 2005; Korinek et al., 1997 and 1998; Morin et al., 1997). For instance, mutations in the *adenomatous polyposis coli (APC)* gene cause a hereditary colorectal cancer syndrome called familial adenomatous polyposis (Kinzler et al., 1991; Nishisho et al., 1991). Axin loss-of-function mutations are found in hepatocellular carcinomas, while oncogenic β-catenin mutations are described in colon cancer and melanoma (Rubinfeld et al., 1997). Consequently, intense efforts have been made to target this pathway for therapeutic purposes (Clevers and Nusse, 2012).

A key feature of the Wnt/β-catenin pathway is the regulated proteolysis of the downstream effector β-catenin by the β-catenin degradation complex. The principal components of this complex are APC, Axin and Glycogen synthase kinase 3β (GSK3β) (Kramps et al., 2002; Hamada et al., 1999; Salic et al., 2000; Lee at al., 2003). Axin, a critical scaffold protein in the β-catenin degradation complex, is the rate-limiting factor of Wnt signaling and its protein levels are regulated by the Ubiquitin-Proteasome System (UPS) (Li et al., 2012). Axin is targeted for

degradation by the combined action of the TNKS and the ubiquitin E3-ligase Iduna/Ring finger protein 146 (RNF146) (Zhang et al., 2011). Both genetic and pharmacological studies suggest that UPS-dependent degradation of Axin occurs in a specific temporal order. Iduna initially exists in an inactive state but binding to its iso- or PARsylated targets causes allosteric activation of the enzyme (DaRosa et al., 2014). In the first step, TNKS binds to Axin and ADP-ribosylates Axin using NAD+. Then, Iduna recognizes and binds to ADP-ribosylated Axin via its WWE domain and poly-ubiquitylates Axin. Following the ADP-ribosylation and ubiquitination, post-translationally modified Axin is rapidly degraded by the proteasome (DaRosa et al., 2014; Wang et al., 2016 a, b; Croy et al., 2016; Callow et al., 2011). This tight control suggests a crucial function for Iduna to regulate the Wnt-β catenin pathway.

Because the stability of Axin is partially regulated by TNKS-mediated ADP ribosylation, specific small-molecule inhibitors have been developed to inhibit Wnt-signaling (Lu et al., 2009; Huang et al., 2009). For example, XAV939 targets the ADP-ribose polymerase activity of TNKS and increases Axin levels, which in turn destabilizes β-catenin to inhibit Wnt signaling (Huang et al., 2009). There are two TNKS isoforms in mammalian cells (Hsiao et al., 2006). *Tnks1*$^{-/-}$ and *Tnks2*$^{-/-}$ mice are overall normal; however, double knockout of *Tnks1/2* causes early embryonic lethality, which indicates their redundancy in mouse development (Hsiao et al., 2006; Chiang et al., 2008). On the other hand, inactivation of the single *Drosophila Tnks* gene produces viable flies that have slightly increased Axin levels and abnormal proliferation of intestinal stem cells, but otherwise display no overt defects (Wang et al., 2016 a, b; Feng et al., 2014; Yang et al., 2016; Tian et al., 2016). The exact physiological function of Iduna, however, remains to be determined. In order to address this question, I generated and characterized *Drosophila* Iduna

loss-of-function mutants and demonstrate a critical function of this pathway for stem cells in the *Drosophila* intestinal tract.

The *Drosophila* genomes encode four isoforms of *CG8786/Iduna/RNF146*, which is evolutionarily conserved from *Drosophila* to human. In this study, I concentrated on the physiological function of Iduna in the adult *Drosophila* midgut*,* which shares several striking similarities with the mammalian small intestine but offers greater anatomical and genetic accessibility (Micchelli and Perrimon, 2006; Ohlstein and Spradling, 2006; Markstein et al., 2014). Under normal conditions, Wingless signaling controls stem cell proliferation and cell fate specification in adult midgut (Tian et al., 2016). Here, I showed that Iduna has a physiological function to regulate the proteolysis of both TNKS and Axin. Inactivation of *Iduna* results in increased numbers of midgut stem cells and progenitors due to over-proliferation. I found that Axin accumulation in enterocytes promotes the secretion of Unpaired, a cytokine that binds to the Domeless receptor and activates the JAK-STAT pathway in stem cells and thereby promotes stem cell division. Significantly, reducing *Axin* expression by half restores the numbers of ISC. These findings indicate that regulation of Axin proteolysis by Iduna is necessary to control intestinal homeostasis in *Drosophila,* and it provides physiological evidence for the idea that the functions of TNKS and Iduna are tightly coupled.

2.3 Results

2.3.1 Iduna plays a role in Axin degradation

To examine the *in vivo* function of *Drosophila* Iduna, CRISPR-Cas9 genome editing was used to generate *Iduna* mutants. *Iduna* is located on the 3rd chromosome of *Drosophila*. I designed a specific guide RNA that targets *Iduna*`s first exon and identified two mutant alleles by Sanger sequencing: $Iduna^{17}$ and $Iduna^{78}$, which have 4-nucleotides and 2-nucleotides deletions, respectively (Fig 2.1A-B). These deletions are close to the translation start side of *Iduna*.

Next, I assessed the levels of mRNA and protein expression in these mutants. Using reverse transcript PCR analyses, I found significantly reduced amounts of *Iduna* transcripts in the $Iduna^{78}$ mutant. On the other hand, I was unable to detect any *Iduna B* and *C/G* transcripts in the $Iduna^{17}$ allele (Fig 2.1C). Moreover, no Iduna protein was detected in either of these mutants, indicating that they represent null-mutations (Fig 2.1D). Finally, genetic analyses of these alleles in trans to a larger deletion indicate that both alleles are complete loss-of-function mutations. *Iduna* mutants were crossed to *Drosophila* deficiency lines [Df(3L) Exel6135, Df(3L) ED228)] and also to each other and all combinations were viable as trans-heterozygotes.

I examined the larval development of *Iduna* mutants and Oregon R but did not observe any differences in the numbers of hatched eggs (Fig 2.2A-B), pupated larvae or eclosed adult *Drosophila* (Fig 2.2C) between *Iduna* mutants and wild type. *Iduna*-null adult flies had no overt morphological defects when compared with wild type controls, although, *Iduna* mutants did not live as long as control flies (Fig 2.3A). *Iduna* inactivation, therefore, decreased average lifespan compared to wild type (Fig 2.3B).

Figure 2.1 *Iduna*^{17} and *Iduna*^{78} are null mutants. A- *Iduna*^{17} and *Iduna*^{78} have deletions of 4 and 2 nucleotides, respectively, introduced early stop codons and led to truncations of Iduna protein. sgRNA against Iduna was designed to generate small nucleotide deletions, close to its translation initiation site. The three nucleotides were highlighted with red to indicate the location of Cas9 cleavage site. **B-** *Iduna* loss-of-function mutants, *Iduna*^{17} and *Iduna*^{78}, were isolated by Sanger sequencing. **C-** *Iduna*^{17} had no detectable *Iduna* transcripts, and Iduna^{78} had severely reduced *Iduna* mRNA based on RT-PCR. 7-day-old adult females were analyzed for expressions of *Iduna*, *Ribosomal protein 49* (a house keeping gene) and *Ornitate aminotransferase.* **D-** *Iduna*^{17} and *Iduna*^{78} have no detectable protein. Endogenous Iduna protein was detected by immunoblotting. Anti-Iduna antibody was generated in guinea pigs and 20μg total protein lysates of 7-day-old adult females were analyzed by immunoblotting. β-actin was used as a loading control. Both *Iduna* alleles have no detectable protein and behave genetically as null-alleles.

Figure 2.1

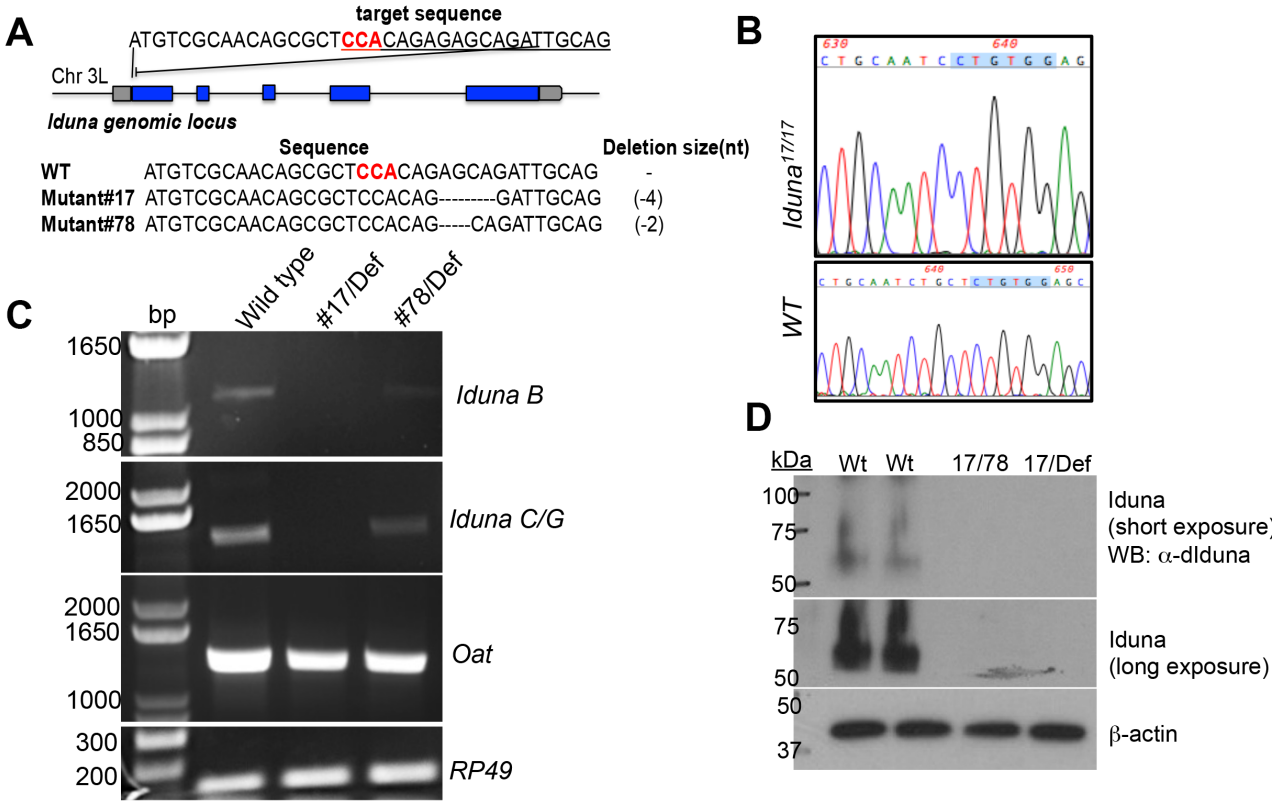
A
target sequence
ATGTCGCAACAGCGCTCCACAGAGAGCAGATTGCAG
Chr 3L
Iduna genomic locus
Sequence
Deletion size(nt)
WT ATGTCGCAACAGCGCTCCACAGAGCAGATTGCAG -
Mutant#17 ATGTCGCAACAGCGCTCCACAG---------GATTGCAG (-4)
Mutant#78 ATGTCGCAACAGCGCTCCACAG-----CAGATTGCAG (-2)
B
Iduna17/17
WT
C
bp
Wild type
#17/Def
#78/Def
1650
1000
850
Iduna B
2000
1650
Iduna C/G
2000
1650
1000
Oat
300
200
RP49
D
kDa
Wt
Wt
17/78
17/Def
100
75
50
Iduna
(short exposure)
WB: α-dIduna
75
50
Iduna
(long exposure)
50
37
β-actin

Figure 2.2

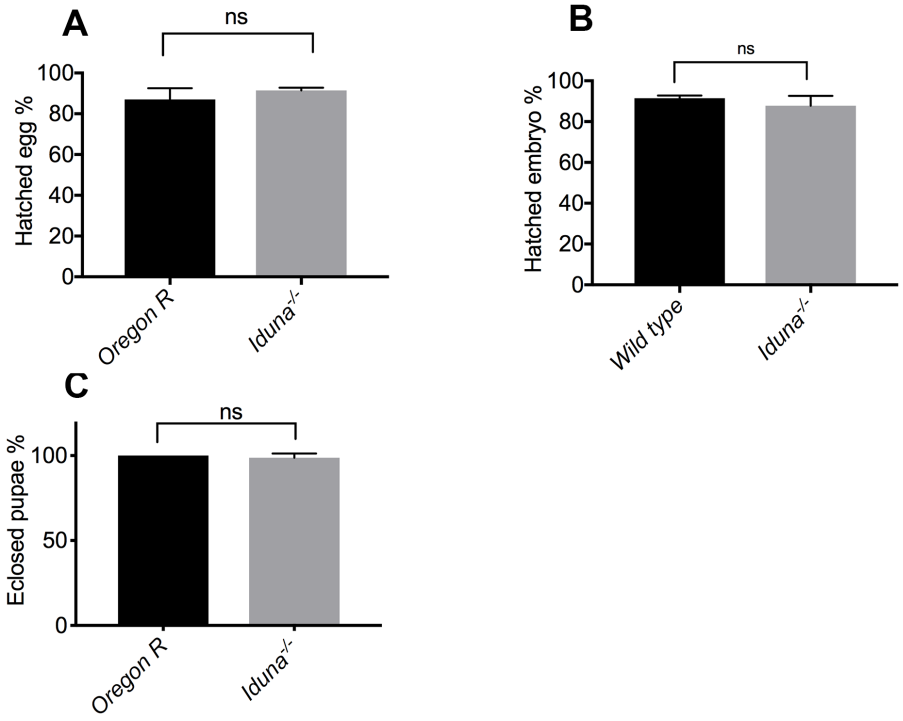

Figure 2.2 *Iduna* inactivation does not cause developmental defects in *Drosophila.* **A-** *Iduna* mutants (*Iduna*$^{-/-}$*: Iduna*$^{17/17}$) did not have defects in hatching their eggs. n>250 for each genotype. **B-** *Iduna* transheterozygous (*Iduna*$^{-/-}$*: Iduna*$^{17/78}$) mutants did not have defects in hatching their embryos. n>100 for each genotype. **C-** *Iduna* mutant larvae could be pupated and eclosed to adult *Drosophila.* n>100 for each genotype. Oregon R flies used as wild type flies. Two-tailed Student`s *t-test* was used for statistical analyses. Error bars represented as means ± s.d. ``ns`` means ``not significant``.

Figure 2.3

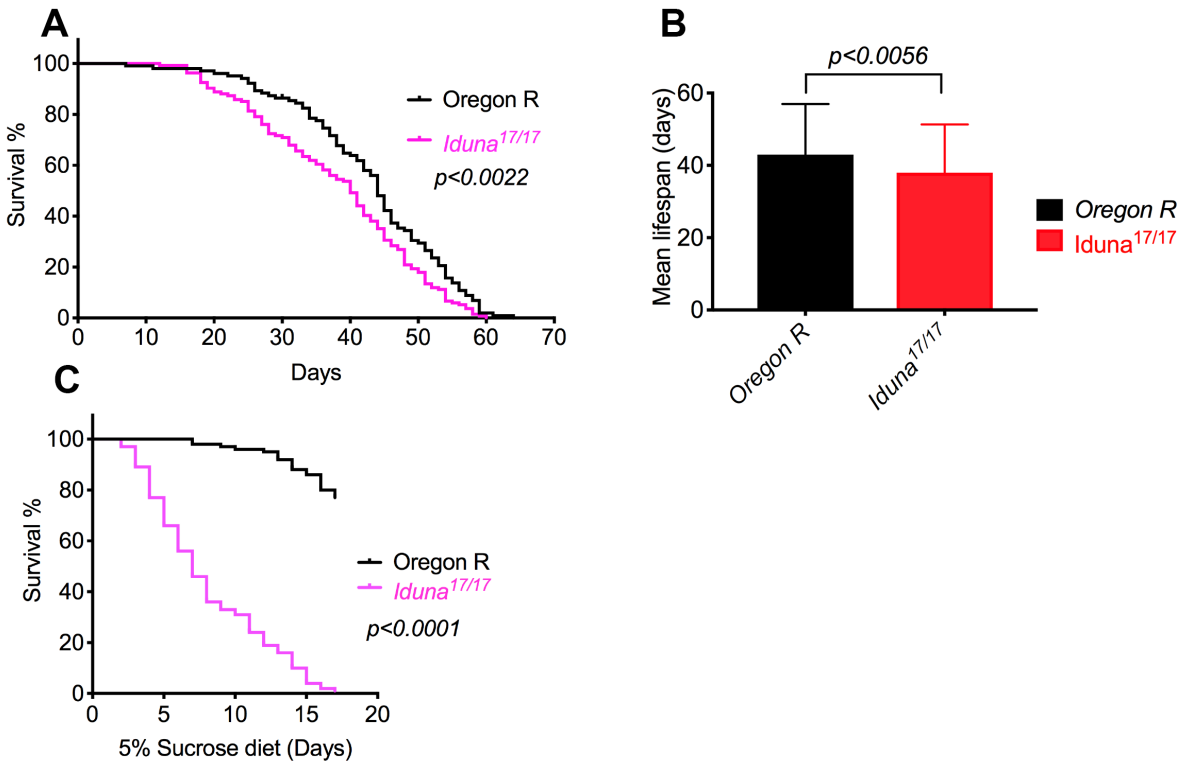

Figure 2.3 Loss-of-function mutants of *Iduna* display increased mortality under reduced nutrient conditions. A- *Iduna*$^{17/17}$ mutant flies lived slightly shorter than wild type flies. **B-** *Iduna* inactivation decreased average lifespan compared to wild type flies. Flies were aged matched at 24-25^{0}C. n>100 from each genotype. **C-** *Iduna*$^{17/78}$ flies were analyzed on 5% sucrose diet. For statistical analyses, I used the Mantel-Cox and Gehan-Breslow-Wilcoxon tests to compare survival curves between *Iduna* mutants and Oregon R wild type flies. 2-day-old mutant or wild type female flies were collected and kept on 5% sucrose diet at 28^{0}C. n=100 from each genotype.

However, they displayed increased mortality upon nutrient deprivation. I challenged two-day-old mutant and wild type adult females with a 5% sucrose diet at 28^0C. Mutant flies died within 17 days, while 70-80% of wild type flies were still viable at this time (Fig 2.3C).

Iduna is one of the key components of the machinery that degrades Axin whose ADP-ribosylation by TNKS is crucial for mammalian Wnt-β catenin signaling (Li at al., 2012). I detected increased levels of endogenous Axin in the lysates from *Iduna* mutant midguts compared to controls (Fig 2.4A). Mammalian Iduna recognizes both ADP-ribosylated (ADPR) TNKS and Axin via the R163 residue in its WWE domain (Zhang et al., 2011). The R163 residue is conserved in evolution and corresponds to R252 in the *Drosophila* WWE domain (Fig 2.4B). To examine the level of endogenous ADPR-Axin in *Iduna* mutants, ADPR-Axin was pulled down with wild type-WWE or R252A-WWE-mutant recombinant proteins (Fig 2.4C). This analysis revealed that *Iduna* mutants had a more than two-fold increase in ADPR-Axin in their midguts compared to the wild type (Fig 2.4D-E). These results suggest that Iduna promotes Axin degradation *in vivo*. To further understand the contribution of *Iduna* inactivation for both TNKS and Axin proteolysis in *Drosophila*, *UAS-Flag-Tnks* and *UAS-GFP-Axin* transgenes were mis-expressed under an eye-specific driver, *GMR*, in an *Iduna* mutant background (Fig 2.5A). To detect mis-expressed GFP-Axin and Flag-TNKS levels, total proteins were extracted from 5-day-old male heads and analyzed by immunoblotting (Fig 2.5C and E). I found that *Iduna* mutants had 2.5-fold more mis-expressed GFP-Axin protein when compared to the control (Fig 2. 5D). These mutants also had 3.5-fold more ectopic expressed Flag-tagged TNKS as well (Fig 2. 5F).

Figure 2.4 *Iduna* inactivation leads to increased Axin protein levels in the midgut. A- Iduna mutant midguts have elevated levels of Axin protein compared with controls. Midguts of 7-day-old adult females were dissected, lysed and analyzed by Axin immunoblotting. β-Actin was used as a loading control. **B-** Mammalian Iduna recognizes ADP-ribosylated (ADPR) Axin via the R163 residue in its WWE domain. The R163 residue is conserved in evolution and corresponds to R252 in the Drosophila WWE domain. *Hs, Homo sapiens; Mm, Mus musculus; Dm, Drosophila melanogaster.* **C-** Recombinant wild type and R252A mutants were used as biochemical sensors to pull down the ADPR-Axin from Drosophila midguts. Myc-tagged WWE proteins were expressedand purified from Drosophila S2R+ cells by immunoprecipitation. **D-** Inactivation of *Iduna* leads to accumulation of ADPR-Axin. Wild-type Myc-tagged-WWE protein pulled down ADPR-Axin. In contrast, the R252A mutant did not interact with modified Axin. Following immunoprecipitation (IP), eluted proteins were analyzed with an anti-PAR antibody. The 50 kDa heavy chain IgG is indicated on the blot. **E-** *Iduna* inactivation results in 2.3-fold more ADPR-Axin protein in the midgut. Western blot quantification of two independent experimental replicates; ADPR-Axin levels were normalized to the control lines. Flies were fed with regular diet at 24-25°C. Two-tailed Student`s *t-test* was used for statistical analyses. Error bars represented as means ± s.d. $p<0.001$ is indicated as *** and $p<0.0001$ was marked as ****.

Figure 2.4

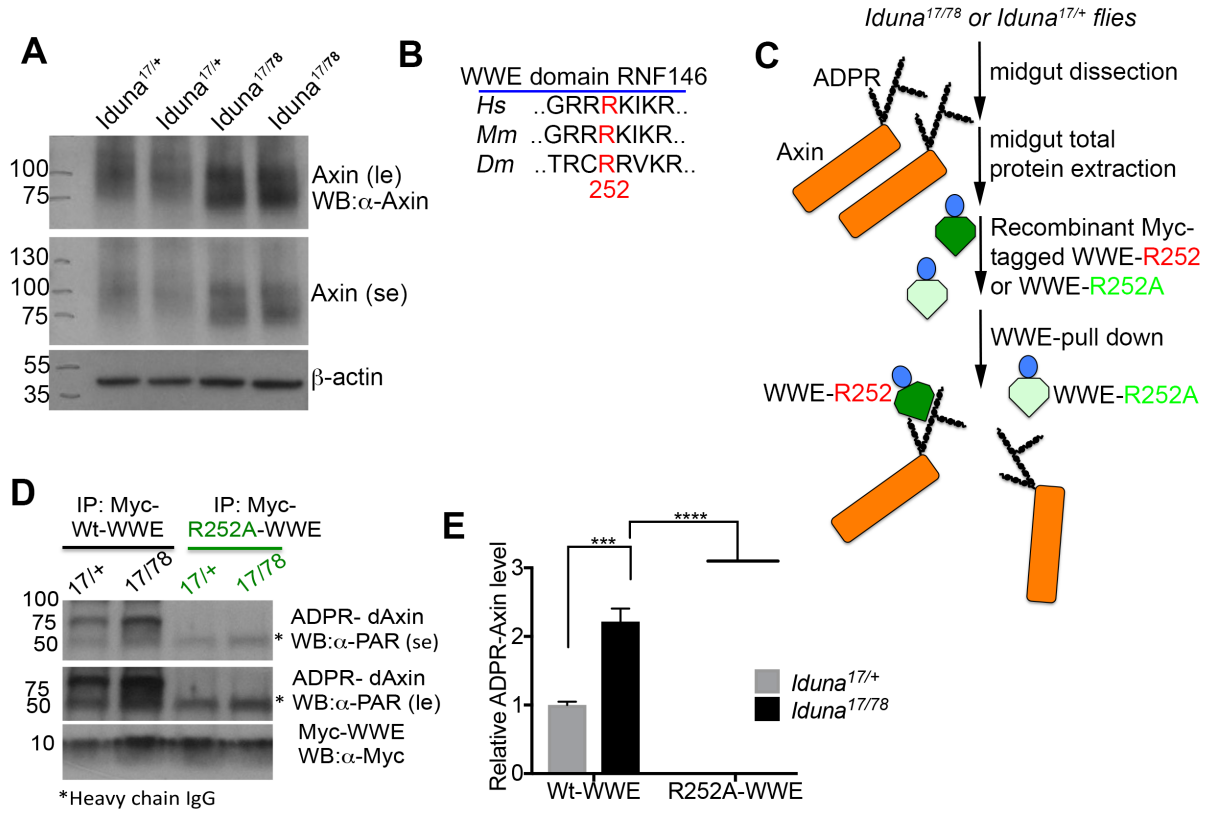
A
Iduna17/+
Iduna17/+
Iduna17/78
Iduna17/78
100
75
Axin (le)
WB:α-Axin
130
100
75
Axin (se)
55
35
β-actin
B
WWE domain RNF146
Hs ..GRRRKIKR..
Mm ..GRRRKIKR..
Dm ..TRCRRVKR..
252
C
Iduna17/78 or Iduna17/+ flies
ADPR
Axin
midgut dissection
midgut total protein extraction
Recombinant Myc-tagged WWE-R252 or WWE-R252A
WWE-pull down
WWE-R252
WWE-R252A
D
IP: Myc-Wt-WWE
IP: Myc-R252A-WWE
17/+
17/78
17/+
17/78
100
75
50
ADPR- dAxin
* WB:α-PAR (se)
75
50
ADPR- dAxin
* WB:α-PAR (le)
10
Myc-WWE
WB:α-Myc
*Heavy chain IgG
E
***
****
Relative ADPR-Axin level
3
2
1
0
Iduna17/+
Iduna17/78
Wt-WWE
R252A-WWE

Figure 2.5 *Iduna* depletion leads to increased Axin and TNKS protein levels in the *Drosophila* eye. A- Mis-expression of GFP-Axin in 5-day-old adult male eyes did not result in an obvious eye phenotype. **B-** Mis-expressed TNKS however led to rough eye phenotype in 5-day-old adult males. *Iduna* inactivation promoted the eye phenotype. **C-** *Iduna* inactivation leds to mis-expressed GFP-Axin elevation. A *UAS-GFP-Axin* reporter transgene was expressed under *GMR* driver in the *Iduna* mutants or wild type. **D-** *Iduna* mutants had 2.5-fold increased GFP-Axin protein. Quantification of mis-expressed GFP-Axin immunoblottings. Results are based on two repeats of independent replicates and Axin protein levels were normalized to β-actin. **E-** Flag-tagged mis-expressed TNKS protein accumulates in *Iduna* mutants. A *UAS-Flag-Tnks* reporter transgene was expressed under the *GMR-Gal4* driver in *Iduna* mutants or wild type. **F-** *Iduna* mutants had 3.5-fold increased levels of Flag-tagged TNKS. Quantification of Flag-TNKS immunoblottings. 5-day-old adult male heads were dissected and 20μg of total protein lysates were analyzed by immunoblotting to assess the levels of GFP-Axin or Flag-tagged TNKS using α-GFP or α-Flag antibodies, respectively. Western blot quantification was performed based on two independent experimental replicates, and protein levels were normalized with β-actin. Oregon R flies were used as a wild type control. Flies were fed with regular diet at 24-25^{0}C. Two-tailed Student`s *t-test* was used for statistical analyses. Error bars represented as means ± s.d. *** $p<0.001$

Figure 2.5

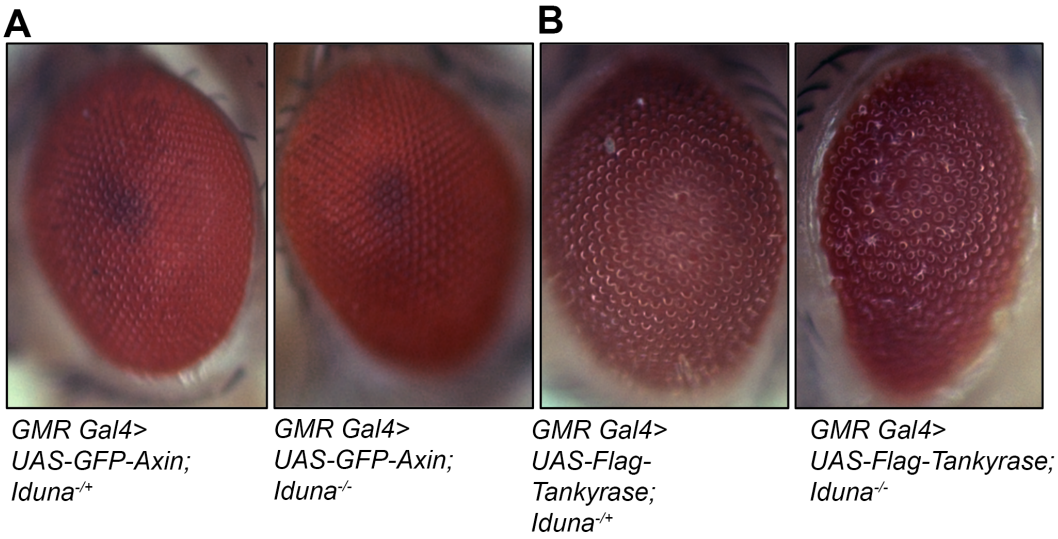
A
B
GMR Gal4> UAS-GFP-Axin; Iduna-/+
GMR Gal4> UAS-GFP-Axin; Iduna-/-
GMR Gal4> UAS-Flag-Tankyrase; Iduna-/+
GMR Gal4> UAS-Flag-Tankyrase; Iduna-/-

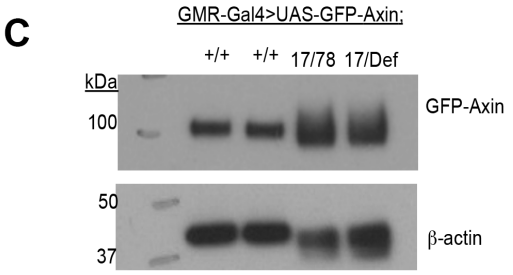
C
GMR-Gal4>UAS-GFP-Axin;
+/+ +/+ 17/78 17/Def
kDa
100
GFP-Axin
50
37
β-actin

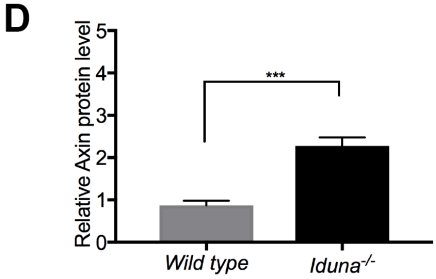
D
Relative Axin protein level
0
1
2
3
4
5
***
Wild type
Iduna-/-

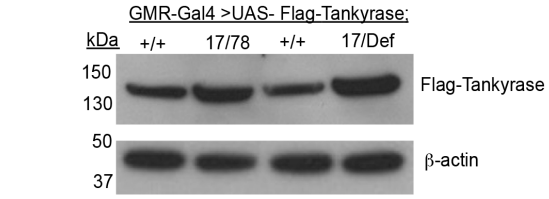
E
GMR-Gal4 >UAS- Flag-Tankyrase;
kDa
+/+ 17/78 +/+ 17/Def
150
130
Flag-Tankyrase
50
37
β-actin

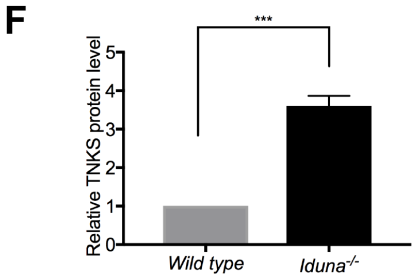
F
Relative TNKS protein level
0
1
2
3
4
5
***
Wild type
Iduna-/-

When I examined the eye morphology, GFP-Axin mis-expression did not cause an obvious eye phenotype (Fig 2.5A). In contrast, mis-expressed Flag-tagged TNKS led to a rough eye phenotype, which was more severe when *Tnks* was mis-expressed in *Iduna*$^{-/-}$ homozygous mutants compared to *Iduna*$^{-/+}$ heterozygous animals (Fig 2.5B). Recently, it was also reported that mis-expressed TNKS promotes apoptosis in the *Drosophila* eye due to the activation of JNK signaling (Feng et al., 2018).

In order to examine whether Axin is a target for Iduna-mediated degradation, I also mis-expressed a *UAS-GFP-Axin* transgene under the enterocyte (EC) specific temperature sensitive *Myo1A-Gal4* driver (Fig 2.6A) and saw 2-2.5-fold more Axin in *Iduna* mutants compared to controls (Fig 2.6B). To investigate the cellular levels of *Myo1A* driven GFP-Axin in ECs, I examined *FRT80B, Iduna* mutant clones and found that mutant EC clones had more GFP-Axin when compared to their neighboring cells (Fig 2.6C). Taken together, these observations suggest that Iduna plays a role in promoting the degradation of both Axin and TNKS.

2.3.2 Iduna is required to control the proliferation of intestinal progenitors in the *Drosophila* midgut

Attenuations in the Wingless pathway affect the proliferation of stem cells in the *Drosophila* midgut. For instance, inactivation of *Tcf*, *arr, armadillo, dsh,* and *pygo* leads to suppression of Wingless signaling, which in turn causes more stem cell division (Kramps et al., 2002; Wang et al., 2016a and 2016b; Tian et al., 2016). Furthermore, *Apc* and *Tnks* mutations cause elevation of Axin, which reduces Wingless signaling which in turn promoting mitosis of stem cells in the *Drosophila* midgut (Wang et al., 2016 a, b; Tian et al., 2016). Hence, the Wingless signaling pathway is required to control ISC proliferation in *Drosophila* (Xu et al, 2011; Cordero et al., 2012; Tian et al., 2016).

Since *Iduna* mutants have elevated Axin, I considered that *Iduna* inactivation might cause aberrant proliferation of stem cells in the *Drosophila* midgut. Just as the mammalian intestine (Korinek et al., 1998), the *Drosophila* midgut has intestinal stem cells (ISCs), which give rise to all intestinal compartments (Micchelli and Perrimon, 2006; Ohlstein and Spradling, 2006). ISCs specifically give rise to two types of daughter progenitor cells: undifferentiated enteroblast (EBs) and pre-enteroendocrine cells (Pre-EE). EBs and pre-EEs differentiate into ECs and EEs cells, respectively (Ohlstein and Spradling, 2006; Xu et al., 2011) (Fig 2.7A). ISCs can be distinguished from ECs by their cell size and marker proteins (Ohlstein and Spradling 2006; Xu et al., 2011). ISCs are small, express cell membrane-associated Armadillo, and lack nuclear expression of Prospero (Fig 2.7B). In contrast, nuclear Prospero staining is a marker of small-sized differentiated EE cells (Fig 2.7B).

ISCs are also marked by the expression of *escargot (esg),* a transcription factor, whose GFP reporter allows tracing of stem and progenitor cells during development (Ohlstein and Spradling, 2006) (Fig 2.7B). Using the *esg>GFP* marker, I first analyzed 9-day-old female flies which were fed with a 5% sucrose diet for seven days at 28^0C and saw an approximately twofold increase in the numbers of *esg>GFP* positive ISCs/progenitors in the midgut of *Iduna* mutants compared to controls (Fig 2.8A-B). *Iduna* inactivation increased the numbers of $Arm^+/Pros^-$ stem cells in midguts (Fig 2.8C) upon nutrient deprivation.

Figure 2.6 *Iduna* inactivation causes increased mis-expressed Axin protein levels in the midgut. A- *Iduna* mutant midguts had elevated mis-expressed GFP-Axin protein. Midguts of 7-day-old adult females, which were expressing GFP-Axin under the temperature sensitive *Myo1A-Gal4* driver, were dissected, lysed and analyzed by GFP immunoblotting. *Iduna* mutants had more Axin protein compared to the wild type. 20μg total intestinal lysates were analyzed by GFP immunoblotting and α-tubulin was used as a loading control. **B-** Loss-of-*Iduna* resulted in 2.2-fold GFP-Axin accumulation in the midgut. Western blot quantification was performed based on two independent experimental replicates, and protein levels were normalized to α-Tubulin. **C-** *Iduna* mutant clones have elevated mis-expressed GFP-Axin compared to their WT neighbors. A *UAS-GFP-Axin* transgene was expressed under the temperature sensitive *Myo1A-Gal4* driver in the FRT80B-*Iduna*^{17} mutant. Midgut mutant clones were induced during larval development by daily incubation at 37^{o}C for 1h. Adult female FRT80B-Nls-Red/FRT80B-*Iduna*^{17} flies were collected after eclosion, incubated at 28-29^{0}C and analyzed on day 7. Unlabeled cells represent *Iduna* mutant clones, whereas cells stained for nuclear RFP are either wild type or *Iduna* heterozygous. $p<0.001$ is indicated as *** and $p<0.0001$ was marked as ****. Two-tailed Student`s *t-test* was used for statistical analyses. Error bars represented as means ± s.d. Scale bars: 10μm

Figure 2.6

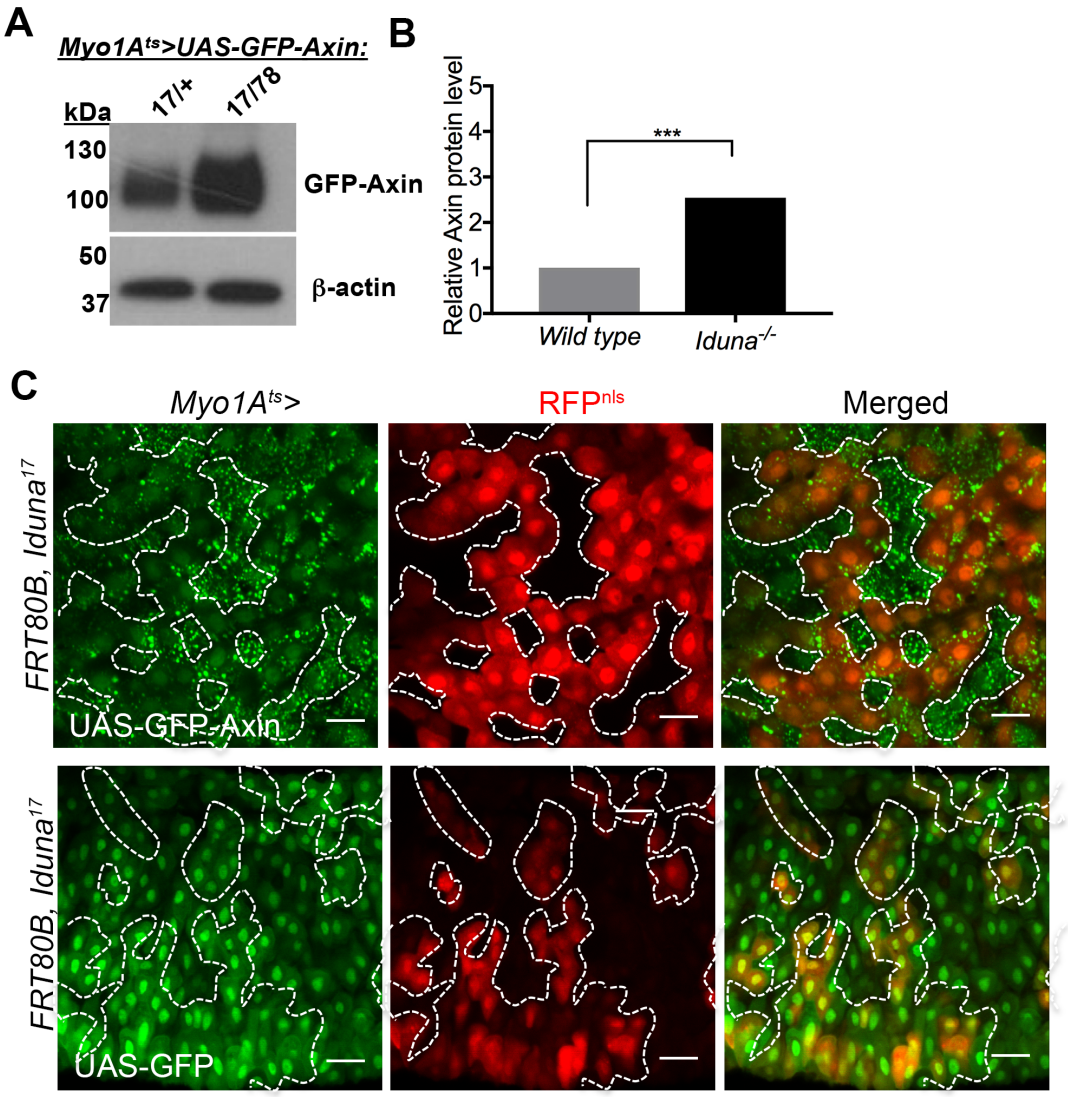
A
Myo1A^ts>UAS-GFP-Axin:
kDa
17/+
17/78
130
100
GFP-Axin
50
37
β-actin
B
Relative Axin protein level
***
Wild type
Iduna-/-
C
Myo1A^ts>
RFPnls
Merged
FRT80B, Iduna17
UAS-GFP-Axin
FRT80B, Iduna17
UAS-GFP

To test whether the increased number of ISCs was dependent on nutrient deprivation, I examined midguts of 7-day-old female mutants and controls on regular diet. I saw again an approximately twofold increase in the numbers of both *esg*>GFP positive (Fig 2.8E-F) and $Arm^{+}/Pros^{-}$ stained (Fig 2.8G-H) stem cells-progenitors under these conditions. Therefore, increased ISC numbers in *Iduna* mutants are independent of diet.

To exclude the possibility that *Iduna* mutant flies raised on regular diet had reduced nutrient uptake, I monitored fly feeding by an acid blue 9 colorimetric assay (Mattila et al., 2018). I noticed no decrease in food intake in *Iduna* mutants kept on regular diet at 24-25^{0}C compared to controls (Fig 2.8D). These results show that *Iduna* inactivation promotes the numbers of midgut stem cells independent of diet and food intake. Finally, I analyzed the midgut cell composition in *Iduna* mutant and control flies. I observed a slight increase in the total midgut cell number of *Iduna* mutants (Fig 2.9A). However, there were no significant differences in the number of EC and EE cells (Fig 2.9B-C). Therefore, Iduna is not required for differentiation of ISCs (Fig 2.9D-E). Collectively, these observations indicate that *Iduna* inactivation selectively affects ISC numbers.

Figure 2.7

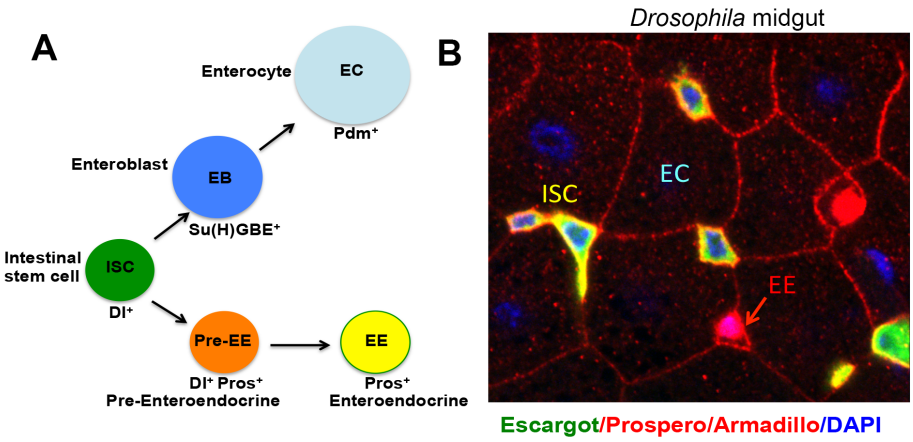

Figure 2.7 Intestinal stem cells in the *Drosophila* midgut give rise to ECs and EE cells. A- ISCs give rise to two different types of daughter progenitors, undifferentiated EBs and Pre-EEs. EBs and pre-EEs differentiate into ECs and EEs cells, respectively. **B-** ISCs and ECs can be distinguished by their cell sizes, high level of membrane-associated Armadillo, and lack of nuclear Prospero. On the other hand, differentiated EEs are small and can be identified by nuclear Prospero staining. Finally, small-sized ISCs are stained with Armadillo but not with nuclear Prospero. In the image, small ISCs were co-stained with escargot (green), and Armadillo (red). Small EEs were shown with the red arrow and stained with Armadillo (red) and nuclear Prospero (red). Bigger cells are enterocytes whose cell membrane is stained with Armadillo (red). DAPI staining in blue marks the cell nucleus.

Figure 2.8 *Iduna* mutants have increased numbers of intestinal stem and progenitor cells in their midgut. **A-** Upon nutrient deprivation, there is an approximately twofold increase in the numbers of *esg>GFP* expressing stem cells/progenitors in the midgut of *Iduna* mutants compared to controls. **B-** Quantification of *esg>GFP* positive stem cells and progenitors from adult flies of indicated genotypes. n=6 from each genotype. **C-** *Iduna* inactivation increases the numbers of $Arm^{+}/Pros^{-}$ ISCs upon nutrient deprivation. 9-day-old female flies, fed with 5% sucrose diet for seven days at 28^{0}C, were examined in A-B and C. **D-** There is no decrease in food intake in *Iduna* mutant when flies kept under the regular diet. Quantification of adult fly nutrient uptake by a calorimetric assay from regular dietary condition in *Iduna* mutants and Oregon R. **E-** Under normal diet, inactivation of *Iduna* also promotes the proliferation of the *esg-GFP*-labeled intestinal stem and progenitor cells in the *Drosophila* midgut. **F-** Quantification of *esg>GFP*$^{+}$ stem cells and progenitors from adult flies of indicated genotypes. In wild type, 25-30% of posterior midgut cells are stem cells, as assessed by *esg>GFP* expression. In contrast, 55-60% of the total cell population in *Iduna* mutants expressed the stem marker *esg>GFP*, representing a greater than 2-fold increase. **G-** *Iduna* mutants have more $Arm^{+}/Pros^{-}$ ISCs in the midgut. **H-** Quantification of $Arm^{+}/Pros^{-}$ ISCs from adult flies of indicated genotypes. The midguts of 7-day-old adult females were analyzed by confocal microscope. For the consistency, posterior midgut R5 region was analyzed in this study. $Iduna^{17/+}$ flies were used as control. n>12 from each genotype. Two-tailed Student`s *t-test* was used for statistical analyses. Error bars represented as means ± s.d. Scale bars: 10 μm. $p<0.001$ was indicated as *** and $p<0.0001$ was marked as ****.

Figure 2.8

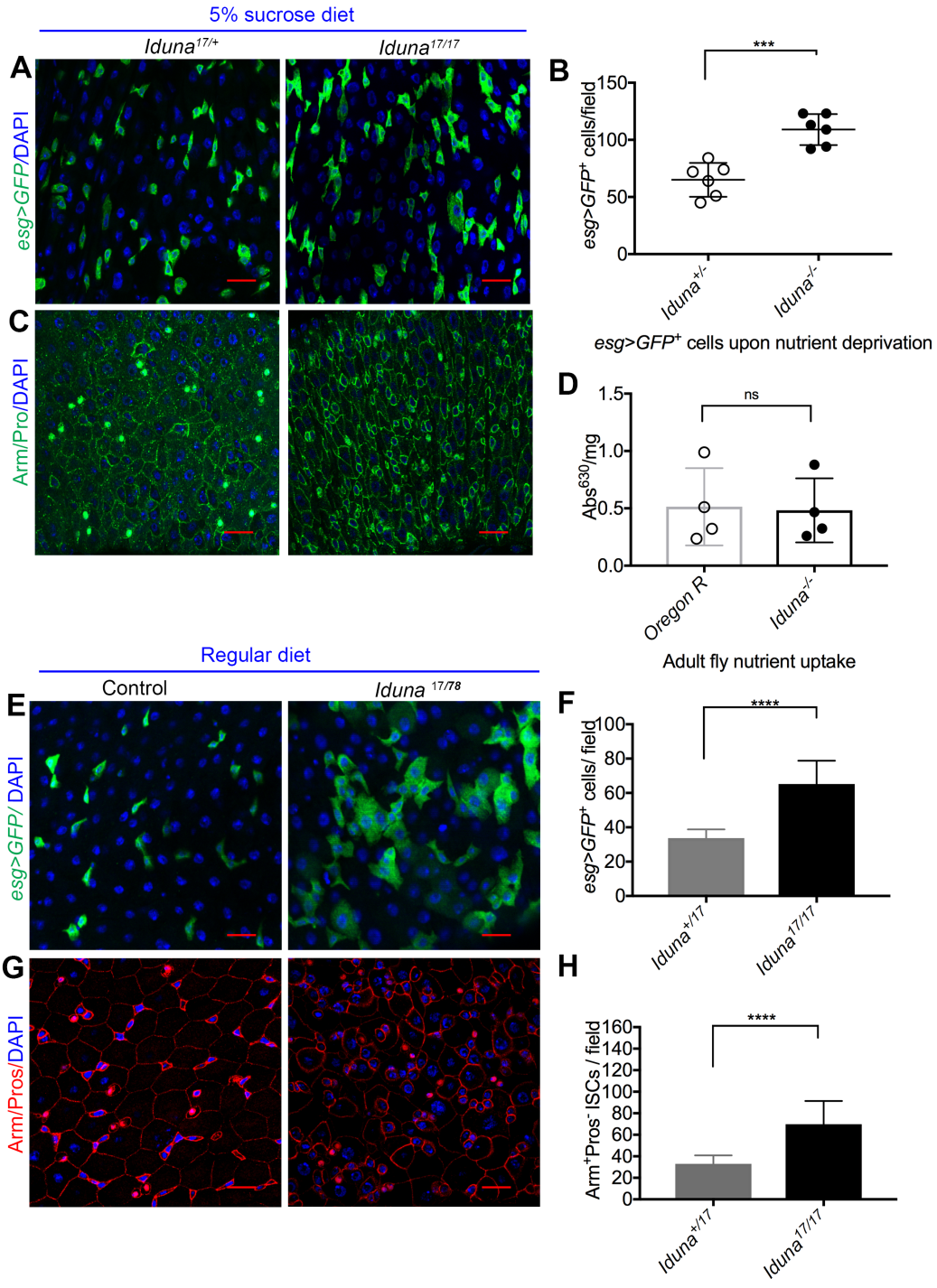
5% sucrose diet
Iduna17/+
Iduna17/17
A
esg>GFP/DAPI
B
esg>GFP+ cells/field
***
Iduna+/-
Iduna-/-
esg>GFP+ cells upon nutrient deprivation
C
Arm/Pro/DAPI
D
Abs630/mg
ns
Oregon R
Iduna-/-
Adult fly nutrient uptake
Regular diet
Control
Iduna 17/78
E
esg>GFP/ DAPI
F
esg>GFP+ cells/ field
****
Iduna+/17
Iduna17/17
G
Arm/Pros/DAPI
H
Arm+Pros- ISCs / field
****
Iduna+/17
Iduna17/17

Figure 2.9 Iduna is not required for differentiation of ISC. A- There were more cells in the midgut of *Iduna* mutants. **B- C-** No differences in the numbers of ECs and EEs were observed in *Iduna* mutants. **D-** Iduna is not required for the differentiation of ISCs into ECs. ECs were marked with GFP expressed under the control of EC specific driver, *Myo1A-Gal4*. Control cells are shown with nuclear RFP, and *Iduna* mutant clones are marked with a white line. **E-** Genetic depletion of *Iduna* did not affect the differentiation of ISCs into EEs. Mutant clones in 7-day-old adult midguts were analyzed. Small nuclear Prospero-positive EEs are labeled with yellow arrows in *Iduna* mutant clones. Control cells are labeled with nuclear RFP, and mutant clones are marked with a white line. Two-tailed Student`s *t-test* was used for statistical analyses. Error bars represented as means ± s.d. Scale bars: 10μm

Figure 2.9

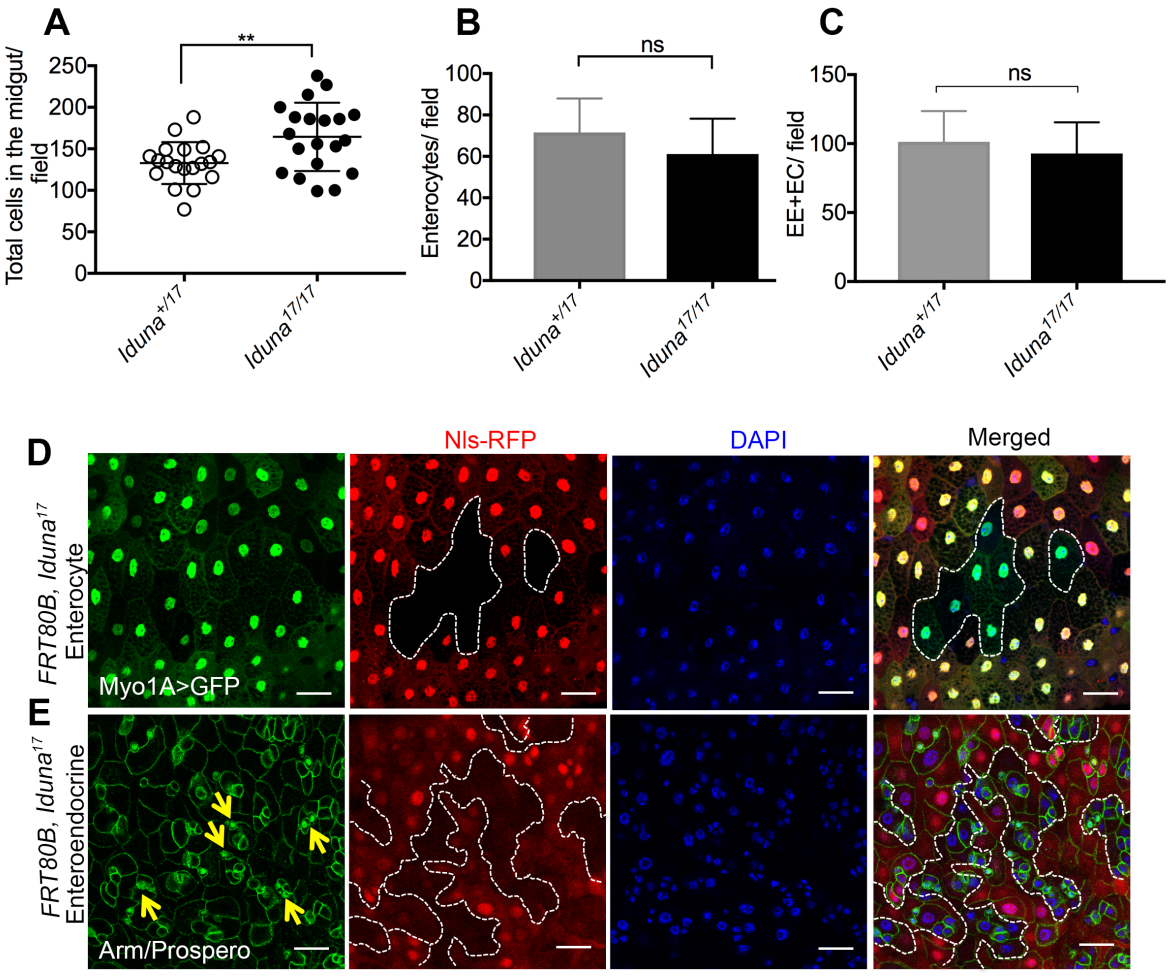
A
B
C
**
ns
ns
Total cells in the midgut/ field
Enterocytes/ field
EE+EC/ field
250
200
150
100
50
0
100
80
60
40
20
0
150
100
50
0
Iduna+/17
Iduna17/17
D
E
NIs-RFP
DAPI
Merged
FRT80B, Iduna17 Enterocyte
Myo1A>GFP
FRT80B, Iduna17 Enteroendocrine
Arm/Prospero

The observed increase in stem cell numbers could be the result of aberrant stem cell proliferation or inhibition of their differentiation. To distinguish between these possibilities, I first assessed cell proliferation by dissecting 7-day-old mutant and wild type females. Following an hour EdU-labeling of the dissected midguts, I observed that *Iduna* mutants had more EdU-positive cells (Fig 2.10A-C). Moreover, phospho-Ser-Histone H3 (pH3) immunostaining (Fig 2.10D-E) also revealed a significant increase in $pH3^{+}$ mitotic cells in the midgut of 7-day-old female *Iduna* mutants (Fig 2.10D-F). These findings suggest that stem cells undergo increased proliferation in the midgut of *Iduna* mutants. To address whether there was an inhibition of differentiation in *Iduna* mutants, I generated *FRT80B, Iduna* mutant clones (Theodosiou and Xu, 1998). I found that ECs and EEs were present in the 5-day-old female mutant clones, demonstrating that Iduna was not essential for differentiation of ISCs into daughter cells (Fig 2.9D-E).

2.3.3 Regulation of Axin proteolysis by Iduna is necessary for normal ISC proliferation

One possible mechanism by which Iduna may control the proliferation of ISCs in the *Drosophila* midgut is through modulating the concentration of Axin. To determine whether a reduction of the elevated Axin levels could reduce ISC numbers in *Iduna* mutants, they were recombined with *Axin* mutants and then back-crossed with *Iduna* mutants to generate flies that were homozygous mutant for $Iduna^{-/-}$ and heterozygous for $Axin^{+/-}$. Strikingly, a reduction of the *Axin* gene dosage by 50% restored ISC numbers to wild type levels in *Iduna* mutants (Fig 2.11A). Compared to 7-day-old female controls, *Iduna* mutants had an approximately twofold increase in the number of $Arm^{+}/Pros^{-}$ as well as $pH3^{+}$ mitotic stem cells (Fig 2.11B-C).

Figure 2.10 *Iduna* inactivation enhances proliferation of intestinal stem cells. A-B- Genetic depletion of *Iduna* leads to over-proliferation of intestinal stem cells in the midgut. EdU was used as a proliferation marker in 7-day-old mutant or wild type female flies. Following fixation, EdU incorporation was analyzed by confocal microscope. **C-** Increased numbers of EdU^+ stem cells were seen in *Iduna* mutants, indicating increased cell proliferation. Posterior midguts were analyzed for quantification. **D-E-** *Iduna* mutants display elevated phospho-Ser-Histone 3 (pH3)-positive ISCs**. F-** Iduna inactivation leads to an increase of $pH3^+$ mitotic stem cells in the midgut. Quantification of $pH3^+$ proliferating cells was done in the whole midgut. 7-day-old mutant or wild type female flies were examined. Flies were fed with regular diet at 24-25^{o}C. n>12 from each genotype. Two-tailed Student`s *t-test* was used for statistical analyses. Error bars represented as means ± s.d. Scale bars: 10μm. $p<0.0001$ was marked as ****.

Figure 2.10

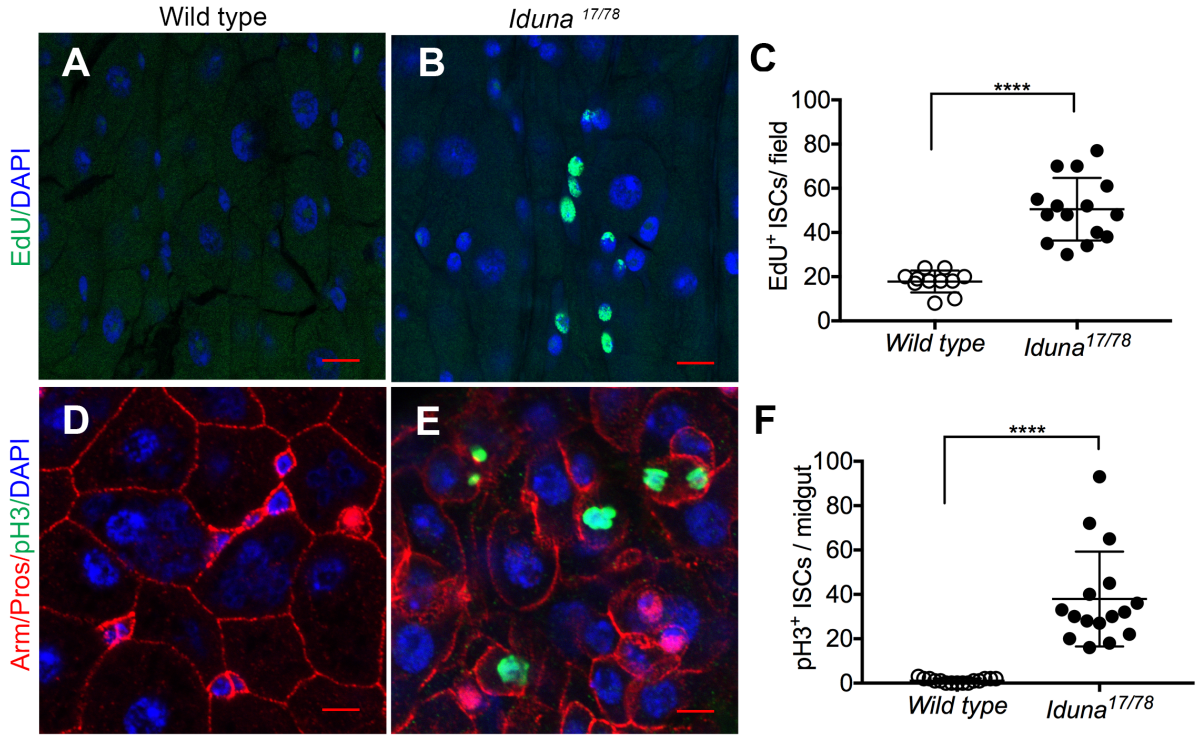
Wild type
Iduna 17/78
A
B
C
EdU/DAPI
EdU+ ISCs/ field
****
100
80
60
40
20
0
Wild type
Iduna17/78
D
E
F
Arm/Pros/pH3/DAPI
pH3+ ISCs / midgut
****
100
80
60
40
20
0
Wild type
Iduna17/78

On the other hand, reducing the *Axin* gene dosage by 50% in an *Iduna*-null background yielded numbers of ISCs and the $pH3^+$ stem cells comparable to 7-day-old wild type females. These results suggest that small changes in the levels of Axin have profound effects on stem cell number, and that regulation of Axin degradation by Iduna is necessary for normal ISC proliferation.

I observed that *Iduna* mutants had 2-fold more Axin in the *Drosophila* midgut. This indicates that defects in Axin degradation might cause over-proliferation of stem cells due to inhibition of Wingless signaling. Therefore, I analyzed a reporter for the Wingless pathway target gene, *frizzled-3* (*fz3*). It was previously reported that *fz3-RFP* reporter activity is high at the major boundaries between compartments (Buchon et al., 2013; Tian et al., 2016; Wang et al., 2016 a, b). *fz3-RFP* was strongly expressed in enterocytes at three distinct sites of the midgut: around R1a, R2c, and R5 (Buchon et al., 2013). Therefore, enterocytes are the primary sites of the Wingless pathway activation during intestinal homeostasis (Tian et al., 2016). I analyzed 3-day-old *fz3-Gal4>GFP* females and consistently observed that *fz3>GFP* was expressed in gradients in the foregut, posterior midgut, as well as the border between the posterior midgut and hindgut (Fig 2.11D). Here, I focused on the posterior midgut-hindgut border to investigate the effect of Iduna on Wingless signaling. Upon *fz3-Gal4* driven RNAi-mediated *Iduna* depletion, I found that *fz3>GFP* activity decreased significantly (Fig 2.11E). I concluded that Iduna stimulates Wingless activity in the posterior midgut by promoting degradation of Axin.

The proliferation of stem cells in the *Drosophila* midgut is regulated by intrinsic signals and also interactions with neighboring cells (Zhou et al., 2013; Tian et al., 2016).

Figure 2.11 A 50% reduction of *Axin* restores ISC numbers in the *Drosophila* midgut. A- Reducing the *Axin* gene dosage by half restores the number of $Arm^{+}/Pros^{-}$ ISCs. *AxinS044230* is a complete *Axin*-null mutant, and *AxinE77* is a loss-of-function truncation allele (Q406X). Midguts of 7-day-old adult females of the indicated genotypes were dissected and analyzed by confocal microscope following Armadillo, Prospero and DAPI staining. $Axin^{+/-}$, $Iduna^{17/+}$ served as control. Reducing the Axin gene dosage by 50% in $Iduna^{17/17}$ mutants decreased the number of ISCs to normal levels. **B-** Quantification of ISC numbers. Reducing the *Axin* gene dosage by half fully suppressed the increased numbers of $Arm^{+}/Pros^{-}$ ISCs in $Iduna^{17/17}$ null-mutants. **C-** Reducing *Axin* gene expression suppressed the proliferation of ISCs in the $Iduna^{17/17}$ null-mutant. $p<0.0001$ was marked as ****. **D-** *frizzled 3 (fz3)* is a Wingless target gene and a GFP-reporter construct was used here to visualize Wg-activity in the midgut (Buchon et al., 2013; Tian et al., 2016; Wang et al., 2016 a, b). In wild type, *fz3>GFP* is highly expressed in a graded fashion in the foregut (f), the posterior midgut (p) as well as the posterior midgut-hindgut border, but not in the anterior midgut (a) or the hindgut proper (h). Right-hand image is a higher magnification image of the *fz3>GFP* near the midgut-hindgut boundary (Scale bar: 20μm). 7-day-old female midguts were analyzed. **E-** *fz3-Gal4* driven *Iduna* depletion inhibits Wingless activity. RNAi-mediated down-regulation of *Iduna* led to significant reduction of *fz3>GFP*; *white*-RNAi served as a control. The arrow indicates the border between the posterior midgut and the hindgut (b). 3-day-old female midguts were analyzed. Flies were fed with regular diet at 24-25^{0}C. One-way ANOVA was used for statistical analyses. Error bars represented as means ± s.d. Scale bars: 10μm.

Figure 2.11

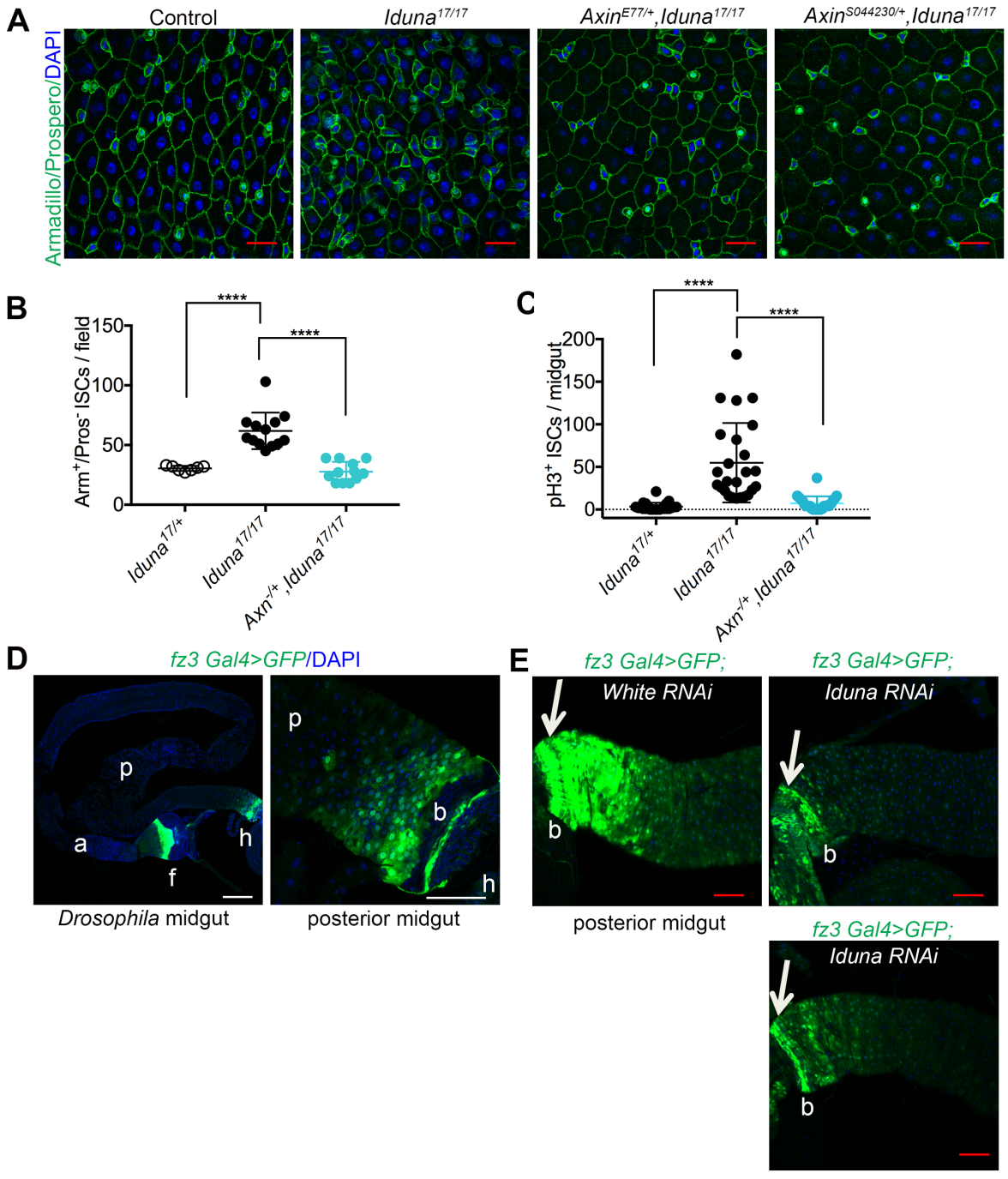
A
Control
Iduna17/17
AxinE77/+,Iduna17/17
AxinS044230/+,Iduna17/17
Armadillo/Prospero/DAPI
B
Arm+/Pros- ISCs / field
150
100
50
0
****
****
Iduna17/+
Iduna17/17
Axn-/+,Iduna17/17
C
pH3+ ISCs / midgut
200
150
100
50
0
****
****
Iduna17/+
Iduna17/17
Axn-/+,Iduna17/17
D
fz3 Gal4>GFP/DAPI
p
a
h
f
p
b
h
Drosophila midgut
posterior midgut
E
fz3 Gal4>GFP;
White RNAi
fz3 Gal4>GFP;
Iduna RNAi
b
b
posterior midgut
fz3 Gal4>GFP;
Iduna RNAi
b

Figure 2.12 *Iduna* depletion in ECs leads to over-proliferation of ISCs. A- Over-proliferation of ISCs in *Iduna* mutants is non-cell autonomous. RNAi-mediated *Iduna* knock-down was carried out in the ECs and ISCs/EBs using *Myo1A-Gal4* and *esg-Gal4* drivers, respectively. **B-** Knock-down of *Iduna* in ECs using the *Myo1A-Gal4* driver led to over-proliferation of $Arm^{+}/Pros^{-}$ ISCs. In contrast, no changes in ISC proliferation were observed upon down-regulation of *Iduna* in ISCs using *esg-Gal4*-driven *Iduna* RNAi. *Myo1A-Gal4*>GFP served as a control. **C-** EC-specific knock-down of *Iduna* increased the number of $pH3^{+}$ progenitors. **D-** Ectopic expression of *Iduna* in ECs inhibits over-proliferation of ISCs. A UAS-Myc-tagged Iduna C/G transgene was generated to perform rescue experiments. **E- F-** Expression of the UAS-Myc-Iduna C/G transgene with the *Myo1A-Gal4* driver resulted in a reduction of the numbers of $pH3^{+}$ **(E-)** and $Arm^{+}/Pros^{-}$ **(F-)** ISCs in the midgut of *Iduna* mutants. Flies were fed with regular diet at 24-25^{0}C. 7-day-old female midguts were analyzed for ISC and mitotic markers. One-way ANOVA was used for statistical analyses. $p<0.0001$ was marked as ****. Error bars represented as means ± s.d. Scale bars: 10μm.

Figure 2.12

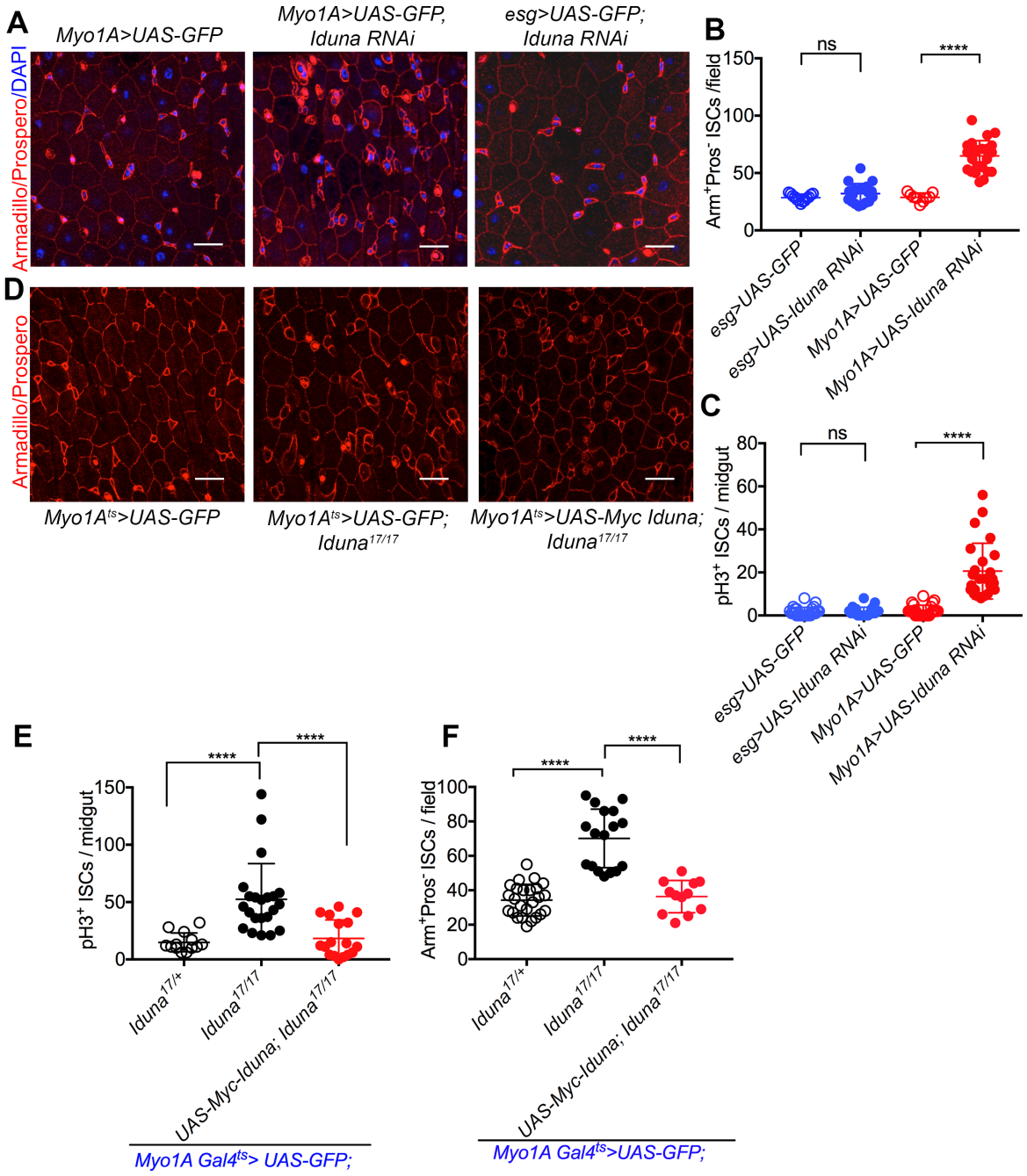
A
Myo1A>UAS-GFP
Myo1A>UAS-GFP, Iduna RNAi
esg>UAS-GFP; Iduna RNAi
Armadillo/Prospero/DAPI
B
ns
****
Arm+Pros- ISCs /field
esg>UAS-GFP
esg>UAS-Iduna RNAi
Myo1A>UAS-GFP
Myo1A>UAS-Iduna RNAi
C
ns
****
pH3+ ISCs / midgut
esg>UAS-GFP
esg>UAS-Iduna RNAi
Myo1A>UAS-GFP
Myo1A>UAS-Iduna RNAi
D
Armadillo/Prospero
Myo1Ats>UAS-GFP
Myo1Ats>UAS-GFP; Iduna17/17
Myo1Ats>UAS-Myc Iduna; Iduna17/17
E
****
****
pH3+ ISCs / midgut
Iduna17/+
Iduna17/17
UAS-Myc-Iduna; Iduna17/17
Myo1A Gal4ts> UAS-GFP;
F
****
****
Arm+Pros- ISCs / field
Iduna17/+
Iduna17/17
UAS-Myc-Iduna; Iduna17/17
Myo1A Gal4ts>UAS-GFP;

To further investigate whether the observed effects could reflect a cell-autonomous requirement of Iduna in ISCs, or alternatively a requirement in other cells of the midgut, *Iduna* was specifically targeted in ECs as well as midgut stem and progenitor cells by using the *Myo1A-Gal4* and *esg-Gal4* drivers, respectively (Fig 2.12A-B). I examined 7-day-old females expressing *Iduna*-RNAi under the *Myo1A* or *esg* drivers. RNAi-mediated knock-down of *Iduna* in ECs caused a significant increase in $Arm^{+}/Pros^{-}$ stem cell numbers (Fig 2.12B). However, stem cell/progenitor cell-specific knock-down of *Iduna* did not affect either the stem cell numbers or mitosis in the midgut (Fig 2.12B-C). This suggests that *Iduna* inactivation causes stem cell over-proliferation by a non-cell-autonomous mechanism, and that perhaps ECs are responsible for stem cell over-proliferation in *Iduna* mutants. To further test this idea, I ectopically expressed *Iduna* in ECs and investigated if this could suppress stem cell proliferation in *Iduna* mutants (Fig 2.12D). Indeed, consistent with this model, I saw that *Myo1A-Gal4* driven *UAS-Iduna* was able to restore normal numbers of stem cells and progenitors (Fig 2.12E-F). Taken together, my results indicate that Iduna plays a physiological role to regulate Wingless signaling in ECs, which is critical for proper ISC proliferation.

I found that *Iduna* mutants have increased mortality upon nutrient deprivation (Fig. 1C). Following 7 days on a 5% sucrose diet at 28^{0}C, *Iduna* mutants had more *esg>GFP* positive cells in the midgut (Fig 2.8A-C). Therefore, I considered that under reduced nutrient diet, hyper-proliferation of ISCs might be responsible for elevated mortality. To test this idea, I first inactivated *Iduna* in enterocytes by expression of three different RNAi lines under the *Myo1A* driver.

Figure 2.13 RNAi-mediated *Iduna* depletion in ECs does not cause mortality upon nutrient deprivation. A- Three different *Iduna* RNAi lines were expressed under the *Myo1A* driver. *white*-RNAi was used as a control. **B-** There was no significant change on the mean lifespan between *white* and *Iduna*-RNAi expressing flies. n=60 for each genotype. **C-** *Iduna*-RNAi in EBs also did not result in increased lethality upon 5% sucrose diet at 28^0C. n=70 for each genotype. **D-** Ectopic expression of *Iduna* under *Myo1A* driver in ECs does not rescue elevated mortality of *Iduna* mutants under reduced nutrient diet. 2-day-old mutant or wild type female flies were collected and kept on 5% sucrose diet at 28^0C for the experiments in A-D. **E-** EC-specific ectopic expression of I*duna* rescues the hyper-proliferation of midgut stem cells upon nutrient deprivation. 2-day-old females were collected at 24-25^0C and their regular diet was replaced with 5% sucrose diet at 28^0C. 9-day-old female flies were examined with α-Armadillo and Prospero antibodies. One-way ANOVA was used for statistical analyses. Error bars represented as means ± s.d. Scale bars: 10μm. For statistical analyses of sucrose diet, I used the Mantel-Cox and Gehan-Breslow-Wilcoxon tests to compare survival curves between *Iduna* mutant and control flies. Scale bars: 10μm.

Figure 2.13

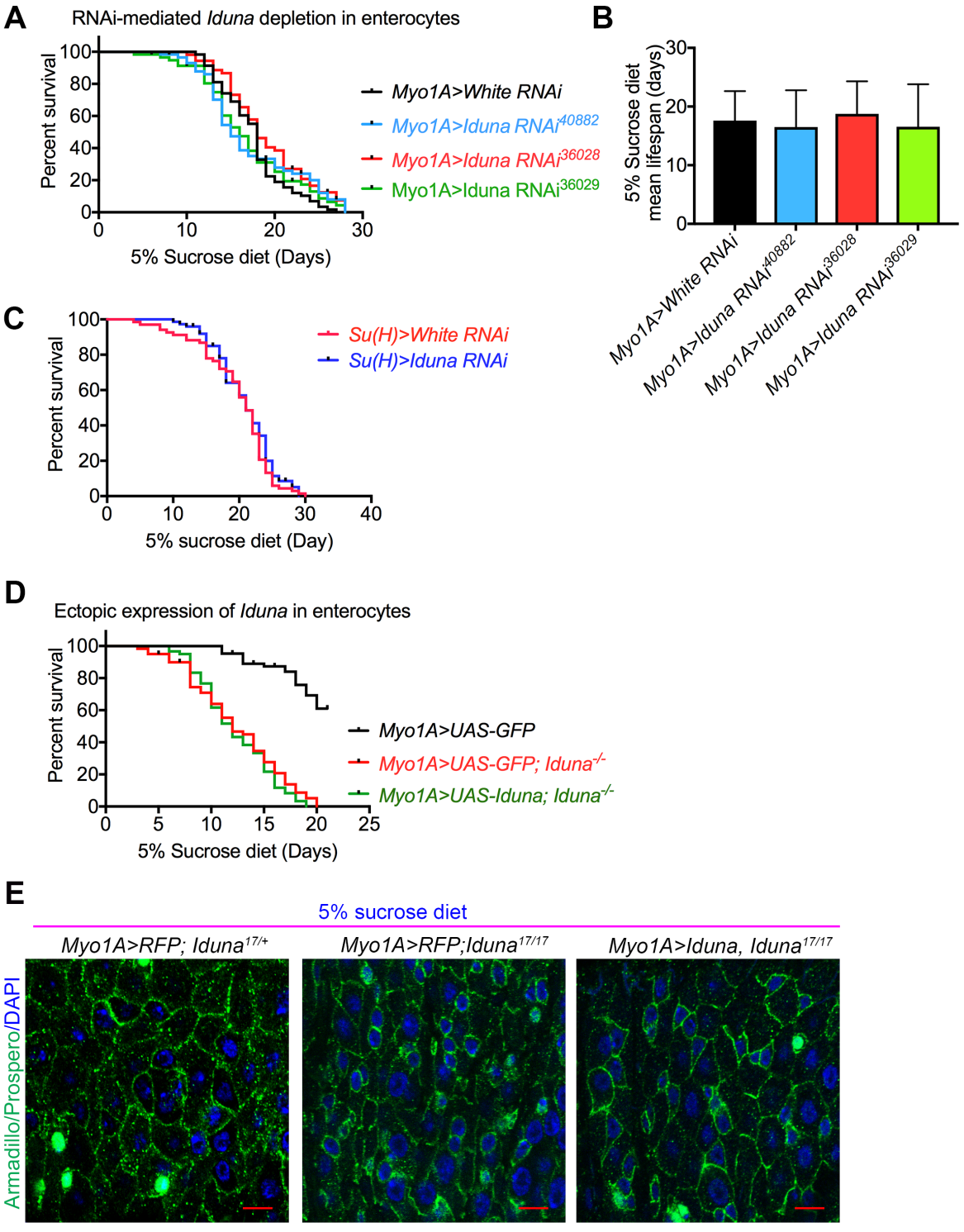
A
RNAi-mediated Iduna depletion in enterocytes
Percent survival
5% Sucrose diet (Days)
Myo1A>White RNAi
Myo1A>Iduna RNAi40882
Myo1A>Iduna RNAi36028
Myo1A>Iduna RNAi36029
B
5% Sucrose diet mean lifespan (days)
Myo1A>White RNAi
Myo1A>Iduna RNAi40882
Myo1A>Iduna RNAi36028
Myo1A>Iduna RNAi36029
C
Percent survival
5% sucrose diet (Day)
Su(H)>White RNAi
Su(H)>Iduna RNAi
D
Ectopic expression of Iduna in enterocytes
Percent survival
5% Sucrose diet (Days)
Myo1A>UAS-GFP
Myo1A>UAS-GFP; Iduna-/-
Myo1A>UAS-Iduna; Iduna-/-
E
5% sucrose diet
Myo1A>RFP; Iduna17/+
Myo1A>RFP;Iduna17/17
Myo1A>Iduna, Iduna17/17
Armadillo/Prospero/DAPI

I showed that RNAi-mediated *Iduna* depletion did not increase lethality compared with *white*-RNAi (Fig 2.13A). There was also no significant change on the mean lifespan between *white* and *Iduna*-RNAi expressing flies (Fig 2.13B). I also tested EB specific *Iduna* depletion and again found no significant effects on longevity upon nutrient deprivation (Fig 2.13C).

Finally, I expressed UAS-*Iduna* transgene *under Myo1A driver* in ECs to rescue the elevated mortality in the mutants. Whereas the *Iduna* transgene rescued the hyper-proliferation phenotype (Fig 2.13E), it failed to rescue the mortality of mutants on 5% sucrose diet (Fig 2.13D). These findings suggest that Iduna mortality is not caused by dysregulation of midgut stem cell proliferation and point to another role of Iduna in promoting survival under stress conditions.

The fly midgut provides essential physiological functions of the living organism including food digestion and nutrient absorption. It is also a key organ for lipid uptake and distribution. Under normal feeding conditions, lipids digested from dietary food are absorbed by ECs, resynthesized into triglyceride (TG), and packaged into lipoprotein particles that are transported to peripheral tissues for energy supply or storage in a specialized tissue, known as the fat body (Song et al., 2014). Upon starvation, flies consume their lipid storages. Since *Iduna* mutants displayed increased mortality on the reduced nutrient diet, I examined adult fat bodies to test if there might be a lipid deposition defect in *Iduna* mutants. 7-day-old adult females were starved for 12h and 24h. Stored lipids were visualized in the abdominal fat bodies of starved flies by Nile Red staining. Remarkably, stored lipid levels in abdominal fat body cells were visibly reduced upon starvation in *Iduna* mutants (Fig 2.14). I found that *Iduna* mutants constantly lost their fat storages during 24h starvation. Although wild type flies also reduced their fat bodies in 12h, they

sustained their fat reservoirs in 24h (Fig 2.14). My results suggest that Iduna may also have essential role(s) in energy metabolism.

2.3.4 Depletion of *Iduna* promotes stem cell proliferation through the JAK-STAT pathway

In order to further investigate the mechanism by which Iduna affected ISC proliferation, I explored the function of additional signaling pathways implicated in this system. Because the JAK-STAT pathway has a well-known role in stem cell proliferation, I looked for possible effects of *Iduna* mutants here (Zeidler et al., 2000; Zoranovic et al., 2013; Zhou et al., 2013; Markstein et al., 2014). I analyzed the JAK-STAT pathway via a 10xStat-GFP reporter in the midgut (Bach et al., 2007). Under regular physiological conditions, Stat-GFP reporter expression was mainly seen in small sized cell populations in the midgut that appear to represent ISCs for several reasons (Fig 2.15). First, Prospero-positive EEs were negative for Stat-GFP (Fig 2.15A). Second, ECs stained with Armadillo were also not expressing the Stat-GFP reporter. Finally, Delta-lacZ positive but Prospero-negative cells for the most part expressed Stat-GFP. However, a minor population of small sized cells was GFP positive but Delta-lacZ negative (white arrows, Fig 2.15B). These cells appeared to be undifferentiated progenitors, such as EBs. 7-day-old *Iduna* mutants had more Stat-GFP positive cells when compared to controls (Fig 2.15A-F, Fig 2.17A-B). I also generated *FRT80B, Iduna* midgut mutant clones and observed that these clones had elevated JAK-STAT signaling (Fig 2.16A-B).

Figure 2.14

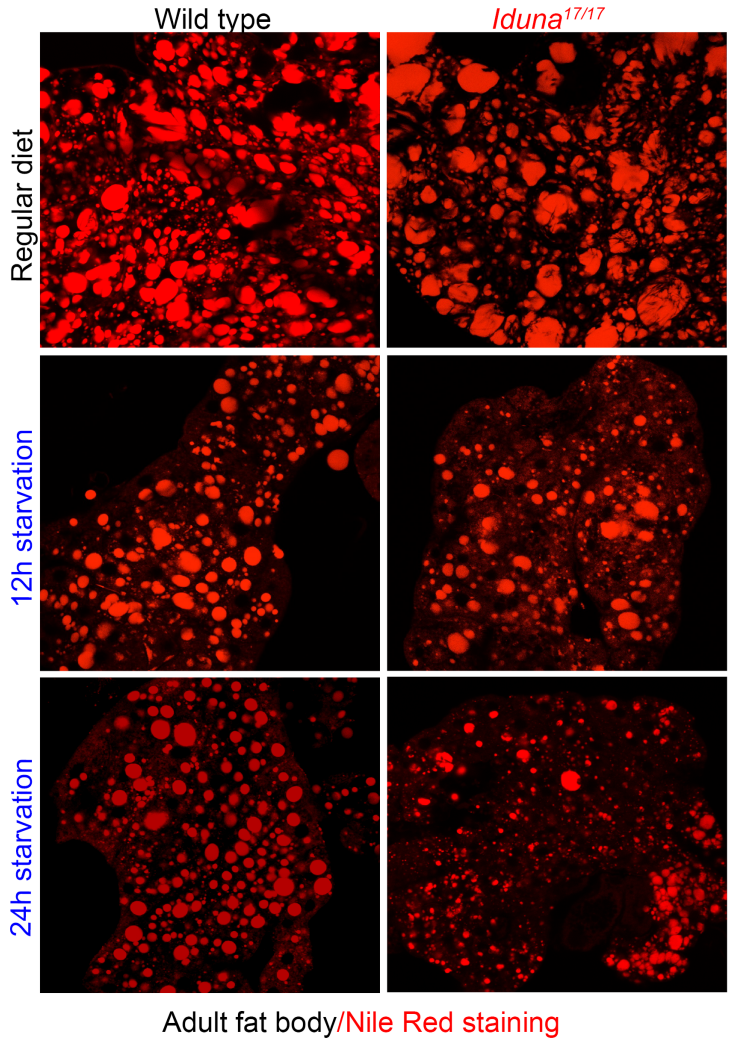

Figure 2.14 *Iduna* inactivation promotes fat body wasting upon starvation. 7-day-old adult females were starved for 12h and 24h. Abdominal fat bodies were dissected and stained with Nile Red. Compared to control flies, *Iduna* mutants had severe fat lost during starvation. Oregon R was used as wild type flies.

To confirm elevated JAK-STAT signaling in *Iduna* mutant stem cells, I stained midguts from 7-day-old females for Delta, a previously identified target gene of the JAK-STAT pathway (Jiang et al., 2009). I found that there was indeed more Delta protein in *Iduna* mutants, consistent with elevated JAK-STAT activity (Fig 2.16F).

To test whether activation of JAK-STAT signaling was responsible for aberrant ISC proliferation, I knocked down *Stat92E*, a transcription factor in the JAK-STAT pathway, in ECs as well as in ISCs and EBs. I did not detect dramatic changes in the numbers of mitotic cells when *Stat92E* transcription factor was depleted in ECs (Fig 2.17C). Interestingly, knock-down of *Stat92E* in midgut stem and progenitor cells was sufficient to suppress their increased cell division (Fig 2.17C).

My observations raise the question of how ECs signal ISC proliferation. One possibility is that ECs secrete a factor that activates the JAK-STAT pathway in neighboring ISCs. The JAK-STAT pathway can be activated by cytokines, such as *unpaired* (UPD, UPD2, UPD3) in the *Drosophila* midgut (Ghiglione et al., 2002; Zhou et al., 2013). Since UPD3 is produced in differentiated ECs and in differentiating EBs, I explored the possibility that UPD cytokines could mediate ISC over-proliferation in *Iduna* mutants. For this purpose, I first inactivated *Iduna* with the *upd3-Gal4* driver and found that RNAi-mediated knock-down of *Iduna* resulted in a significant increase of *upd3>GFP* reporter expression in the midgut (Fig 2.17E, Fig 2.18A). *upd3>GFP*-positive cells were mainly ECs, and not EEs or ISCs (Fig 2.17E, Fig 2.18B-C). I then knocked down *Iduna* in ECs and performed a q-PCR to test whether *Iduna* depletion in ECs induced unpaired expression. I detected that EC-specific *Iduna* inactivation resulted in elevated *upd3* gene expression compared to *white*-RNAi (Fig 2.17D). To suppress the over-proliferation of ISC in *Iduna* mutants, I finally reduced *upd2* and *upd3* gene dosages. Strikingly, I found that

heterozygosity in Δ*upd2-upd3* fully suppressed ISC proliferation in *Iduna* mutants (Fig. 2.17F). Secreted UPD proteins bind to the Domeless receptor on ISCs (Ghiglione et al., 2002). Therefore, I tested whether decreasing Domeless levels could also suppress stem cell over-proliferation in *Iduna* mutants. Again, this prediction was experimentally confirmed (Fig 2.17F).

Collectively, these observations suggest that *Iduna* inactivation causes a decrease in Wingless signaling in ECs which in turn causes elevated JAK-STAT signaling in ISCs, thereby, resulting in their over-proliferation. I concluded that inactivation of *Iduna* causes decrease in Wingless signaling in ECs, which in turn leads to increased secretion of UPD2-3 from these cells to stimulate over-proliferation of ISCs through the JAK-STAT pathway (Fig 2.17G).

Figure 2.15 Under regular physiological conditions, the Stat-GFP reporter is mainly expressed in midgut stem cells and EBs. A- A 10xStat-GFP reporter was mainly positive in small sized- cells but Prospero-stained EEs were negative for Stat-GFP in the midguts. **B-** Delta-lacZ positive but Prospero negative cells were mainly positive for Stat-GFP expression. A small population of cells (white arrow) were small-sized and GFP positive but Delta-lacZ negative. Those could be undifferentiated progenitors like EBs. **C-** $Arm^{+}/Pros^{-}$ small-sized stem and progenitor cells have Stat-GFP reporter activity. 5-day-old female flies were dissected and stained with α-Armadillo and α-Prospero antibodies. Scale bars: 10μm.

Figure 2.15

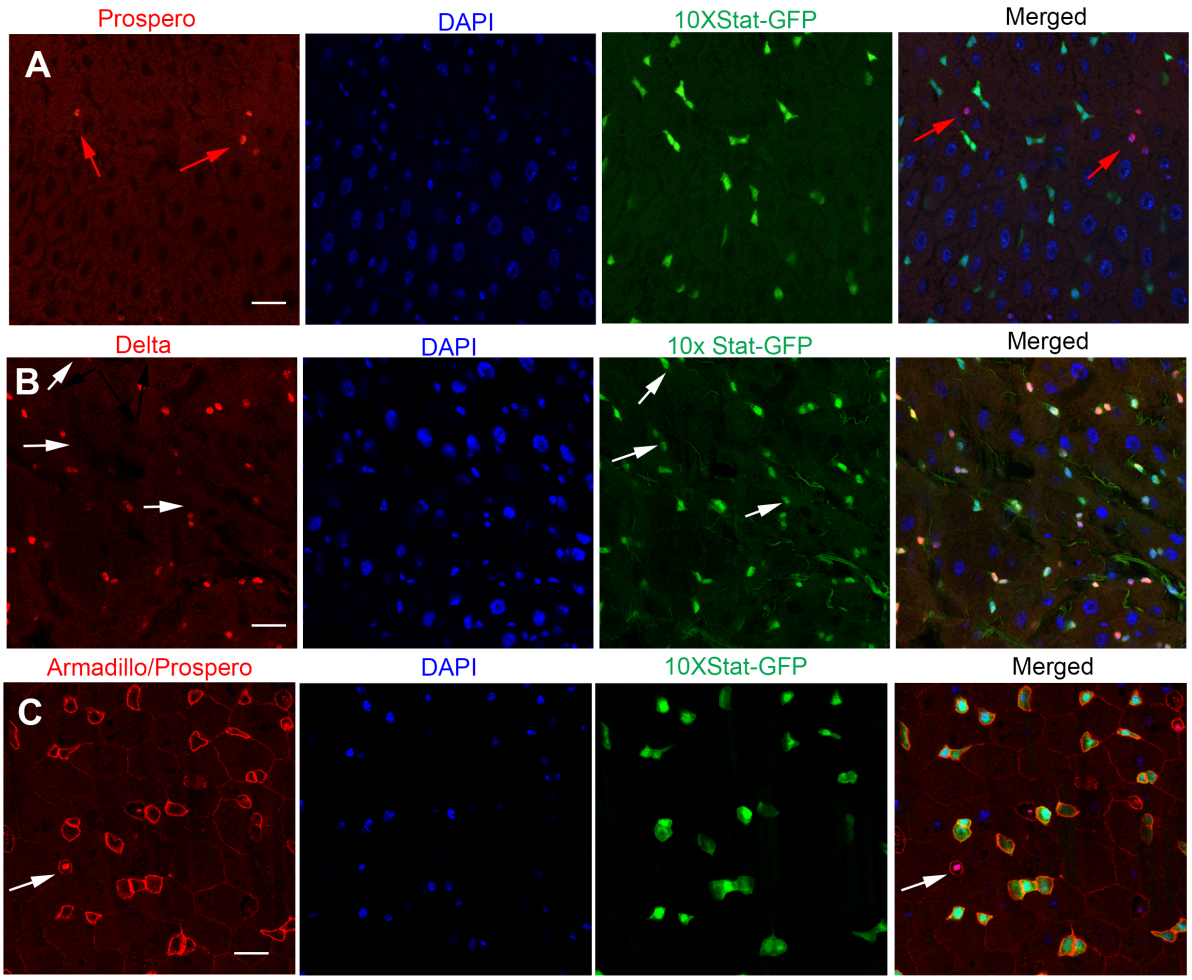
Prospero
DAPI
10XStat-GFP
Merged
A
Delta
DAPI
10x Stat-GFP
Merged
B
Armadillo/Prospero
DAPI
10XStat-GFP
Merged
C

Figure 2.16 *Iduna* mutants have increased numbers of Stat-GFP positive cells. A- *Iduna* mutant clones had elevated Stat-GFP signaling in ISCs. 10xStat-GFP is a reporter for STAT signaling activity. *Iduna* mutant clones displayed strongly increased staining of this reporter. Posterior midguts of 7-day-old females were analyzed. **B-** The quantification of Stat-GFP reporter expression in *Iduna* mutant clones. GFP intensity was measured with Image J and normalized with control cells. *Iduna* mutant clones showed 4-5-fold higher reporter expression. **C- E-** *Iduna* mutants have more Stat-GFP positive ISCs and progenitors in midguts. Posterior midguts of 7-day-old females were analyzed. n>6 for each genotype. $p<0.0001$ is indicated as ****. **F-** Delta protein is elevated in the midguts of *Iduna* mutants. Posterior midguts of 7-day-old females were stained for Delta. Flies were collected and kept on regular diet at 24-25^{0}C. Two-tailed Student`s *t-test* was used for statistical analyses. Error bars represented as means ± s.d. Scale bars: 10μm

Figure 2.16

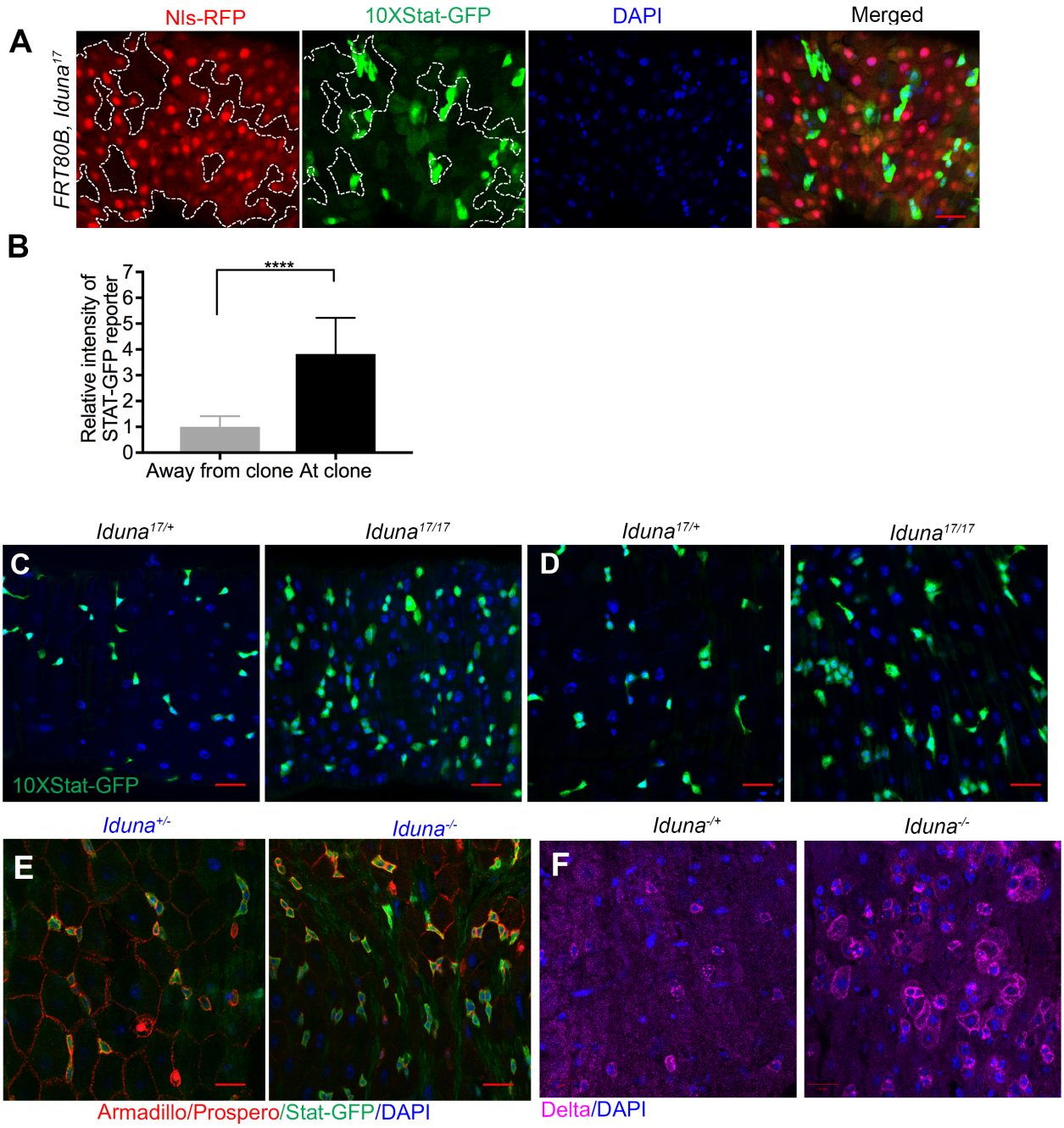
A
Nls-RFP
10XStat-GFP
DAPI
Merged
FRT80B, Iduna17
B
****
Relative intensity of STAT-GFP reporter
0
1
2
3
4
5
6
7
Away from clone
At clone
Iduna17/+
Iduna17/17
C
10XStat-GFP
D
Iduna17/+
Iduna17/17
Iduna+/-
Iduna-/-
E
Armadillo/Prospero/Stat-GFP/DAPI
Iduna-/+
Iduna-/-
F
Delta/DAPI

Figure 2.17 Loss of *Iduna* activates the JAK-STAT pathway non-cell autonomously to promote ISC proliferation. **A**- *Iduna* mutants have elevated Stat-GFP signaling in ISCs. *10xStat-GFP* is a reporter for STAT signaling activity. *Iduna* mutants displayed strongly increased GFP reporter. Posterior midguts of 7-day-old females were analyzed. **B-** The quantification of Stat-GFP expressing midgut cells. **C-** Knock-down of the *Stat92E* transcription factor in ISCs and EBs blocked ISC over-proliferation in *Iduna* mutants. In contrast, RNAi-mediated depletion of *Stat92E* in ECs did not affect proliferation of ISCs. 7-day-old female midguts were dissected and analyzed. **D-** *Iduna* depletion resulted in the upregulation of *upd3* mRNA expression in ECs. Myo1A driven *Iduna*-RNAi and *white*-RNAi expressing 7-day-old females were dissected for their midguts. Total RNA was isolated and cDNA libraries were prepared. *upd3* transcripts were amplified and analyzed by q-PCR. **E**- RNAi-mediated *Iduna* down-regulation induced *upd3>GFP* reporter activity. *Iduna* was knocked-down using RNAi driven by *upd3-Gal4*, and *GFP* was used as a reporter for *upd3* gene expression. ECs were stained with α-Armadillo antibody. EEs and ISCs were negative for *upd3>GFP* expression. *white*-RNAi served as a control. Posterior midguts of 3-day-old females were analyzed. **E-** Reduction of either *upd2 and upd3* or their receptor *Domeless* suppressed over-proliferation of ISCs in *Iduna* mutants. Upon reduction of *upd2* and *upd3* gene dosage in *Iduna* mutants, I observed significantly less mitotic stem cells in *Iduna* mutants, comparable to wild type levels. Likewise, a 50% reduction of *Domeless* resulted in the suppression of ISC over-proliferation in *Iduna* mutants. On the other hand, these reductions in gene dosage of *upd2, upd3* and *Domeless* did not affect mitosis of ISCs in a wild type background. 7-day-old female midguts were quantified by $pH3^+$ staining. Flies were fed with regular diet at 24-25^{0}C. n>12 from each genotype. One-way ANOVA was used for statistical analyses. Error bars represented as means ±

s.d. Scale bars: 10μm. *p<0.0001* was marked as ****. **G-** Model for the role of *Iduna* in the regulation of ISC proliferation. My model suggests that inactivation of *Iduna* causes Axin elevation which in turn decreases Wingless signaling activation in ECs and increases secretion of UPD cytokines from these cells. These cytokines activate JAK-STAT signaling through the Domeless receptor on neighboring ISCs and thereby induce ISC proliferation in the *Drosophila* midgut.

Figure 2.17

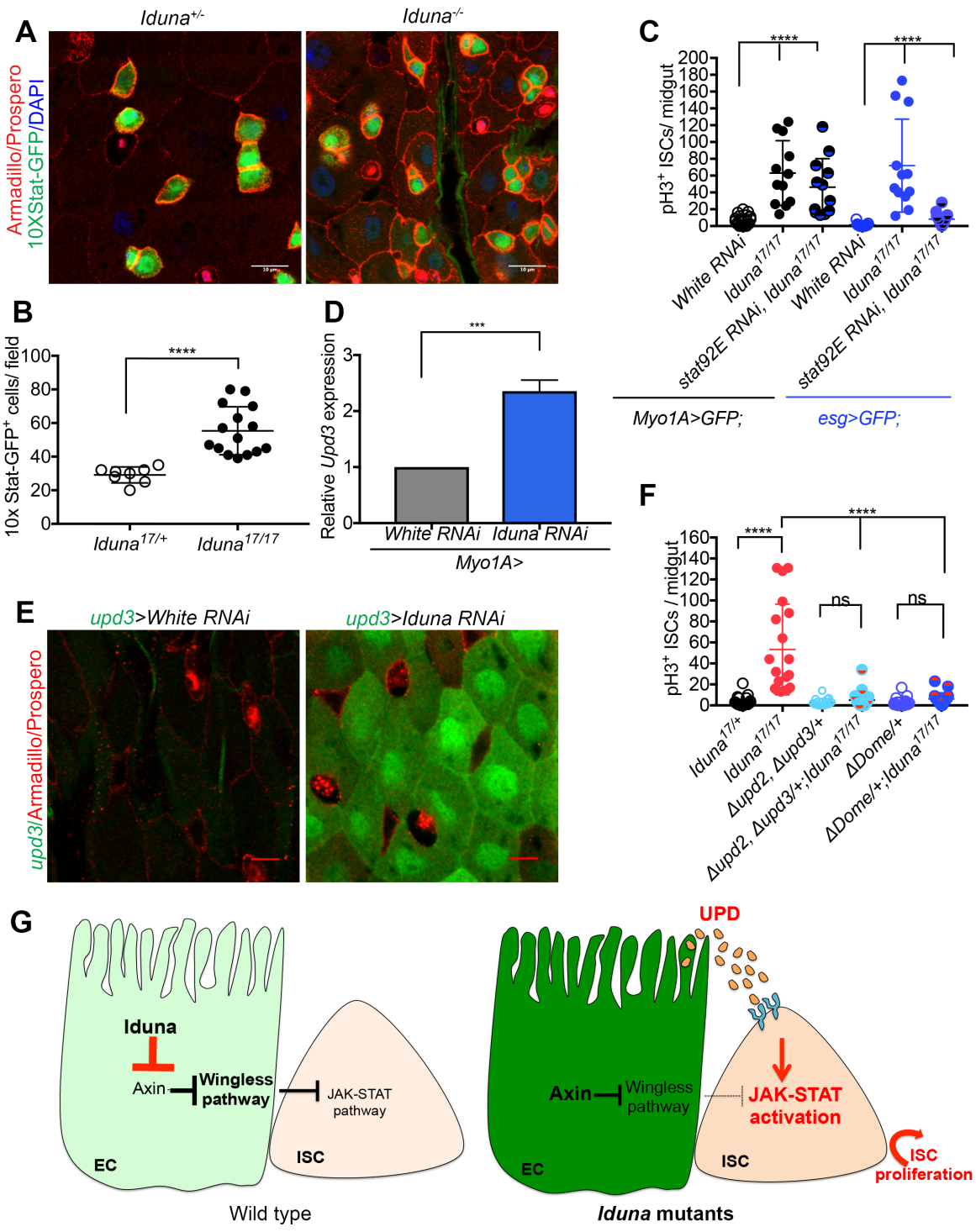
A
Iduna+/-
Iduna-/-
Armadillo/Prospero
10XStat-GFP/DAPI
B
10x Stat-GFP+ cells/ field
****
Iduna17/+
Iduna17/17
C
pH3+ ISCs/ midgut
****
****
White RNAi
Iduna17/17
stat92E RNAi, Iduna17/17
Myo1A>GFP;
esg>GFP;
D
Relative Upd3 expression
***
White RNAi
Iduna RNAi
Myo1A>
E
upd3>White RNAi
upd3>Iduna RNAi
upd3/Armadillo/Prospero
F
pH3+ ISCs / midgut
****
****
ns
ns
Iduna17/+
Iduna17/17
Δupd2, Δupd3/+
Δupd2, Δupd3/+;Iduna17/17
ΔDome/+
ΔDome/+;Iduna17/17
G
Iduna
Axin
Wingless pathway
JAK-STAT pathway
EC
ISC
Wild type
UPD
Axin
Wingless pathway
JAK-STAT activation
EC
ISC
ISC proliferation
Iduna mutants

Figure 2.18 RNAi-mediated *Iduna* depletion increases *upd3>GFP* reporter activity. A- Knock-down of *Iduna* results in upregulation of *upd3*. *Iduna* was down-regulated by two different UAS-RNAi lines (#36029 and #40882) under *upd3-Gal4 driver*. *upd3>GFP* was used as a reporter for *upd3* gene expression. *white*-RNAi served as control. **B- C-** *upd3 was* upregulated in the ECs. Dissected midguts were stained with α-Armadillo and α-Prospero antibodies. ECs expressed *upd3>GFP* but EEs and ISCs did not. Posterior midguts of 3-day-old females were analyzed. Scale bars: 10μm.

Figure 2.18

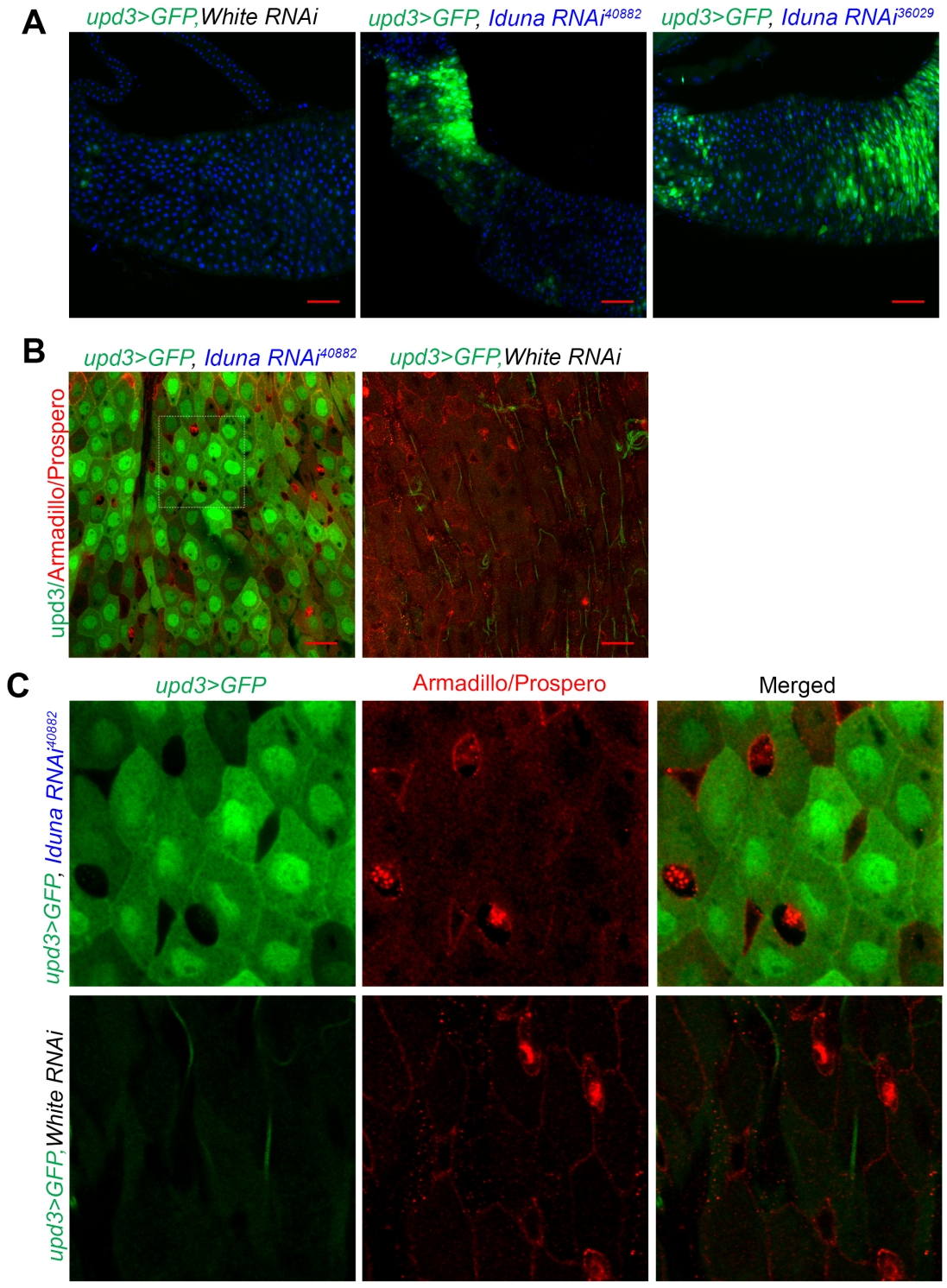
A
upd3>GFP,White RNAi
upd3>GFP, Iduna RNAi40882
upd3>GFP, Iduna RNAi36029
B
upd3>GFP, Iduna RNAi40882
upd3>GFP,White RNAi
upd3/Armadillo/Prospero
C
upd3>GFP
Armadillo/Prospero
Merged
upd3>GFP, Iduna RNAi40882
upd3>GFP,White RNAi

2.4 Material and Methods

Fly stocks: Flies were kept at a 12-hour light/dark cycle. All crosses were performed at 22-25°C unless stated otherwise. The following fly stocks were used for this study (Bloomington Drosophila Stock Center (BDSC) and Vienna Drosophila Resource Center (VDRC) number (#) given in parentheses):

The stocks used in here: Df(3L)Exel6135 (BDSC# 7614), Df(3L)ED228 (BDSC# 8086), Df(3L)ED229 (BDSC# 8087), esg-Gal4, UAS-GFP (a gift of Dr. Norbert Perrimon; Micchelli and Perrimon, 2006), esgK606 (a gift of Dr. Norbert Perrimon; Micchelli and Perrimon, 2006), *10xStat-GFP*, Bach et al., 2007), UAS-GFP-Axin (BDSC# 7224), FRT82B, *Axin044230* (a gift of Dr. Wei Du; Hamada et al., 1999), FRT82B, *AxinE77* (a gift of Dr. Jessica Treisman; Collins and Treisman, 2000), Myo1A-Gal4, tub-Gal80ts, UAS-GFP (a gift of Dr. Norbert Perrimon; Micchelli and Perrimon, 2006), upd3-Gal4, UAS-GFP (a gift of Dr. Norbert Perrimon; Markstein et al., 2014), *Δupd2/3* (BDSC# 129), *ΔDome* (BDSC# 12030), UAS-*Stat92E* RNAi (BDSC# 26889), UAS-CG8786/*dIduna* RNAi#1 (BDSC# 40882), UAS-CG8786/*dIduna* RNAi#2 (VDRC#43533), UAS-CG8786/*dIduna* RNAi#3 (VDRC#36028), UAS-CG8786/*dIduna* RNAi#4 (VDRC#36029), and *white* RNAi (BDSC#33623), *fz3-Gal4* (BDSC#36520). The rest of *Drosophila* lines, which were studied here, were obtained from Steller Lab stocks. Oregon R flies were used as control and only adult female flies were analyzed in this study.

***Drosophila* egg collection:** A $10cm^2$ apple-agar plate was set up with embryo collection cage to provide a substrate for egg laying. Prior to adding the plate, a small quantity of yeast paste was smeared onto the center of the apple-agar. To provide moisture, water-soaked tissue paper was layered under embryo collection cages. 10-15-day-old adult flies were collected to cages, which

were then placed into a fly incubator at 24^0C for 4 hours. Then, laden eggs were counted and 50 of them were plated into one corner of $10cm^2$ apple-agar plates, in which had a straight yeast paste smear at the center. Agar plates finally were incubated in the incubator. After 24h, hatched eggs were counted.

To analyze larval development, hatched 1st instar larvae were counted and placed into a fresh agar plate with yeast paste until they were reached to the 3rd instar larvae. After counting, larvae were placed into vials containing regular food. They were counted both when they pupated and again when they eclosed.

5% sucrose diet: $5mm^2$ Whatman filter papers were soaked with 1ml 5% sucrose solution and placed into the empty vials. The 5% sucrose solution was used as reduced nutrient diet. Eclosed adult females were collected at 24-25^0C. When they were 2-day-old, their regular diet was replaced to 5% sucrose diet at 28^0C. 20 of 2-day-old wild type or *Iduna* mutant female flies were grouped and kept on 5% sucrose solution-soaked filter paper containing vials at 28^oC. Following the fly count, dead flies were removed and 1ml 5% sucrose-soaked filter papers were replaced daily.

Food intake measurement: Female flies of *Iduna* mutant and Oregon R were collected after they eclosed. Before measuring food intake, the flies were kept on the regular food for 6 days. The flies then transferred to the regular food supplemented with 0.5% (w/v) Acid Blue 9 (erioglaucine disodium salt, Sigma 861146) for 4 hours. Quadruplicates of 5 flies per sample were then homogenized in 250µl 1xPBS and cellular debris was removed by centrifugation. Food intake was quantified by measuring the absorbance of the supernatant at 630nm and normalized to the wet weight of the flies.

***CG8786/dRNF146/dIduna* CRISPR/Cas9 editing:** I used the CRISPR optimal target finder website (tools.flycrispr.molbio.wisc.edu/targetFinder) to identify an appropriate guide RNA (gRNA) target sequence within *dIduna* (Gratz et al., 2013, 2014). I purchased the forward 5`-GTCGCTAGCTGCAATCTGCTCTG-3` and reverse 5`-AAACCAGAGCAGATTGCAGCTAG-3` oligos (IDT, Inc.) annealed, and followed the protocol; from Port et al., 2014 to clone the annealed oligos into pCFD3-dU6:3-gRNA plasmid (Addgene, plasmid# 49410, Port et al., 2014). Transformants were verified via Sanger sequencing (Genewiz, Inc.). The gRNA plasmid was injected into 300 embryos of custom *vasa*-Cas9 *Drosophila* (BestGene, Inc.). The injection was yielded 89 G_o progeny, and I established 70 individual fly lines, a couple of which possible *Iduna* loss-of-function mutations.

Isolation of the *Iduna* mutants and genetic mapping of *Iduna* –loss-of-function mutations: Total DNA was isolated from the 3rd instar (L3) larvae or 5-day-old adults of *Iduna* homozygous mutants and controls by using the Roche genomic DNA extraction kit (Roche). To confirm the mutant line, PCR fragments were amplified with specific primers (forward primer 5`-CAGCCCGAGCTGGTCATACTCAG-3`, reverse primer 5`-CGGCTTTCTGGGCTACCTAC-3`) binding within 5` UTR of *Iduna* and within the coding region of the gene. To identify the mutation site, the entire coding region was PCR amplified and PCR products were sent for DNA sequencing (Genewiz, Inc.).

Cloning and generation of UAS-CG8786 transgenic *Drosophila*: Adult flies were directly homogenized in 1ml TRIzol (Life Technologies) and total RNA was isolated according to the manufacturer's protocol. cDNA library was prepared from 5 μg total RNA, by using oligo(dT) amplification and the Superscript III First Strand synthesis kit (Invitrogen). cDNA library was used to amplify the *Iduna* transcripts with the primers (forward 5`-

ATGTCGCAACAGCGCTCCACAG-3`; *Iduna* B isoform reverse primer 5`-TCAGTAGAGCTTTAGGTATACC-3`; *Iduna* C/G isoform reverse primer 5`-TCAGTAGAGCTTTAGGTATACCG-3`). Amplified *dIduna* transcripts were cloned into pUAST (DGRC, Drosophila Genomic Resource Center) and pAc5.1 (Thermo Scientific) vectors by considering the appropriate restriction digestion sites. Following the bacterial transformation, all of the cloned genes were sequenced. To generate UAS-CG8786 transgenic *Drosophila,* Myc-tagged pUAST-CG8786/dIduna plasmid was injected into w1118 embryos (Best Gene, Inc.) We obtained successful transgenic lines.

Total RNA isolation, cDNA synthesis and Q-PCR: Posterior midguts of 7-day-old adult flies were directly homogenized in 1 ml TRIzol (Life Technologies) and total RNA was isolated according to the manufacturer's protocol (miRNeasy mini kit, QIAGEN). cDNA library was prepared from 5 μg total RNA, by using oligo(dT) amplification and the Superscript III First Strand synthesis kit (Invitrogen). cDNA library was used to amplify *Upd3* and *Rp32l* transcripts with the forward 5`-AGGCCATCAACCTGACCAAC-3`, reverse 5`-ACGCTTCTCCATCAGCTTGC-3` and forward 5`-CCCAAGGGTATCGACAACAGA-3`, reverse 5`-CGATCTCGCCGCAGTAAAC-3` primers, respectively. Those primers were designed via the online tool of DRSC/TRiP Functional Genomics Resources, Harvard Medical School and purchased from IDT, Inc.

Cloning and generation of the wild type and mutants UAS-Flag-*Tnks* transgenic *Drosophila*: I previously described *Drosophila* TNKS (Park and Steller, 2013) and its ORF was cloned into pUAST vector from pcDNA3.1-Flag-*Tnks*. To generate UAS-Flag-*Tnks* transgenic *Drosophila,* Flag-tagged pUAST-*Tnks* plasmid was injected into w1118 embryos (Best Gene,

Inc.) I obtained successful transgenic *Drosophila* lines and those were utilized in conjunction with tissue-specific *Gal4* drivers.

Nile Red Staining: 7-day-old female midguts and fat bodies were dissected in ice cold 1xPBS and kept on ice until required sample size obtained. Tissues were then fixed in ice cold 4% paraformaldehyde/PBS for 20 min at room temperature and washed with 1xPBS for 3x10 min. Tissues were stained with 0.25ug/ml Nile Red/PBS solution for 30 min at room temperature. Following the staining, samples were washed in 1xPBS for 3x10 min at room temperature. Specimens were finally mounted in Fluoromount-G (Southern Biotech) and analyzed with confocal microscope.

Clone analyses and RNAi experiments: Mutant clones were utilized to generate mitotic clones. 2nd instar larvae were subjected to an hour heat shock in a 37^{0}C water bath per day until they reached the pupa stage and maintained at 24^{0}C. 3-day-old adult females were analyzed.

For RNAi experiment, crosses were performed at 24^{0}C and the progeny of the desired genotypes were collected on the day of eclosion and maintained at 24^{0}C for 7 days before dissection. In the case of using temperature sensitive driver, eclosed virgin females were collected and kept at 29^{0}C for 7 days before intestinal dissection.

Cell culture: S2R+ cells were maintained at 25°C in supplemented Grace's Insect Medium (supplemented with 10% heat inactivated FBS, 100U/ml penicillin, 100µg/ml streptomycin) in spinner flasks.

Development of polyclonal antibodies: Full-length GST-tagged-Iduna C/G protein was expressed and purified from BL21 DE3 *E. coli* strain. Polyclonal antisera were generated in two guinea pigs (Cocalico, Inc.). For Western blot analyses, serum was used in 1:1000 dilutions.

Western blot analyses: 50-100µg dissected tissues or total larvae/flies were lysed in lysis buffer [50mM HEPES-KOH pH 7.4, 150mM NaCl, 0.05% Triton-X100, complete EDTA-free protease inhibitor cocktail (Roche)] using a 1 ml tissue grinder. Lysates were cleared by centrifugation at 13,000 g for 20 min at 4°C. Protein concentrations of supernatants were determined by BCA assay (Pierce). 1µg/µl lysate was prepared with 3X sample buffer in 100µl total volume (200mM Tris-HCl, pH 6.8, 200mM dithiothreitol (DTT), 8% SDS, 24% glycerol, 0.04% bromophenol blue), heated at 95°C for 10 min and samples were separated by SDS-PAGE for 1 h at 120V, by using standard 1X SDS Tris base-glycine running buffer. Proteins on the gels were blotted onto a PVDF membrane, in a 1X transfer buffer (25mM Tris base, 190mM Glycine, 20% MeOH, 0.05% SDS), and transferred (Bio-Rad) at 100V for 90 min. Membranes were taken through a standard immunoblot protocol followed by enhanced chemiluminescent detection (Crescendo ECL, Millipore) using a Lumimager (Fuji, LAS-3000). Primary antibodies: anti-Flag-HRP (1/1000, Sigma-Aldrich, A8592), anti-Flag (1/1000, CST, D6W5B 14793), anti-PAR (1/1000, Trevigen, 4335-MC-100), anti-Myc tag (1/1000, CST, 9B11, 2276), anti-Axin Drosophila (Santa Cruz, dT20, sc15685), anti-tubulin DM1A clone (1/1000, Sigma-Aldrich, T9026), mouse anti-GFP-HRP (1/2500, clone B2, Santa Cruz Biotechnology, sc-9996-HRP), rabbit anti-β-Actin-HRP (1/5000, clone 13E5, Cell Signaling Technology, 5125), donkey anti-rabbit-HRP (1/5000, Jackson ImmunoResearch, 711-035-152), donkey anti-mouse-HRP (1/5000, Jackson ImmunoResearch, 715-035-150), donkey anti-guinea pig-HRP (1:5000, Jackson ImmunoResearch, 706 006 148).

Immunofluorescence: Adult intestines were dissected in 1xPBS and fixed in 4% paraformaldehyde in PBS for 45 minutes at room temperature. Tissues then were first washed with 0.1% Tween 20-PBS, then washed with 0.1% TritonX-100-PBS and finally permeabilized

in 0.5% TritonX 100-PBS for 30 minutes. After blocking with 10% BSA in 0.1% Tween 20-PBS for 1 hour at room temperature, primary antibody incubation in 10% BSA in 0.1% Tween 20-PBS was performed for overnight at 4^{o}C. 3X 5 min 0.1% Tween 20-PBS washed intestines then were then incubated in secondary antibodies for 1 hour at room temperature. Specimens were finally mounted in Fluoromount-G (Southern Biotech) and analyzed with confocal microscope (LSM780, Zeiss). Primary antibodies: mouse anti-Arm (Wang et al., 2016; N2 7A1, DSHB, 1:50), mouse anti-Prospero (Wang et al., 2016; MR1A, DSHB, 1/50), mouse anti-GFP (GFP-12A6, DSHB, 1/100), mouse anti-β-galactosidase (Tian et al., 2016); 401A, DSHB, 1/100), mouse anti-Delta (Wang et al., 2016; C594.9B, DSHB, 1/100), rabbit anti-phosho-S10-Histone3 (Wang et al., 2016; 06-570, Millipore, 1/1000). The secondary antibodies were goat anti-mouse-Alexa 488 plus (Thermo Fisher Scientific, A32723), goat anti-mouse-Alexa 568 (Thermo Fisher Scientific, A11031), goat rabbit-Alexa 546 (Thermo Fisher Scientific, A11035), goat rabbit-Alexa 488 (Thermo Fisher Scientific, A11034), goat anti-rabbit-Alexa 633 (Thermo Fisher Scientific, A21071) and used at 1/1000.

Quantification of Stat-GFP immunostaining intensity: Images from R5 region were taken with a 63x objective. Each Stat-GFP^{+} stem cell was identified using Imaris software (Bitplane). The main intensity in those cells within a field (40 μm x 40 μm) surrounding an *Iduna* mutant clone or an equal field at least 50 μm away from the mutant clone was measured. The relative intensity was calculated and shown in the figure (Wang et al., 2016). Statistical analyses were performed with Prism software (GraphPad).

Immunoprecipitation: S2R+ cells were seeded at 5x10^{6} cells/10 cm^{2} culture plates and incubated overnight at 25^{0}C. Cells were then co-transfected with 5μg of each plasmid by using Mirus-insect transfection reagent. Negative controls were transfected with empty plasmids. 48

hours later, transfected cells were harvested. The cell pellets were washed within cold 1X PBS. This step was repeated 3 times. Pellets were re-suspended in 600µl 1% Triton X-100 lysing buffer. Re-suspended pellets were incubated on ice for 15 minutes and mixed gently and periodically. Total lysates were centrifuged at 13,000 rpm at 4^0C for 30 minutes. The supernatant was removed and 100µl was stored as total lysate. 25µl Protein A/G (Thermo Scientific) beads were washed with lysing buffer for 3 times. 200µl of supernatant was incubated with the mixture of washed protein A-G beads on a rotator at 4^0C for 30 minutes. In a parallel way, 25µl Protein A/G was washed with lysing buffer for 3 times. At the end of incubation period, the beads-supernatant mixture was centrifuged at 2,000 rpm at 4^0C for 1 minute. Pre-cleaned supernatant was collected and added to beads. Antibody was added to supernatant-beads and incubated at 4^0C on a rotator for 4 hours. The beads-supernatant-antibody mixture was centrifuged at 2,000 rpm at 4^0C for 1 minute and beads were washed with lysing buffer for 3 times. In the final step, the beads were re-suspended in 50µl of 3X sample buffer to perform immunoblotting.

Recombinant protein purification from S2R+ cells: S2R+ cells were seeded at $5x10^6$ cells/10 cm^2 culture plates and incubated overnight at 25^0C. Then, Flag or Myc-tagged gene of interests were transfected and based on the small tag, a recombinant protein was immunoprecipitated with Flag or Myc agarose beads as described above. Finally, by using Flag or Myc peptides, tagged proteins were eluted and quantified by BCA (Pierce, ThermoFisher Scientific).

Quantification and statistics: ISC quantification, dissected midguts were stained with Armadillo and Prospero. Images of the R5 region (Buchon et al., 2013) were obtained with a 63X objective and total number of $Arm^+/Pros^-$ cells in a field were counted. Quantifications of immunoblot were done with Image J. Two-tailed Student *t-test* and One-way ANOVA were used as statistical analyses and those were done with Prism (GraphPad) software.

3 *In vivo* functional analyses of lysine 598 in *Drosophila* TNKS

3.1 Summary

ADP-ribosylation is a strikingly dynamic and reversible post-translational modification. TNKS is conserved from flies to human. Although auto-poly-ADP-ribosylation is a degradation signal for TNKS, regulation of its poly-ADP-ribose activity is still a mystery. The ADP-ribosylation sites in TNKS have not been mapped to the specific residue(s) yet. Iduna is a binding partner of TNKS. Iduna-dependent TNKS degradation requires its PARsylation. My work revealed that lysine 598 is an ADP-ribosylation site in *Drosophila* TNKS. $Tnks^{K598A}$ knock-in flies live significantly shorter compared to control flies. Strikingly, $Tnks^{K598A}$ adult flies exhibit climbing deficits with age. $Tnks^{K598A}$ flies reduced the levels of phosphorylated JNK and poly-ADP-ribosylated proteins. Unlike *Tnks*-null mutants, $Tnks^{K598A}$ does not cause hyper-proliferation of stem cells in the adult midgut. I finally identified that K598A mutation prominently reduces the binding of certain proteins. As a result, I suggest that K598 residue is essential for building up the interaction between TNKS and certain partners.

3.2 Introduction

ADP-ribosylation is a post-translational modification (PTM) that regulates many essential biological functions including DNA repair, chromatin structure, unfolded protein response, and apoptosis. ADP-ribose transferases (ARTs) attach ADP ribose (ADP-r) units to acceptor proteins by using NAD+. Some ARTs can subsequently add more ADP-r units to target proteins to generate poly-ADP-ribose (PAR) chains. Glutamic acid, aspartic acid, lysine, arginine, cysteine, or phosphorylated serine amino acid residues can be modified by ARTs (DaRosa et al., 2018; Martello et al., 2016; Zhang et al., 2013).

PAR moieties are negatively charged polymers. Although poly-ADP-ribosylation (PARsylation) has an estimated half-live of only 1-6 min, it may influence the fate of proteins through several mechanisms, including a direct effect on protein activity, stability, or recruitment of binding partners (Guettler et al., 2011). Several enzymes can reverse protein ADP-ribosylation. NUDIX9 and NUDT16 process both mono-ADP-ribose (MAR) and PAR units. Impairments in the hydrolysis of PAR chains involve in various disease conditions such as cancer, neurodegeneration, oxidative stress, neural injury, and regeneration (Deng, 2009; Hanai et al., 2004; Martire et al., 2015; Brochier et al., 2015). Therefore, protein PARsylation and its regulation are essential.

Tankyrases (TNKS/PARP5) have essential roles in cellular pathways including telomere length maintenance, Notch signaling, and Wnt signaling (Bhardwaj et al., 2014). TNKS contains catalytic PARP domain, α-steril oligomerization motif (SAM) and large ankyrin repeat clusters (ARCs), known for substrate recognition and binding (Smith et al., 1998; De Rycker and Price, 2004). Although SAM-dependent polymerization strikingly enhances its PARP activity, auto-

PARsylation inhibits TNKS polymerization (De Rycker and Price, 2004; Nottbohm et al., 2007; Fan et al., 2018).

The fly genome has a highly conserved *Tnks* gene. Loss-of *Tnks* is not required for viability in *Drosophila*. TNKS-mediated ADP-ribosylation activates Wingless signaling (Croy et al., 2016; Feng et al., 2014; Yang et al., 2016; Wang et al., 2016). Loss-of *Tnks*, therefore, causes Axin elevation that blocks Wingless signaling in enterocytes and activates JAK-STAT signaling to promote stem cell division in the fly midgut (Wang et al., 2016). On the other hand, the conditional depletion of *Tnks1/2* in mice results in a rapid decrease of Lgr5+ stem cells and promotes stem cell death in the small intestine. As a result, mortality of double knockout mice increases (Ye et al., 2018).

Here, I showed that Iduna is a TNKS-binding protein that plays an important role in TNKS degradation after its auto-PARsylation. Using a mass spectrophotometry-based approach, I identified lysine 598 as an ADP-ribosylation site in *Drosophila* TNKS. I then generated $Tnks^{K598A}$ knock-in flies by using CRISPR-Cas9 genome engineering to investigate *in vivo* function(s) of K598 residue in *Drosophila*. Finally, I found that 11 interactors of TNKS have considerably reduced binding to the K598A mutant. This points to a critical function of K598 in mediating interactions between TNKS and various binding partners. In the future, it will be interesting to determine the functional consequences of these interactions.

3.3 Result

3.3.1 Iduna interacts with TNKS and plays a role in TNKS degradation in *Drosophila*

TNKS is a well-defined substrate of Iduna both in both vertebrates and *Drosophila*. Auto-PARsylation of TNKS is a degradation signal (Zhang et al., 2011). Loss-of *Iduna* leads to elevation of mis-expressed TNKS in *Drosophila* eye (Gultekin and Steller, 2019). However, it is still a mystery of how TNKS is rapidly destructed. To understand TNKS degradation, I focused on PARsylation and Iduna-mediated ubiquitylation of TNKS.

Iduna recognizes and ubiquitylates the PARsylated proteins through its WWE and RING domains, respectively (Fig 3.1A). I deleted the functional RING, WWE, and PAR domains to determine the structure and functions of Iduna. These mutants were then co-expressed with TNKS in *Drosophila* S2R+ cells. Wild type Iduna led to degradation of TNKS while the mutants did not led destruction of TNKS, resulting in elevated protein levels of TNKS in cells (Fig 3.1B). This confirmed that Iduna plays a role in TNKS degradation.

TNKS recognizes peptide motifs, which consist of six minimal consecutive amino acids. The canonical TNKS-binding motif (TBM) is Rxx#DG that starts with arginine in the 1st position and ends up glycine as the 6th amino acid residue whereas x can be any amino acid, and # is a small hydrophobic amino acid (DaRosa et al., 2018). Iduna has a putative TNKS binding motif, RATEDG, in the WWE domain (Fig 3.1C). To test if this motif was necessary for TNKS binding, Flag-TNKS was immunoprecipitated with wild type or a motif deficient mutant of Iduna in S2R+ cells. The deletion mutants were also co-immunoprecipitated with TNKS (Fig 3.1D).

Figure 3.1 *Drosophila* Iduna interacts with TNKS and ubiquitinylates *Drosophila* TNKS. A- Iduna has evolutionarily conserved WWE, PAR, and RING functional domains, responsible for the degradation of its ADP-ribosylated target proteins. Truncation mutants of Iduna were generated to conduct structure-function analyses in S2R+ cells. **B-** Truncation mutants of Iduna prevented *Drosophila* TNKS degradation. TNKS was co-expressed with wild type or the truncation mutants of Iduna in S2R+ cells. Labeled proteins were detected by immunoblotting. **C-** Iduna has several putative TNKS-binding motifs (TBMs): On the RING domain RLPCG, and RATEDG on the WWE configuration. **D-** Iduna interacts with TNKS. Flag-TNKS was co-expressed with wild type or the truncation mutants of Iduna in S2R+ cells. Co-IP was done with anti-Flag, and WB was conducted with anti-GFP and anti-Flag. **E-** Iduna was co-localized with TNKS in S2R+ cells. *UAS-RFP-Tnks* was co-expressed with *UAS-AcGFP-Iduna* under *Act5C* driver in S2R+ cells. **F-** Iduna ubiquitylated TNKS in S2R+ cells. Flag-TNKS was co-expressed and AcGFP- wild type or Iduna mutants in S2R+ cells. After 24h, S2R+ cells were treated with 5μM Bortezomib. 10h later, cells were collected and lysed. HA-conjugated A/G beads were used to pull down Flag-TNKS. Western blotting was performed with an anti-HA antibody. **G-** Ubiquitin ligase activity of Iduna depended on 141-Histidine and 147-Cysteine residues in the RING domain. **H-** Ubiquitin ligase deficient Iduna did not degrade TNKS. Flag-TNKS was co-expressed with AcGFP- mutant or wild type Iduna in S2R+ cells. Labeled proteins were analyzed by immunoblotting. β-actin was a loading control.

Figure 3.1

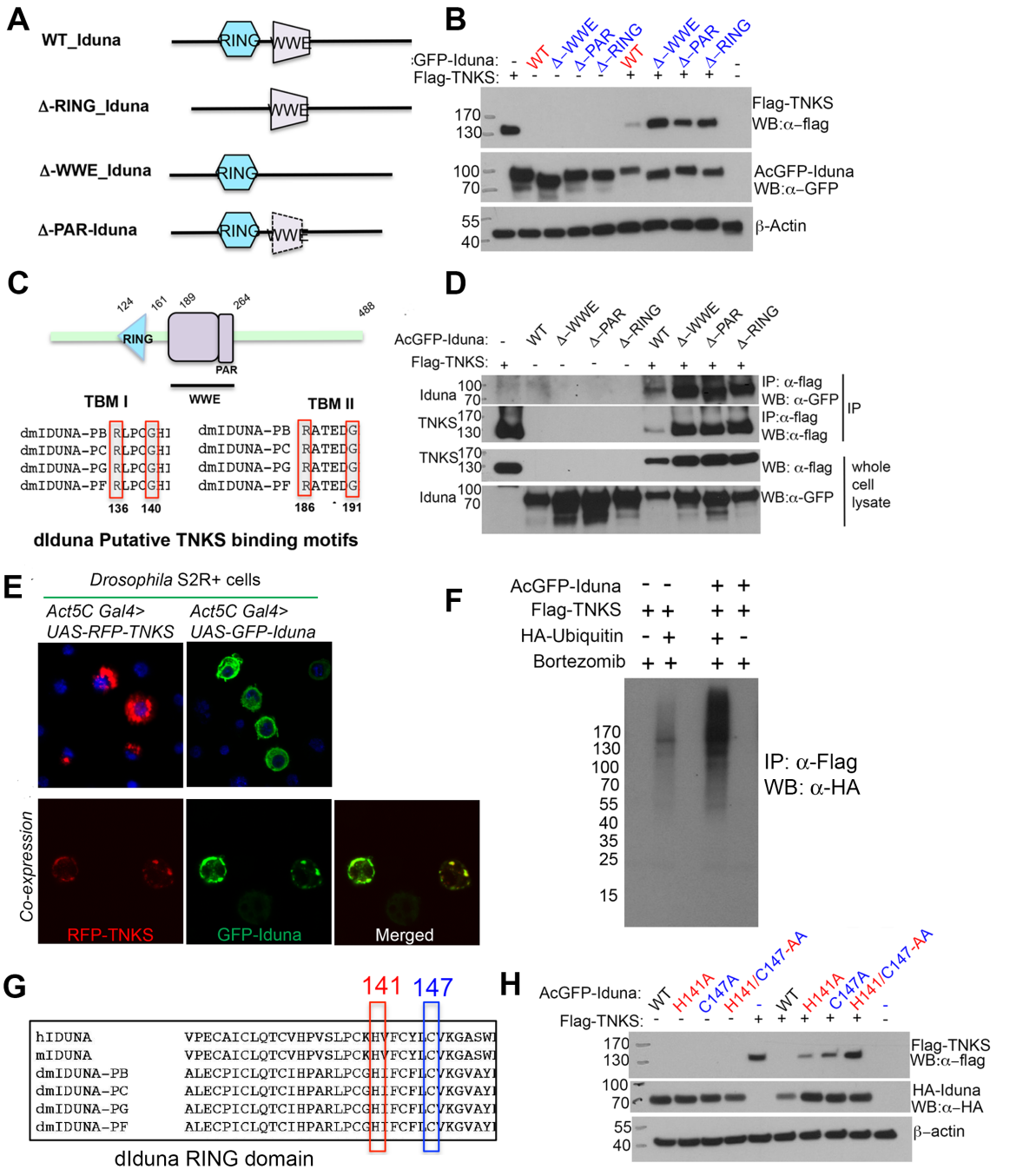
A
WT_Iduna
Δ-RING_Iduna
Δ-WWE_Iduna
Δ-PAR-Iduna
RING
WWE
B
GFP-Iduna:
Flag-TNKS:
WT
Δ–WWE
Δ–PAR
Δ–RING
Flag-TNKS WB:α–flag
AcGFP-Iduna WB:α–GFP
β-Actin
C
RING
PAR
WWE
TBM I
TBM II
dmIDUNA-PB RLPCGHI RATEDG
dmIDUNA-PC RLPCGHI RATEDG
dmIDUNA-PG RLPCGHI RATEDG
dmIDUNA-PF RLPCGHI RATEDG
dIduna Putative TNKS binding motifs
D
AcGFP-Iduna:
Flag-TNKS:
IP: α-flag
WB: α-GFP
IP:α-flag
WB:α-flag
WB: α-flag
WB:α-GFP
whole cell lysate
E
Drosophila S2R+ cells
Act5C Gal4> UAS-RFP-TNKS
Act5C Gal4> UAS-GFP-Iduna
Co-expression
RFP-TNKS
GFP-Iduna
Merged
F
AcGFP-Iduna
Flag-TNKS
HA-Ubiquitin
Bortezomib
IP: α-Flag
WB: α-HA
G
141 147
hIDUNA VPECAICLQTCVHPVSLPCKHVFCYLCVKGASWI
mIDUNA VPECAICLQTCVHPVSLPCKHVFCYLCVKGASWI
dmIDUNA-PB ALECPICLQTCIHPARLPCGHIFCFLCVKGVAYI
dmIDUNA-PC ALECPICLQTCIHPARLPCGHIFCFLCVKGVAYI
dmIDUNA-PG ALECPICLQTCIHPARLPCGHIFCFLCVKGVAYI
dmIDUNA-PF ALECPICLQTCIHPARLPCGHIFCFLCVKGVAYI
dIduna RING domain
H
AcGFP-Iduna:
Flag-TNKS:
WT
H141A
C147A
H141/C147-AA
Flag-TNKS WB:α–flag
HA-Iduna WB:α–HA
β–actin

Figure 3.2 TNKS degradation requires its poly-ADP-ribosylation and Iduna plays a role in TNKS degradation *in vivo*. A- TNKS ADP-ribosylates its target proteins through its PARP domain. **B-** M1064, H1041, and E1148 are the catalytic PARP residues, conserved from flies to human. **C-** Alanine mutations on these residues led to a deficiency in auto-poly-ADP-ribosylation (PARsylation). Mutant proteins were purified from *Drosophila* S2R+ cells by using Flag-beads. **D-** TNKS auto-ADP-ribosylation is necessary for its Iduna-dependent degradation. Wild type *Drosophila* TNKS or the PARP deficient M1064V, H1041A, E1148A mutants of TNKS were co-expressed with and without Iduna in S2R+ cells. **E-** The small molecule inhibitor of TNKS, XAV939 blocks the auto-ADP-ribosylation of TNKS that leads to TNKS elevation in S2R+ cells. Transfected S2R+ cells were treated with 20μM XAV939. Ribosylated TNKS proteins were detected by anti-PAR immunoblotting after TNKS-immunoprecipitation. β-actin was a loading control. **E-** RNAi-mediated *Iduna*-depletion causes an elevation of miss-expressed TNKS in *Drosophila. UAS-HA-Tnks* transgene was expressed under the temperature sensitive *Tub>Gal4* driver. *Iduna* inactivation by RNAi led to TNKS accumulation. 7-day-old female flies were lysed. Total proteins were analyzed by Western blotting. *white*-RNAi was a negative control. **F-** Quantification of Western blotting. The experiment was repeated two times with two independent replicates. Lines indicated means ± s.d. (standard deviation) ***$p<0.001$ Statistical analyses were done by two-tailed Student`s *t-test*. **H-** *Iduna*-RNAi caused an accumulation of PARsylated TNKS in *Drosophila* midguts. *UAS-Iduna* RNAi or *white*-RNAi and *UAS-HA-Tnks* transgenes were expressed under the temperature sensitive *Tub>Gal4* driver. 7-day-old female flies were dissected and stained with α-PAR, α-HA and DAPI.

Figure 3.2

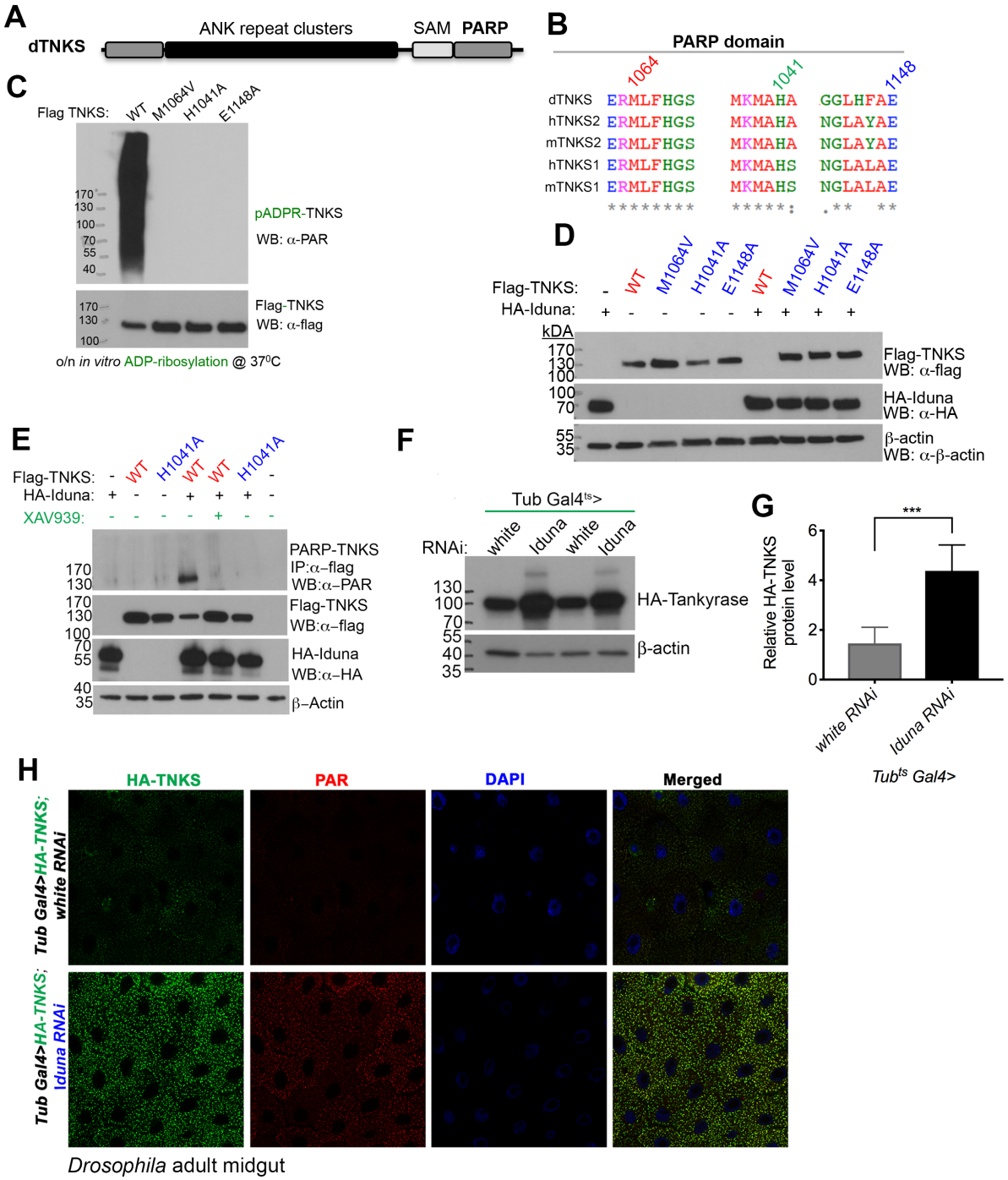

Drosophila adult midgut

That suggests the interaction between Iduna and TNKS is independent of ADP-ribosylation and ubiquitylation. Therefore, Iduna has more than one TBMs, one of which is sufficient to bind TNKS. In addition to immunoprecipitation, Iduna was co-localized with TNKS in S2R+ cells (Fig 3.1E). Taken together, TNKS can work together with Iduna to control the degradation of its substrates.

I next focused on ubiquitin ligase activity of Iduna. I first showed that Iduna ubiquitylated TNKS by conducting *in vivo* ubiquitylation in S2R+ cells (Fig 3.1E). I then characterized the RING domain of Iduna. Histidine and cysteine residues in the RING domain are responsible for ubiquitin ligase activity in both mouse and human Iduna (Kang et al., 2011). Both residues are conserved in *Drosophila* (Fig 3.1F). I mutated both residues into alanine to test their ubiquitin ligase functions. Each mutant (H141A or C147A) partially led to TNKS degradation compared to the wild type Iduna (Fig 3.1G). However, the H141/C147-AA mutant was completely unable to degrade TNKS (Fig 3.1H). As a result, TNKS degradation requires Iduna-dependent ubiquitylation.

3.3.2 Poly-ADP-ribosylation is essential for TNKS degradation

Auto-ADP-ribosylation is crucial to control TNKS stability. Auto-PARsylation is catalyzed by PARP domain (Fig 3.2A), which is 86% similar to its corresponding amino acid sequences in mouse and human TNKS. Mammalian PARP of TNKS has several catalytic amino acid residues including M1064, H1041, and E1148 (Callow et al., 2011). These residues are conserved in *Drosophila* (Fig 3.2B). Recombinant Flag-M1064A, H1041A, and E1148A TNKS were deficient for auto-PARsylation (Fig 3.2C).

Unlike wild type TNKS, these TNKS mutants were also resistant to degradation in the presence of wild type Iduna in S2R+ cells (Fig 3.2D-E). Auto-PARsylation of TNKS is

necessary for its stability. As a proof of concept, a small molecule inhibitor of TNKS, XAV939, blocked its auto-PARsylation as well as Iduna-dependent-degradation. As a control, the PARP deficient H1041A mutant had no auto-PARsylation. Therefore, it was stable to Iduna-dependent degradation (Fig 3.2E). RNAi-mediated *Iduna* inactivation also led to an elevation of miss-expressed TNKS *in vivo* (Fig 3.2F-G). *Iduna* knock-down resulted in an accumulation of PARsylated TNKS in the *Drosophila* midgut (Fig 3.2H). These results together demonstrate that ADP-ribosylation is necessary for degradation of TNKS in *Drosophila*.

3.3.3 Lysine 598 (K598) is an ADP-ribosylation residue in *Drosophila* TNKS

ADP-ribosylation is a highly dynamic PTM with an estimated half-life of only 1-6 min (Palazzo et al., 2015). Although auto-PARsylation is essential for TNKS degradation, the ADP-ribosylation site(s) in TNKS have not been mapped to the specific residue(s) yet. To this end, I developed a mass spectrophotometry (MS) approach to identify the amino acid residue(s) in *Drosophila* TNKS (Fig 3.4A).

Since human NUDT16 (hNUDT16) removes both poly- and mono-ADP-ribosylation, hNUDT16 cleavage can be a tool to trim the complex protein ADP-ribosylation into an easily detectable mark by mass spectrometry (Palazzo et al., 2015). To test if hNUDT16 could exhibit phosphodiesterase activity against PARsylated TNKS, I first expressed *Drosophila* TNKS in *Drosophila* S2R+ cells and *hNudt16* in *E. coli*. Subsequently, I purified both Flag-tagged dTNKS and His-tagged hNUDT16 proteins by using cobalt and Flag conjugated beads, respectively (Fig 3.3A-B). I first PARsylated TNKS *in vitro* for 1 hour (Fig 3.4B, lane 1) and then incubated the purified hNUDT16 with PARsylated TNKS for 3 hours. Strikingly, the recombinant hNUDT16 showed significant ability to remove the PAR signal from TNKS (Fig

4.3B). I further tested the range of hNUDT16 concentrations by PAR hydrolysis assay (Fig 3.4B, lanes 2-6). PAR modification was visualized by Western blot, using an antibody specifically recognizing poly- and oligo chains of ADP-r but not MAR. I detected molecular shifts of TNKS with and without modification in an hNUDT16-concentration-dependent manner *in vitro*. hNUDT16, therefore, efficiently hydrolyzes PAR modification in TNKS.

In my MS approach, following *in vitro* ADP-ribosylation, PARsylated *Drosophila* TNKS was cleaved by hNUDT16, leaving a ribose-5`-phosphate (R5P) footprint of ADP-ribosylation in target amino acids. After trypsin digestion, R5P-containing peptides were enriched via TiO_2 pull down and analyzed by MS (Fig 3.4A). With MS, R5P can be detectable in the peptides of interest (Palazzo et al., 2015). I identified several peptides, having R5P (Fig 3.4C). However, only one peptide, GKYDICK, had an R5P molecular marker with an expected molecular size (Fig 3.5A). I identified K598 residue as one of the ADP-r acceptor sides in TNKS (Fig 3.5B). K598 is the first investigated PARsylation site in TNKS.

K598 localizes in the ARC4 repeat of *Drosophila* TNKS (Fig 3.4D and Fig 3.6A-B). I first aligned the amino acid sequences of TNKS from different species and found that K598 is conserved in evolution. Both human and mouse orthologs of *Drosophila* TNKS shares high identity with ARC4 (Fig 3.4D) suggesting that K598 may have a conserved function. I then mutated lysine 598 to alanine (K598A) to examine its PARP activity. I purified Flag-K598A TNKS from S2R+ cells and carried out ADP-ribosylation assays. Strikingly, the K598A mutation completely blocked auto-PARsylation of TNKS *in vitro* just like PARP-deficient TNKS M1064V, H1041A and E11418A mutants (Fig 3.4E).

Figure 3.3 Expression and purification of recombinant *Drosophila* TNKS and human NUDT16. A- *UAS-Flag-TNKS* was expressed under *Actin5C-Gal4* driver in S2R+ cells. After 48h, transfected S2R+ cells were lysed to purify Flag-tagged TNKS by Flag-antibody conjugated beads. Purified TNKS was stained with colloidal blue on the SDS-poly-acrylamide gel. **B-** Expression and purification of His-tagged *hNudt16* from *E. coli* after IPTG induction. Cobalt beads were used to purify the His-tagged protein. Colloidal blue staining was used to visualize the purified proteins.

Fig 3.3

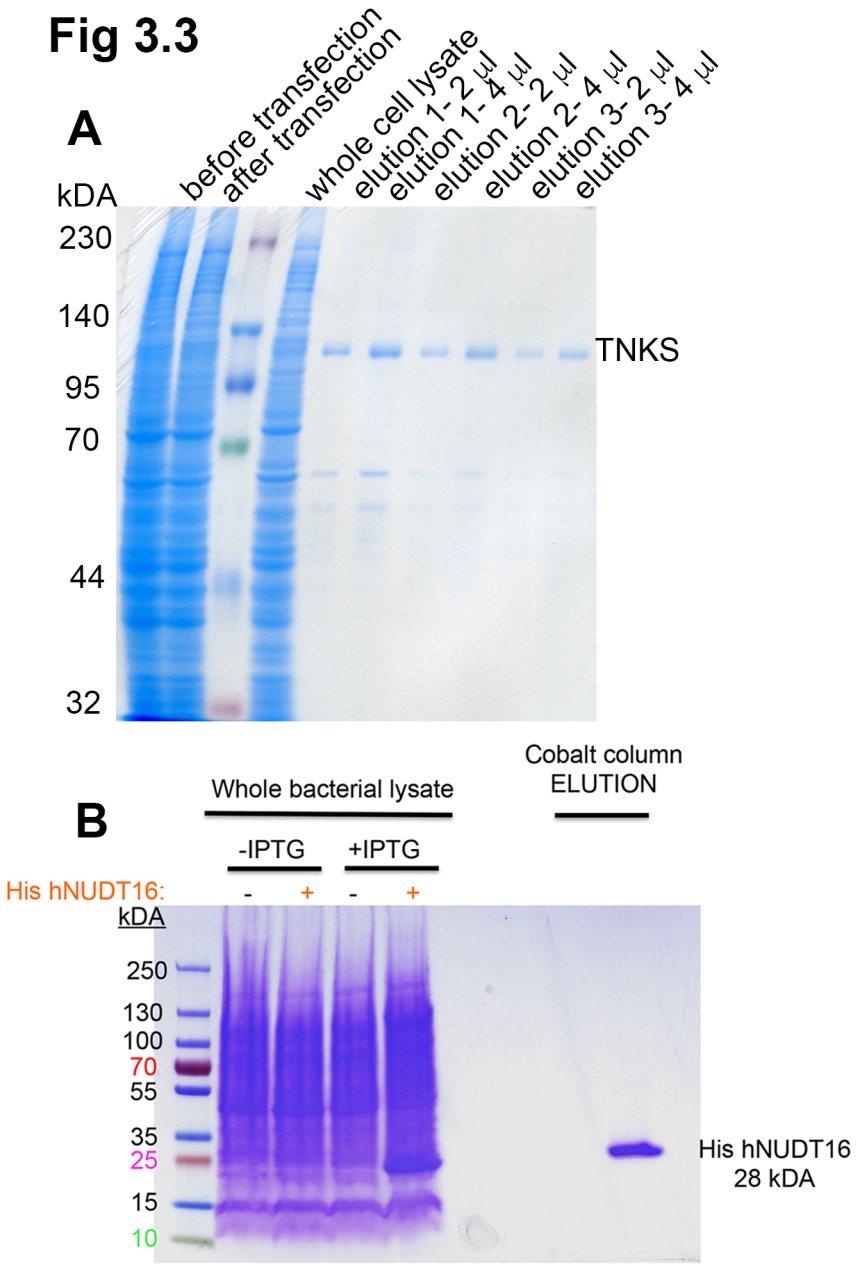
A
before transfection
after transfection
whole cell lysate
elution 1- 2 µl
elution 1- 4 µl
elution 2- 2 µl
elution 2- 4 µl
elution 3- 2 µl
elution 3- 4 µl
kDA
230
140
95
70
44
32
TNKS
B
Whole bacterial lysate
Cobalt column
ELUTION
-IPTG
+IPTG
His hNUDT16:
- + - +
kDA
250
130
100
70
55
35
25
15
10
His hNUDT16
28 kDA

Figure 3.4 Mass spectrophotometric approach identifies ADP-ribose acceptor residues of TNKS. A- I had developed an MS-based approach to identify ADP-ribose acceptor residues in TNKS. After *in vitro* ADP-ribosylation of TNKS, human NUDT16 removed PARsylation in TNKS. **B-** Human NUDT16 cleaves the poly-ADP-ribose modification in TNKS *in vitro.* By using NAD+, purified TNKS auto-poly-ADP-ribosylated *in vitro* (Lane 1). Recombinant hNUDT16 removed the PAR polymers from TNKS. Flag-TNKS was purified from S2R+ cells. For 3h, hNUDT16 digested PAR units in TNKS in a concentration-dependent manner (Lanes 2-6). **C-** hNUDT16 left a small molecular footprint, ribose-5`-phosphate (R5P) in TNKS. $TiO_2$ pull down enriched R5P-containing peptides, which were finally detected by mass spectrophotometry (MS). GKYDICK peptide in *Drosophila* TNKS has a ribose-5`-phosphate molecular marker. **D-** K598 residue is conserved from flies to human. K598 residue in *Drosophila* TNKS corresponds to K604 in human TNKS2. **E-** K598A mutant TNKS did not PARsylated by itself in the presence of NAD+ *in vitro.* TNKS proteins were expressed and purified from S2R+ cells. PARP deficient TNKS mutants (M1064V, H1041A, and E1148A) were also tested in the ribosylation assay. The modification was detected with an anti-PAR antibody. Unmodified TNKS was recognized by a Flag-immunoblotting. **F-** *Drosophila* TNKS PARsylated V5-Axin through TNKS-binding motif (TBM) *in vitro*. On the other hand, TNKS did not modify TBM deleted V5-Axin. Flag-TNKS and V5- wild type Axin or V5-D-TBM-Axin were expressed and purified from S2R+ cells. ADP-ribosylation was conducted *in vitro* with the purified proteins from S2R+ cells. **G-** K598A mutant was unable to modify GFP-Axin *in vitro*. GFP-Axin was expressed under the temperature sensitive *Tub-Gal4* driver and purified from *Drosophila*. **H-** K598 in *Drosophila* TNKS corresponds to K604 in human TNKS2. TBM of Axin is conserved from flies to human. Glutamic acid is a negative and lysine is a positive charged amino acid. Hence, the 7th

and 8th glutamic acid residues in the TBM of human AXIN can form a strong stable salt bridge interaction with K604 in human TNKS2.

Figure 3.4

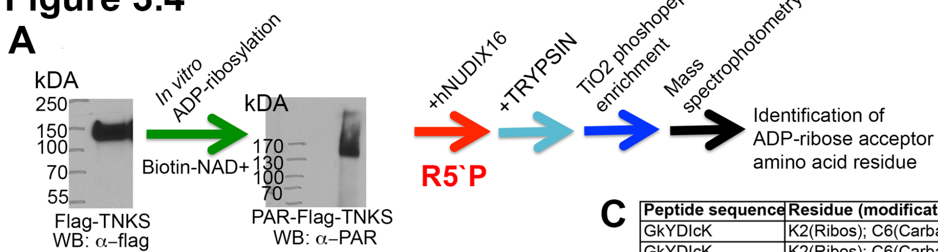

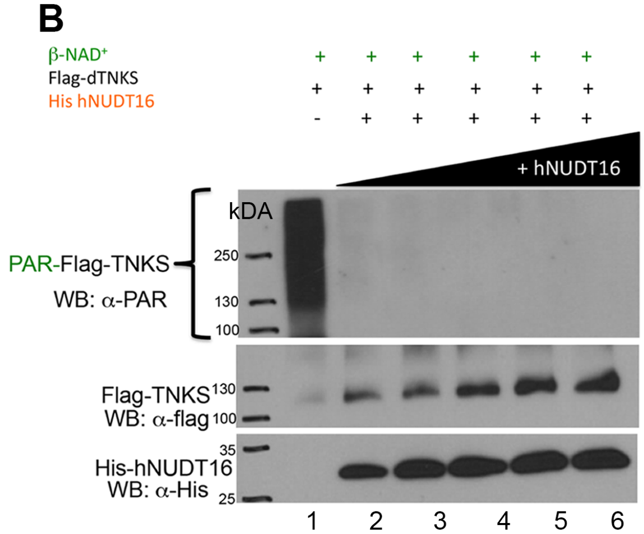

C

Peptide sequence	Residue (modification)	Residue TNKS
GkYDIcK	K2(Ribos); C6(Carbamidomethyl)	K598
GkYDIcK	K2(Ribos); C6(Carbamidomethyl)	K598
GkYDIcK	K2(Ribos); C6(Carbamidomethyl)	K598
GkYDIcK	K2(Ribos); C6(Carbamidomethyl)	K598
GkYDIcK	K2(Ribos); C6(Carbamidomethyl)	K598
GkYDIcK	K2(Ribos); C6(Carbamidomethyl)	K598
GkYDIcK	K2(Ribos); C6(Carbamidomethyl)	K598
GkYDIcK	K2(Ribos); C6(Carbamidomethyl)	K598
GkYDIcK	K2(Ribos); C6(Carbamidomethyl)	K598
GkYDIcK	K2(Ribos); C6(Carbamidomethyl)	K598
GkYDIcK	K2(Ribos); C6(Carbamidomethyl)	K598
GkYDIcK	K2(Ribos); C6(Carbamidomethyl)	K598
GkYDIcK	K2(Ribos); C6(Carbamidomethyl)	K598
GkYDIcK	K2(Ribos); C6(Carbamidomethyl)	K598
GkYDIcK	K2(Ribos); C6(Carbamidomethyl)	K598
GkYDIcK	K2(Ribos); C6(Carbamidomethyl)	K598
GkYDIcK	K2(Ribos); C6(Carbamidomethyl)	K598
GkYDIcK	K2(Ribos); C6(Carbamidomethyl)	K598
GkYDIcK	K2(Ribos); C6(Carbamidomethyl)	K598
GkYDIcK	K2(Ribos); C6(Carbamidomethyl)	K598
eSDHDVAELLR	E1(Ribos)	E628
GkYDIcK	K2(Ribos); C6(Carbamidomethyl)	K598
GkYDIcK	K2(Ribos); C6(Carbamidomethyl)	K598
NRDGATPAdLVK	D9(Ribos)	D618
NRDGAtPADLVK	T6(Ribos)	T621
NRdGATPADLVK	D3(Ribos)	D624
GkYDIcK	K2(Ribos); C6(Carbamidomethyl)	K598
GkYDIcK	K2(Ribos); C6(Carbamidomethyl)	K598
rYAHRRQEIAE	R1(Ribos)	R1018

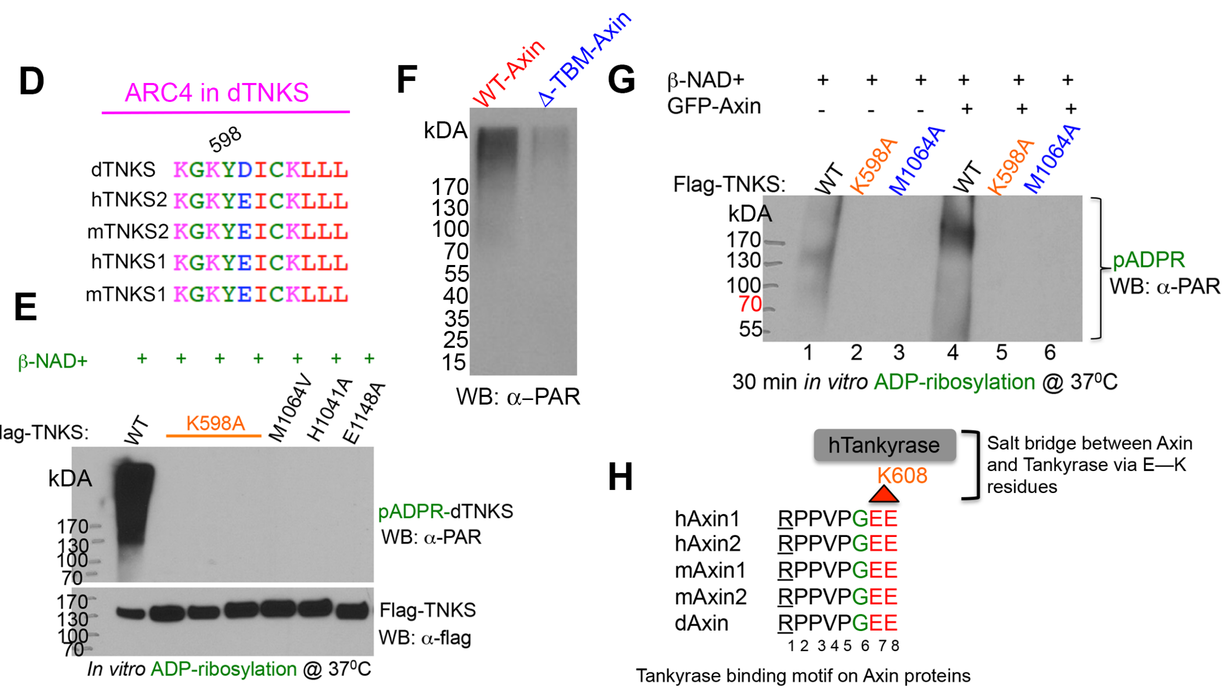

Figure 3.5 The GKYDICK peptide in *Drosophila* TNKS has R5P, detected by MS. A- The peptide has an expected molecular mass with R5P modification. The K598 in the GKYDICK peptide was identified as one of the ADP-ribose acceptor residues. **B-** Lysine 598 is an ADP-ribose acceptor residue in *Drosophila* TNKS.

Figure 3.5

A

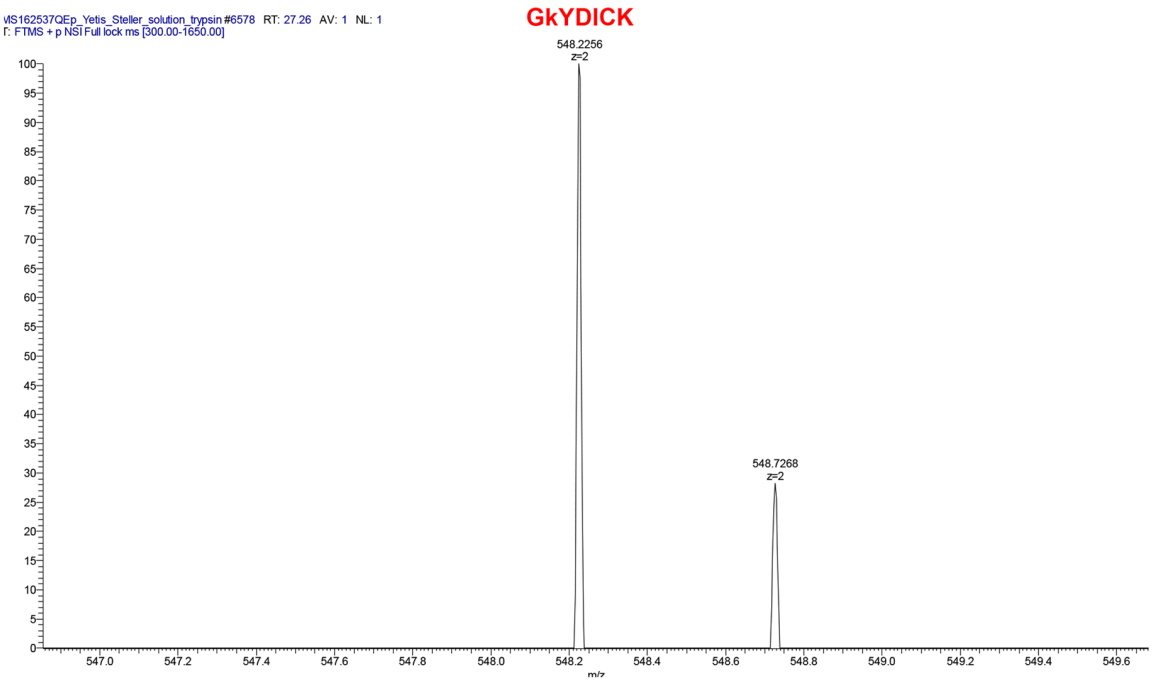

B

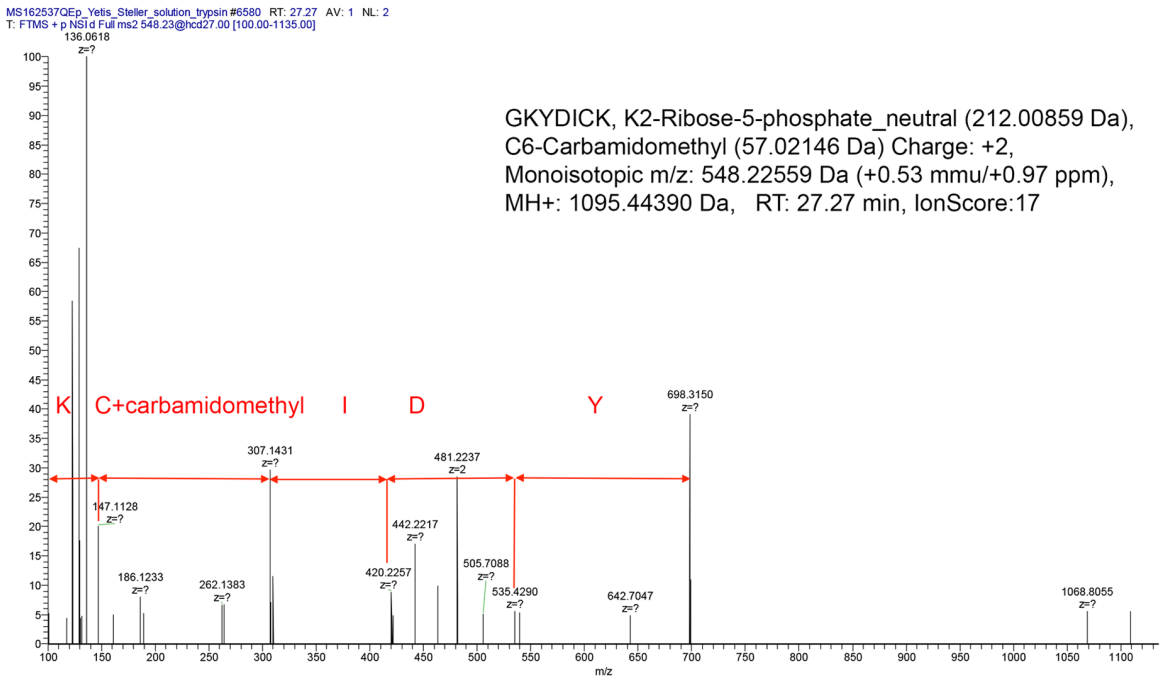

GKYDICK, K2-Ribose-5-phosphate_neutral (212.00859 Da), C6-Carbamidomethyl (57.02146 Da) Charge: +2, Monoisotopic m/z: 548.22559 Da (+0.53 mmu/+0.97 ppm), MH+: 1095.44390 Da, RT: 27.27 min, IonScore:17

Figure 3.6

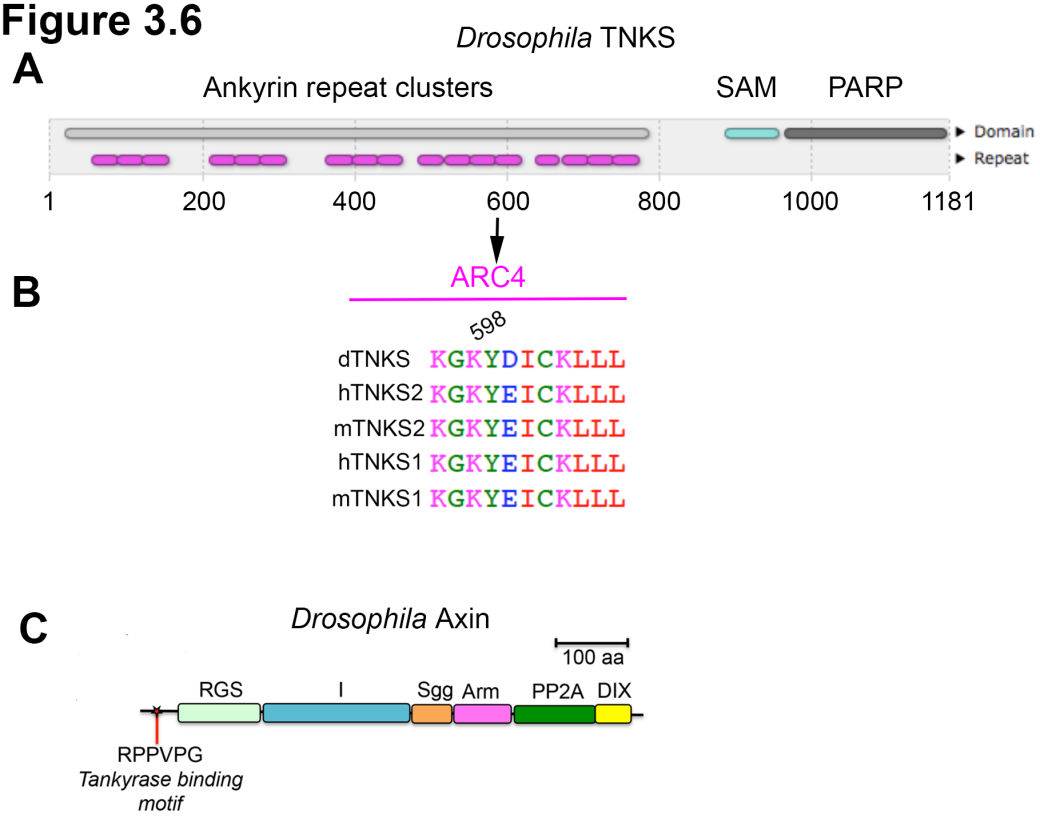

Figure 3.6 Lysine 598 is one of the ADP-acceptor residues in *Drosophila* TNKS. A-Lysine 598 localizes in the ARC4 repeat of *Drosophila* TNKS, that is conserved during evolution. **B-** K598 in Drosophila TNKS is corresponding to K604 residue in human TNKS. **C-** *Drosophila* Axin has an N-terminus TBM. Axin is a scaffold protein that recruits and interacts with different proteins through its various domains.

Axin, the rate-limiting factor in the Wingless pathway, is a target protein of TNKS in *Drosophila* as well. Axin also functions as a scaffold as it recruits different proteins through its various domains. It interacts with Adenomatous Polyposis Coli (APC) protein via its RGS domain and also binds to Shaggy (GSK3 in mammals) and Armadillo (β-catenin in mammals) through its BCD domain. TNKS recognizes and binds to Axin through its TNKS-binding motif (TBM) (Fig 3.6C).

I demonstrated that TNKS was unable to PARSylate Axin when its TBM was mutated. Hence, TBM is necessary for TNKS-dependent PARsylation of Axin (Fig 3.4F). I next tested PARP activity of K598A on its substrate Axin. I purified GFP-tagged Axin from flies and conducted *in vitro* ADP-ribosylation assay with wild type, K598A, and M1064V mutants of TNKS. Wild type TNKS PARsylated GFP-Axin as well as itself (Fig 3.4G). However, both K598A and M1064V TNKS mutants were unable to modify GFP-tagged Axin in this *in vitro* assay (Fig 3.4G). These results suggest that K598A may be a loss-of-function mutation of TNKS.

K598 residue in *Drosophila* TNKS corresponds to K604 in human TNKS2 (Fig 3.4H). Independent of my investigation, K604 residue in human TNKS2 was shown to be essential for AXIN1 interaction (Guettler et al., 2011). Based on fluorescence polarization peptide binding assays, the binding of TBM in AXIN1 was indeed highly sensitive to the K604A mutant peptide of TNKS2 (Guettler et al., 2011). It suggests that the position 7 and 8- glutamic acid residues in the TBM of AXIN can form a robust stabilizing salt bridge interaction with K604 of TNKS2 (Guettler et al., 2011). Taken together, I suggest that K598 residue may be necessary for ADP-ribosylation of Axin in *Drosophila*.

Figure 3.7 *Tnks*^{K598A} knock-in mutation is introduced into *Drosophila Tnks* gene by CRISPR-Cas9 genome engineering. A- A specific sgRNA was designed to target K598 residue. To mutate lysine residue to alanine, single-stranded DNA was designed and injected together with the sgRNA into Cas9-expressing embryos. **B-** I first screened the established fly lines with PCR and Styl-RFLP since K598A mutation changed one of the Styl restriction enzyme recognition sites. Several *Drosophila* lines were identified as K598A mutant, whose PCRs failed to give 2 DNA fragments (328 and 308 nucleotides). **C-** Identified *Tnks*^{K598A} knock-in mutants by Sanger sequencing. Corresponding *Tnks* sequences from wild type, heterozygous and homozygous flies were compared for K598 codon. **D-** *Tnks*^{K598A} mutants are viable, fertile and do not have obvious morphological defects. *Tnks*^{K598A} knock-in mutants did not have defects in hatching their embryos. n>200 for each genotype. **E-** *Tnks*^{K598A} knock-in mutants did not have defects in eclosing their pupae. n>100 for each genotype. Each line indicated means ± s.d. Statistical analyses were done with two-tailed Student`s *t-test.*

Figure 3.7

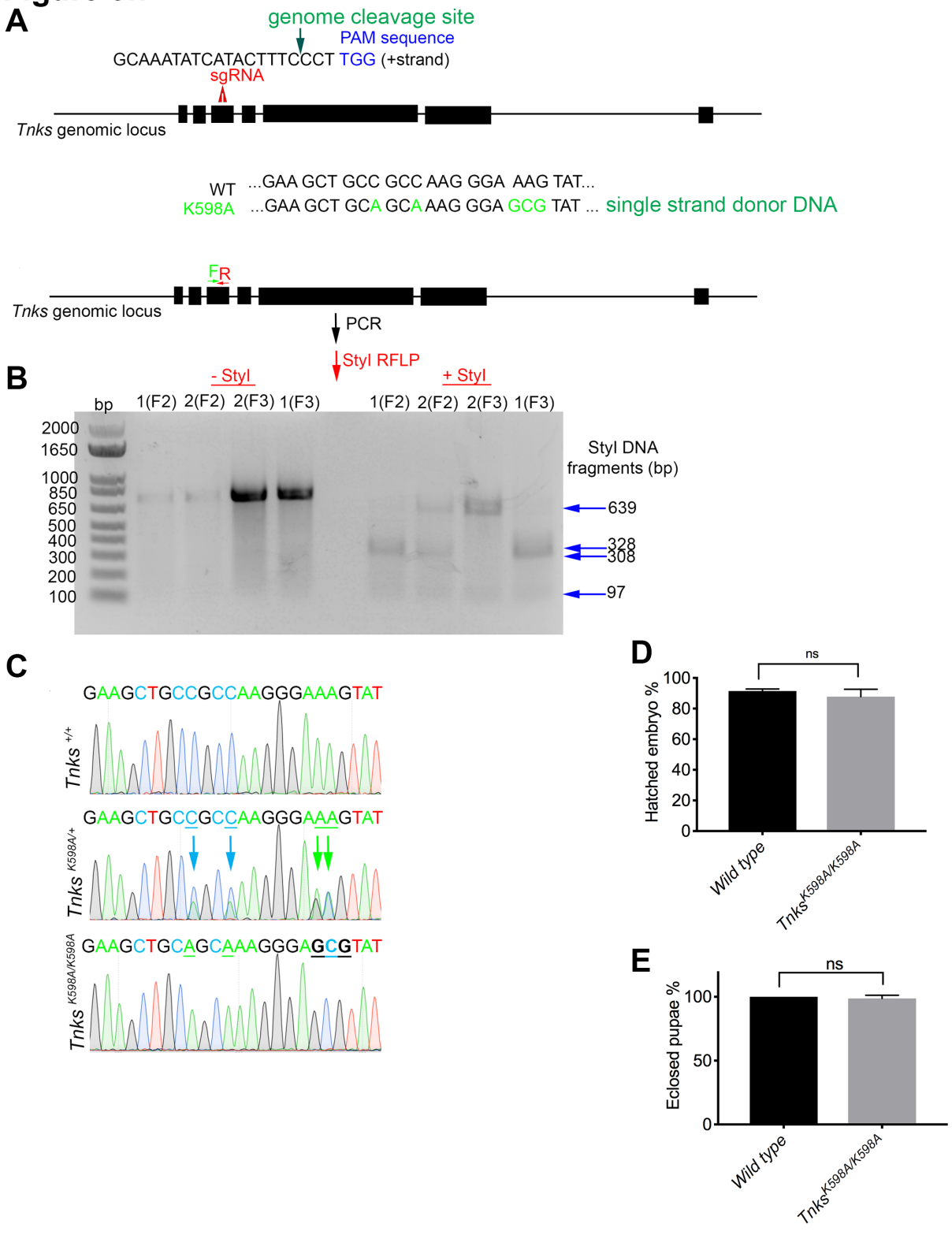
A
genome cleavage site
PAM sequence
GCAAATATCATACTTTCCCT TGG (+strand)
sgRNA
Tnks genomic locus
WT ...GAA GCT GCC GCC AAG GGA AAG TAT...
K598A ...GAA GCT GCA GCA AAG GGA GCG TAT ... single strand donor DNA
F
R
Tnks genomic locus
PCR
StyI RFLP
B
- StyI
+ StyI
bp
1(F2) 2(F2) 2(F3) 1(F3)
1(F2) 2(F2) 2(F3) 1(F3)
2000
1650
1000
850
650
500
400
300
200
100
StyI DNA fragments (bp)
639
328
308
97
C
GAAGCTGCCGCCAAGGGAAAGTAT
Tnks +/+
GAAGCTGCCGCCAAGGGAAAGTAT
Tnks K598A/+
GAAGCTGCAGCAAAGGGAGCGTAT
Tnks K598A/K598A
D
ns
Hatched embryo %
100
80
60
40
20
0
Wild type
Tnks K598A/K598A
E
ns
Eclosed pupae %
100
50
0
Wild type
Tnks K598A/K598A

To investigate the physiological function(s) of K598 residue in *Drosophila*, I generated $Tnks^{K598A}$ knock-in mutant, in which the lysine 598 residue in *Tnks* gene was replaced with an alanine residue (Fig 3.7A). Both sgRNA and donor DNA injected into Cas9-expressing embryos. I finally established possible $Tnks^{K598A}$ knock-in fly lines. After StyI restriction fragment length polymorphism (RFLP) analyses and complementary Sanger sequencing (Fig 3.7B), I identified $Tnks^{K598A}$ mutant flies (Fig 3.7C).

3.3.4 $Tnks^{K598A}$ knock-in mutation reduces lifespan and JNK signaling in *Drosophila*

I first examined the larval development of $Tnks^{K598A}$ and Oregon R flies but did not observe any differences in the numbers of hatched embryos (Fig 3.7D), pupated larvae, and eclosed adult *Drosophila* (Fig 3.7E), between $Tnks^{K598A}$ mutants and wild type flies.

Similar to $Tnks^{19}$ and $Tnks^{503}$-null mutants, $Tnks^{K598A}$ adult flies are viable, fertile, and have no apparent morphological defects when compared with wild type flies (Wang et al., 2016). Strikingly, both K598A females and males had significantly shorter lifespans compared to control flies (Fig 3.8A-B). Surprisingly, $Tnks^{K598A}$ adult flies reduce their climbing behavior with age (Fig 3.8C, Fig 3.9A-C). *Tnks* knock-out flies also have prominently shorter lifespan and impaired climbing ability due to the JNK pathway (Li et al., 2019). To address if K598 residue was important for JNK signaling in *Drosophila*, I analyzed the protein levels of phosphorylated JNK (p-JNK) and indicated that $Tnks^{K598A}$ flies have less p-JNK proteins when they were 4-week old compared to their controls (Fig 3.8D-E). Only two PARP family members, TNKS and PARP-1, exist in *Drosophila* and modify their substrate proteins via PARsylation (Krishnakumar and Kraus, 2010). Consistently, the levels of PARsylated proteins were reduced in the $Tnks^{K598A}$ mutants compared to their controls (Fig 3.8F-G).

Figure 3.8 *Tnks*^{K598A} mutation significantly reduces lifespan in *Drosophila*. **A**- K598A females and **B-** males had significantly shorter lifespan than control flies. Both females and males *Tnks*^{K598A} mutants were independently analyzed on a regular diet at 24-25^{0}C. For statistical analyses, I used the Mantel-Cox and Gehan-Breslow-Wilcoxon tests to compare survival curves between *Tnks*^{K598A} mutants and control flies. n>100 for each genotype. **C-** *Tnks*^{K598A} adult flies reduced their climbing abilities with age. *Tnks*^{K598A} mutation did not affect climbing behavior in flies when they were 3-day-old (Week 0). n>100 for each genotype. Female flies were tested for their climbing for 4 weeks. n>100 for each genotype. **D-** *Tnks*^{K598A} flies have less phosphorylated-JNK proteins when they were 4-week old compared to their controls. Whole fly protein lysates were used in Western blot analysis. p-JNK levels were detected by antibody. **E-** Quantification of p-JNK levels. Normalization was done with α-Tubulin. **F-** Protein PARsylation was decreased in the *Tnks*^{K598A} mutants compared to their control. PARsylation was detected by α-PAR antibody. **G-** Decline in the global PARsylation was quantified and normalized with α-Tubulin. Each line indicated means ± s.d. Statistical analyses were done with two-tailed Student`s *t-test* or 2-way ANOVA. ****$p< 0.0001$ for C.

Figure 3.8

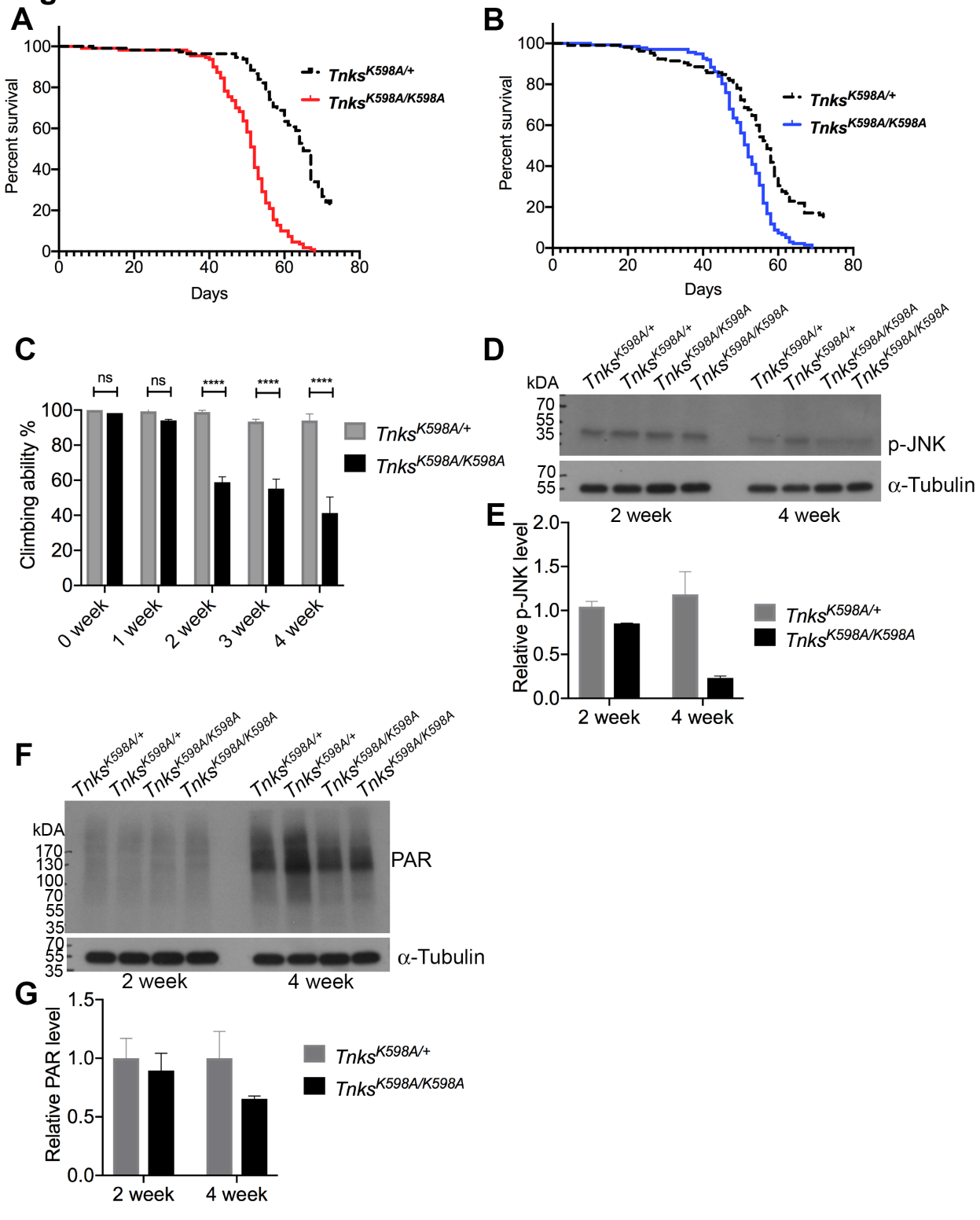
A
Percent survival
Days
Tnks K598A/+
Tnks K598A/K598A
B
Percent survival
Days
Tnks K598A/+
Tnks K598A/K598A
C
Climbing ability %
ns
ns
****
****
****
0 week
1 week
2 week
3 week
4 week
Tnks K598A/+
Tnks K598A/K598A
D
kDA
p-JNK
α-Tubulin
2 week
4 week
E
Relative p-JNK level
2 week
4 week
Tnks K598A/+
Tnks K598A/K598A
F
kDA
PAR
α-Tubulin
2 week
4 week
G
Relative PAR level
2 week
4 week
Tnks K598A/+
Tnks K598A/K598A

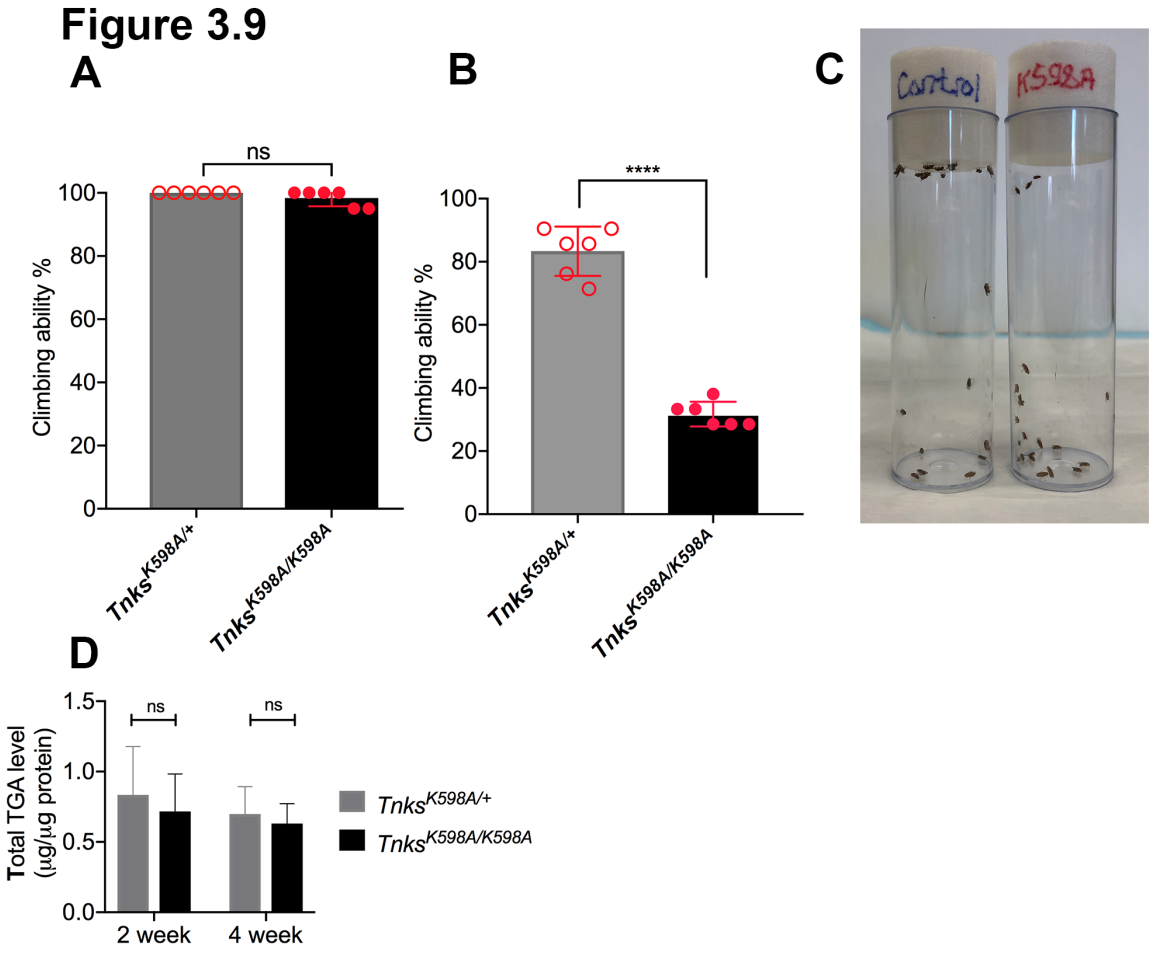

Figure 3.9 *Tnks*^{K598A} mutation significantly reduces their climbing behavior in *Drosophila*. **A-** *Tnks*^{K598A} mutation did not affect climbing behavior in flies when they were 3-day-old. n>100 for each genotype. **B-** *Tnks*^{K598A} adult flies reduced their climbing abilities with age. 45-day-old females were tested for their climbing. n>100 for each genotype. **C-** Image from 45-day-old female flies during their climbing assay. n=21 for each genotype. **D-** TAG levels did not change in *Tnks*^{K598A} mutants during aging. Quantification of total triglycerides (TGA). Each line indicated means ± s.d. Statistical analyses were done with two-tailed Student`s *t-test*.

*****p< 0.0001* for B.

Figure 3.10 *Apc1, pygo,* and *Arm* are indispensable for Wingless-dependent regulation of stem cell proliferation in the adult midgut. A- FRT-RFP was a control mutant clones, which did not promote the proliferation of *esg-LacZ*$^{+}$ stem and progenitor cells. **B-** *Apc1* is required for ISC hyper-proliferation in adult fly midguts. FRT82B, *Apc1* is an *Apc1*-null mutant. **C-** Wingless co-transcription factor *pygo*-null mutants had an increased number of *esg-LacZ*$^{+}$ cells. **D-** Armadillo is essential to prevent over-proliferation of stem cells. FRT19A, *arm* is *arm*-null mutant. Posterior midguts from 7-day-old *FRT-RFP* animals were dissected and stained with α-β-gal. *FRT-RFP* mutant clones did not have RFP signals. These flies carried *esg-lacZ* reporter in their backgrounds.

Figure 3.10

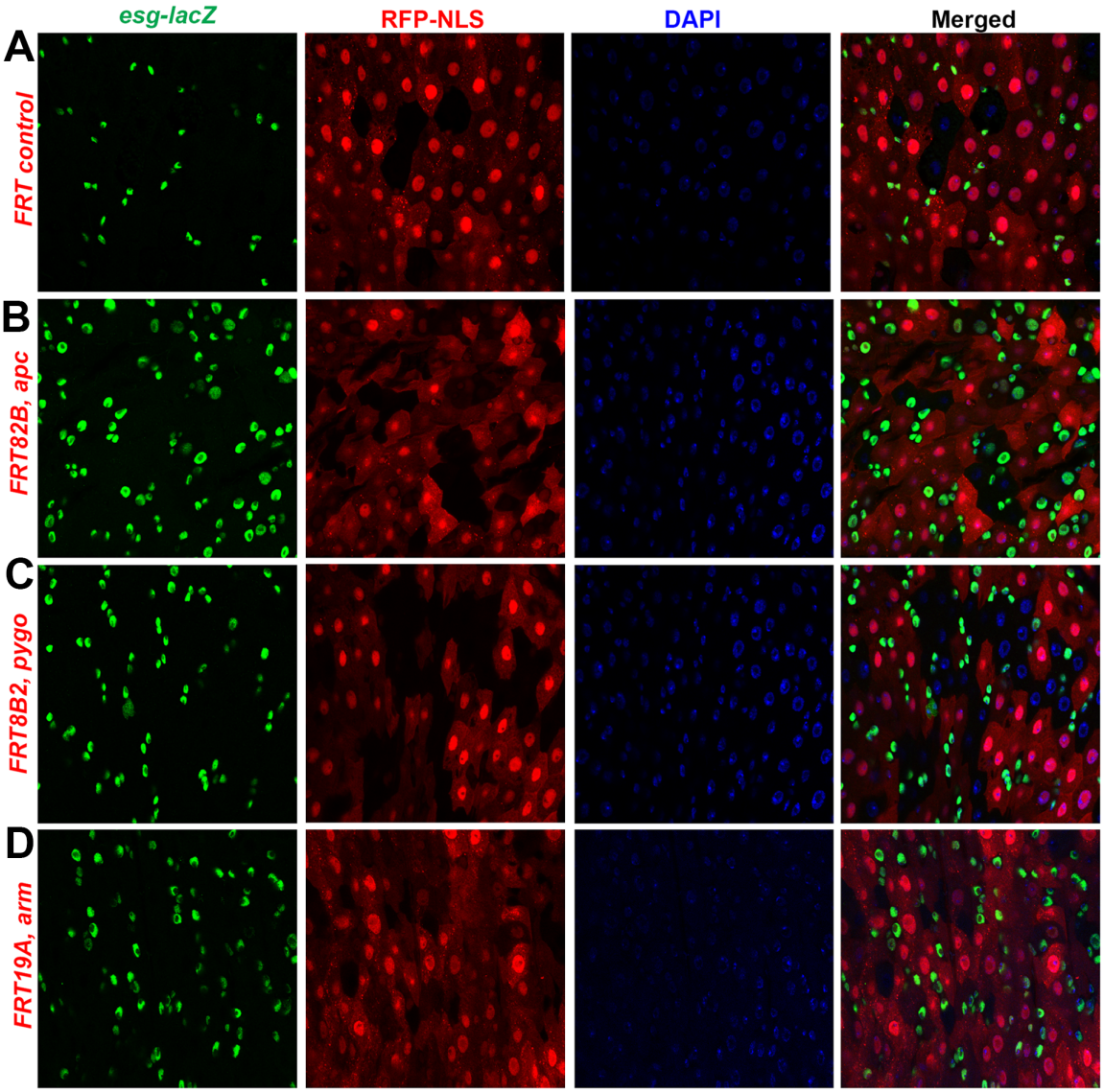
esg-lacZ
RFP-NLS
DAPI
Merged
A
FRT control
B
FRT82B, apc
C
FRT8B2, pygo
D
FRT19A, arm

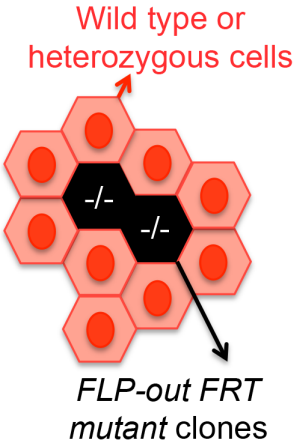
Wild type or
heterozygous cells
-/-
-/-
FLP-out FRT
mutant clones

Figure 3.11 *Tnks* prevents the over-proliferation of ISCs. A- *Tnks*^{503} mutant clones had increased number of Arm^{+}/Pros^{-} stem cells compared to FRT82B control clones in the *Drosophila* midgut. Posterior midguts from 7-day-old *FRT-RFP* animals were dissected and stained with a-Armadillo and a-Prospero antibodies. Armadillo stained cell membranes. **B-** *Tnks* deletion in mutant clones resulted in promotion of *esg>GFP*$^{+}$ stem and progenitor cell numbers in adult midguts compared to FRT82B control clones. Posterior midguts from 7-day-old *FRT-RFP* flies were analyzed. Flies had *esg>GFP* in their backgrounds. Mutant clones were defined by the absence of an RFP signal. Scale bar: 10μm.

Figure 3.11

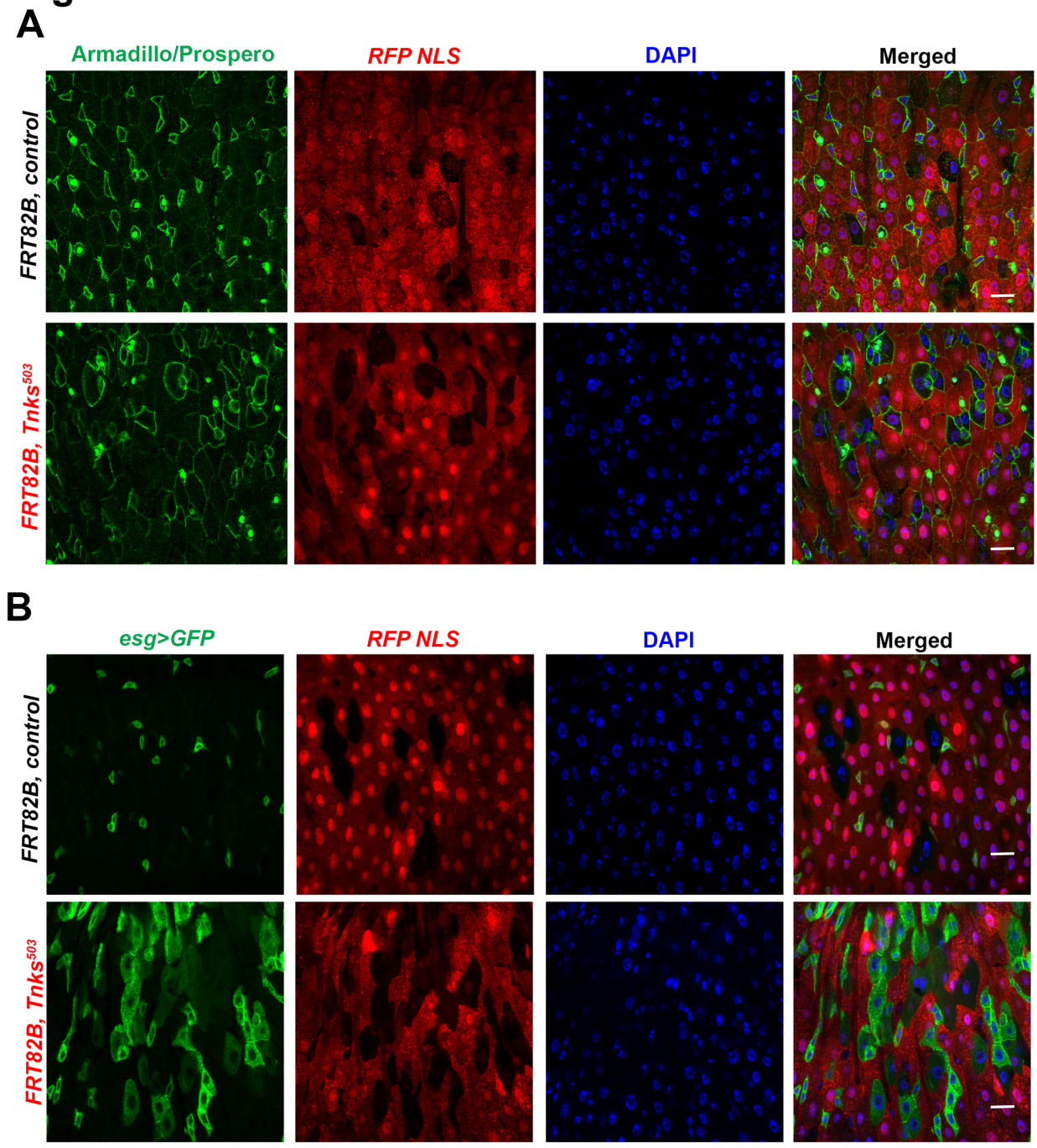
A
Armadillo/Prospero
RFP NLS
DAPI
Merged
FRT82B, control
FRT82B, Tnks503
B
esg>GFP
RFP NLS
DAPI
Merged
FRT82B, control
FRT82B, Tnks503

Figure 3.12 *Tnks* is essential in ECs to prevent hyper-proliferation of midgut stem cells. A- TNKS is crucial to control Axin levels in the ECs. Inactivation of *Tnks* elevated mis-expressed Axin levels in adult midguts. GFP-Axin transgene was mis-expressed in ECs under the *Myo1A* driver. 5-day-old flies were dissected. Midguts were lysed to conduct Western blotting. Tubulin was used as a loading control. **B-** *Tnks* mutants had more *esg-LacZ* stained midgut stem cells and progenitors. **C-** *Tnks* deletion promotes the number of *esg>GFP* cells. **D-** Ectopic expression of *UAS-Flag-Tnks* transgene in ECs suppressed the increased number of ISCs in *Tnks* mutants. *Myo1A-Gal4* was used to express *Tnks* in ECs. $Arm^{+}/Pros^{-}$ stem cells were quantified from posterior midguts. **E-** Quantification of $pH3^{+}$ cells in whole midguts. n>5. Both $Tnks^{19/19}$ and $Tnks^{503/503}$ are *Tnks*-null flies. Heterozygous flies ($Tnks^{503/+}$ or $Tnks^{19/+}$) were used as control flies. Each dot represented an animal and lines indicated means ± s.d. ****$p<0.0001$. Statistical analyses were done with One-way ANOVA.

Figure 3.12

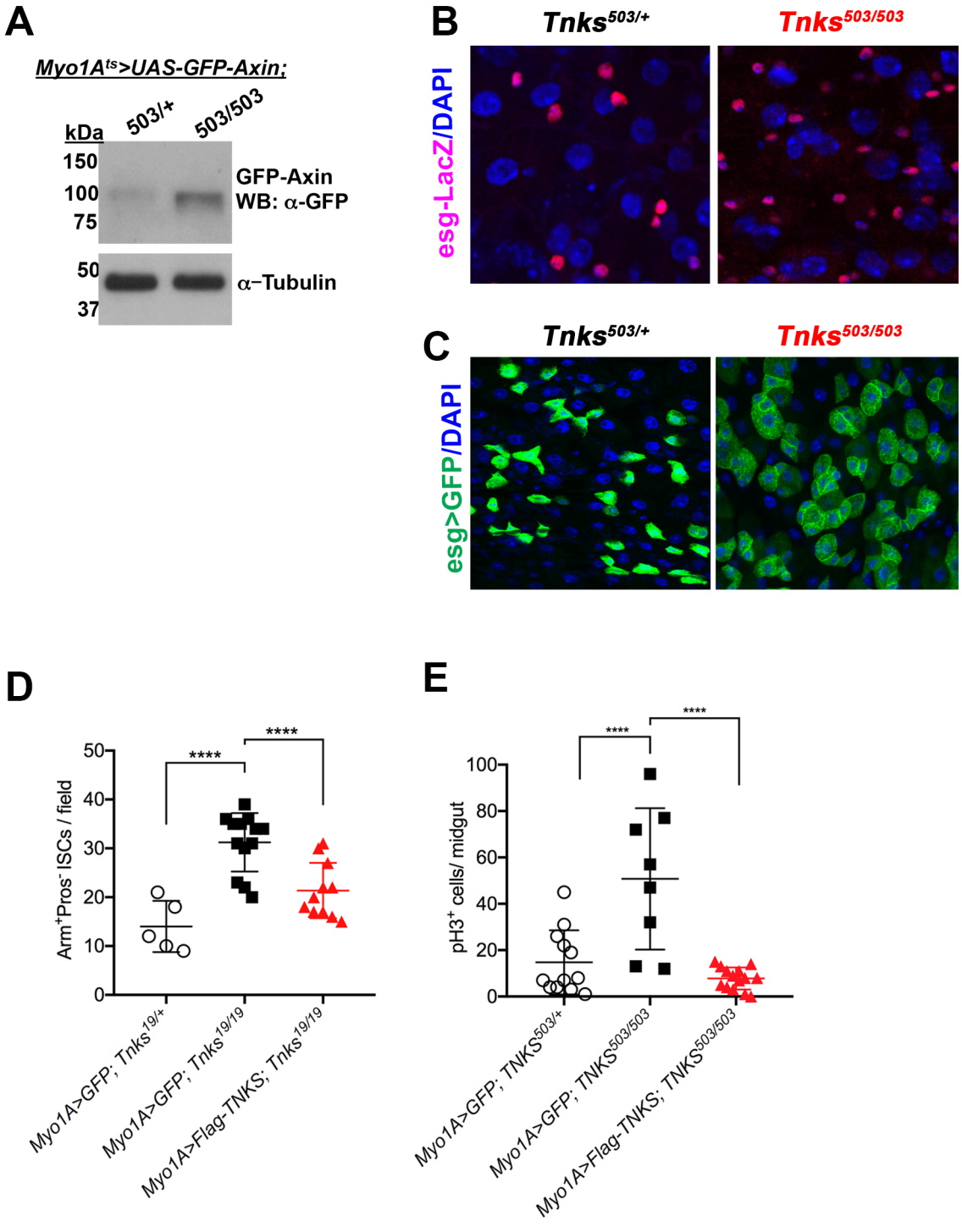
A
Myo1A^ts>UAS-GFP-Axin;
kDa
503/+
503/503
150
100
75
GFP-Axin
WB: α-GFP
50
37
α–Tubulin
B
Tnks503/+
Tnks503/503
esg-LacZ/DAPI
C
Tnks503/+
Tnks503/503
esg>GFP/DAPI
D
Arm+Pros- ISCs / field
****
****
Myo1A>GFP; Tnks19/+
Myo1A>GFP; Tnks19/19
Myo1A>Flag-TNKS; Tnks19/19
E
pH3+ cells/ midgut
****
****
Myo1A>GFP; TNKS503/+
Myo1A>GFP; TNKS503/503
Myo1A>Flag-TNKS; TNKS503/503

Decrease in the global PARsylation suggested that *Tnks*^{K598A} mutants might be a defect in energy storage. To test that, I examined levels of total triglycerides (TGA). However, I found that TAG levels were not altered in these mutants during aging (Fig 3.9D). I, therefore, reasoned that *Tnks*^{K598A} might be a hypomorph of *Drosophila* TNKS.

My previous *in vitro* results suggested that *Tnks*^{K598A} might be a loss-of-function mutant that might lead to Axin elevation and the promotion of stem cell proliferation in *Drosophila*. To test this, I analyzed midguts of both *Tnks*-null and *Tnks*^{K598A} mutants. As indicated previously, the Wingless pathway is essential to control midgut stem cell proliferation. ECs are responsible for activating Wingless signaling in the midgut. When Wingless signaling decreases due to Axin elevation in ECs, midgut stem cells undergo aberrant proliferation under homeostatic conditions.

Apc1, *pygo* (Pygorus-Wingless transcription co-factor) and *arm* (Armadillo-Wingless transcription factor, β-catenin in mammals) are indispensable for Wingless-dependent regulation of stem cell proliferation in the adult midgut. Therefore, the genetic depletions of them result in an increased number of esgcargot-LacZ positive (*esg-LacZ*$^{+}$) midgut stem and progenitor cells around RFP negative mutant clones compared to FRT-RFP^{-} control clones (Fig 3.10A-D).

3.3.5 Unlike *Tnks*-null mutants, *Tnks*^{K598A} knock-in mutation does not promote proliferation of ISCs in *Drosophila*

TNKS is a positive regulator of Wingless signaling. I found that *Tnks*-null mutant clones had an increased number of Arm^{+}/Pros^{-} midgut stem cells (Fig 3.11A) as well as *esg*>*GFP*$^{+}$ stem and progenitor cells in *Drosophila* midguts (Fig 3.11B). *Tnks* depletion caused accumulation of mis-expressed GFP-Axin in ECs (Fig 3.12A). Loss-of *Tnks* non-autonomously promoted stem cell division; as a consequence, there were an increased number of *esg*>*GFP*$^{+}$

Figure 3.13 Pharmacological inhibition of Axin degradation suppresses Wingless signaling. **A-** XAV939 and Bortezomib treatment inhibited Axin degradation in *Drosophila* midguts. 2-day-old female *FRT82B, Axn^{h}, BAC-Axin-V5* flies were treated with Bortezomib or XAV939. DMSO was also supplemented in the low melt fly food as a control of drug treatments. *Axn^{h}* is a loss-of function mutant of Axin. This mutation leads to lethality in *Drosophila*. BAC-Axin-V5 transgenic line rescues the lethality of *Axn*^{h} mutant. After 5-day XAV939 or Bortezomib treatment, midguts were dissected for V5-immunostaining. Axin accumulation was observed in dissected midguts. **B-** XAV939 treatment caused Axin accumulation. After 5-day XAV939 or Bortezomib treatment, total proteins were extracted from these flies and analyzed by V5-immunoblotting. ``se`` meant short exposure of immunoblotting while ``le`` meant long exposure. **C-** Quantification of V5-Axin immunoblotting upon XAV939 treatment. **D-** Bortezomib treatment resulted in Axin elevation. **E-** Quantification of V5-Axin immunoblotting after Bortezomib treatment. **F-** Bortezomib inhibited Wingless signaling. *fz3>GFP* reporter activity mainly reduced in the posterior midgut. 5-day Bortezomib-fed female flies were dissected, and *fz3>GFP*-expression in posterior midguts was examined with confocal microscope.

Figure 3.13

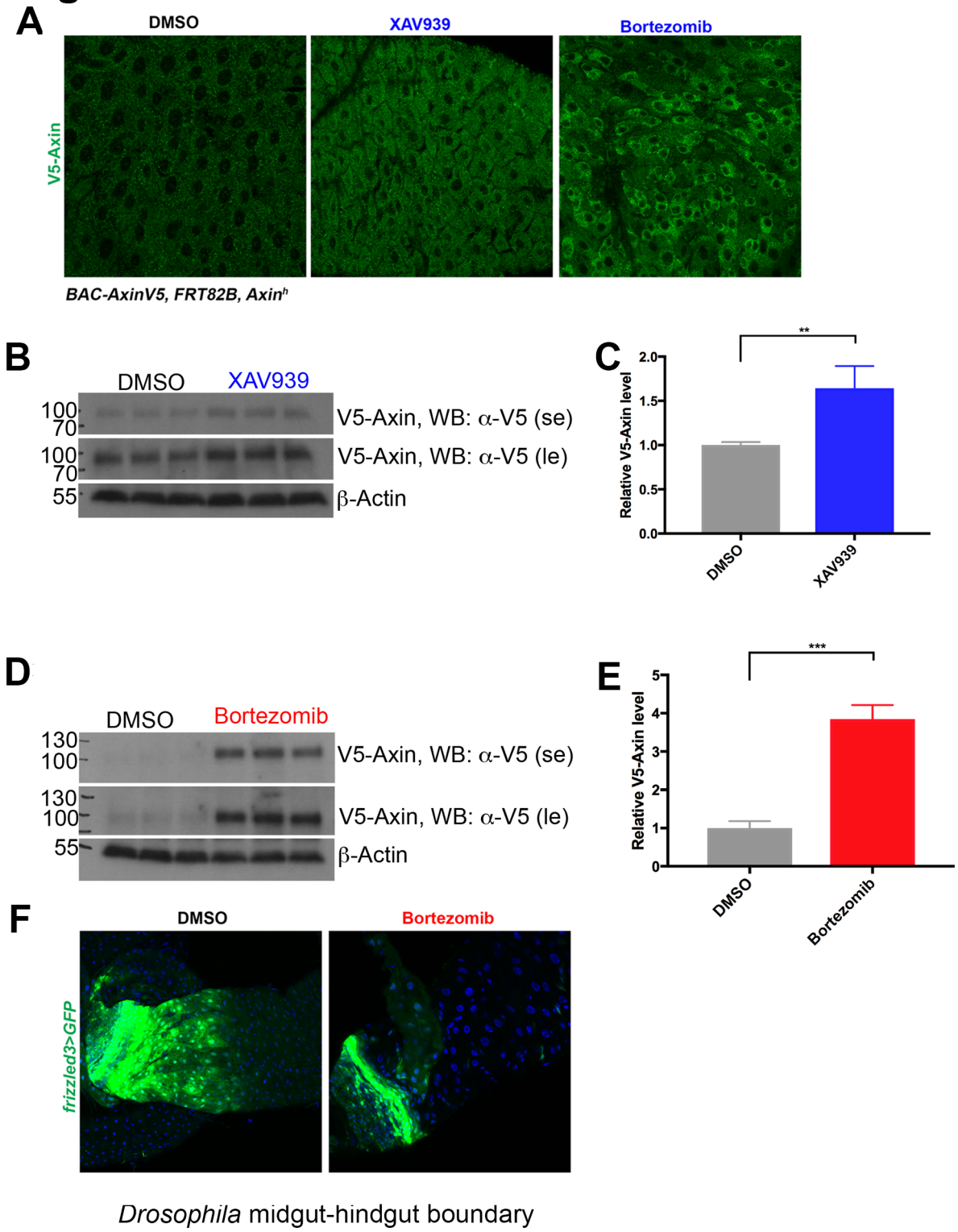

Drosophila midgut-hindgut boundary

Figure 3.14 XAV939 and Bortezomib induce JAK-STAT signaling to promote ISC proliferation. A- XAV939 and Bortezomib treatments drived stem cell hyper-proliferation in adult midguts compared to DMSO-fed flies. **B-** XAV939 and Bortezomib triggered JAK-STAT signaling, traced with a 10xStat-GFP reporter. **C-** XAV939 and Bortezomib induced *upd3>GFP* expression. **D-** XAV939 or Bortezomib increased stem cell proliferation in adult midguts. 2-day-old Oregon R female flies were fed with 50μM XAV939 or Bortezomib for 5 days. Midguts were then dissected and stained with α-pH3 antibody. $pH3^+$ mitotic cells were quantified in each midgut analyzed. Posterior midguts were imaged by confocal microscope. n>10. Each dot represented an animal and lines indicated means ± s.d. ****$p< 0.0001$. Statistical analyses were done with One-way ANOVA. Scale bar: 10μm.

Figure 3.14

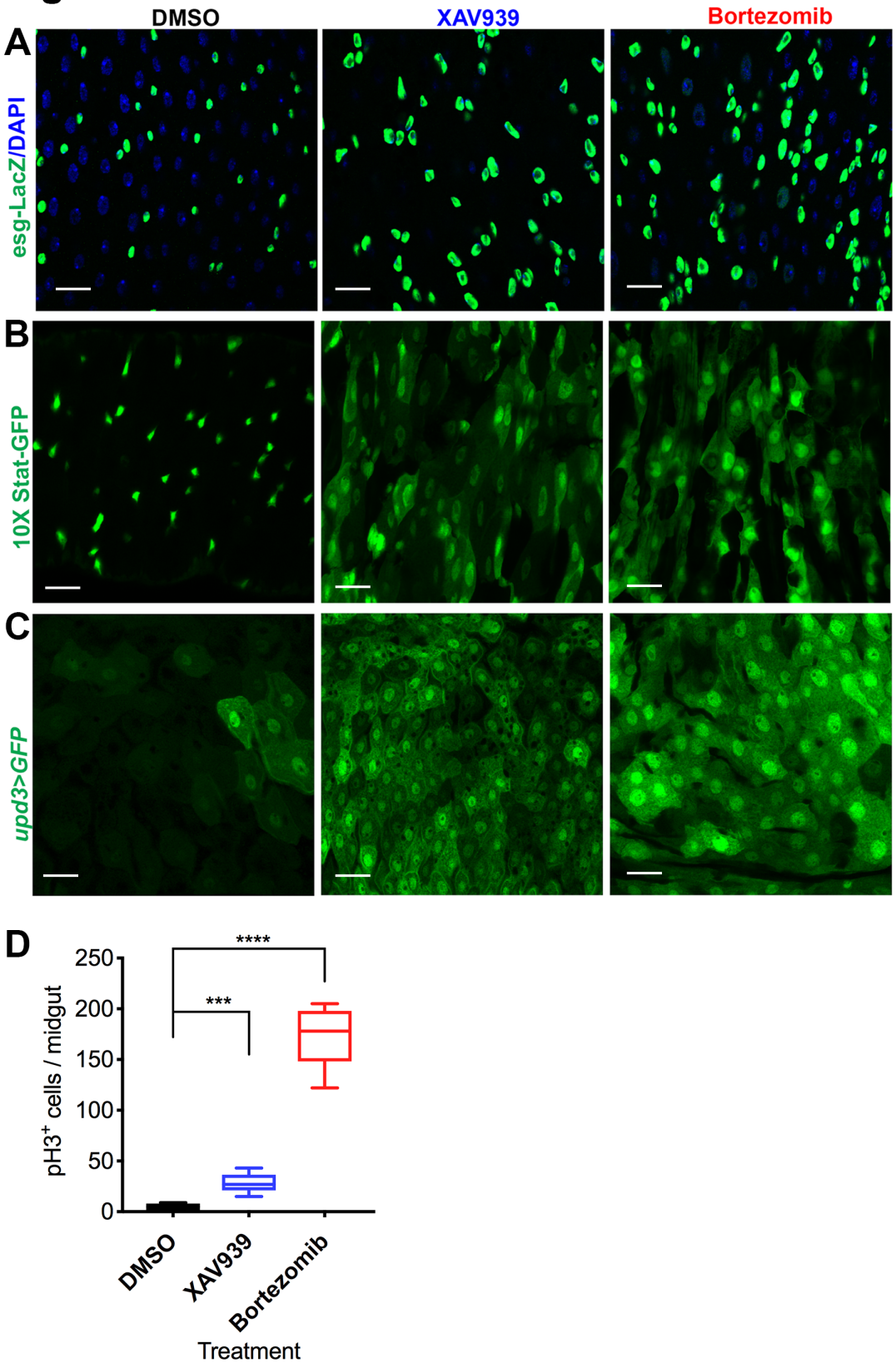
DMSO
XAV939
Bortezomib
A
esg-LacZ/DAPI
B
10X Stat-GFP
C
upd3>GFP
D
pH3+ cells / midgut
250
200
150
100
50
0
****
***
DMSO
XAV939
Bortezomib
Treatment

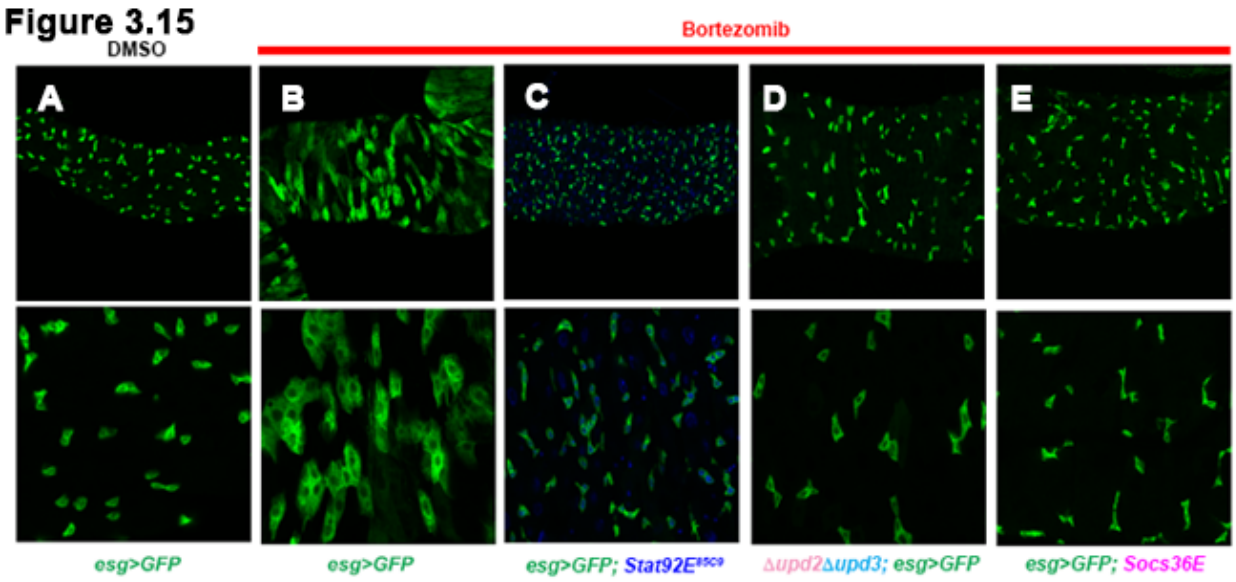

Figure 3.15 Bortezomib-mediated ISC proliferation requires JAK-STAT activation. A- DMSO treatment did not affect stem cell division in midguts. **B-** Bortezomib treatment led to over-proliferation of midgut stem cells. **C-** Depletion of the *Stat92E* transcription factor suppressed Bortezomib-induced stem cell division. **D-** Inactivation of *upd2*/*3* reversed the proliferation effect of Bortezomib on stem cells. **E-** The reduction of JAK-STAT signaling in ISCs by the expression of *UAS-Socs36E* reduced the proliferation response to Bortezomib. A *UAS-Socs3E* transgene expression was driven by *esg-Gal4>GFP*. 2-day-old Oregon R female flies were fed with 50μM XAV939 or Bortezomib for 5 days. These flies had *esg-Gal4>GFP* in their backgrounds. Posterior midguts were imaged by confocal microscope. n>5 for each experimental condition.

Figure 3.16 *Tnks*^{K598A} knock-in mutation does not affect stem cell proliferation in the adult midgut. A- *Tnks*^{503}-null flies have more Arm^{+}/Pros^{-} midgut stem cells. **B-** Unlike *Tnks*-null flies, *Tnks*^{K598A} mutation did not affect Arm^{+}/Pros^{-} stem cell numbers. *Tnks*^{K598A} did not caused any changes in the JAK-STAT pathway. A 10xStat-GFP reporter fly line was used to monitor JAK-STAT signaling. **C-** The quantification of Arm^{+}/Pro^{-} ISCs in midguts of *Tnks-null (Tnks503)* flies. **D-** The quantification of Arm^{+}/Pro^{-} ISCs in midguts of *Tnks*$^{K598A/+}$ flies. *Tnks*$^{K598A/+}$ flies were used as control flies. **E-** *Tnks*^{K598A} flies did not affect *upd3>GFP* expression. *Tnks*$^{K598A/+}$ flies were used as control flies. **F-** The quantification of pH3^{+} mitotic cells. There were no differences in the average of pH3^{+} cell numbers between heterozygous or homozygous *Tnks*^{K598A} flies. Oregon R flies were used as wild type flies. Scale bar: 50μm. 7-day-old female flies were dissected, and posterior midguts were examined with confocal microscope. Each dot represented an animal. Graphs indicated means ± s.d. Statistical analyses were done with two-tailed Student`s *t-test*. ns means not significant**.** Scale bars: 10μm for A, C and 50μm for E.

Figure 3.16

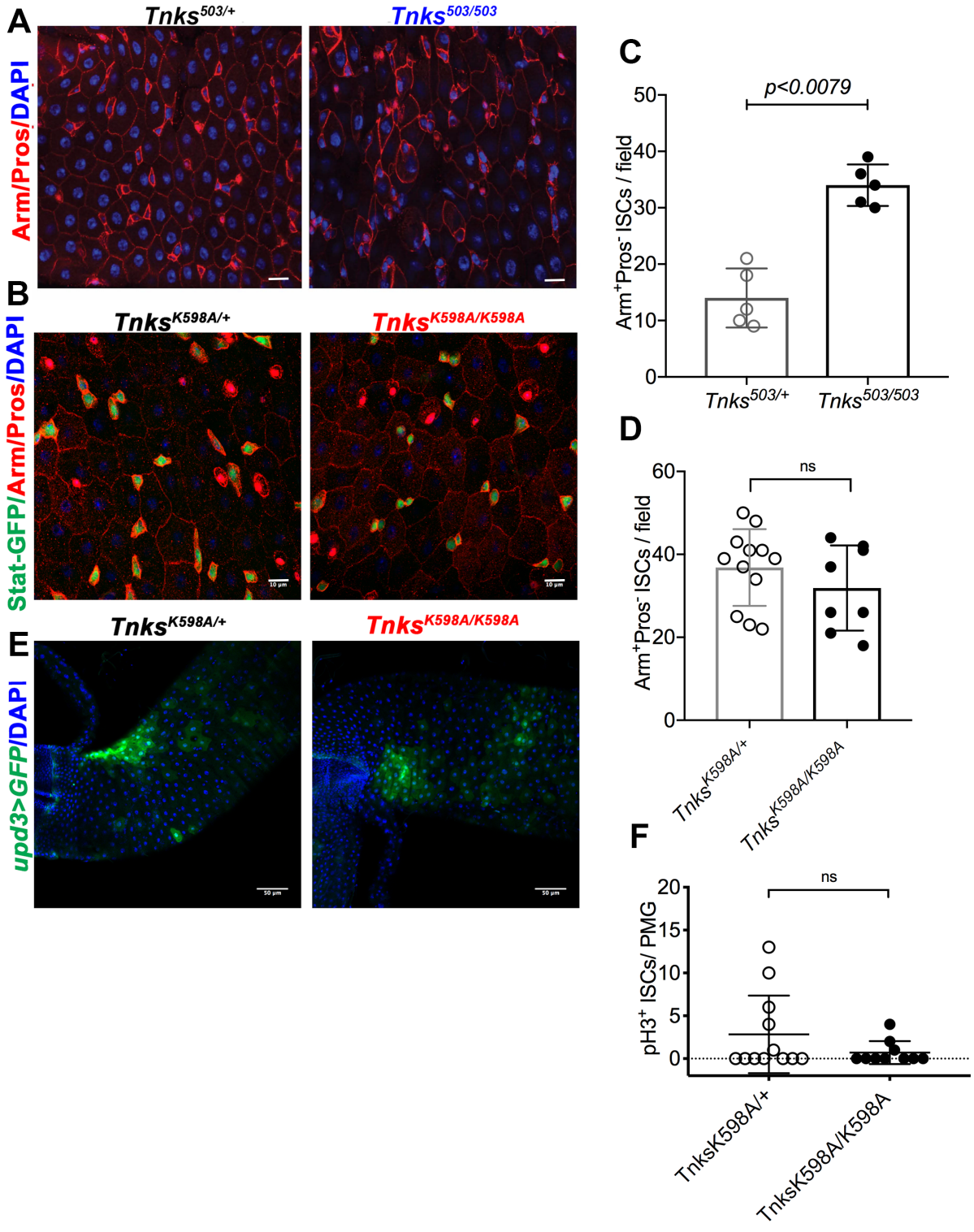
A
Tnks503/+
Tnks503/503
Arm/Pros/DAPI
B
TnksK598A/+
TnksK598A/K598A
Stat-GFP/Arm/Pros/DAPI
E
TnksK598A/+
TnksK598A/K598A
upd3>GFP/DAPI
C
p<0.0079
Arm+Pros- ISCs / field
0
10
20
30
40
50
Tnks503/+
Tnks503/503
D
ns
Arm+Pros- ISCs / field
0
20
40
60
TnksK598A/+
TnksK598A/K598A
F
ns
pH3+ ISCs/ PMG
0
5
10
15
20
TnksK598A/+
TnksK598A/K598A

stem and progenitor cells in adult midguts (Fig 3.12B-E). Ectopic expression of Flag-tagged TNKS in ECs suppressed over-proliferation of ISCs in *Tnks*-null mutants (Fig 3.12D-E).

Both pharmacological inhibition of Axin ADP-ribosylation by XAV939, and its 26S proteasome-dependent degradation by Bortezomib, led to an accumulation of endogenous Axin in *Drosophila* midguts (Fig 3.13A). I also detected increased levels of endogenous Axin in the whole-body protein lysates from XAV939 or Bortezomib fed flies (Fig 3.13B-E). High levels of Axin suppressed the expression of *frizzled3*, an indicator of Wingless signaling activity, in the midgut. Therefore, I observed more *esg>GFP*$^{+}$ stem and progenitor cells after XAV939 or Bortezomib treatment (Fig 3.14A). Similar to *Tnks*-null mutants, XAV939 and Bortezomib treatments both triggered the JAK-STAT pathway (Fig 3.14B) and stem cell proliferation (Fig 3.14D) in *Drosophila* midguts.

In response to stress, ECs express and secrete UPD cytokines to activate JAK-STAT signaling, which is essential for ISC to proliferate. I, therefore, used *upd3-Gal4* enhancer trap to monitor *upd3* induction in midguts and found that *upd3* expression correlated with the effects of XAV939 or Bortezomib treatment (Fig 3.14C).

When I reduced JAK-STAT signaling in *esg>GFP*$^{+}$ cells, either by inactivation of transcription factor *Stat9E* and *upd2-3* cytokines or by over-expression of *Socs36E*-the inhibitor of the JAK-STAT pathway, Bortezomib treatment-induced hyper-proliferation response was suppressed (Fig 3.15).

I next analyzed 7-day-old female *Tnks*-null as well as *Tnks*^{K598A} mutants. I only found an increase in the numbers of Arm^{+}/Pro^{-} stem cells in *Tnks*-null midguts compared to control flies (Fig 3.16A, C). However, *Tnks*^{K598A} mutant did not promote the numbers of Arm^{+}/Pros^{-} stem cells in midguts (Fig 3.16B). I did not indicate any significant change in the number of stem cells

(Fig 3.16D) and $pH3^+$ mitotic ISCs in $Tnks^{K598A}$ flies (Fig 3.16F). Furthermore, both Stat-GFP reporter activity (Fig 3.16D) and *upd3>GFP* gene expression were not induced by $Tnks^{K598A}$ (Fig 3.16E). Taken together, K598 does not involve in the ADP-ribosylation of Axin as well as its degradation *in vivo*.

I finally tested the effect of K598 residue on TNKS degradation in S2R+ cells. Unlike PARP-deficient mutants, K598A mutant still underwent proteolytic degradation in the presence of Iduna in S2R+ cells (Fig 3.17A-B). XAV939 stabilized both K598A and wild type TNKS (Fig 3.17B). Flag-tagged wild type or K598A TNKS was co-expressed with Iduna in S2R+ cells to see the PARsylation levels of TNKS. An equal amount of total proteins was pulled down via Flag beads and then immunoblotted with a PAR antibody. While there was less ADP-ribosylation in K598A compared to wild type TNKS, it was still adequate for its degradation (Fig 3.17B). Therefore, I suggest that K598 residue in the ARC4 domain may be essential for other physiological function(s) instead of Axin and TNKS ADP-ribosylation and their degradations.

3.3.6 Lysine 598 is essential for TNKS-binding to certain proteins

$Tnks^{K598A}$ knock-in mutants have several phenotypes that overlapped with *Tnks*-null mutants. To investigate the most affected molecular target(s) of K598, I conducted Co-IP-MS analysis (Fig 3.18A). I expressed Flag-tagged wild type (Fig 3.19A) or K598A TNKS (Fig 3.19B) in S2R+ cells and pulled down Flag-tagged TNKS to reveal which binding partner(s) were significantly reduced for K598A TNKS (Fig 3.18B). We then compared wild type TNKS interactome with the interactome of K598A (Fig 3.18B-C). As a result, we identified 11 proteins as the most prominently affected binding partners of TNKS.

Figure 3.17

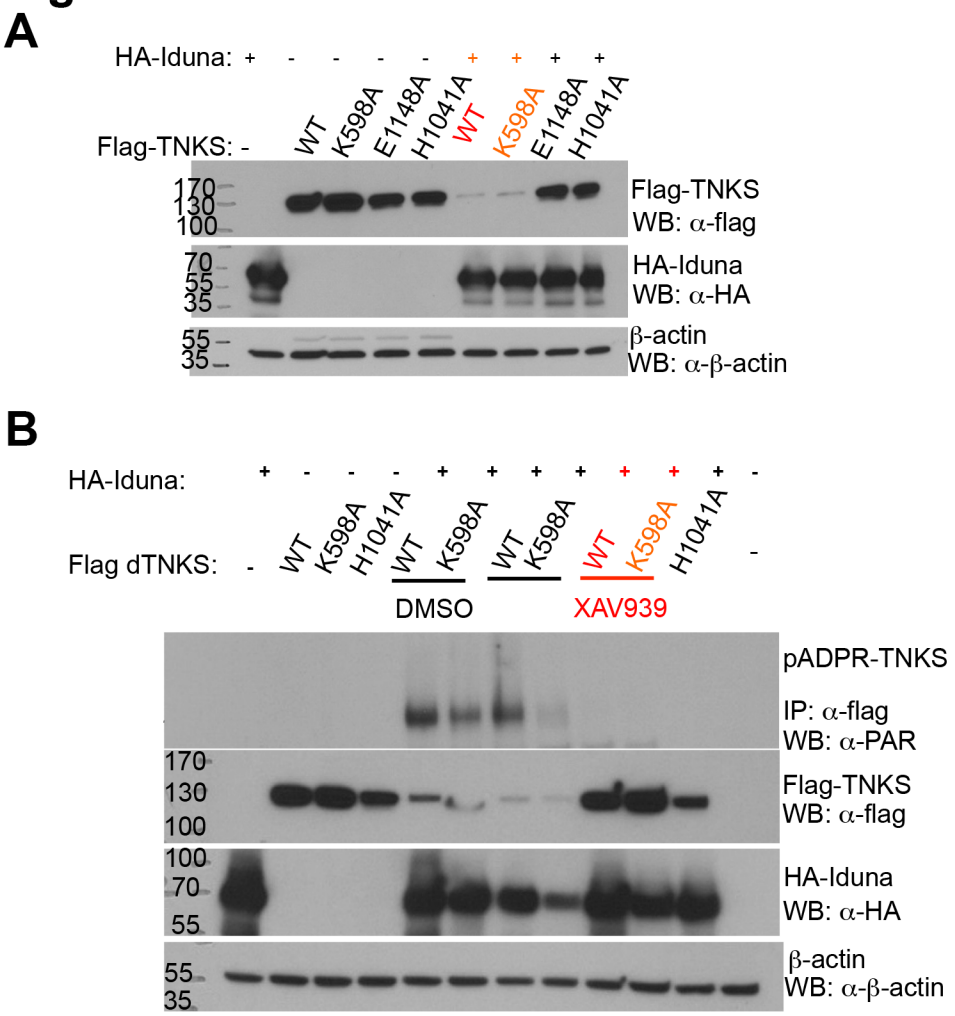

Figure 3.17 K598A TNKS is auto-poly-ADP-ribosylated and degraded in S2R+ cells. A- Iduna degraded K598A mutant in S2R+ cells, whereas PARP-deficient mutants were resistant against Iduna-dependent TNKS degradation. **B-** XAV939 treatment inhibited Iduna-mediated destruction of K598A mutant protein. TNKS wild type or the mutants were expressed in S2R+ cells. 20μM XAV939 and DMSO treatments were done 24h after transfection. Following 48 h of XAV939 treatment, S2R+ cells were collected and lysed for Western blotting against Flag-TNKS. β-actin was used as a loading control. PARsylated TNKS was detected with a PAR antibody after Flag-TNKS immunoprecipitation (IP).

Figure 3.18 IP-MS identifies 11 proteins as the most prominently affected binding partners of TNKS. **A-** MS-Based approach to identify the binding partners of *Drosophila* TNKS. **B-** Flag-peptide-eluted proteins were analyzed with silver staining before MS analysis. **C-** K598A mutation significantly reduces the binding of several proteins. S2R+ cells expressing wild type Flag-TNKS or K598A Flag-TNKS were collected for an anti-Flag Co-IP. Shown here is a volcano plot of label-free quantitative MS results. Biological triplicates were conducted and analyzed. The cut-off line for significance is P-value<0.001 ($-\log_{10}P > 3$) and fold difference $\log_2 < -1$. Statistically significant proteins were labeled in red. **D-** TNKS K598A mutation prominently reduces binding affinity of 11-proteins, identified by IP-MS. Statistically significant proteins are listed in this table. Given *p*-values represent the statistical significance, calculated from the three-independent pull-down analyses. Binding abilities of each protein to K598A TNKS are compared to the interactions with the wild type TNKS protein. Proteins name and their possible functions are searched in the Uniprot's *Drosophila* proteome.

Figure 3.18

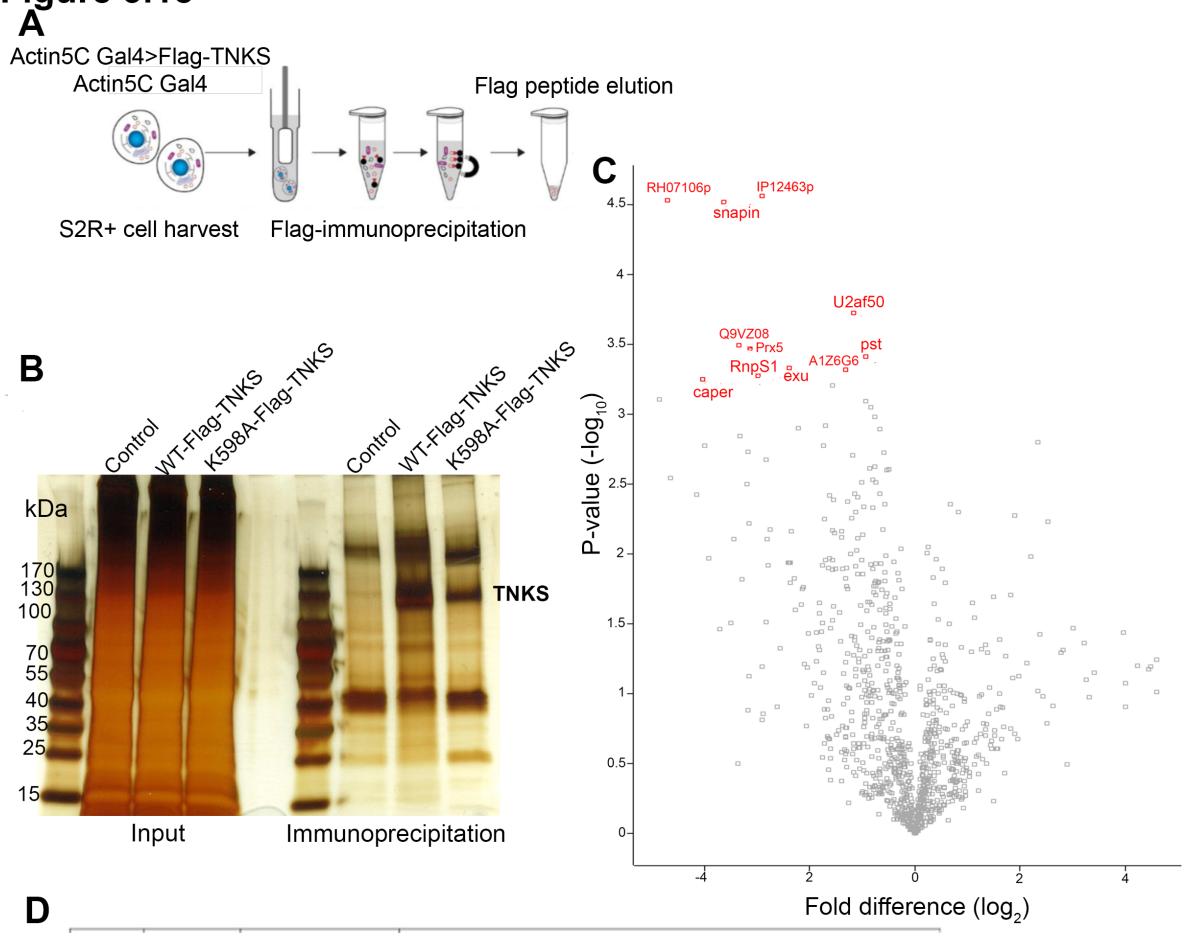

D

p value	mut vs wt	Protein name	Molecular function
4.53205	-4.70459	RH07106p	Hsp70 protein binding
3.25288	-4.03001	caper	mRNA binding, mRNA splicing, via spliceosome, positive regulation of ERK1 and ERK2 cascade, and positive regulation of Ras protein signal transduction
4.51909	-3.62254	snapin	Biogenesis of lysosome-related organelles complex-1
3.49675	-3.34514	Receptor-mediated endocytosis protein 6 homolog	Receptor-mediated endocytosis
3.46725	-3.12817	Prx5-RA	Thioredoxin peroxidase activity, negative regulation of apoptotic process, response to oxidative stress and negative regulation of innate immune response
3.27861	-2.98015	RnpS1	Negative regulation of transposition, DNA-mediated and RNA splicing
4.562	-2.90473	IP12463p	Putative cyclic GMP-AMP synthase /cADPR synthase
3.33297	-2.37962	EXU	Protein homodimerization activity, bicoid mRNA localization, anterior/ posterior axis specification, embryo and regulation of pole plasm oskar mRNA localization
3.31734	-1.31995	A1Z6G6	Scyl pseudokinases
3.72618	-1.16889	U2af50	mRNA splicing, via spliceosome, neurogenesis, nuclear export, and positive regulation of RNA export from nucleus
3.41301	-0.932608	pst	Learning or memory, olfactory learning, long-term memory and protein secretion

Figure 3.19 MS-based approach to identify wild type *Drosophila* TNKS and K598A TNKS interactomes. A- Wild type GKYDICK peptide **B-** GAYDICK peptides were detected by MS. GKYDICK peptide is in wild type TNKS, whereas GAYDICK is in K598A TNKS.

Figure 3.19

A

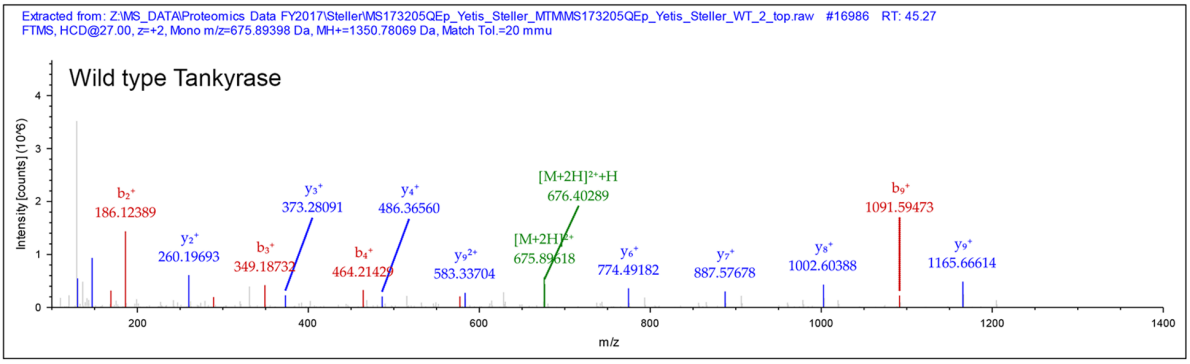

#1	b+	b2+	Seq.	y+	y2+	#2
1	58.02875	30	G			11
2	186.1237	94	K	1293.76	647.3836	10
3	349.187	175	Y	1165.665	583.3361	9
4	464.214	233	D	1002.602	501.8045	8
5	577.2981	289	I	887.5747	444.291	7
6	737.3287	369	C-Carbamidomethyl	774.4907	387.749	6
7	865.4237	433	K	614.46	307.7336	5
8	978.5078	490	L	486.365	243.6862	4
9	1091.592	546	L	373.281	187.1441	3
10	1204.676	603	L	260.1969	130.6021	2
11			K	147.1128	74.06004	1

B

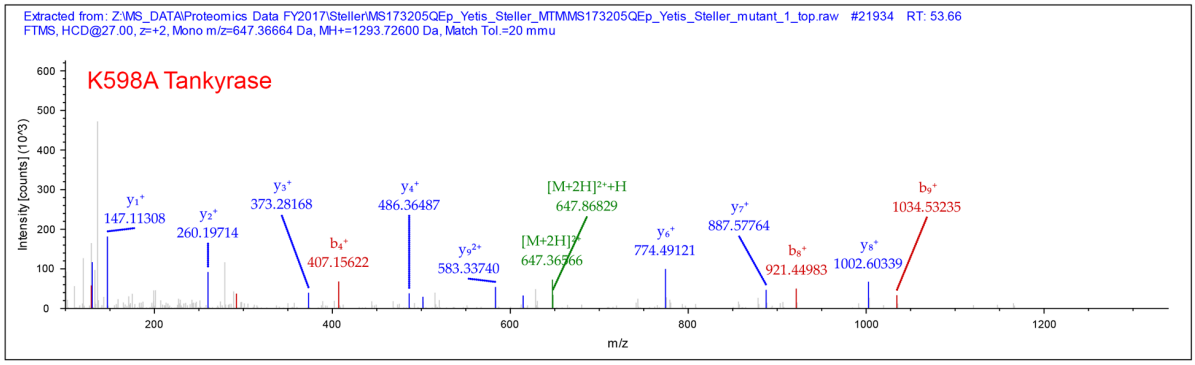

#1	b+	b2+	Seq.	y+	y2+	#2
1	58.02875	30	G			11
2	129.0659	65	A	1236.702	618.8547	10
3	292.1292	147	Y	1165.665	583.3361	9
4	407.1561	204	D	1002.602	501.8045	8
5	520.2402	261	I	887.5747	444.291	7
6	680.2709	341	C-Carbamidomethyl	774.4907	387.749	6
7	808.3658	405	K	614.46	307.7336	5
8	921.4499	461	L	486.365	243.6862	4
9	1034.534	518	L	373.281	187.1441	3
10	1147.618	574	L	260.1969	130.6021	2
11			K	147.1128	74.06004	1

These proteins are RH07106p Hsp70 binding protein, Caper, Snapin, Receptor-mediated endocytosis protein 6 homolog, Prx5, RnpS1, IP12463p putative cADPR synthase, Exu, A1Z6G6, U2af50, Pst (Fig 3.18C). These proteins have various suggested functions (3.18D). As a result, I suggested that K598 promotes the formation of complexes between TNKS and these proteins. It, therefore, points out a critical function of K598 in various biological processes. In the future, it will be interesting to investigate the functional consequences of these interactions.

3.4 Material and Methods

Fly stocks: Flies were kept at a 12-hour light/dark cycle. All crosses were performed at 22-25°C unless stated otherwise. The following fly stocks were used for this study (Bloomington Drosophila Stock Center (BDSC) and Vienna Drosophila Resource Center (VDRC) number (#) given in parentheses):

The stocks used in here: *Tnks*^{K598A} (generated in this study), *esg-Gal4, UAS-GFP* (a gift of Dr. Norbert Perrimon; Micchelli and Perrimon, 2006), *esgK606* (a gift of Dr. Norbert Perrimon; Micchelli and Perrimon, 2006), *10XStat-GFP* (Bach et al., 2007), *BAC-AxinV5* (a gift of Jean-Paul Vincent, Gerlach et al., 2014), *FRT 82B, Axn*^{h}*, BAC-AxinV5* (a gift of Jean-Paul Vincent, Gerlach et al., 2014), *UAS-GFP-Axin* (BDSC# 7224), *Myo1A-Gal4, tub-Gal80ts, UAS-GFP* (a gift of Dr. Norbert Perrimon; Micchelli and Perrimon, 2006), *upd3-Gal4, UAS-GFP* (a gift of Dr. Norbert Perrimon; Markstein et al., 2014), *Δupd2/3* (BDSC# 129), *ΔDome* (BDSC# 12030), *Tnks*^{503} (a gift of Dr. Yahsi Ahmed, Wang et al., 2016), *Tnks*^{19} (a gift of Dr. Yahsi Ahmed, Wang et al., 2016), *UAS-Tnks-HA* (a gift of Dr. Yahsi Ahmed, Wang et al., 2016), *UAS-CG8786/dIduna* RNAi#1 (BDSC# 40882), *UAS-CG8786/dIduna* RNAi#2 (VDRC#43533), *UAS-CG8786/dIduna* RNAi#3 (VDRC#36028), *UAS-CG8786/dIduna* RNAi#4 (VDRC#36029), and *white* RNAi (BDSC#33623), *fz3-Gal4* (BDSC#36520). The rest of *Drosophila* lines, which were studied here, were obtained from Steller Lab stocks. Oregon R flies were used as control and only adult female flies were analyzed in this study.

***Drosophila* egg collection:** Please refer to Chapter 2, Material and methods.

Fly Climbing: Newly eclosed male or female flies were separated and raised on standard food for 3 days or 1 month. Cohorts of 60 flies were pre-divided into 3 groups and transferred, without anesthesia, into graduated vials. The vials were gently tapped to force the flies down to

the bottom. The climbing behavior was observed for 18 s and repeated 3 times with 2-min intervals.

Low-melt fly food: This fly food was developed by Markstein et al., 2014. They developed this fly food formula for mixing drugs in low volumes. It contains low-melt agarose and standard agarose in place of agar. Low-melt fly food was prepared with distilled water containing 2% (wt/vol) autoclaved yeast, 7% (vol/vol) corn syrup, and 1.5% (wt/vol) agarose (composed of 1 part standard agarose to 11 parts of low-melt agarose). Following its sterilization, the food was stored at 4^0C, boiled and mixed as liquid with drugs at 37^0C. The resulting food-plus drug mixtures solidified at 30^0C into soft fly-edible gels.

CRISPR/Cas9 genome editing for *Tnks*^{K598A}: CRISPR optimal target finder website (tools.flycrispr.molbio.wisc.edu/targetFinder) was used to identify an appropriate guide RNA (gRNA) target sequence within TNKS-ARC4 domain (Gratz et al., 2013, 2014). I found GCAAATATCATACTTTCCCT **TGG** sgRNA to target lysine 598 in TNKS. By using the forward 5`-GTCGCAAATATCATACTTTCCCT-3` and reverse 5`-AAACAGGGAAAGTATGATATTTG-3` oligos (IDT, Inc.). I cloned the sgRNA into pCFD3-dU6:3-gRNA plasmid (Addgene, plasmid# 49410, Port et al., 2014). Transformants were verified via Sanger sequencing (Genewiz, Inc.). I purchased single strand DNA as a HDR donor sequence for **K598A** mutation- CTATGAGGTAACCGAACTGCTG GTC AAG CAC GGA GCC AAT GTA AAT GTA TCG GAT TTG TGG AAG TTT ACT CCT CTT CAT GAA GCT GCa GCa AAG GGA **gcG** TAT GAT ATT TGC AAG CTG CTC TTG AAA CAT GGC GCT GAT CCA ATG AAG AAG AAT CGG GAT GGC GCG ACA CCA (IDT, Inc). The gRNA plasmid and the HDR donor sequence were injected into 300 embryos of *Act5C*-Cas9

Drosophila (BestGene, Inc.). The injection was yielded 95 G_o progeny, and I established 125 individual fly lines, a couple of which could possibly have the *Tnks*^{K598A} mutations.

Isolation of the *Tnks*^{K598A} mutants: Total DNA was isolated from 5-day-old adults of established *K598A* lines. To screen the mutant lines, PCR fragments were amplified with specific primers (forward primer 5`-F: CCCTTGAGGGACTTACGGCCGC-3`, reverse primer 5`-CTTGTCCTGTGCATTAACATCGGCTC-3`). Amplified PCR products were then digested with Styl restriction enzyme, which gave two DNA fragments. PAM sequence mutation on sgRNA changed the restriction digestion site. Therefore, StyI did not digest the PCR product. Based on Styl-RFLP, I identified more than 10 fly lines. To verify the mutation, amplified PCR products were sent for DNA sequencing (Genewiz, Inc.).

Clone analyses and RNAi experiments: Please refer to Chapter 2, Material and methods.

Cell culture: Please refer to Chapter 2, Material and methods.

Western blot analyses: Please refer to Chapter 2, Material and methods.

Primary antibodies: anti-Flag-HRP (1/1000, Sigma-Aldrich, A8592), anti-Flag (1/1000, CST, D6W5B 14793), anti-PAR (1/1000, Trevigen, 4335-MC-100), anti-Myc tag (1/1000, CST, 9B11, 2276), anti-Axin Drosophila (Santa Cruz, dT20, sc15685), anti-tubulin DM1A clone (1/1000, Sigma-Aldrich, T9026), mouse anti-GFP-HRP (1/2500, clone B2, Santa Cruz Biotechnology, sc-9996-HRP), rabbit anti-β-Actin-HRP (1/5000, clone 13E5, Cell Signaling Technology, 5125), donkey anti-rabbit-HRP (1/5000, Jackson ImmunoResearch, 711-035-152), donkey anti-mouse-HRP (1/5000, Jackson ImmunoResearch, 715-035-150), donkey anti-guinea pig-HRP (1:5000, Jackson ImmunoResearch, 706 006 148).

Immunofluorescence: Please refer to Chapter 2, Material and methods.

Primary antibodies: mouse anti-Arm (Wang et al., 2016; N2 7A1, DSHB, 1:50), mouse anti-Prospero (Wang et al., 2016; MR1A, DSHB, 1/50), mouse anti-GFP (GFP-12A6, DSHB, 1/100), mouse anti-β-galactosidase (Tian et al., 2016); 401A, DSHB, 1/100), mouse anti-Delta (Wang et al., 2016; C594.9B, DSHB, 1/100), rabbit anti-phosho-S10-Histone3 (Wang et al., 2016; 06-570, Millipore, 1/1000). The secondary antibodies were goat anti-mouse-Alexa 488 plus (Thermo Fisher Scientific, A32723), goat anti-mouse-Alexa 568 (Thermo Fisher Scientific, A11031), goat rabbit-Alexa 546 (Thermo Fisher Scientific, A11035), goat rabbit-Alexa 488 (Thermo Fisher Scientific, A11034), goat anti-rabbit-Alexa 633 (Thermo Fisher Scientific, A21071) and used at 1/1000.

Immunoprecipitation: Please refer to Chapter 2, Material and methods.

Recombinant protein purification from S2R+ cells: Please refer to Chapter 2, Material and methods.

Expression and Purification of of human NUDT16: 1.5 ml of transformed Rosetta2 (DE) cells were grown in terrific broth (TB) medium in the presence of 100µg/ml kanamycin and 34µg/ml chloramphenicol at 37◦C. When the absorbance (A) reached 2.0, the temperature was decreased to 18^0C. When the A reached 3.0, the expression of recombinant protein was induced with 0.2mM IPTG and continued overnight. Bacterial pellet was prepared by centrifuge at 5000 rpm for 5 minutes. The pellet were then re-suspended in a buffer composed by 20mM Tris/HCl, pH 8.0, 150mM NaCl, 10mM imidazole, 5µM 2-mercaptoethanol, 10% glycerol and supplemented with Complete Protease Inhibitor (Roche). Re-suspended bacterial pellet was then sonicatated in order to lyse bacterial cells. After 10-15 min ice incubation, the lysate was clarified by centrifugation and supernatant applied on 5ml of Cobalt beads (GE Healthcare) for affinity purification. The histidine-tagged hNUDT16 was eluted in 300mM imidazole. Finally, the

elution buffer of the protein was exchanged with a buffer composed of 25mM Tris, pH 8.0, 300mM NaCl, 10%glycerol and 1mM DTT. Proteins were then concentrated to 10mg/ml using 10 kDa Amicon-Ultra centrifugal filter (Millipore).

***In vitro* ADP-ribosylation:** 20 mgs of Flag-tagged *Drosophila* TNKS protein (purified from S2R+ cells) were automodified in 100 µL of a reaction buffer containing 100mM Tris-HCl pH 8.0, 10mM MgCl2, 10mM DTT, 25µM NAD+ for 1h at 24-25°C.

hNUDT16 digestion: After the auto-modification reaction of TNKS, 5 µL of purified hNUDT16 was added to digest TNKS-bound pADPr (3h at 30 °C). The $MgCl_2$ (Sigma) concentration was adjusted to 15mM to allow full Nudix hydrolase activity. Auto-modified TNKS was then incubated for 3h at 30^0C with hydrolytic enzymes in 10 µl of reaction mixture.

Mass spectrophotometry for ADP-ribose acceptor side identification: Flag-TNKS was purified from S2R+ cells and 60mg ADP-ribosylated *in vitro*. After ADP-ribosylation, it was incubated with hNUDT16 for 3h at 30^0C. After enzymatic reactions, proteins were precipitated by cold acetone. Pellets were dissolved in 6M guanidium-chloride (Sigma), reduced with TCEP (Pierce) and alkylated with chloroacetamide (Sigma). After a 10-fold dilution with 50mM ammonium bicarbonate (Fluka), proteins were digested using 200ng of trypsin Gold (Promega) for 16 h at 37◦C. Samples were then desalted. Later, dried samples were reconstituted in 5 µL of 0.1% trifluoroacetic acid (TFA) and 25 µL of 6%TFA/80%ACN. Twenty microliters of a 10mg/mL water solution of TiO2 (ZirChrom Separations, Inc.) beads was added to a homemade gel-loading tip that contained a glass fiber frit. Gentle air pressure supplied from a syringe was applied to speed the flow of solvent and beads were always left wet. Ten microliters of 6%TFA/80%ACN was used to wash the beads. Sample was passed through the column three times and the final elute was collected. Two wash steps were each performed twice: first with 10

μL of 6%TFA/80% ACN followed by 10 μL of 0.1% TFA. Each wash elute was collected. Ten microliters of 5% ammonium hydroxide was used to elute the capture peptides. Sixty microliters of 2% FA was used to immediately adjust the final elution pH. All samples were dried to near completion and reconstituted in 5% ACN/ 0.1% FA for mass spectrometry analysis. MS was performed by The Rockefeller University Proteomics core facility.

Co-IP Mass spectrophotometry to identify TNKS-binding partners: S2R+ cells were transfected with *Act5C-Gal4* and *UAS-Flag-Tnks* or *UAS-Flag-K598A-Tnks*. After 72h, S2R+ cells were collected and. *Act5C-Gal4* expressing S2R+ cells were used as a negative control in IP experiment. Both Flag-tagged TNKS and *Act5C-Gal4* expressing cells were lysed and immunoprecipitated with Flag beads in lysing buffer. Finally, IP samples (3 from control and 3 from Flag-TNKS expression) were eluted with Flag-peptide. Eluted proteins were cleaned up by using SDS-PAGE, reduced (10mM DTT) and alkylated (30mM iodoacetamide), followed by digestion with a cocktail of LysC and Trypsin Gold. Digestions were halted by adding trifluoroacetic acid (TFA) and digests then were desalted and analyzed by reversed phase nano-LC-MS/MS using either a Fusion Lumos or a Q-Exactive Plus (Thermo Fisher Scientific) both operated in high/high mode. Data were searched and quantified against Uniprot's *Drosophila* proteome databases using ProteomeDiscoverer v. 1.4.0.288 (Thermo Scientific) combined with Mascot v. 2.5.1 (Matrix Science) and/or MaxQuant v. 1.6.0.13. Oxidation of methionine and protein N-terminal acetylation were allowed as variable modifications and all cysteines were treated as being carbamidomethylated. Peptide matches were filtered using a Percolator-calculated false discovery rate (FDR) of 5%.

Statistics: Student *t-test* and ANOVA were used as statistical analysis and those were done with Prism (GraphPad) software.

Acknowledgment: Dr. Milica Tesic Mark from The Rockefeller University proteomics core facility, conducted MS analyses for ADP-ribose acceptor side identification as well as TNKS-interactome.

4 ADP-ribosylation by TNKS provides a molecular scaffold for rapid protein degradation

4.1 Summary

ADP-ribosylation affects the fate of proteins by directly modulating their activity or stability. By and large, TNKS-mediated poly-ADP-ribosylation is tightly coupled to the 26S proteasome-mediated proteolysis. Auto-poly-ADP-ribosylation is an inhibitory post-translational modification for TNKS as well. Here, I find that the ubcD1 E2 ubiquitin-conjugating enzyme (an E2 ubiquitin ligase) participates in Iduna-dependent TNKS degradation by binding to a poly-ADP-ribose scaffold. Strikingly, adding low concentration of poly-ADP-ribose polymers provides a signal to stimulate auto-ubiquitylation of Iduna in the presence of ubcD1. Similarly, ubcD1 promotes Iduna-dependent ubiquitylation of PARsylated TNKS *in vitro*. *ubcD1*-RNAi results in elevation of Iduna, Tankyrase, and Axin proteins in *Drosophila*. These results demonstrate that ubcD1 mediates Iduna-dependent degradation of certain proteins. Finally, TNKS can colocalize with active 26S proteasomes in the *Drosophila* midgut. Inhibition of PARP activity by XAV939 suppresses this co-localization. As a result, I suggest that poly-ADP-ribosylation may play a role as a molecular scaffold that brings together TNKS, ubcD1 E2 ubiquitin-conjugating enzyme, Iduna E3 ubiquitin ligase, and the substrates to close proximity for rapid degradation of target proteins.

4.2 Introduction

As one of the poly-ADP-ribose polymerases (PARPs), TNKS consumes NAD+ to synthesize poly-ADP-ribose (PAR). Although TNKS-mediated poly-ADP-ribosylation (PARsylation) is largely associated with the 26S proteasome-mediated protein degradation, it can also promote the activity of several proteins. TNKS-mediated PARsylation of PI31 and JNK enhances proteasome assembly and signal transduction, respectively rather than destruction of PI31 and JNK in *Drosophila* (Park and Steller, 2013; Li et al., 2019). Furthermore, several TNKS-interacting proteins do not undergo PARsylation. GDP-mannose-4, 6-dehydratase is a cytoplasmic TNKS1 binding-protein that inhibits PARP activity of TNKS (Bisht et al., 2012).

PAR is a negatively charged biopolymer that has an impact on protein stability as well as degredation. TNKS can reside in multiple subcellular localizations and participate in various biological processes including telomere homeostasis, and Wnt/β-catenin signaling. In 3T3-L1 adipocytes, TNKS localizes in GLUT4 vesicles near the Golgi (Chi and Lodish, 2000). PARsylation can also recruit PAR-binding proteins into a close proximity. PAR-binding proteins, ``PAR readers``, recognize PAR polymers through PAR-binding motif (PBM). Following the PAR reading, certain proteins co-localize on the PAR scaffold to assemble protein complexes during stress granule formation, DNA repair and ribosomal RNA maturation (McGurk et al., 2018; Duan et al., 2018; Boamah et al., 2012; Caldecott, 2014; Fatokun et al., 2014; Hotiger et al., 2015; Hsiao and Smith, 2008; Krietsch et al., 2013; Teloni and Altmeyer, 2016; Catara et al., 2017; Isabella et al., 2012; Leung et al., 2011). For instance, nuclear PARP1 facilitates ribosomal RNA (r-RNA) biogenesis in *Drosophila*. PARP1 becomes automodifed upon each act of transcription start within r-RNA gene. Auto-PARsylated PARP1 serves as a chaperoning machine during the whole cycle of ribosome maturation in the nucleus. The

dynamic PARP1-mediated PAR scaffold brings a subset of nucleolar proteins to the proximity of precursor r-RNA and coordinates the order of events including r-RNA processing, modification and loading of subsets of ribosomal proteins to mature pre-ribosome in *Drosophila* (Boamah et al., 2012). Depletion of *Parp* leads to removal of PAR-binding proteins from nucleoli, which disrupt processing, modification, and folding of ribosomal RNA in *Drosophila* (Boamah et al., 2012).

In this chapter, I demonstrated that ubcD1 E2 ubiquitin ligase is involved in Iduna-dependent TNKS degradation. Loss-of *ubcD1* resulted in an elevation of mis-expressed Iduna, and TNKS as well as endogenous Axin in *Drosophila*. I found that the E2 ubiquitin ligase ubcD1 promotes auto-ubiquitylation of Iduna in the presence of PAR. However, ubcD1 does not interact with Iduna or TNKS, ubcD1 plays a role in Iduna-dependent TNKS ubiquitinylation. Moreover, ubcD1 is capable of binding ADP-ribose scaffold because of its PAR-binding motifs. I finally showed that TNKS co-localizes with active 26S proteasomes in the *Drosophila* midgut. Taken together, I provided evidence that ADP ribosylation by TNKS brings ubcD1, Iduna, and the target protein into close proximity for accelerating degradation of the target protein.

4.3 Results

4.3.1 Proteomic screen to identify TNKS-binding partners for the regulation of its stability

TNKS-mediated PARsylation is mainly related to UPS-mediated protein destruction. PARsylation destabilized both TNKS itself and Axin by recruiting a PAR-directed E3 ubiquitin ligase Iduna in *Drosophila* (Gultekin and Steller, 2019). Thanks to PAR reader proteins, ADP-ribosylation can mediate the assembly of protein complexes. Therefore, I suggest that ADP-ribosylation provided by TNKS may provide a molecular scaffold for rapid degradation of TNKS itself or its substrates. To this end, I conducted a Co-IP-MS of Flag-tagged TNKS to identify its binding partners.

The *Drosophila* TNKS interactome was then narrowed down to the proteins, related to the Ubiquitin-Proteasome system since they might regulate TNKS degradation. I found that the E2 ubiquitin-conjugating enzymes Ben and Morgue, E3 ubiquitin ligase Iduna, deubiquitinating enzymes (DUBs) Usp30 and Usp10, and finally 19S proteasome subunits Rpt1, 2, 3, and 6 were significantly co-immunoprecipitated with Flag-tagged TNKS in S2R+ cells (Table 4.1). I assessed an RNAi-based validation screen to ask if these binding-partners might be involved in TNKS degradation. HA-tagged TNKS-expressing transgenic flies were crossed with RNAi lines under the temperature sensitive *Tub-Gal4* driver. HA-tagged TNKS was then detected via immunoblotting from whole-body protein lysate. A screen for compatible E2 ubiquitin conjugating enzymes in an *in vitro* RNF146 auto-ubiquitinylation assay reveals UbcH5a as a functional partner for human Iduna (Zhang et al., 2011). *Drosophila ubcD1* is ortholog of the human *UbcH5a* gene. Although, Flag-TNKS did not pull down ubcD1 in my IP-MS, I included *ubcD1* gene into the RNAi screen (Fig 4.2A).

Table 4.1 *Drosophila* TNKS interactome that can be related to TNKS ubiquitinylation and degradation. *Drosophila* Tankyrase interactome is narrowed down to the proteins that can be related to TNKS degradation. Flag-tagged TNKS was expressed under Act5C-Gal4 driver in S2R+ cells and pulled down with Flag beads.

Protein partner	P value ($-\log_{10}$)	Fold difference ($\log_2$)
TNKS (bait)	4.96	10.67
Ubiquitin carboxyl-terminal hydrolase 30 homolog (Usp30)	3.61	4.87
Ubiquitin-conjugating enzyme E2 N (Ben)	2.10	2.21
Usp10	2.41	2.18
Morgue	2.53	1.99
Iduna	2.03	1.10
Rpt6	1.67	1.03
Rpt1	3.02	1.04
Rpt3	3.20	0.77
Rpt2	2.15	0.59

Figure 4.1 ubcD1 plays a role in TNKS degradation. A- Both Usp30 and Usp10 have roles in the regulation of TNKS protein stability. *Usp10* depletion by RNAi resulted in TNKS elevation. Decrease in the *Usp30* gene dosage by half resulted in reduction in the protein level of TNKS. **B-** RNAi-mediated *ubcD1* inactivation led to an elevation of HA-tagged TNKS protein**.** *UAS-HA-Tnks* transgene was expressed under the temperature sensitive *Tub-Gal4* driver. 7-day-old adult females were lysed. Western blotting was done with an anti-HA antibody**. C-** *ubcD1* knockdown also resulted in an accumulation of PARsylated TNKS. Western blot was performed with an anti-PAR antibody. a-Tubulin was a loading control. **D-** *ubcD1* deficient larvae had more HA-tagged TNKS. 3rd instar larvae were dissected and midguts were stained against HA and Armadillo. **E-** *ubcD1* knockdown resulted in elevation of HA-tagged TNKS as well as PAR polymers in adult midguts. 7-day-old adult females were dissected. Dissected midguts were stained against HA and PAR.

Figure 4.1

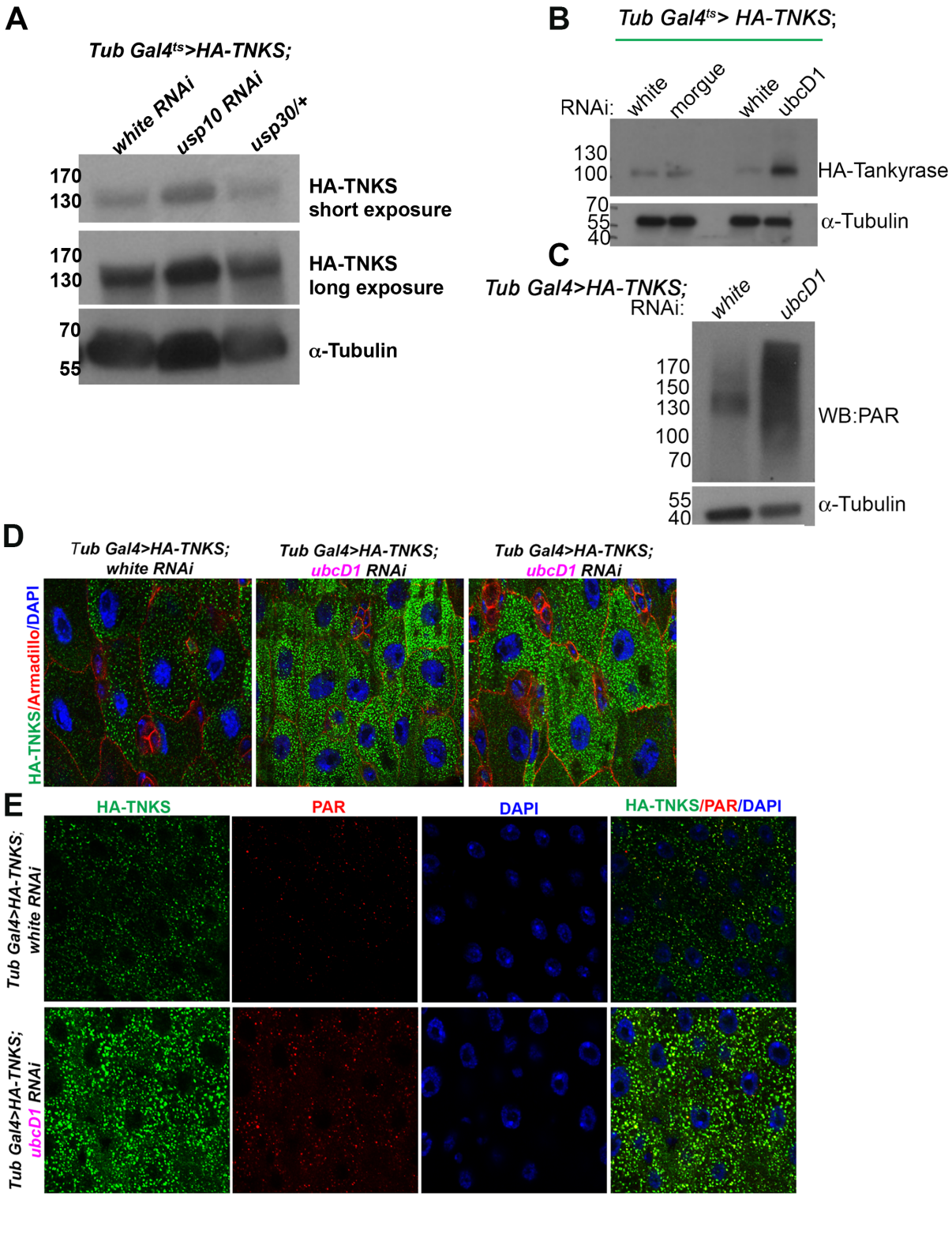
A
Tub Gal4ts>HA-TNKS;
white RNAi
usp10 RNAi
usp30/+
170
130
HA-TNKS
short exposure
170
130
HA-TNKS
long exposure
70
55
α-Tubulin
B
Tub Gal4ts> HA-TNKS;
RNAi:
white
morgue
white
ubcD1
130
100
HA-Tankyrase
70
55
40
α-Tubulin
C
Tub Gal4>HA-TNKS;
RNAi:
white
ubcD1
170
150
130
100
70
WB:PAR
55
40
α-Tubulin
D
Tub Gal4>HA-TNKS;
white RNAi
Tub Gal4>HA-TNKS;
ubcD1 RNAi
Tub Gal4>HA-TNKS;
ubcD1 RNAi
HA-TNKS/Armadillo/DAPI
E
HA-TNKS
PAR
DAPI
HA-TNKS/PAR/DAPI
Tub Gal4>HA-TNKS;
white RNAi
Tub Gal4>HA-TNKS;
ubcD1 RNAi

I found that *Usp10* depletion by RNAi resulted in TNKS elevation. In contrast, reducing the *Usp30* gene dosage by half led to decrease in the protein level of TNKS (Fig 4.1A). These results suggested that both both Usp30 and Usp10 have roles in the regulation of TNKS protein stability. On the other hand, *morgue*-RNAi did not cause any change in the protein level of TNKS. Since Morgue has a putative TNKS-binding motif, RNAi result can suggest that Morgue ubiquitin-conjugating enzyme may work together with TNKS to regulate protein stability of one of the target proteins of TNKS. However, RNAi-mediated *ubcD1* inactivation led to an elevation of HA-tagged TNKS (Fig 4.1B). *ubcD1* knockdown also resulted in an accumulation of PARsylated TNKS (Fig 4.1C). Finally, both larval (Fig 4.1D) and adult midguts (Fig 4.1E) had more HA-tagged TNKS as well as PAR polymers when *ubcD1* was depleted (Fig 4.1E).

4.3.2 ubcD1 promotes TNKS degradation

ubcD1 also known as *effete*, encodes a 147-amino acid ubiquitin-conjugating enzyme that is similar to the mammalian ubcH5 class (Fig 4.2A). As a result of amino acid sequence alignment, ubcD1 is conserved from flies to human (Fig 4.2B). I next assessed if *ubcD1* genetically interacted with Iduna, by crossing *ubcD1*-RNAi flies to *Myo1A^{ts}>UAS-GFP-Myc-Iduna*. I found that inactivation of *ubcD1* resulted in an elevation of Iduna protein (Fig 4.3A-B). Hence, ubcD1 promotes ubiquitinylation activity of Iduna in *Drosophila*.

By and large, ubiquitin ligases physically interact with their ubiquitin-conjugating enzymes to transfer ubiquitin to their substrates. To test if ubcD1 protein interacted with Iduna, I carried out a Co-IP assay. ubcD1 and Iduna co-expressing flies were lysed to pull down AcGFP-Iduna. Surprisingly, Iduna did not co-immunoprecipitate with ubcD1 in *Drosophila* (Fig 4.3C).

Figure 4.2

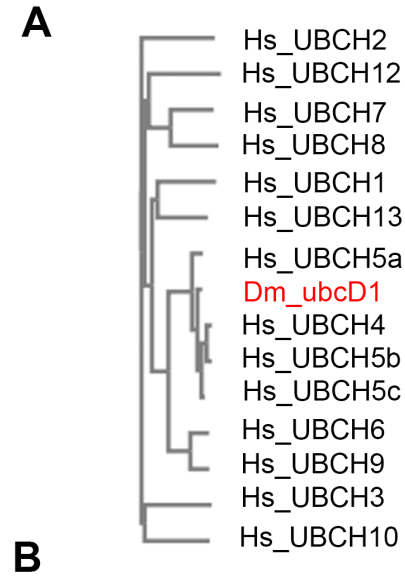


```
Hs_UbcH5a       MALKRIQKELSDLQRDPPAHCSAGPVGDDLFHWQATIMGPPDSAYQGGVFFLTVHFPTDY   60
Mm_UBCH5a       MALKRIQKELSDLQRDPPAHCSAGPVGDDLFHWQATIMGPPDSAYQGGVFFLTVHFPTDY   60
Bt_UBCH5a       MALKRIQKELSDLQRDPPAHCSAGPVGDDLFHWQATIMGPPDSAYQGGVFFLTVHFPTDY   60
Dm_ubcD1        MALKRINKELQDLGRDPPAQCSAGPVGDDLFHWQATIMGPPDSPYQGGVFFLTIHFPTDY   60
                ******:***.** *****:********************** *********:******

Hs_UbcH5a       PFKPPKIAFTTKIYHPNINSNGSICLDILRSQWSPALTVSKVLLSICSLLCDPNPDDPLV   120
Mm_UBCH5a       PFKPPKIAFTTKIYHPNINSNGSICLDILRSQWSPALTVSKVLLSICSLLCDPNPDDPLV   120
Bt_UBCH5a       PFKPPKIAFTTKIYHPNINSNGSICLDILRSQWSPALTVSKVLLSICSLLCDPNPDDPLV   120
Dm_ubcD1        PFKPPKVAFTTRIYHPNINSNGSICLDILRSQWSPALTISKVLLSICSLLCDPNPDDPLV   120
                ******:****:****************************:**********************

Hs_UbcH5a       PDIAQIYKSDKEKYNRHAREWTQKYAM      147
Mm_UBCH5a       PDIAQIYKSDKEKYNRHAREWTQKYAM      147
Bt_UBCH5a       PDIAQIYKSDKEKYNRHAREWTQKYAM      147
Dm_ubcD1        PEIARIYKTDREKYNELAREWTRKYAM      147
                *:**:***:*:****. *****:****
```

Figure 4.2 ubcD1 is conserved from flies to human. **A-** *ubcD1/effete* encodes a 147-amino acid ubiquitin-conjugating enzyme that a member of mammalian ubiquitin-conjugating ubcH5 class. *Hs, Homo sapiens; Mm, Mus musculus; Bt, Bos taurus; Dm, Drosophila melanogaster.* Amino acid sequences were aligned and pyhlogenetic tree was drawn with Clustal Omega software. **B-** ubcD1 is conserved from flies to human.

Figure 4.3 ubcD1 regulates the ubiquitin ligase activity of Iduna. A- *ubcD1* knockdown elevated AcGFP-Iduna in *Drosophila* midguts. **B-** The quantification of AcGFP-Iduna protein levels upon *ubcD1*-RNAi. *UAS-AcGFP-Myc-Iduna* transgene was expressed under the temperature sensitive *Myo1A-Gal4* driver. 7-day-old adult females were lysed. Western blotting was done with an anti-GFP antibody**. C-** Iduna did not pull down ubcD1. *UAS-AcGFP-Myc-Iduna* or *UAS-ubcD1-HA* or *UAS-AcGFP-Myc-Iduna, UAS-ubcD1-HA* transgenes were expressed under the temperature sensitive *Tub-Gal4* driver. 7-day-old adult females were lysed. Immunoprecipitation was conducted with anti-GFP antibody Western blotting was done with GFP and HA antibodies.

Figure 4.3

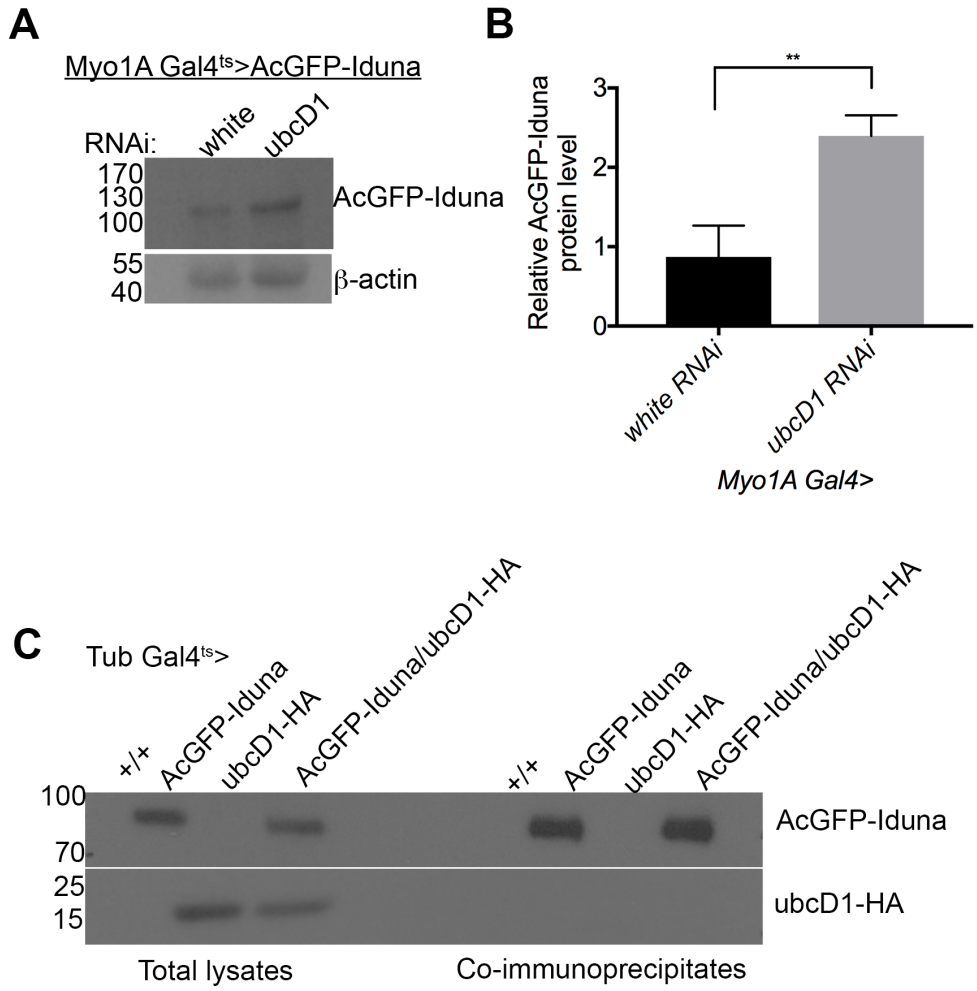
A
Myo1A Gal4ts>AcGFP-Iduna
RNAi:
white
ubcD1
170
130
100
AcGFP-Iduna
55
40
β-actin
B
Relative AcGFP-Iduna protein level
**
3
2
1
0
white RNAi
ubcD1 RNAi
Myo1A Gal4>
C
Tub Gal4ts>
+/+
AcGFP-Iduna
ubcD1-HA
AcGFP-Iduna/ubcD1-HA
100
70
25
15
AcGFP-Iduna
ubcD1-HA
Total lysates
Co-immunoprecipitates

This result suggests Iduna may not directly bind to ubcD1 and TNKS or PAR modification may be required for ubcD1 and Iduna to interact.

To determine if ubcD1 directly mediated Iduna auto-ubiquitylation, I reconstituted ubiquitylation reaction *in vitro* by using recombinant E1, ubcD1, and Iduna. Ubiquitinylation of Iduna was detected by immunoblotting against GST-ubiquitin. In this assay, ubcD1 slightly promoted Iduna auto-ubiquitinylation. In the presence of PAR polymers, ubcD1 induced auto-ubiquitinylation of Iduna (Fig 4.4A).

Next, PARsylated TNKS was used to test if ubcD1 was required for the substrate ubiquitinylation of Iduna. Following TNKS ADP-ribosylation *in vitro,* a ubiquitinylation assay was conducted. I found that ubcD1 together with Iduna ubiquitinylated PARsylated TNKS (Fig 4.4B). These results demonstrate that ubcD1 participates in Iduna-dependent ubiquitinylation and PAR or substrate PARsylation promotes this activity.

4.3.3 ubcD1 can bind to PAR polymer

Although TNKS interacts with its protein partners through TBM, ubcD1 does not have a canonical TBM motif. Since ubcD1 did not bind to Iduna directly, I suggested that ubcD1 might bind to the PAR polymer. The most common PAR-binding module is the PBM (Teloni and Altmeyer, 2016). Alignment of the PBM $[HKR]_1$-x_2-x_3-$[AIQVY]_4$-$[KR]_5$-$[KR]_6$-$[AILV]_7$-$[FILPV]_8$ to ubcD1 revealed that it had two putative PBMs: One PBM is MALKRINK in the amino terminus and the second PBM is LAREWTRKYAM found in the carboxyl end of *Drosophila* ubcD1 protein (Fig 4.5A). *UAS-ubcD1-HA* was expressed in the fly midgut. Under denaturating conditions, I observed that ubcD1-HA co-immunoprecipitated with PAR polymers from fly lysates (Fig 4.5B).

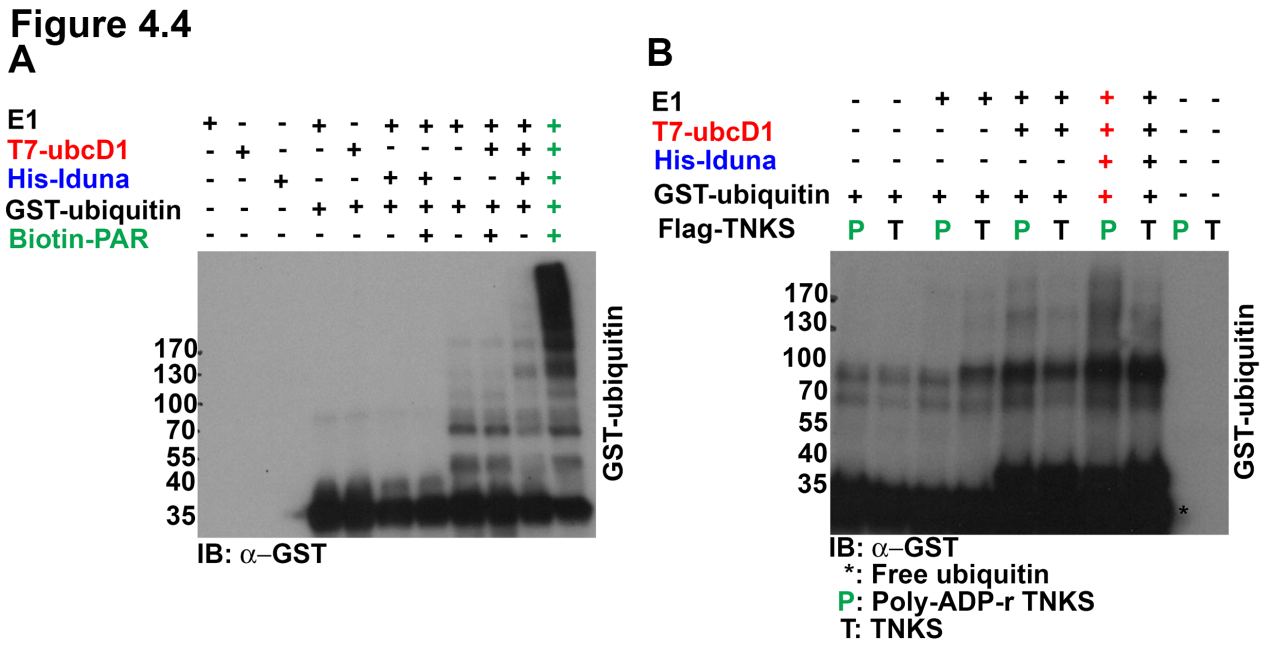

Figure 4.4 ubcD1 directly mediates Iduna-dependent ubiquitinylation in the presence of PAR. **A-** The reconstitution of ubiquitinylation reaction *in vitro* by using recombinant E1, ubcD1, and Iduna. Auto-ubiquitinylation of Iduna was detected by GST-immunoblotting. **B-** ubcD1 is involved in Iduna-dependent ubiquitylation of TNKS. Ubiquitinylation was reconstituted *in vitro* using recombinant E1, ubcD1, and Iduna. Flag-tagged TNKS was purified from S2R+ cells and was ADP-ribosylated *in vitro*. Ubiquitylation was detected by GST-immunoblotting.

Figure 4.5 ubcD1 binds to PAR polymer through PAR-binding motifs. A- *Drosophila* ubcD1 aligned with a canonical PBM that suggested the existence of two PBMs**,** PBM1-MALKRINK at the amino terminus and PBM2-LAREWTRKYAM at the carboxyl terms. **B-** ubcD1-HA co-immunoprecipitated with PARsylated proteins from fly lysates. *UAS-ubcD1-HA* transgene was expressed under *Myo1A-Gal4* driver. 7-day-old adult flies were dissected and midguts were lysed for immunoprecipitation. IP and IB were done with anti-HA and anti-PAR antibodies, respectively. IgG pull down was a negative control. **C-** ubcD1 bound to PAR. Recombinant GST-tagged ubcD1 was spotted onto a nitrocellulose membrane with a negative control GST and incubated with biotin-PAR polymers. Dot blot was carried with an anti-streptavidin antibody.

Figure 4.5

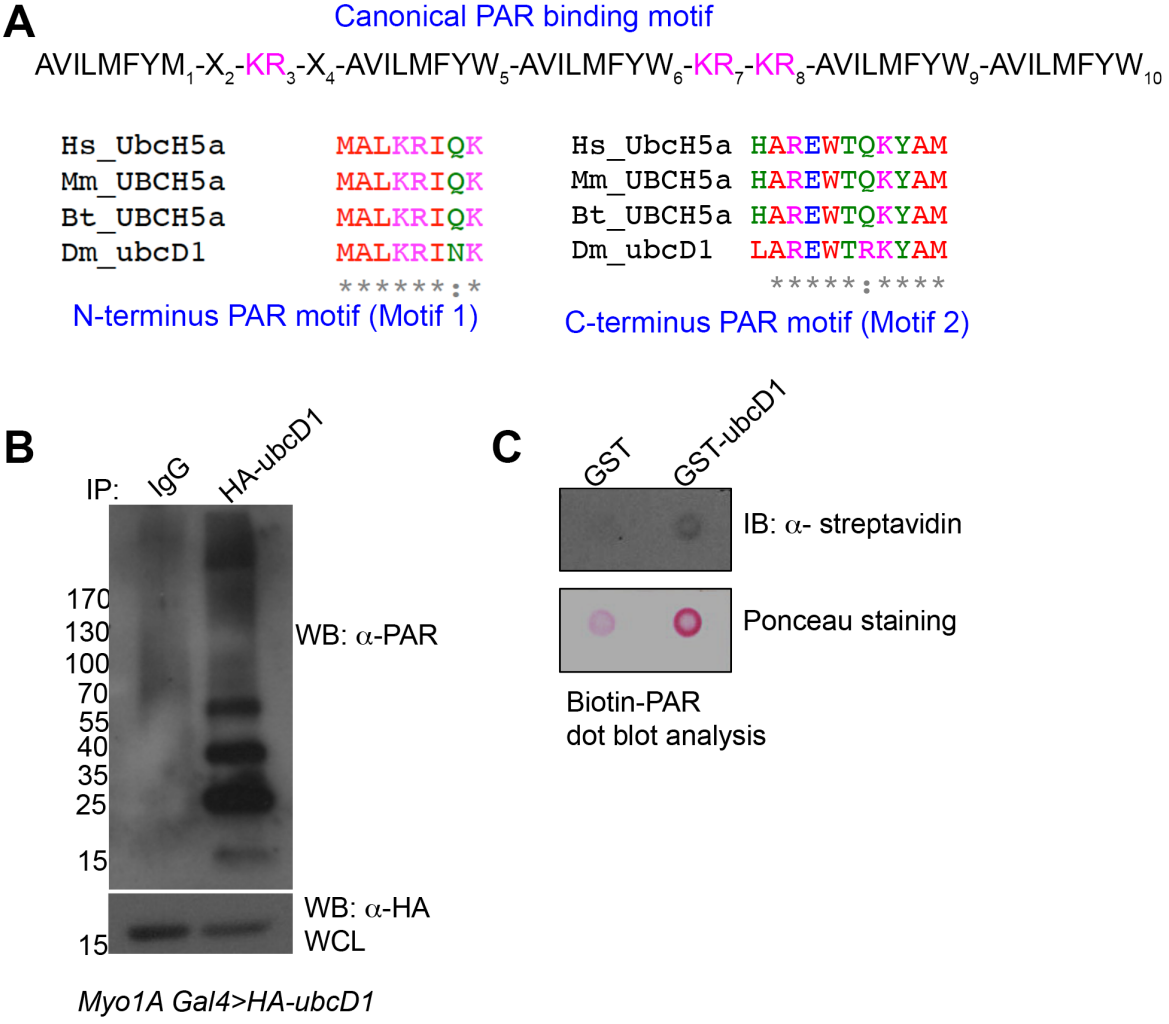
A
Canonical PAR binding motif
AVILMFYM1-X2-KR3-X4-AVILMFYW5-AVILMFYW6-KR7-KR8-AVILMFYW9-AVILMFYW10
Hs_UbcH5a MALKRIQK
Mm_UBCH5a MALKRIQK
Bt_UBCH5a MALKRIQK
Dm_ubcD1 MALKRINK
Hs_UbcH5a HAREWTQKYAM
Mm_UBCH5a HAREWTQKYAM
Bt_UBCH5a HAREWTQKYAM
Dm_ubcD1 LAREWTRKYAM
N-terminus PAR motif (Motif 1)
C-terminus PAR motif (Motif 2)
B
IP: IgG
HA-ubcD1
170
130
100
70
55
40
35
25
15
WB: α-PAR
WB: α-HA
WCL
15
Myo1A Gal4>HA-ubcD1
C
GST
GST-ubcD1
IB: α- streptavidin
Ponceau staining
Biotin-PAR
dot blot analysis

Figure 4.6 *ubcD1* inactivation promotes stem cell division in the *Drosophila* midgut. A- There were slightly more *esg>GFP*$^{+}$ stem and progenitor cells in FRT82B, *ubcD1*$^{-/-}$ clones compared to FRT82B control clones. 7-day-old adult females were dissected to analyze *esg-GFP*+ cells. **B-** *ubcD1*-RNAi midguts had more Arm^{+}/Pros^{-} stem cells compared to *white*-RNAi. UAS-RNAi flies crossed with *Myo1A-Gal4* lines. 7-day-old females were dissected to analyze stem cell numbers by confocal microscopy. Dissected midguts were stained with anti-Armadillo and Prospero antibodies. Posterior midguts were imaged with a confocal microscope. **C-** *ubcD1*-RNAi resulted in elevation of endogenous Axin. **D-** The quantification of pH3^{+}-stained cells in midguts. 7-day-old female flies were analyzed by pH3 immunostaining. pH3^{+} cells were counted in posterior midguts. **E-** *ubcD1*-RNAi induced an *upd3>GFP* reporter compared to *white* knock-down. 14-day-old posterior midguts were analyzed with a confocal microscope for *upd3>GFP*. Statistical analyses was done with the Two-tailed Student`s *t-test*. n>5. ****$p>0.0001$. Statistics represented as mean ± s.d. Scale bar: 10μm.

Figure 4.6

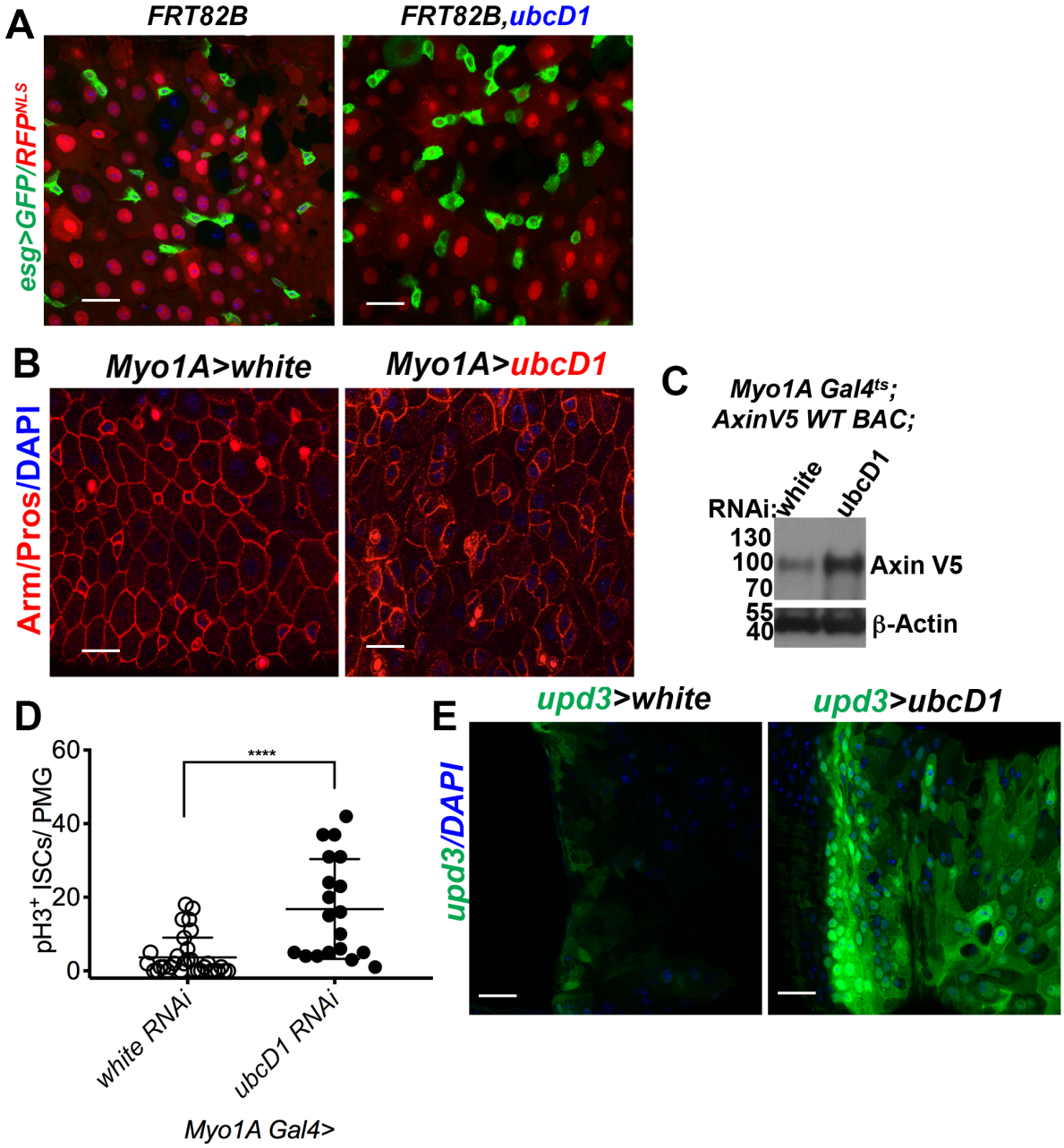
A
FRT82B
FRT82B,ubcD1
esg>GFP/RFP^NLS
B
Myo1A>white
Myo1A>ubcD1
Arm/Pros/DAPI
C
Myo1A Gal4^ts;
AxinV5 WT BAC;
RNAi: white
ubcD1
130
100
70
55
40
Axin V5
β-Actin
D
pH3+ ISCs/ PMG
60
40
20
0
****
white RNAi
ubcD1 RNAi
Myo1A Gal4>
E
upd3>white
upd3>ubcD1
upd3/DAPI

To ascertain whether ubcD1 could bind to PAR, I carried out a PAR-binding dot blot. Recombinant GST-tagged ubcD1 was spotted onto a nitrocellulose membrane with a negative control GST and incubated with the biotin-PAR polymer. After immunoblotting with an anti-streptavidin antibody, I found that ubcD1 bound to PAR (Fig 4.5C). These data suggest that ubcD1 is capable of binding ADP-ribose scaffold to mediate Iduna-dependent ubiquitinylation.

I previously showed that both *Tnks* and *Iduna* inactivation lead to Axin elevation and stem cell over-proliferation in the *Drosophila* midgut. To examine the function of *ubcD1* in midgut stem cells *in vivo*, I generated mosaic animals with *ubcD1*$^{-/-}$ by using Flipase/FRT system. I found there were slightly more *esg>GFP*$^{+}$ stem and progenitor cells around FRT82B, *ubcD1*$^{-/-}$ clones compared to FRT82B control clones (Fig 4.6A). I also demonstrated that *ubcD1-RNAi* caused endogenous Axin elevation (Fig4.6B), increased numbers of Arm^{+}/Pros^{-} stem cells (Fig 4.6C), increased number of pH3^{+} cells (Fig 4.6D) and increased *upd3>GFP* reporter activity (Fig 4.6E). These results are consistent with *in vitro* function of ubcD1 in promoting TNKS and Axin degradation.

4.3.4 TNKS-mediated ADP-ribosylation can provide a molecular platform for rapid degradation of PARsylated proteins

My hypothesis suggests that ADP-ribosylation might be a molecular scaffold to concentrate the 26S proteasome locally and accelerate the degradation of TNKS or its PARsylated substrates. Therefore, I tested if TNKS co-localized with the 26S proteasome in the cell. To accomplish this, I miss-expressed *UAS-Flag-Tnks* in adult fly midguts under *Myo1A* driver, and dissected midguts were incubated with a fluorescent probe (Me4BodipyFL-

AhxLeu3VS) for 26S proteasome labeling (Berkers et al., 2007). I found that Flag-tagged TNKS co-localized with the 26S proteasome in ECs (Fig 4.7A). To address the importance of the PARsylation scaffold for the proteasome-TNKS interaction, I treated TNKS-expressing midguts with a small molecule inhibitor of TNKS, XAV939. I observed that both Flag-TNKS and 26S proteasomes changed their localizations upon XAV939 treatment (Fig 4.7B). TNKS protein level increased whereas the cytoplasmic proteasome localization diminished. As a conclusion, this result suggested that PARsylation might be a signal for proteasome recruitment into a local environment.

One possible mechanism by which the proteasome might be transported to the ADP-ribosylation scaffold is through an adaptor protein. Our lab previously demonstrated that PI31 physiologically required for the optimal 26S proteasome activity *in vivo*. Loss-of *PI31* causes a reduction of protein breakdown in several tissues and organismal lethality (Bader et al., 2011). PI31 is regulated by several different mechanisms including TNKS-dependent ADP-ribosylation and p38-mediated phosphorylation. ADP-ribosylation of PI31, for instance, alters its binding affinity for 20S proteasome alpha subunits and 19S assembly chaperones. As a consequence, the 26S proteasome assembly and activity are enhanced (Park and Steller, 2013). Furthermore, our lab has recently demonstrated that PI31 plays a role as an adaptor protein in proteasome transport, required for synaptic structure and function (Liu et al., 2019). PI31 binds directly to proteasomes with dynein light chain proteins (DYNLL1/2). *PI31* depletion, therefore, inhibits proteasome movements in axons. Finally, p38 MAP kinase-mediated phosphorylation of PI31 promotes its binding to DYNLL1/2. Phosphorylation deficient PI31 reduces proteasome transport in axons (Liu et al., 2019). I, therefore, tested if PI31 might have a role in ADP-ribosylation-dependent protein destruction.

Figure 4.7 The co-localization of TNKS and proteasomes depends on PARP activity TNKS. **A-** ECs cells expressed *Flag-Tnks* under *Myo1A* driver. Dissected midguts were incubated with a fluorescent probe (Me4BodipyFL-AhxLeu3VS) for 26S proteasome labeling in a conditioned media for 3h. **B-** Dissected midguts were treated with 20μM XAV939 for 3h. 7-day-old females were studied. After 4% PFA fixation, midguts were stained against Flag and analyzed by confocal microscope. Scale bar: 10μm.

Figure 4.7

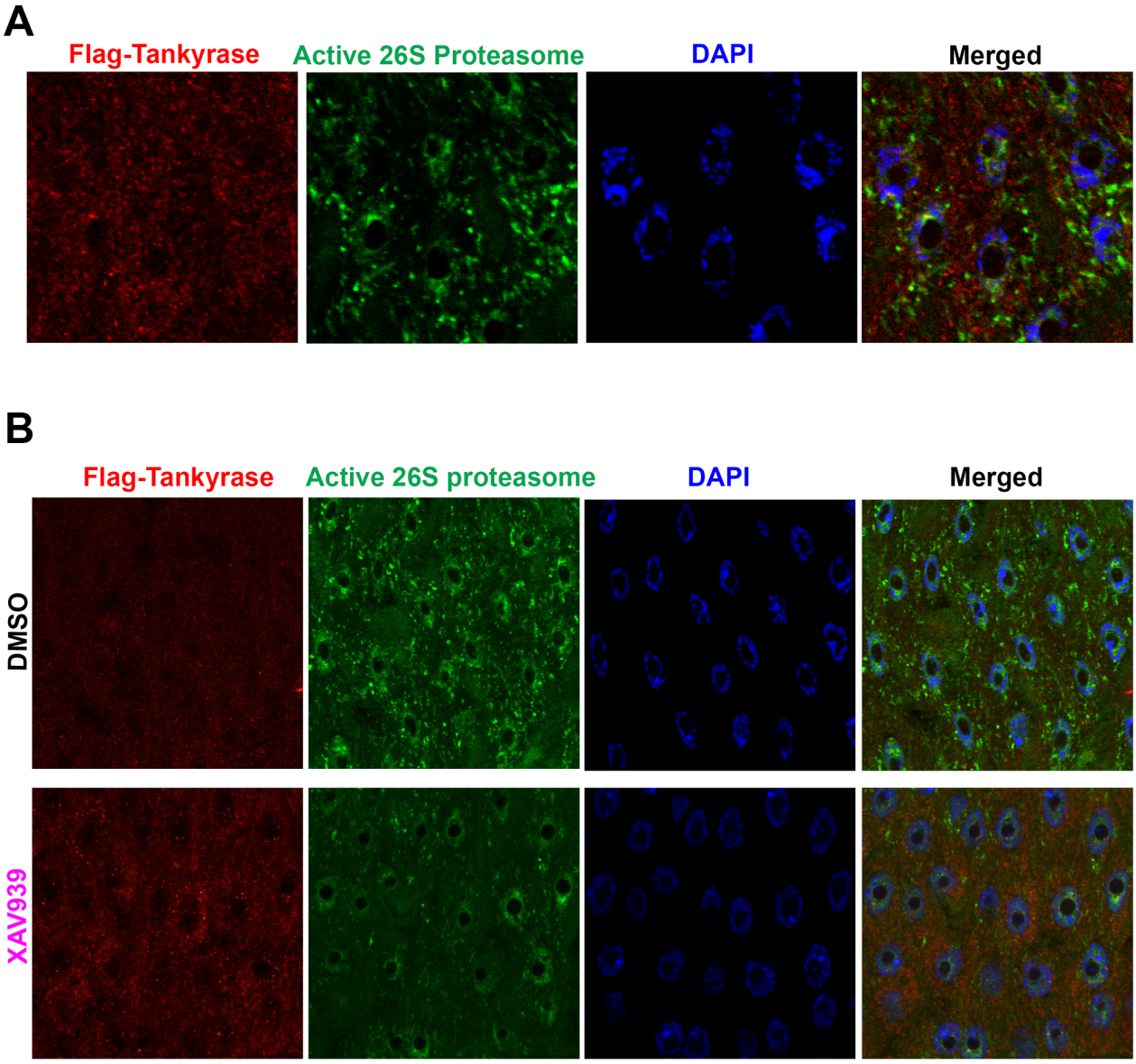
A
Flag-Tankyrase
Active 26S Proteasome
DAPI
Merged
B
Flag-Tankyrase
Active 26S proteasome
DAPI
Merged
DMSO
XAV939

I showed TNKS ADP-ribosylated PI31 *in vitro*, and this modification was sensitive to XAV939 treatment and hNUDT16 cleavage (Fig 4.8A). While TNKS-mediated ADP-ribosylation is mainly related to the protein breakdown through the 26S proteasome, loss-of *Tnks* did not result in PI31 elevation (Fig 4.8B), suggesting that ADP-ribosylation is not a degradation signal for PI31. I also demonstrated the whole protein lysate of *PI31* mutant larvae did not display Axin accumulation (Fig 4.8C). To examine the function of PI31 in Armadillo degradation *in vivo*, I generated mosaic animals with $PI31^{-/-}$ cells by using Flipase/FRT system. *PI31* inactivation in mutant clones did not affect Armadillo destruction in wing imaginal discs (Fig 4.8D), thereby suggesting that PI31 might not affect in PARsylation-mediated protein turn-over in all tissues.

Another possible mechanism to explain how the 26S proteasome might affect rapid degradation of PARsylated proteins was that the 26S proteasome might bind to a PAR scaffold through PAR-binding module in its subunits. I found that the 19S subunits Rpt1, 2, 3, and 6 were significantly co-immunoprecipitated with Flag-tagged TNKS in S2R+ cells (Table 4.1). When their amino acid sequences were aligned with the canonical PBM, the Rpt proteins of 19S regulatory particle had many essential core lysine-arginine amino acids (RR, KK or RK) but not the β-or α-subunits of the 20S proteasome did not. Detailed analyses revealed that Rpt2, 3 and 6 had several canonical PBMs (Fig 4.9). I, therefore, suggest that PBMs on Rpt subunits may facilitate the binding of 26S proteasomes to PARsylation scaffold. As a consequence, PARsylation can bring TNKS, Iduna, ubcD1, substrates, and the 26S proteasome together into close proximity, thereby accelerating the breakdown of substrates (Fig 4.10).

Figure 4.8 PI31 does not affect in Axin and Armadillo degradation in L3 larvae. A- TNKS ADP-ribosylated PI31 *in vitro*. His-tagged *Drosophila* PI31 was expressed and purified from *E. coli*. ADP-ribosylation of PI31 was a covalent modification that was sensitive to XAV939 treatment and hNUDT16 digestion. **B-** PI31 ADP-ribosylation is not a proteolysis signal in *Drosophila*. *Tnks* inactivation did not result in PI31 elevation. 7-day-old males were lysed for PI31 immunoblotting (IB: α-dPI31). **C-** Depletion of *PI31* does not affect endogenous Axin levels in L3 larvae. *PI31$^{-/-}$; BAC-Axin-V5* or +/+; *BAC-Axin-V5* larvae were lysed for immunoblotting (IB: α-V5). α-Tubulin and β-actin were loading controls. **D-** *FRT42D, PI31* mutant clones were analyzed for Armadillo levels. Dissected 3rd instar wing imaginal discs were stained with an Armadillo antibody. I did not observe an elevation of Armadillo in *PI31$^{-/-}$* mutant clones. Scale bar: 25μm.

Figure 4.8

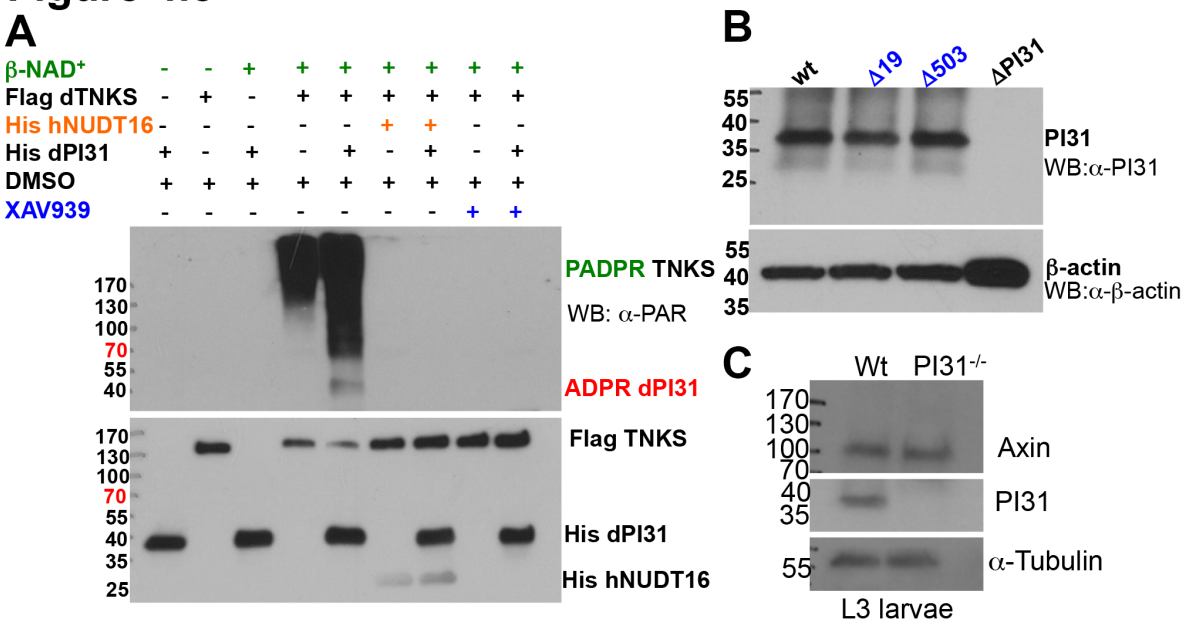
A
β-NAD+
Flag dTNKS
His hNUDT16
His dPI31
DMSO
XAV939
PADPR TNKS
WB: α-PAR
ADPR dPI31
Flag TNKS
His dPI31
His hNUDT16
B
wt
Δ19
Δ503
ΔPI31
PI31
WB:α-PI31
β-actin
WB:α-β-actin
C
Wt
PI31-/-
Axin
PI31
α-Tubulin
L3 larvae

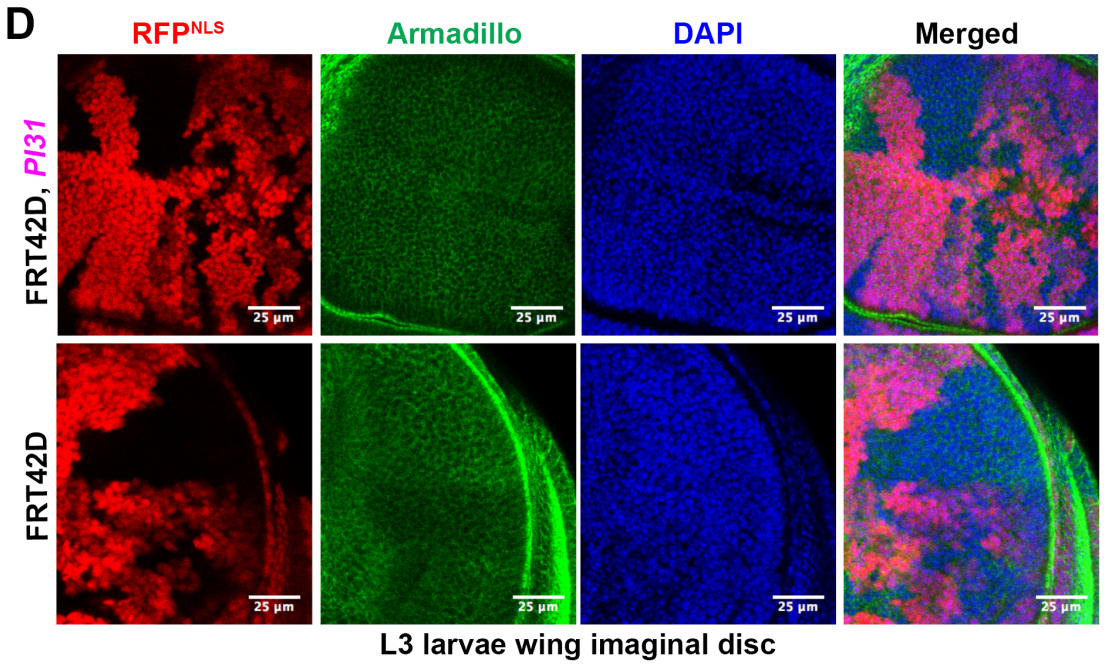
D
RFPNLS
Armadillo
DAPI
Merged
FRT42D, PI31
FRT42D
25 μm
L3 larvae wing imaginal disc

Figure 4.9

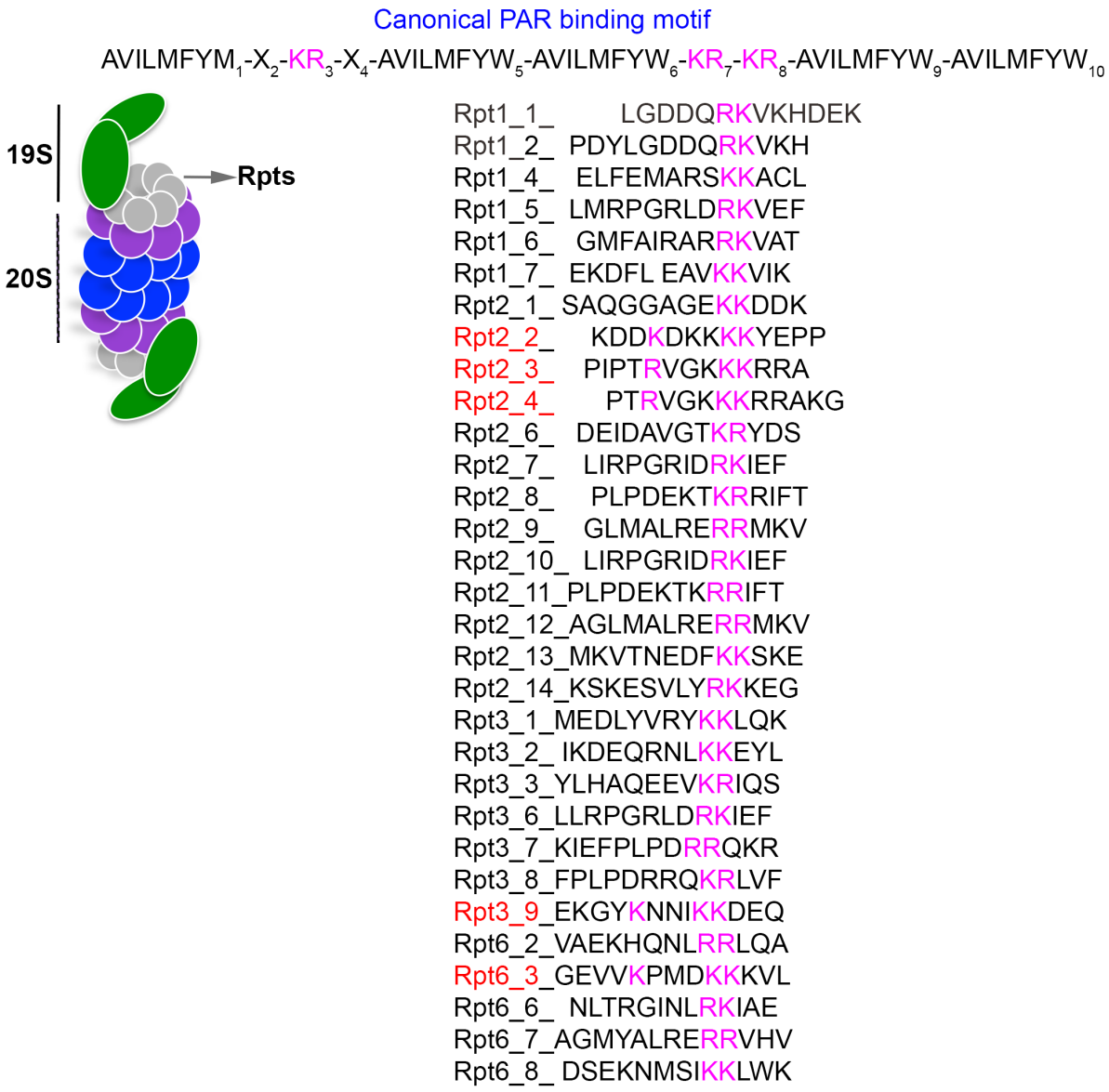

Figure 4.9 Rpt2, 3 and 6 subunits of the 19S regulatory particles of the proteasome have several canonical PAR-binding motifs. The canonical PBM consists of core lysine and arginine residues: AVILMFYM$_1$-X$_2$-KR$_3$-X$_4$-AVILMFYW$_5$-AVILMFYW$_6$-KR$_7$-KR$_8$-AVILMFYW$_9$-AVILMFYW$_{10}$. Core residues were highlighted with pink. The canonical PBM-containing peptides of Rpt2, 3 and 6 were colored as red.

Figure 4.10 ADP-ribosylation by TNKS provides a molecular scaffold that brings substrates, E2 and E3 ubiquitin ligases and proteasomes into close proximity, thereby accelerating target protein degradation. I propose that TNKS forms a complex with Iduna, which is inactive when bound to non-PARylated TNKS in the cell. After substrate binding to TNKS and subsequent PARylation, Iduna binds to PAR. This binding causes a conformational change in the RING domain of Iduna, which activates its ubiquitin ligase activity, enabling the poly-ubiquitinylation of the substrate. The ubcD1 ubiquitin-conjugating enzyme promotes ubiquitin ligase function of Iduna by binding to ADP-ribose. As a consequence, TNKS may increase its PARsylation activity to assemble PAR scaffold. Finally, 26S proteasomes may be recruited to the scaffold and concentrated in a local environment for rapid destruction of the target protein.

Figure 4.10

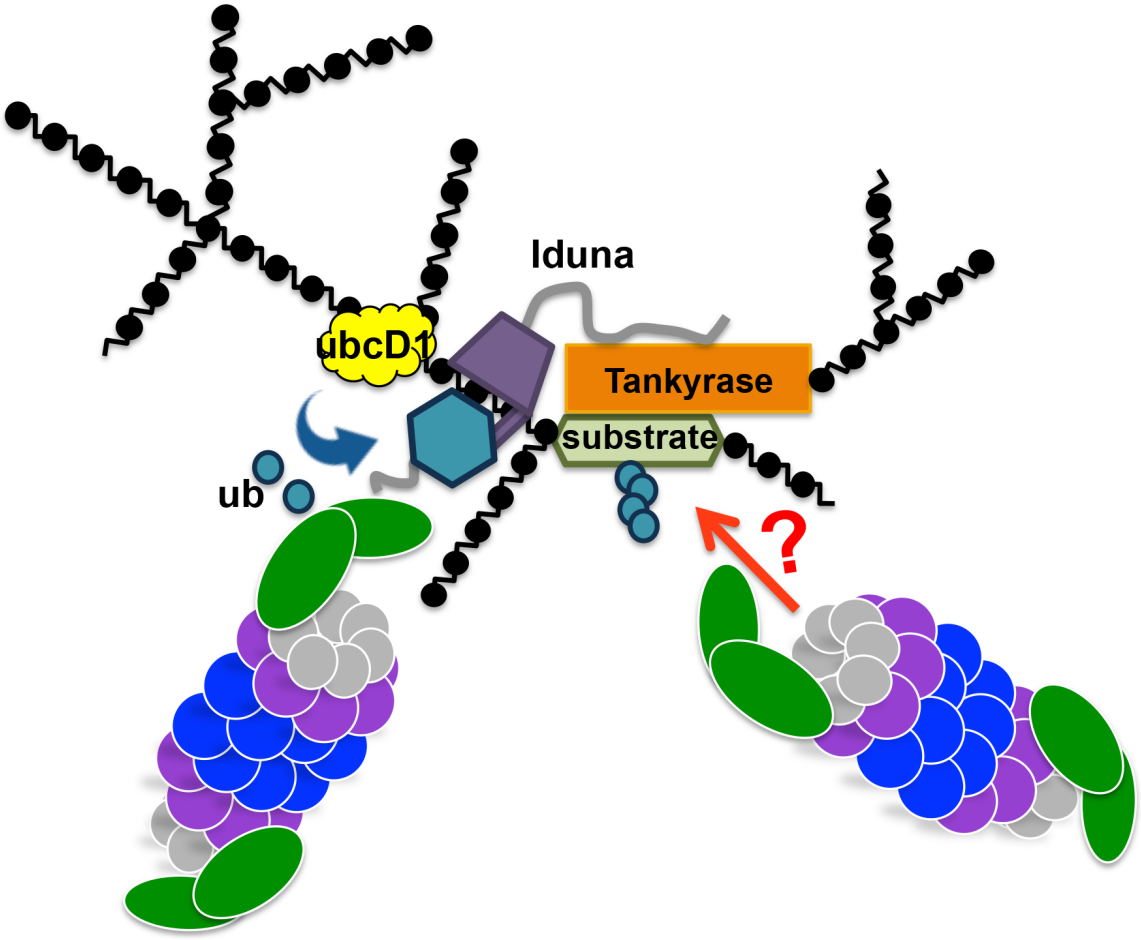

4.4 Material and Methods

Fly stocks: Flies were kept at a 12-hour light/dark cycle. All crosses were performed at 22-25°C unless stated otherwise. The following fly stocks were used for this study (Bloomington Drosophila Stock Center (BDSC) and Vienna Drosophila Resource Center (VDRC) number (#) given in parentheses):

The stocks used in here: esg-Gal4, UAS-GFP (a gift of Dr. Norbert Perrimon; Micchelli and Perrimon, 2006), BAC-AxinV5 (a gift of Jean-Paul Vincent, Gerlach et al., 2014), *FRT 82B, Axn^{h}, BAC-AxinV5* (a gift of Jean-Paul Vincent, Gerlach et al., 2014), UAS-GFP-Axin (BDSC# 7224), Myo1A-Gal4, tub-Gal80ts, UAS-GFP (a gift of Dr. Norbert Perrimon; Micchelli and Perrimon, 2006), upd3-Gal4, UAS-GFP (a gift of Dr. Norbert Perrimon; Markstein et al., 2014), *Tnks^{503}* (a gift of Dr. Yahsi Ahmed, Wang et al., 2016), *Tnks^{19}* (a gift of Dr. Yahsi Ahmed, Wang et al., 2016), PI31$^{-/-}$ (Bader et al., 2009), UAS-ubcD1-HA (Ryoo et al., 2002), UAS-Flag-Tnks (Gultekin and Steller, 2019), UAS-Tnks-HA (a gift of Dr. Yahsi Ahmed, Wang et al., 2016), UAS-CG8786/*dIduna* RNAi#1 (BDSC# 40882), UAS-CG8786/*dIduna* RNAi#2 (VDRC#43533), UAS-CG8786/*dIduna* RNAi#3 (VDRC#36028), UAS-CG8786/*dIduna* RNAi#4 (VDRC#36029), and *white* RNAi (BDSC#33623), *ubcD1* RNAi (BDSC#31875), *ubcD1* RNAi (BDSC#35431), *morgue* RNAi (BDSC#31059). The rest of *Drosophila* lines, which were studied here, were obtained from Steller Lab stocks. Oregon R flies were used as control and only adult female flies were analyzed in this study.

Clone analyses and RNAi experiments: Please refer to Chapter 2, Material and methods.

Cell culture: Please refer to Chapter 2, Material and methods.

Western blot analyses: Please refer to Chapter 2, Material and methods.

Primary antibodies: anti-dPI31 (rabbit, generated in this study, 1/2500), anti-V5 (1/1000, Abcam, ab27671), anti-Flag-HRP (1/1000, Sigma-Aldrich, A8592), anti-Flag (1/1000, CST, D6W5B 14793), anti-GST HRP (1/1000, GenScript, A00866-100), anti-PAR (1/1000, Trevigen, 4335-MC-100), anti-Myc tag (1/1000, CST, 9B11, 2276), anti-Axin Drosophila (Santa Cruz, dT20, sc15685), anti-tubulin DM1A clone (1/1000, Sigma-Aldrich, T9026), mouse anti-GFP-HRP (1/2500, clone B2, Santa Cruz Biotechnology, sc-9996-HRP), rabbit anti-β-Actin-HRP (1/5000, clone 13E5, Cell Signaling Technology, 5125), donkey anti-rabbit-HRP (1/5000, Jackson ImmunoResearch, 711-035-152), donkey anti-mouse-HRP (1/5000, Jackson ImmunoResearch, 715-035-150), donkey anti-guinea pig-HRP (1:5000, Jackson ImmunoResearch, 706 006 148).

Immunofluorescence: Please refer to Chapter 2, Material and methods.

Primary antibodies: rabbit anti-HA (Sigma, H6908, 1:1000), mouse anti-Flag (Sigma, M2-F1804, 1:5000), anti-V5 (Abcam, ab27671, 1:1000), mouse anti-Arm (Wang et al., 2016; N2 7A1, DSHB, 1:50), mouse anti-Prospero (Wang et al., 2016; MR1A, DSHB, 1/50), mouse anti-GFP (GFP-12A6, DSHB, 1/100), mouse anti-β-galactosidase (Tian et al., 2016); 401A, DSHB, 1/100), mouse anti-Delta (Wang et al., 2016; C594.9B, DSHB, 1/100), rabbit anti-phosho-S10-Histone3 (Wang et al., 2016; 06-570, Millipore, 1/1000). The secondary antibodies were goat anti-mouse-Alexa 488 plus (Thermo Fisher Scientific, A32723), goat anti-mouse-Alexa 568 (Thermo Fisher Scientific, A11031), goat rabbit-Alexa 546 (Thermo Fisher Scientific, A11035), goat rabbit-Alexa 488 (Thermo Fisher Scientific, A11034), goat anti-rabbit-Alexa 633 (Thermo Fisher Scientific, A21071) and used at 1/1000.

Immunoprecipitation: Please refer to Chapter 2, Material and methods.

Recombinant protein purification from S2R+ cells: Please refer to Chapter 2, Material and methods.

Antibody production against *Drosophila* PI31: To generate a polyclonal antibody against Drosophila PI31, GST-PI31 was expressed in BL21 Star (DE3) *E. coli* cells (Thermo Fisher Scientific, C601003), and purified using Glutathione Sepharose 4B beads (GE Healthcare, 17-0756-01). The purified protein was injected into rabbits and the antisera were collected (Cocalico).

***In vitro* ADP-ribosylation:** 20 micrograms of Flag-tagged *Drosophila* TNKS protein (purified from S2R+ cells) were automodified in 100 µL of a reaction buffer containing 100mM Tris-HCl pH 8.0, 10mM MgCl2, 10mM DTT, 25µM NAD+ for 1h at 24-25°C.

***In vitro* ubiquitinylation assays:** For Iduna auto-ubiquitinylation, 50ng E1, 100ng T7–ubcD1, 700ng His-Iduna, and PAR were used in each reaction. For TNKS ubiquitinylation, 750ng Flag-tagged TNKS (purified from S2R+ cells, *in vitro* ADP-ribosylated and not) 50ng E1, 100ng T7–ubcD1, 100ng His-Iduna, and PAR were used in each reaction. *In vitro* ubiquitinylation assays were carried out in a total volume of 20 µl. The reaction mixture contained also 40mM Tris-HCl at pH 7.6, 5mM $MgCl_2$, 1mM dithiothreitol, 5mg GST-ubiquitin, 100ng ubiquitin–aldehyde, 2mM ATP. Reactions were incubated for 1h at 37 °C before addition of sample buffer and resolution on 4-20 % SDS–PAGE gels. Finally, Western blotting was carried out.

Quantification and statistics: Please refer to Chapter 2, Material and methods.

5 DISCUSSION

5.1 Iduna regulates stem cell proliferation and intestinal homeostasis

We investigated the *in vivo* function of *Iduna* and identified a critical role of this enzyme for the control of stem cell proliferation in the *Drosophila* midgut. Mammalian Iduna is an unusual E3 ubiquitin ligase that specifically binds to and poly-ubiquitylates ADP-ribosylated substrates to promote their rapid degradation by the proteasome. However, the physiological function of Iduna remains largely unclear.

Here, I generated *Drosophila Iduna*-null-mutants and used them to show that Iduna has a crucial *in vivo* function for the degradation of ADP-ribosylated TNKS and Axin to control stem cell proliferation. In particular, I focused on the role of *Iduna* in the *Drosophila* midgut. I found that *Iduna* inactivation caused a slight but significant increase in Axin protein levels in ECs, which in turn caused over-proliferation of ISCs. This non-cell autonomous effect on stem cell proliferation is depended on UPD2-UPD3 cytokines that are secreted from ECs. These findings suggest a model in which loss of *Iduna* function, which decreases the Wingless pathway activity due to elevated Axin levels in ECs, in turn causes increased secretion of UPD2-3 from these cells to activate the JAK-STAT pathway in ISCs. Importantly, a 50% reduction in *Axin* gene dosage blocked the over-proliferation of stem cells in *Iduna* mutants, demonstrating the necessity to tightly regulated Axin levels in this system. Whereas many other cell types appear to tolerate fluctuations in the amount of Axin protein, proper Wingless signaling in the *Drosophila* midgut appears to critically depend on restricting Axin levels by Iduna.

The activity of Iduna depends on binding to ADP-ribosylated substrates via its WWE domain. Recognition and binding to its ADP-ribosylated target proteins change the

structural confirmation of Iduna. Subsequently, Iduna is activated to ubiquitylate its targets for proteasome-mediated degradation. It was previously reported that TNKS forms a tight complex with Iduna to control the proteolysis of target proteins (DaRosa et al., 2014). I could not detect any obvious morphological differences between *Iduna* mutants and wild type. Although this may seem somewhat surprising, it is consistent with complete inactivation of *Tnks* in *Drosophila,* which also causes no overt abnormalities (Feng et al., 2014; Wang et al., 2016 a,b; Yang et al., 2016). As for *Iduna*, *Tnks* mutants have no obvious effects on wing development and the expression of Wingless target genes in larval wing discs, despite the fact that Axin levels are increased (Feng et al., 2014; Wang et al., 2016a and 2016b; Yang et al., 2016). Our interpretation of these findings is that most tissues can tolerate relatively modest (2-3-fold) changes of Axin. For example, it appears that a greater than 3-fold increase of endogenous Axin is required for functional consequences of altered Wingless signaling in *Drosophila* embryos (Yang et al., 2016) and 3-9-fold changes are needed in wing discs (Wang et al., 2016a). On the other hand, the *Drosophila* midgut appears much more sensitive to reduced Wingless signaling.

An independent study demonstrated that inactivation of *Drosophila Tnks* led to increased Axin protein accumulation in the *Drosophila* midgut and promoted ISC proliferation (Wang et al., 2016). These results are consistent with previously reported cell-based studies suggesting that Iduna mediates TNKS-dependent degradation of Axin and thereby positively regulates Wnt signaling (Huang et al., 2009; Croy et al., 2016; Callow et al., 2011). On the other hand, it is notable that inactivation of two highly diverse types of enzymes, *Tnks*, a PARP, and *Iduna*, an E3 ubiquitin ligase, produced

similar phenotypes. Both TNKS and Iduna have many other targets outside the Wnt-pathway, and based on biochemical observations, it has been proposed that they may play roles in DNA repair, telomere length, vesicle trafficking, Notch-signaling, centrosome maturation, neuronal protection and cell death (Bai, 2012; Gibson and Kraus, 2012; Riffell et al., 2012). However, *Iduna* and *Tnks* mutant flies are viable and do not show any obvious defects under normal growth conditions. This indicates that the major non-redundant physiological function of both Tnks and Iduna in *Drosophila* is to regulate Wingless-mediated intestinal stem cell proliferation, and provides physiological evidence for the idea that the function of both proteins is indeed tightly coupled. In addition, our study identifies a role of UPD-Domeless in this pathway. These results may have implications for the regulation of this highly conserved pathway in mammals. For example, conditional inactivation of *Iduna* in mouse bones leads to increased numbers of osteoclasts and inflammation (Matsumoto et al., 2017a). In this system, down-regulation of *Iduna* leads to accumulation of Axin1 and 3BP2. This, in turn, attenuates β-catenin degradation and activates SRC kinase, respectively, thereby promoting the release of inflammatory cytokines in the bone (Matsumoto et al., 2017a). On the other hand, *Iduna* depletion reduces proliferation of osteoblasts and promotes adipogenesis in the mouse skeleton (Matsumoto et al., 2017b). Despite the obvious differences between mammalian bone and the *Drosophila* midgut, both systems show overall striking similarities in the use of TNKS/Iduna to restrict Axin levels to achieve proper levels of Wnt/β-catenin signaling during tissue homeostasis. Finally, my study indicates that Axin may have a more general function as a scaffold protein that recruits multiple proteins and permits a crosstalk with other pathways that modulate Wnt/β-catenin signaling.

5.2 Iduna can play a role in energy metabolism in *Drosophila*

The PARsylation activity of TNKS regulates diverse physiological processes including energy metabolism. PARP activity consumes NAD+ as a co-substrate to post-translationally modify various acceptor proteins including TNKS itself. PARsylation by TNKS often tags the acceptors for ubiquitylation and proteasomal degradation. In insulin-secreting cells, glucose and fatty acid consumptions stimulate the auto-PARsylation of TNKS; consequently, its breakdown is promoted. Elevation of NAD+ levels primarily mediates this glucose effect on TNKS (Zhong et al., 2015). Furthermore, TNKS binds to IRAP1 (insulin-responsive aminopeptidase) and co-localizes with GLUT-4 vesicles near the Golgi in 3T3-L1 adipocytes (Chi and Lodish, 2000). Because of its Golgi localization, TNKS can have an impact on the exocytosis of specific cargos in adipocytes. Upon insulin stimulation, MAP kinase phosphorylates TNKS, which in turn enhances its PARP activity in adipocytes. As a result, it is suggested that TNKS-mediated PARsylation of Golgi-associated proteins may affect the sorting or stability of GLUT4 vesicles (Chi and Lodish, 2000). Moreover, genetic depletion of *Tnks* in adipose tissue increases glucose tolerance and adiponectin levels in female mice (Zhong et al., 2016). Global TNKS knockouts also share these phenotypes (Yeh et al., 2009). The similarity between global knockout and tissue-specific deletion suggest that the impact of TNKS on systemic metabolism largely comes from its PARsylation activity in adipocytes (Zhong et al., 2016).

Mice with loss of *Iduna* within the osteoblast lineage have increased fat stores and are glucose intolerant with severe osteopenia because of defective osteoblastogenesis and

subsequent impaired osteocalcin production. Hence, Iduna controls bone production, glucose, and lipid metabolism (Matsumoto et al., 2017b).

TNKS also influences lifespan, stress tolerance and energy storage in *Drosophila* (Li et al., 2018). The knockdown of *Tnks* in muscle causes similar effects to those of *Tnks*-null mutants and its ubiquitous knockdown. They exhibit shortened lifespan, impaired climbing ability, increased sensitivity to oxidative stress and starvation, and reduced TAG and glycogen storage (Li et al., 2018). Similar to TNKS, Iduna affects longevity in *Drosophila*. *Iduna* mutants have slightly shorter lifespans than their wild type controls. They display increased mortality upon reduced nutrient diet. Remarkably, *Iduna* depletion reduces stored lipids in abdominal fat body cells upon starvation. I have shown that *Iduna*-null flies steadily lost their fat stores during a 24h starvation, while wild type control flies were able to sustain their fat reservoirs for 24h. These results point out another role of Iduna in promoting survival under stress conditions. I, therefore, suggest that Iduna may have an essential function(s) in energy metabolism as well. The exact mechanism by which starvation caused increased mortality in *Iduna* mutants remains to be determined.

5.3 Lysine 598 in TNKS affects longevity in *Drosophila*

I explored the importance of PARsylation-mediated proteolysis by focusing on TNKS-mediated ADP-ribosylation and the E3 ubiquitin ligase function of Iduna. PARsylation is a degradation signal for TNKS and Axin. However, the ribosylation and the PARsylation-dependent ubiquitylation sites that target TNKS and Axin for degradation are not yet known. With an MS-based approach, I reveal that K598 residue is

one of the ADP-ribose acceptor sides in *Drosophila* TNKS. *In vitro* ADP-ribosylation assays suggested that K598A might be a loss-of-function mutation of *Tnks* since it was unable to ADP-ribosylate *Drosophila* Axin as well as itself *in vitro*. However, I found that K598A mutant was auto-ADP-ribosylated and degraded in S2R+ cells. Lysine 598 is located in the ARC4 domain, which is conserved from flies to human. This residue corresponds to lysine 604 in human TNKS2. It was previously demonstrated that K604 in human TNKS2 might be essential for Axin1-binding as well as its degradation. Therefore, it was suggested $K604^{TNKS}$ might form strong salt bridge interactions between 7^{th} and 8^{th} glutamine residues in Axin`s TBM. Although there are no crystal structures for ARC4 to bind Axin1/2 yet, recent reports have demonstrated that ARC1, 3 and 5 repeats in human TNKS2 are necessary for Axin recognition and binding.

TNKS is a negative regulator of Axin. As a result, *Tnks*-null flies have elevated Axin in *Drosophila*. Loss-of *Tnks* promotes stem cell proliferation through non-cell autonomous JAK-STAT activation. As a consequence, there are more stem and progenitor cells in *Drosophila* midguts. On the other hand, $Tnks^{K598A}$ knock-in flies do not promote the cell division of ISCs. Hence, $Tnks^{K598A}$ is not a complete loss-of-function mutation of *Tnks*. Taken together, I suggest that K598-ADP ribosylation can have an essential function(s) for other protein(s) rather than Axin.

$Tnks^{K598A}$ adult flies are viable, fertile, and have no apparent morphological defects. However, $Tnks^{K598A}$ flies live significantly shorter than their control flies. $Tnks^{K598A}$ adult flies also decline their climbing abilities with age. Similarly, *Tnks*-null flies have prominently shorter lifespan. Loss-of *Tnks* or its muscle-specific inactivation impairs longevity, stress tolerance, and energy storage in adult flies through regulation of

the JNK pathway. TNKS PARsylates JNK, which positively controls JNK signaling. PARsylation is not a degradation signal for JNK. Instead, TNKS triggers degradation-independent K63-ubiquitination of JNK to promote its kinase activity *in Drosophila* (Li et al., 2019). Taken together, I suggest that K598 in TNKS may have a role in JNK signaling in the *Drosophila* muscle.

I finally conducted a Co-IP-MS to identify the most affected binding protein(s) of TNKS when lysine 598 was mutated to alanine. I, therefore, investigated that 11 proteins that prominently lost their binding-affinities to TNKS due to this mutation. As a result, I suggest that K598 may have various physiological functions together with these binding partners. For instance, RH07106p is the most affected binding-partner of TNKS. RH07106p is an Hsp70-binding protein. It has a putative transmembrane domain, and is expected to localize on the endoplasmic reticulum membrane. Its molecular functions are not known yet. Likewise, K598A TNKS does not pull down Snapin, a component of the biogenesis of lysosome-related organelles complex-1 (BLOC-1). It functions in different biological processes including intracellular protein transport, synaptic vehicles priming, and neurotransmitter release.

In conclusion, my results point out that lysine 598 can be essential to interact with several binding-partners of TNKS. Further molecular studies on the affected interaction partners of TNKS can be helpful to further investigate the physiological function(s) of lysine 598.

5.4 ubcD1 ubiquitin-conjugating enzyme promotes ubiquitin ligase activity of Iduna

I described the ubiquitin-conjugating function of ubcD1 for Iduna-dependent ubiquitylation. Loss-of *ubcD1* results in elevations of Iduna, TNKS and Axin proteins in *Drosophila*. ubcD1 boosts auto-ubiquitylation of Iduna in the presence of PAR and promotes degradation of Iduna, TNKS and Axin *in vivo*. ubcD1 can bind to PAR scaffold through its PBMs.

I also showed that Flag-tagged TNKS significantly co-immunoprecipitates with Ben, morgue, Usp10, and Usp30 in S2R+ cells. Similar to ubcD1, Ben and Morgue are ubiquitin-conjugating enzymes. It is possible that they may have functions on TNKS-dependent protein breakdown although *morgue*-RNAi does not have an impact on the stability TNKS itself. On the other hand, Usp10 and Usp30 are ubiquitin-specific proteases, which can remove ubiquitin chains and stabilize proteins. USP25 positively regulates Wnt signaling by mediating the deubiquitylation of TNKS in human cells. Conversely, si-RNA-dependent USP25 deficiency promotes TNKS degradation, which in turn causes suppression of Wnt signaling (Xu et al., 2017). However, the functions of usp10 and usp30 on TNKS or its substrates are not known yet. Future work, therefore, is required to address the contribution of these E2 ubiquitin ligases and deubiquitinating enzymes for TNKS-mediated proteolysis.

5.5 ADP-ribosylation can provide a molecular scaffold for TNKS-mediated rapid protein degradation

Finally, I provide evidence that PARsylation can recruit necessary proteins including the 26S proteasome in a local environment to maintain rapid protein degradation. I found that TNKS can colocalize with the 26S proteasome. Reduction of PARsylation by XAV939 blocks cytoplasmic co-localization between TNKS and the 26S proteasome. This result suggests that the 26S proteasome by itself may bind to PAR polymers. Unlike the 20S core particles, the 19S regulatory Rpt proteins consist of many lysine-arginine enrich peptides but Rpt2, 3 and 6 have canonical PBM.

PAR-binding proteins recognize PAR polymers, thereby, driving the localization of proteins and assembly of protein complexes. PARP1-auto-PARsylation provides a molecular platform to recruit all essential proteins into close proximity in response to DNA damage, rRNA biogenesis, and heat shock. Similarly, TNKS-mediated PARsylation is essential for stress granule assembly. TNKS-mediated PARsylation promotes TDP45 liquid-liquid phase separation and protect TDP45 from ALS-associated phosphorylation (Duan et al., 2018; McGurk et al., 2018).

Since Nature uses PAR scaffold in different concepts, I propose a mechanism, by which PARsylation can bring together TNKS, target proteins, E2 and E3 ubiquitin ligases such as ubcD1 and Iduna, respectively and the 26S proteasome into close proximity for accelerating the breakdown of PARsylated proteins. Based on my model, TNKS forms a complex with Iduna, which is inactive when bound to non-PARylated TNKS in the cell. After substrate recognition and binding to the complex, TNKS starts to ADP-ribosylate the substrate. When the target protein has multi-ADP-ribose moieties, Iduna binds an

internal unit of PAR. This binding causes a conformational change in the RING domain of Iduna, which activates its ubiquitin ligase activity, enabling the poly-ubiquitylation of the substrate. As a consequence, TNKS is promoted for its PARsylation activity to assemble PAR scaffold. Finally, 26S proteasomes can be recruited to the scaffold. As a result, rapid protein degradation takes place.

My data has led to a two-step model for regulation of protein degradation by ADP-ribosylation whereby TNKS regulates the formation of the cytoplasmic scaffold of ADP-ribosylation and poly-ADP-ribose regulates the recruitment of 26 proteasomes to the local environment for degradation of target proteins. I can suggest the scaffold model can be a very dynamic and follow the rules of liquid-liquid phase separation. Under regular conditions, TNKS with Iduna can form liquid condensates that can mature, solidify, and undergo liquid-to-solid transitions—or can nucleate aggregation. The oligomerization of TNKS through SAM domain promotes its poly-ADP-ribose polymerase activity. The negatively charged poly-ADP-ribose scaffold, therefore, can promote liquid-liquid phase separation for TNKS-Iduna degradation complex. Importantly, a small molecule inhibitor of TNKS, XAV939 reduces the co-localization of poly-ADP-ribose and proteasomes in the cytoplasm. Thus, poly-ADP-ribosylation may modulate liquid-liquid phase separation, which can accelerate the target protein degradation. Future studies will determine whether TNKS-Iduna complex, ribosylated target proteins, and 26S proteasome can co-phase separate *in vitro*.

5.6 Future perspectives of this thesis

5.6.1 Insights into the *in vivo* functions of Iduna in *Drosophila*

Several *in vivo* functions of Iduna in *Drosophila* were uncovered in this study including its physiological impacts on midgut stem cells and intestinal homeostasis. However, results from this study imply that Iduna has potential regulatory roles in lipid metabolism. Yet, the cause of increased mortality of *Iduna* mutants upon 5% sucrose diet remains to be uncovered. *Iduna* mutants also reduce stored lipids in abdominal fat body cells upon 12h or 24h starvation. *Iduna*-null flies are not able to restore their lipids into fat bodies during a 24h starvation, while wild type flies can. These results demonstrate that Iduna has an important role in promoting survival during starvation. To uncover the physiological relevance of Iduna in *Drosophila*, I performed an RNA-sequencing experiment from the dissected intestines of 15-day-old *Iduna* mutant and control flies. I found that a pancreatic-like lipase, *CG6271* was significantly down-regulated in normal circumstances (Appendix). Both FlyAtlas and FlyGut-seq databases suggest that the expression of *CG6271* gene is high in enteroendocrine cells in the *Drosophila* midgut (Chintapalli et al., 2007; Buchon et al., 2013; Marianes et al., 2013; Dutta et al., 2013). *CG6271* depletion by RNAi under Prospero-Gal4 driver leads to lethality in fly larvae (Data not showed). However, the physiological functions of CG6271 remain to be determined. I suggest that CG6271 may play a role in lipid metabolism and further molecular and cellular studies will address the function of Iduna in lipid metabolism.

5.6.2 Age-related physiological roles of lysine 598 in *Drosophila* TNKS

This study has led to the identification of one of the first ADP-ribosylation acceptor residues in *Drosophila* TNKS. I found that $Tnks^{K598A}$ adult flies are viable, and fertile without any obvious phenotypic defects. However, $Tnks^{K598A}$ mutants live significantly shorter than their controls. $Tnks^{K598A}$ adults also decline their climbing abilities, JNK activation and global protein poly-ADP-ribosylation with age. Finally, I showed that FLAG-tagged K598A TNKS prominently lose its binding-affinity to 11 proteins including RH07106p Hsp70 binding protein, Caper, Snapin, Receptor-mediated endocytosis protein 6 homolog, Prx5, RnpS1, IP12463p putative cADPR synthase, Exu, A1Z6G6, U2af50, Pst.

One of the surprising binding-partner of TNKS is Snapin that does not interact with K598A TNKS. Snapin participates in the biogenesis of lysosome-related organelles. It is a component of the SNARE complex of proteins that is required for synaptic vesicle docking and fusion. Snapin is an essential protein for presynaptic plasticity. Hence, Snapin has important functions including intracellular protein transport, synaptic vehicles priming, and neurotransmitter release (Starcevuc et al., 2004; Ilardi et al., 1999).

Since TNKS is a positive regulator in the JNK signaling pathway, changes in the activity of JNK signaling can suppress or enhance phenotypes of *Tnks* mutant flies. Therefore, we need further studies to investigate how $Tnks^{K598A}$ mutation affects JNK signaling during aging and different stress responses including starvation, bacterial infections, and chemical toxins. Furthermore, these phenotypes in $Tnks^{K598A}$ mutants suggest that there might be problems in organismal metabolism during aging. Various metabolic tissues including muscle, fat body, neuron, and intestine can sense nutrients

and environmental inputs to affect aging-associated cellular functions. Ectopic expression of *UAS-wild type Tnks* in these tissues under tissue-specific drivers can determine the major tissue(s) in which $Tnks^{K598A}$ play its physiological roles. It was previously shown that *Tnks* knock-down in the muscle with Mef2-Gal4 causes shortened lifespan, impaired climbing ability similar to $Tnks^{K598A}$ mutant flies. Finally, comparative interactome between wild type and K598A result suggests Snapin may be a molecular target. Hence, the muscle may be important to further understand the physiological role(s) of K598 residue in *Drosophila*. Cellular and molecular investigations need to be performed on neuromuscular junctions and muscle of $Tnks^{K598A}$ mutants. Complementary electrophysiology experiments need to be can be helpful to further investigate the physiological function(s) of lysine 598 in the muscle.

6 APPENDIX

Figure 6.1 RNA sequencing indicates that *Iduna* depletion down-regulates *CG6271.* 15-day-old adult female flies were dissected for their midguts and directly homogenized in 1 ml TRIzol (Life Technologies). Total RNA was isolated according to the manufacturer's protocol. The Rockefeller University Genomics Core Facility performed RNA quality control test before RNA-sequencing. RNA-seq libraries were generated at The Rockefeller University Genomics Resource Center. Files were delivered in fastq format. For data analysis, reads were aligned against the D. melanogaster genome dm6 with BWA or tophat2 (for poly(A) and total RNA-seq) in standard settings. **A-** Volcano plot of significantly and differentially expressed genes sanity-check the DGE is to see how all genes behave across conditions using a standard "volcano plot". This plot is a special case of the scatter plot where each gene is represented by an individual dot, X-axis shows the degree of fold-change in logarithmic base and the Y-axis is the minus log10 transformation of the raw p-value of statistical significance. The horizontal line shows the significance cut-off hence all genes in the top-left corner are significantly down-regulated and the top-right ones are significantly up-regulated ones. **B-** A list of Significantly and differentially expressed genes (DGE) (FDR 10%). The logFC column is the well-known "log fold-change" value. Positive values represent up-regulation and negative ones down-regulation. The columns AveExpr, t, and B are mostly regarding the DGE statistics and are not informative in terms of the biology. The table is sorted based on the raw p-value and can be considered as an ordered list of genes where the top one is the most relevant. **C-** A heat map of significantly and differentially expressed genes. We showed the number of reads mapped to each gene

using a log-transform for a better color scheme and we will do this for all significant genes. This is a bit hard to interpret by eye, but we definitely would like to see the same conditions clustering together and as a bonus, we might get some interesting groupings of the genes. **D-** *CG6271* is highly expressed in the *Drosophila* midgut (FlyAtlas database). **E-** *CG6271* is expression is enriched in enteroendocrine cells in the R3 region of the midgut. It has a high expression in the visceral muscle in the R2 region of the midgut (FlyGut-Seq Database). **E-** CG6271 is a pancreatic-like lipase in *Drosophila,* which shares 47% similarity with human LPL protein.

Figure 6.1

A

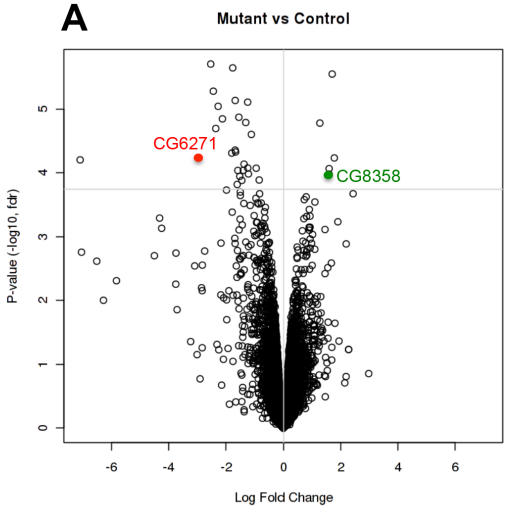

B

Gene	logFC	AveExpr	t	P.Value	adj.P.Val	B
CG3259	-2.5324235	2.658107	-13.016196	1.98E-06	0.008561854	3.956546
CG10562	-1.7647581	6.880549	-12.769397	2.28E-06	0.008561854	5.392056
CG14963	1.7043453	5.425055	12.381076	2.84E-06	0.008561854	5.144027
CR43310	-2.4423336	3.457500	-11.360455	5.28E-06	0.011756842	3.989883
alpha-Est5	-1.6781581	5.707533	-10.840421	7.37E-06	0.011756842	4.359282
Cyp6d4	-1.2433870	6.260636	-10.748260	7.83E-06	0.011756842	4.326968
Cyp6a17	-2.2745149	6.111193	-10.521692	9.11E-06	0.011756842	4.168822
CG6812	-1.5509083	3.050627	-9.952074	1.35E-05	0.013687546	3.280272
CG5724	-2.1236719	6.837044	-9.870486	1.43E-05	0.013687546	3.773949
Oseg4	-1.3104161	3.657283	-9.686262	1.63E-05	0.013687546	3.400771
Syt4	1.2752584	5.982604	9.658879	1.67E-05	0.013687546	3.632019
Cyp6a23	-2.3564401	9.070014	-9.393433	2.03E-05	0.015253024	3.433058
Cyp6a21	-1.1149323	6.661369	-9.109261	2.51E-05	0.017446636	3.252209
Cyp12a5	-1.6798154	7.221268	-8.394041	4.42E-05	0.027758843	2.710714
CG31075	-1.6653272	3.793957	-8.314047	4.72E-05	0.027758843	2.527194
Cyp28a5	-1.7986386	6.911695	-8.265187	4.92E-05	0.027758843	2.608329
CG6271	-2.9577025	3.115061	-8.066407	5.81E-05	0.029437071	2.058155
Ir76a	1.7790618	1.620497	8.054649	5.87E-05	0.029437071	1.517395
Ugt86Dd	-7.0882029	5.253729	-7.973384	6.29E-05	0.029883827	2.034279
TrpA1	-1.3702034	5.794372	-7.794306	7.34E-05	0.033128695	2.219532
CG32407	-1.2413820	5.535908	-7.635119	8.44E-05	0.033280320	2.083579
CG15818	-0.9460242	6.810680	-7.626836	8.50E-05	0.033280320	2.074419
CG10625	1.5983823	3.066627	7.610357	8.62E-05	0.033280320	1.853020
CG18173	-1.3954503	6.511002	-7.542243	9.16E-05	0.033280320	2.000369
CG32024	-1.5876249	4.343815	-7.536068	9.21E-05	0.033280320	1.985623
Ugt36Bc	-1.2177241	7.544371	-7.397908	1.04E-04	0.035239157	1.873875
CG8358	1.5960365	2.733932	7.387141	1.05E-04	0.035239157	1.596200
CG6830	-1.5203065	9.614960	-7.301648	1.14E-04	0.036736286	1.792635
CG16732	-0.8420759	5.930863	-7.158134	1.30E-04	0.039695445	1.652676
CG7912	-1.4473502	4.505639	-7.143148	1.32E-04	0.039695445	1.651243
Cyp9b2	-1.6086006	9.444670	-6.988385	1.53E-04	0.044429338	1.5059

Figure 6.1
C

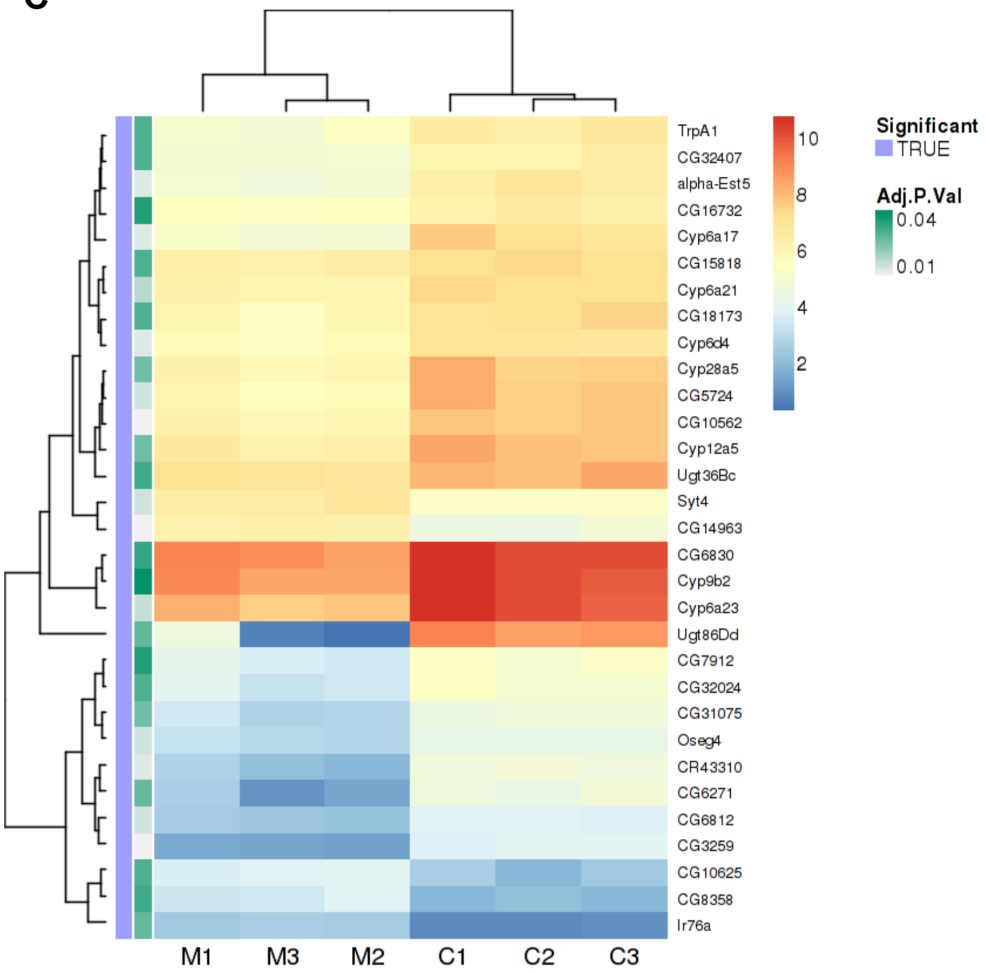
TrpA1
CG32407
alpha-Est5
CG16732
Cyp6a17
CG15818
Cyp6a21
CG18173
Cyp6d4
Cyp28a5
CG5724
CG10562
Cyp12a5
Ugt36Bc
Syt4
CG14963
CG6830
Cyp9b2
Cyp6a23
Ugt86Dd
CG7912
CG32024
CG31075
Oseg4
CR43310
CG6271
CG6812
CG3259
CG10625
CG8358
Ir76a
M1
M3
M2
C1
C2
C3
10
8
6
4
2
Significant
TRUE
Adj.P.Val
0.04
0.01

Figure 6.1

D

Tissue	mRNA Signal	Present Call	Enrichment	Affy Call
Brain	0 ± 0	0 of 4	0.00	None
Head	2 ± 1	0 of 4	0.00	None
Eye	3 ± 1	0 of 4	0.03	None
Thoracicoabdominal ganglion	0 ± 0	0 of 4	0.00	None
Salivary gland	1 ± 0	0 of 4	0.02	None
Crop	0 ± 0	0 of 4	0.00	None
Midgut	2923 ± 168	4 of 4	28.20	Up
Tubule	1 ± 0	0 of 4	0.00	Down
Hindgut	4 ± 2	0 of 4	0.00	None
Heart	1 ± 0	0 of 4	0.02	None
Fat body	2 ± 2	0 of 4	0.03	None
Ovary	0 ± 0	0 of 4	0.00	None
Testis	0 ± 0	0 of 4	0.00	None
Male accessory glands	1 ± 0	0 of 4	0.00	None
Virgin spermatheca	1 ± 0	0 of 4	0.01	None
Mated spermatheca	0 ± 0	0 of 4	0.01	None
Adult carcass	2 ± 0	0 of 4	0.00	None
Larval CNS	0 ± 0	0 of 4	0.01	None
Larval Salivary gland	1 ± 0	0 of 4	0.02	None
Larval midgut	601 ± 352	4 of 4	5.81	None
Larval tubule	0 ± 0	0 of 4	0.00	None
Larval hindgut	1 ± 0	0 of 4	0.01	None
Larval fat body	2 ± 0	0 of 4	0.00	None
Larval trachea	0 ± 0	0 of 4	0.00	None
Larval carcass	0 ± 0	0 of 4	0.01	None
S2 cells (growing)	0 ± 0	0 of 4	0.01	None
Whole fly	103 ± 47	4 of 4		

E

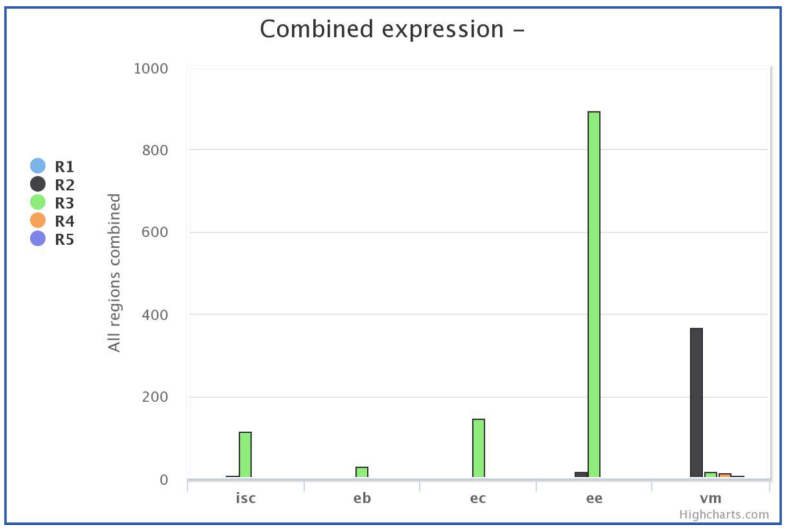

Figure 6.1
F

Protein Alignment: CG6271 and LPL

Sequence 1: NP_651526.1 **Gene:** CG6271 **FLYBASEID:** FBgn0039476 **Length:** 341 **Species:** Drosophila melanogaster
Sequence 2: NP_000228.1 **Gene:** LPL **HGNCID:** 6677 **Length:** 475 **Species:** Homo sapiens

Alignment Length: 329 **Identity:** 95/330 (29%)
Similarity: 155/330 (47%) **Gaps:** 46/330 (14%)

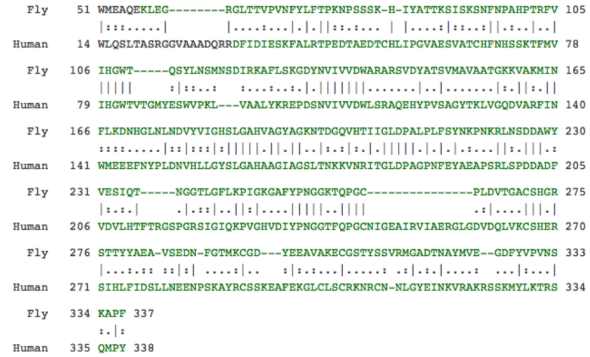

Gene	Sequence	Domain	Region	External ID	Identity
CG6271	NP_651526.1	Lipase	57..337	CDD:278576	94/322 (29%)
		Pancreat_lipase_like	68..333		90/299 (30%)
LPL	NP_000228.1	lipo_lipase	33..473	CDD:132274	92/311 (30%)
		Pancreat_lipase_like	37..334		90/301 (30%)
		PLAT_LPL	341..465	CDD:238856	
		Heparin-binding. {ECO:0000250}	346..441		

Blue background indicates that the domain is not in the aligned region.

7 REFERENCES

Aguilera-Gomez, A., van Oorschot, M.M., Veenendaal, T., Rabouille, C. (2016). In vivo vizualisation of mono-ADP-ribosylation by dPARP16 upon amino-acid starvation. eLife 5: e21475.

Ahel, I., Ahel, D., Matsusaka, T., Clark, A.J., Pines, J., Boulton, S.J., West, S.C. (2008). Poly-ADP-ribose-binding zinc finger motifs in DNA repair/checkpoint proteins. Nature. 451:81–85.

Alvarez-Gonzales, R., Althaus, F.R. (1989). Poly-ADP-ribose catabolism in mammalian cells exposed to DNA-damaging agents. Mutat Res. 218:47–74.

Ame, J.C., Spenlehauer, C., de Murcia, G. (2004). The PARP superfamily. Bioessays. 26:882–893.

Andrabi, S.A., et al. (2006). poly-ADP-ribose (PAR) polymer is a death signal. Proc Natl Acad Sci U S A. Nov 28;103(48):18308-13.

Andrabi, S.A., Kang, H.C., Haince, J.F., Lee, Y.I., Zhang, J., Chi, Z., West, A.B., Koehler, R.C., Poirier, G.G., Dawson, T.M., Dawson, V.L. (2011). Iduna protects the brain from glutamate excitotoxicity and stroke by interfering with poly-ADP-ribose polymer-induced cell death. Nat Med. Jun; 17(6): 692-9.

Andreu, P., Colnot, S., Godard, C., Gad, S., Chafey, P., Niwa-Kawakita, M., Laurent-Puig, P., Kahn, A., Robine, S., Perret, C., Romagnolo, B. (2005). Crypt-restricted proliferation and commitment to the Paneth cell lineage following *Apc* loss in the mouse intestine. Development. 132(6):1443-51.

Asai, M., et al. (2009). PKA rapidly enhances proteasome assembly and activity in in vivo canine hearts. J. Mol. Cell. Cardiol. 46, 452–462.

Apidianakis, Y., et al. (2009). Synergy between bacterial infection and genetic predisposition in intestinal dysplasia. Proc Natl Acad Sci U S A. Dec 8; 106(49): 20883–20888.

Bach, E.A., Ekas, L.A., Ayala-Camargo, A., Flaherty, M.S., Lee, H., Perrimon, N., Baeg, G.H. (2007). GFP reporters detect the activation of the *Drosophila* JAK/STAT pathway in vivo. Gene Expr. Patterns *7*, 323–331.

Bader, M., Benjamin, S., Wapinski, O.L., Smith, D.M., Goldberg, A.L., Steller, H. (2011). A conserved F Box regulatory complex controls proteasome activity in *Drosophila*. Cell *145*, 371–382.

Bai P. (2012). Biology of poly-ADP-ribose polymerases: The Factotums of Cell Maintenance. Molecular Cell. 58-6; 947–958, 1.

Beleke, S. (2012). Regulation of chromatin structure by poly-ADP-ribosylation. Front Genet. Sep 3;3:169.

Belenky, P., Bogan, K.L., and Brenner, C. (2007). NAD+ metabolism in health and disease. Trends Biochem. Sci. *32*, 12–19.

Belle, A., Tanay, A., Bitincka, L., Shamir, R., and O'Shea, E.K. Quanti- fication of protein half-lives in the budding yeast proteome. Proc. Natl. Acad. Sci. USA 103, 13004–13009.

Belote, J.M., Miller, M., Smyth, K.A. (1998). Evolutionary conservation of a testes-specific proteasome subunit gene in *Drosophila*. Gene 215(1): 93-100.

Berkers, C.R. et al. (2007). Profiling Proteasome Activity in Tissue with Fluorescent Probes. Mol. Pharm. 4: 739-748.

Bhardwaj, A., Yang, Y., Ueberheide, B., Smith, S. (2017). Whole proteome analysis of human Tankyrase knockout cells reveals targets of Tankyrase-mediated degradation. Nat Commun 8:2214.

Bisht, K.K., et al. (2012). GDP-mannose-4,6-dehydratase is a cytosolic partner of Tankyrase1 that inhibits its poly-ADP-ribose polymerase activity. Mol Cell Biol. 32 (15), 3044-53.

Boamah K.E., Kotova, E., Garabedian, M., Jarnik, M., Tulin V.A. (2012). Poly-ADP-ribose polymerase 1 (PARP-1) regulates ribosomal biogenesis in *Drosophila* nucleoli. PLoS Genet. Jan; 8(1): e1002442.

Buchon, N., Osman, D., David, F.P.A., Yu Fang, H., Boquete, J.P., Deplancke, B., and Lemaitre, B. (2013). Morphological and Molecular Characterization of Adult Midgut Compartmentalization in *Drosophila*. Cell Rep. *3*, 1725–1738.

Brochier, C., Jones, J.I., Willis, D.E., Langley, B. (2015). Poly-ADP-ribose polymerase 1 is a novel target to promote axonal regeneration. Proc Natl Acad Sci U S A. Dec 8;112(49):15220-5.

Caldecott, K.W. (2014). Protein ADP-ribosylation and the cellular response to DNA strand breaks. DNA Repair (Amst.) 19, 108–113.

Callow, M.G., Tran, H., Phu, L., Lau, T., Lee, J., Sandoval, W.N., Liu, P.S., Bheddah, S., Tao, J., Lill, J.R., et al. (2011). Ubiquitin ligase RNF146 regulates Tankyrase and Axin to promote Wnt signaling. PLoS One 6(7): e22595.

Cambridge, S.B., Gnad, F.N.C., Bermejo, J.L., Kruger, M., and Mann, M. Systems-wide proteomic analysis in mammalian cells reveals conserved, functional protein turnover. J. Proteome Res. 10, 5275–5284.

Chiang, Y.J., Hsiao, S.J., Yver, D., Cushman, S.W., Tessarollo, L., Smith, S., and Hodes, R.J. (2008). Tankyrase 1 and Tankyrase 2 are essential but redundant for mouse embryonic development. PLoS One *3*, e2639.

Chintapalli, V. R., Wang, J., and Dow, J. A. T. (2007). Using FlyAtlas to identify better Drosophila models of human disease. Nature Genetics 39: 715-720.

Cho-Park, P.F., and Steller, H. (2013). Proteasome regulation by ADP-ribosylation. Cell 153, 614–627.

Clevers, H., Nusse, R. (2012). Wnt/β-catenin signaling and disease. Cell 149, 1192–1205.

Chu-Ping, M., Slaughter, C.A., DeMartino, G.N. (1992). Purification and characterization of a protein inhibitor of the 20S proteasome (macropain).
Biochimica et biophysica acta 1119, 303-311.

Collins, R.T., and Treisman, J.E. (2000). Osa-containing Brahma chromatin remodeling complexes are required for the repression of Wingless target genes. Genes Dev. 14, 3140–3152.

Cockman M.E., et al. (2009). Proteomics-based identification of novel factor inhibiting hypoxia-inducible factor (FIH) substrates indicates widespread asparaginyl hydroxylation of ankyrin repeat domain-containing proteins. Mol Cell Proteomics. Mar;8(3):535-46.

Cordero, J.B., Stefanatos, R.K., Scopelliti, A., Vidal, M., and Sansom, O.J. (2012). Inducible progenitor-derived Wingless regulates adult midgut regeneration in *Drosophila*. EMBO J. 31, 3901–3917.

Croy, H.E., Fuller, C.N., Giannotti, J., Robinson, P., Foley, A.V.A., Yamulla, R.J., Cosgriff, S., Greaves, B.D., Von Kleeck, R.A., An, H.H., et al. (2016). The poly(ADP-ribose) polymerase enzyme Tankyrase antagonizes activity of the β-catenin destruction complex through ADP-ribosylation of Axin and APC2. J. Biol. Chem. 291, 12747–12760.

Catara, G., Grimaldi, G., Schembri, L., Spano, D., Turacchio, G., Monte, L.M., Beccari, A.R., Valente, C., Corda, D. (2017). PARP1-produced poly-ADP-ribose causes the PARP12 translocation to stress granules and impairment of Golgi complex functions Sci. Rep.7.p.14035.

Chaudhuri*, A.R.,* Nussenzweig*, A. (2017).* The multifaceted roles of PARP1 in DNA repair and chromatin remodeling. Nat Rev Mol Cell Biol. Oct;18(10):610-621.

Chi, N.W., Lodish, H.F. (2000). Tankyrase is a golgi-associated mitogen-activated protein kinase substrate that interacts with IRAP in GLUT4 vesicles. J Biol Chem. Dec 8;275(49):38437-44.

Cho, S., et al. (2009). PARP-14, a member of the B aggressive lymphoma family, transduces survival signals in primary B cells. Blood 113, 2416–2425.

Daniels, C.M., Ong, S-E., Leung, A.K.L. (2014). The Promise of Proteomics for the Study of ADP-ribosylation. Mol Cell. Jun 18; 58(6): 911–924.

DaRosa, P.A., Wang, Z., Jiang, X., Pruneda, J.N., Cong, F., Klevit, R.E., and Xu, W. (2014). Allosteric activation of the RNF146 ubiquitin ligase by a polyADP-ribosylation signal. Nature. *8*; 517(7533): 223.

DaRosa P.A., et al. (2018). Structural basis for Tankyrase-RNF146 interaction reveals noncanonical tankyrase-binding motifs. Protein Sci. Jun;27(6):1057-1067.

de Bie, P., and Ciechanover, A. (2011). Ubiquitination of E3 ligases: self-regulation of the ubiquitin system via proteolytic and non-proteolytic mechanisms. Cell Death Differ. Sep;18(9):1393-402.

De Rycker, M., Price, C.M. (2004). Tankyrase polymerization is con- trolled by its sterile alpha motif and poly(ADP-ribose) polymerase domains. Mol Cell Biol 24:9802–9812.

Deng, W. (2009). PARylation: strengthening the connection between cancer and pluripotency. Cell Stem Cell. Oct 2;5(4):349-50.

Duan, Y., Du, A., Gu J., Duan, G., Wang, C., Sun, L., et al. (2018). PARylation modulates stress granule assembly, phase separation, and neurotoxicity of disease-related RNA-binding proteins. bioRxiv, 396465. 10.1101/396465.

Dutta, D., Xiang, J., and Edgar, B.A. (2013). RNA expression profiling from FACS-isolated cells of the Drosophila intestine. Curr Protoc Stem Cell Biol 27, Unit2F.2.–2F.2.12.

Elhassan, Y.S., Philp, A.A., and Lavery, G.G. (2017). Targeting NAD+ in Metabolic Disease: New Insights Into an Old Molecule. J. Endocr. Soc. *1*, 816–835.

Eustermann, S., Wu, W.F., Langelier, M.F., Yang, J.C., Easton, L.E., Riccio, A.A., Pascal, J.M., Neuhaus, D. (2015). Structural Basis of Detection and Signaling of DNA Single-Strand Breaks by Human PARP-1. Mol Cell. Dec 3;60(5):742-754.

Eisemann, T., McCauley, M., Langelier, M-F., et al. (2016). Tankyrase-1 ankyrin repeats form an adaptable binding platform for targets of ADP-ribose modi cation. Structure 24:1679–1692.

Fan, C., et al. (2018). Regulation of Tankyrase activity by a catalytic domain dimer interface. Biochem Biophys Res Commun. Sep 10;503(3):1780-1785.

Fancy, S.P.J., et al. (2011). Axin2 as regulatory and therapeutic target in newborn brain injury and remyelination. Nat Neurosci. Jun 26;14(8):1009-16.

Fatokun, A.A., Dawson, V.L., and Dawson, T.M. (2014). Parthanatos: mitochondrial-linked mechanisms and therapeutic opportunities. Br. J. Pharmacol. 171, 2000–2016.

Feng, Y., Li, X., Ray, L., Song, H., Qu, J., Lin, S., and Lin, X. (2014). The *Drosophila* Tankyrase regulates Wg signaling depending on the concentration of dAxin. Cell. Signal. 26, 1717–1724.

Feng, Y., Li, Z., Lv, L., Du, A., Lin, Z., Ye, X., Lin, Y., Lin, X. (2018). Tankyrase regulates apoptosis by activating JNK signaling in Drosophila. Biochem Biophys Res Commun. Sep 18;503(4):2234-2239.

Fevr, T., Robine, S., Louvard, D., and Huelsken, J. (2007). Wnt/ β-catenin is essential for intestinal homeostasis and maintenance of intestinal stem cells. Mol. Cell. Biol. 27, 7551–7559.

Finley, D. (2009). Recognition and processing of ubiquitin-protein conjugates by the proteasome. Annu Rev Biochem. 78:477-513.

Förster A., et al. (2005). The 1.9 A structure of a proteasome-11S activator complex and implications for proteasome-PAN/PA700 interactions. Mol Cell. May 27;18(5):589-99.

Frizzell, K.M., Gamble, M.J., Berrocal, J.G., Zhang, T., Krishnakumar, R., Cen, Y., Sauve, A.A., Kraus, W.L. (2009). Global analysis of transcriptional regulation by poly-ADP-ribose polymerase-1 and poly-ADP-ribose glycohydrolase in MCF-7 human breast cancer cells. J Biol Chem. Dec 4;284(49):33926-38.

Gagné, J.P., Isabelle, M., Lo, K.S., Bourassa, S., Hendzel, M.J., Dawson, V.L., Dawson, T.M., Poirier G.G. (2008). Proteome-wide identification of poly-ADP-ribose-binding proteins and poly-ADP-ribose-associated protein complexes. Nucleic Acids Res. Dec;36(22):6959-76.

Gao, Y., Song, C., Hui, L., et al. (2014). Overexpression of *RNF146* in Non-Small Cell Lung Cancer Enhances Proliferation and Invasion of Tumors through the Wnt/β-catenin Signaling Pathway. PLoS ONE 9(1): e85377.

Gerlach, J.P., Emmink, B.L., Nojima, H., Kranenburg, O., and Maurice, M.M. (2014). Wnt signaling induces accumulation of phosphorylated β-catenin in two distinct cytosolic complexes. Open Biol. 4, 140120–140120.

Gerö, D., Szoleczky, P., Chatzianastasiou, A., Papapetropoulos, A., Szabo, C. (2014). Modulation of poly-ADP-ribose polymerase-1 (PARP-1)-mediated oxidative cell injury by ring finger protein 146 (RNF146) in cardiac myocytes. Mol Med. Jul 31; 20: 313-28.

Gibson, B.A., and Kraus, W.L. (2012). New insights into the molecular and cellular functions of poly-ADP-ribose and PARPs. Nat. Rev. Mol. Cell Biol. 13, 411–424.

Gibson, A.B., and Kraus, W.L. (2012). New insights into the molecular and cellular functions of polyADP-ribose and PARPs Nature Reviews Molecular Cell Biology 13; 411–424.

Goenka, S., Boothby, M. (2006). Selective potentiation of Stat-dependent gene expression by collaborator of Stat6 (CoaSt6), a transcriptional cofactor. Proc. Natl Acad. Sci. USA 103, 4210–4215.

Ghiglione, C., Devergne, O., Georgenthum, E., Carballès, F., Médioni, C., Cerezo, D., Noselli, S. (2002). The *Drosophila* cytokine receptor Domeless controls border cell migration and epithelial polarization during oogenesis. Development. 129, 5437–5447.

Glickman, M.H., Ciechanover, A. (2002). The ubiquitin-proteasome proteolytic pathway: destruction for the sake of construction. Physiol. Rev. Apr 82(2): 373- 428.

Gratz, S.J., Cummings, A.M., Nguyen, J.N., Hamm, D.C., Donohue, L.K., Harrison, M.M., Wildonger, J., and O'connor-Giles, K.M. (2013). Genome engineering of *Drosophila* with the CRISPR RNA-guided Cas9 nuclease. Genetics. 194, 1029–1035.

Gratz, S.J., Ukken, F.P., Rubinstein, C.D., Thiede, G., Donohue, L.K., Cummings, A.M., and Oconnor-Giles, K.M. (2014). Highly specific and efficient CRISPR/Cas9-catalyzed homology-directed repair in *Drosophila*. Genetics *196*, 961–971.

Gultekin, Y., Steller, H. (2019). Axin proteolysis by Iduna is required for the regulation of stem cell proliferation and intestinal homeostasis in *Drosophila*. Development. 146: dev169284.

Guarente, L., Picard, F. (2005). Calorie restriction--the SIR2 connection. Cell. Feb 25;120(4):473-82.

Guo, X., Huang, X. & Chen, M. J. (2017). Reversible phosphorylation of the 26S proteasome. Protein Cell 8, 255–272.

Guettler, S., et al. (2011). Structural basis and sequence rules for substrate recognition by Tankyrase explain the basis for cherubism disease. Cell. Dec 9;147(6):1340-54.

Hayashi, K., Tanaka, M., Shimada, T., Miwa, M., Sugimura, T. (1983). Size and shape of poly-ADP-ribose: examination by gel filtration, gel electrophoresis and electron microscopy. Biochem Biophys Res Commun. 112:102–7.

He, F., Tsuda, K., Takahashi, M., Kuwasako, K., Terada, T., Shirouzu, M., Watanabe, S., Kigawa, T., Kobayashi, N., Güntert, P., Yokoyama, S., Muto, Y. (2012). Structural

insight into the interaction of ADP-ribose with the PARP WWE domains. FEBS Lett. Nov 2; 586(21): 3858-64.

Hottiger, M.O. (2015). Nuclear ADP-ribosylation and its role in chromatin plasticity, cell differentiation, and epigenetics. Annu. Rev. Biochem. 84, 227–263.

Hsiao, S.J., and Smith, S. (2008). Tankyrase function at telomeres, spindle poles, and beyond. Biochimie 90, 83–92.

Hanai, S., Kanai, M., Ohashi, S., Okamoto, K., Yamada, M., Takahashi, H., Miwa, M. (2004). Loss of *poly-ADP-ribose glycohydrolase* causes progressive neurodegeneration in *Drosophila melanogaster*. Proc Natl Acad Sci U S A. Jan 6;101(1):82-6.

Hassa, P.O., Haenni, S.S., Elser, M., Hottiger, M.O. (2006). Nuclear ADP-ribosylation reactions in mammalian cells: where are we today and where are we going? Microbiol Mol Biol Rev. 70:789–829.

Herrera S.C., Bach, E.A. (2019). JAK-STAT signaling in stem cells and regeneration: from Drosophila to vertebratesDevelopment. 146, dev167643.

Hamada, F., Tomoyasu, Y., Takatsu, Y., Nakamura, M., Nagai, S.I., Suzuki, A., Fujita, F., Shibuya, H., Toyoshima, K., Ueno, N., et al. (1999). Negative regulation of Wingless signaling by D-Axin, a Drosophila homolog of Axin. Science. *283*, 1739–1742.

Hershko, A., Ciechanover, A. (1998). The ubiquitin system. Annu Rev Biochem. 67:425-79.

Herr, P., Hausmann, G., Basler, K. (2012). WNT secretion and signaling in human disease. Trends Mol Med. (8):483-93.

Hsiao, S.J., Poitras, M.F., Cook, B.D., Liu, Y., and Smith, S. (2006). Tankyrase 2 poly-ADP-ribose polymerase domain-deleted mice exhibit growth defects but have normal telomere length and capping. Mol. Cell. Biol. *26*, 2044–2054.

Huang, S.M.A., Mishina, Y.M., Liu, S., Cheung, A., Stegmeier, F., Michaud, G.A., Charlat, O., Wiellette, E., Zhang, Y., Wiessner, S., et al. (2009). Tankyrase inhibition stabilizes Axin and antagonizes Wnt signaling. Nature 461, 614–620.

Igarashi, M., Guarente, L. (2016). mTORC1 and SIRT1 Cooperate to Foster Expansion of Gut Adult Stem Cells during Calorie Restriction. Cell. Jul 14;166(2):436-450.

Ilardi, J.M., Mochida, S., Sheng Z.H. (1999). Snapin: a SNARE-associated protein implicated in synaptic transmission. Nature Neuroscience. 2 (2):119–24.

Isabelle, M., Gagne´, J.P., Gallouzi, I.E., and Poirier, G.G. (2012). Quantitative proteomics and dynamic imaging reveal that G3BP-mediated stress granule assembly is poly-ADP-ribose-dependent following exposure to MNNG-induced DNA alkylation. J. Cell Sci. 125, 4555–4566.

Jwa, M. & Chang, P. (2012). PARP16 is a tail-anchored endoplasmic reticulum protein required for the PERK- and IRE1α-mediated unfolded protein response. Nature Cell Biol. 14, 1223–1230.

Jiang, H., Patel P.H., Kohlmaier, A., Grenley, M.O., McEwen, D.G., Edgar, B.A. (2009). Cytokine/Jak/Stat signaling mediates regeneration and homeostasis in the Drosophila midgut. Cell. Jun 26;137(7):1343-55. doi: 10.1016/j.cell.2009.05.014.

Kanai M, Uchida M, Hanai S, Uematsu N, Uchida K, Miwa M. (2000). Poly-ADP-ribose polymerase localizes to the centrosomes and chromosomes. Biochem Biophys Res Commun. 278:385–9.

Kang, H.C., Lee, Y.I., Shin, J.H., Andrabi, S.A., Chi, Z., Gagné, J.P., Lee, Y, Ko, H.S., Lee, B.D., Poirier, G.G., Dawson, V.L., Dawson, T.M. (2011). Iduna is a poly(ADP-ribose) (PAR) dependent E3 ubiquitin ligase that regulates DNA damage. Proc Natl Acad Sci U S A. Aug 23; 108(34): 14103-8.

Kim, H.J., Kim, N.C., et al. (2013). Mutations in prion-like domains in hnRNPA2B1 and hnRNPA1 cause multisystem proteinopathy and ALS. Nature. Mar 28;495(7442):467-73.

Kinzler, K., Nilbert, M., Su, L., Vogelstein, B., Bryan, T., Levy, D., Smith, K., Preisinger, A., Hedge, P., McKechnie, D., et al. (1991). Identification of FAP locus genes from chromosome 5q21. Science. *253*, 661–665.

Kloetzel, P.M. (2004). The proteasome and MHC class I antigen processing. Biochim Biophys Acta. Nov 29;1695(1-3):225-33.

Korinek, V., Barker, N., Morin, P.J., van Wichen, D., de Weger, R., Kinzler, K.W., Vogelstein, B., and Clevers, H. (1997). Constitutive transcriptional activation by a beta-catenin-Tcf complex in $APC^{-/-}$ colon carcinoma. Science *275*, 1784–1787.

Korinek, V., Barker, N., Moerer, P., Van Donselaar, E., Huls, G., Peters, P.J., and Clevers, H. (1998). Depletion of epithelial stem-cell compartments in the small intestine of mice lacking Tcf-4. Nat. Genet. *19*, 379–383.

Kotova E, Jarnik M, Tulin AV. (2009). Poly-ADP-ribose polymerase 1 is required for protein localization to Cajal body. PLoS Genet. Feb;5(2):e1000387.

Kramps, T., Peter, O., Brunner, E., Nellen, D., Froesch, B., Chatterjee, S., Murone, M., Züllig, S., and Basler, K. (2002). Wnt/Wingless signaling requires BCL9/legless-mediated recruitment of pygopus to the nuclear β-catenin-TCF complex. Cell *109*, 47–60.

Krietsch, J., Rouleau, M., Pic, E., Ethier, C., Dawson, T.M., Dawson, V.L., Masson, J.Y., Poirier, G.G., and Gagne´, J.P. (2013). Reprogramming cellular events by poly-ADP-ribose-binding proteins. Mol. Aspects Med. 34, 1066–1087.

Krishnakumar R., Kraus W.L. (2010). The PARP side of the nucleus: molecular actions, physiological outcomes, and clinical targets. Mol Cell. Jul 9;39(1):8-24.

Lee, E., Salic, A., Krüger, R., Heinrich, R., and Kirschner, M.W. (2003). The roles of APC and Axin derived from experimental and theoretical analysis of the Wnt pathway. PLoS Biol. *1*.

Lehmann, S., Loh, S.H.Y., and Martins, L.M. (2016). Enhancing NAD+ salvage metabolism is neuroprotective in a PINK1 model of Parkinson's disease. Biol. Open *6*, 141–147.

Levaot, N., Voytyuk, O., Dimitriou, I., Sircoulomb, F., Chandrakumar, A., Deckert, M., Krzyzanowski, P.M., Scotter, A., Gu, S., Janmohamed, S., Cong, F., Simoncic, P.D., Ueki, Y., La Rose, J., Rottapel, R. (2011). Loss of Tankyrase-mediated destruction of 3BP2 is the underlying pathogenic mechanism of cherubism. Cell. 2011 Dec 9;147(6):1324-39.

Lehtiö, L., Collins, R., van den Berg, S., et al. (2008). Zinc binding catalytic domain of human Tankyrase 1. J Mol Biol 379:136–145.

Leung, A.K. (2014). Poly-ADP-ribose: an organizer of cellular architecture. J. Cell Biol. 205, 613–619.

Leung, A.K., et al. (2011). Poly-ADP-ribose regulates stress responses and microRNA activity in the cytoplasm. Mol Cell. May 20;42(4):489-99.

Li, P., Huang, P., et al. (2018). Tankyrase mediates K63-linked ubiquitination of JNK to confer stress tolerance and influence lifespan in *Drosophila.* Cell Rep. 25, 437–448.

Li, N., Feng, L., et al. (2016). PARP Inhibition Suppresses Growth of EGFR-Mutant Cancers by Targeting Nuclear PKM2. Cell Rep. Apr 26;15(4):843-856.

Li, V.S.W., Ng, S.S., Boersema, P.J., Low, T.Y., Karthaus, W.R., Gerlach, J.P., Mohammed, S., Heck, A.J.R., Maurice, M.M., Mahmoudi, T., et al. (2012). Wnt signaling through inhibition of β-catenin degradation in an intact Axin1 complex. Cell *149*, 1245–1256.

Lin, G., Xu, N., and Xi, R. (2008). Paracrine Wingless signaling controls self-renewal of *Drosophila* intestinal stem cells. Nature *455*, 1119–1123.

Liu, K., Jones, S., Minis, A., Rodriguez, J., Molina, H., Steller, H. (2019). PI31 is an adaptor protein for proteasome transport in axons and required for synaptic development and function. bioRxiv 364463; doi: https://doi.org/10.1101/364463.

Lu, J., Ma, Z., Hsieh, J.C., Fan, C.W., Chen, B., Longgood, J.C., Williams, N.S., Amatruda, J.F., Lum, L., and Chen, C. (2009). Structure-activity relationship studies of small-molecule inhibitors of Wnt response. Bioorganic Med. Chem. Lett. *19*, 3825–3827.

Li, N., Zhang, Y., Han, X., Liang, K., Wang, J., Feng, L., Wang, W., Songyang, Z., Lin, C., Yang, L., Yu, Y., Chen, J. (2014). Poly-ADP ribosylation of PTEN by Tankyrases promotes PTEN degradation and tumor growth. Genes Dev. Dec 29.

Lin, S.-J., Defossez, P.-A., and Guarente, L. (2000). Requirement of NAD and SIR2 for Life- Span Extension by Calorie Restriction in Saccharomyces cerevisiae. Science *289*, 2126–2128.

Lin, W., Amé, J.C., Aboul-Ela, N., Jacobson, E.L., Jacobson, M.K. (1997). Isolation and characterization of the cDNA encoding bovine poly(ADP-ribose) glycohydrolase. J Biol Chem. 272:11895–11901.

Ma, J., Katz, E., Belote, J.M. (2002). Expression of proteasome subunit isoforms during spermatogenesis in *Drosophila melanogaster*. Insect Mol. Biol. 11(6): 627-639.

Martire, S., Mosca, L., d'Erme, M. (2015). PARP-1 involvement in neurodegeneration: A focus on Alzheimer's and Parkinson's diseases. Mech Ageing Dev. 146-148:53-64.

Mariotti, L., Templeton, C.M., Ranes, M., et al. (2016). Tankyrase requires SAM domain-dependent polymerization to support Wnt-beta- catenin signaling. MolCell 63:498–513.

Markstein, M., Dettorre, S., Cho, J., Neumuller, R.A., Craig-Muller, S., and Perrimon, N. (2014). Systematic screen of chemotherapeutics in *Drosophila* stem cell tumors. Proc. Natl. Acad. Sci. *111*, 4530–4535.

Mattila, J., Kokki, K., Hietakangas, V., Boutros, M. (2018) Stem Cell Intrinsic Hexosamine Metabolism Regulates Intestinal Adaptation to Nutrient Content. Dev Cell. Sep 7. pii: S1534-5807(18)30681-6. doi: 10.1016/j.devcel.2018.08.011.

Marianes, A., Spradling, and A.C. Spradling (2013). Physiological and stem cell compartmentalization within the Drosophila midgut. Elife 2.

Martello, R., Leutert, M., et al. (2016). Proteome-wide identification of the endogenous ADP-ribosylome of mammalian cells and tissue. Nat Commun. Sep 30;7:12917.

Matsumoto, Y., La Rose, J., Lim, M., Adissu, H.A., Law, N., Mao, X., Cong, F., Mera, P., Karsenty, G., Goltzman, D., et al. (2017a). Ubiquitin ligase RNF146 coordinates bone dynamics and energy metabolism. J. Clin. Invest. *127*, 2612–2625.

Matsumoto, Y., Larose, J., Kent, O.A., Lim, M., Changoor, A., Zhang, L., Storozhuk, Y., Mao, X., Grynpas, M.D., Cong, F., et al. (2017b). RANKL coordinates multiple osteoclastogenic pathways by regulating expression of ubiquitin ligase RNF146. J. Clin. Invest. *127*, 1303–1315.

McCutchen-Maloney, S.L. et al. (2000). cDNA cloning, expression, and functional characterization of PI31, a proline-rich inhibitor of the proteasome. The Journal of biological chemistry 275, 18557-18565.

McGurk, L., Gomes, E., Guo, L., Mojsilovic-Petrovic, J., Tran, V., Kalb, R.G., Shorter, J., Bonini, N.M. (2018). Poly-ADP-ribose prevents pathological phase separation of TDP-43 by promoting liquid demixing and stress granule localization. Mol Cell. Sep 6;71(5):703-717.e9.

McCubrey, J.A., et al. (2014). GSK-3 as potential target for therapeutic intervention in cancer. Oncotarget. May 30;5(10):2881-911.

McClure, J.M., Wierman, M.B., Maqani, N., and Smith, J.S. (2012). Isonicotinamide enhances Sir2 protein-mediated silencing and longevity in yeast by raising intracellular NAD+ concentration. J. Biol. Chem. *287*, 20957–20966.

Ménissier de Murcia, J., et al. (2003). Functional interaction between PARP-1 and PARP-2 in chromosome stability and embryonic development in mouse. EMBO J. May 1;22(9):2255-63.

Micchelli, C.A., and Perrimon, N. (2006). Evidence that stem cells reside in the adult *Drosophila* midgut epithelium. Nature *439*, 475–479.

Miwa, M., Masutani, M. (2007). PolyADP-ribosylation and cancer. Cancer Sci. Oct;98(10):1528-35.

Miwa, M., Masutani, M. (2007) PolyADP-ribosylation and cancer. Cancer Sci 98: 1528–1535.

Miwa, M., Saikawa, N., Yamaizumi, Z., Nishimura, S., Sugimura, T. (1979). Structure of poly(adenosine diphosphate ribose): identification of 2′-[1″-ribosyl-2″-(or3″)(1‴-ribosyl)]adenosine-5′,5″,5‴-tris (phosphate) as a branch linkage. Proc Natl Acad Sci USA. 76: 595–9.

Miwa, M., Kanai, M., Uchida, M., Uchida, K., Hanai, S. (2006). Roles of poly-ADP-ribose metabolism in the regulation of centrosome duplication and in the maintenance of neuronal integrity. In: Buerkle A, ed. Poly-ADP-ribosylation.Georgetown, Texas: Landes Bioscience. 51–60.

Morrone, S., Cheng, Z., Moon, R.T., et al. (2012). Crystal structure of a Tankyrase-Axin complex and its implications for Axin turnover and Tankyrase substrate recruitment. Proc Natl Acad Sci USA 109:1500–1505.

Morin, P.J., Sparks, B., Korinek, V., Barker, N., Clevers, H., Vogelstein, B., and Kinzler, K.W. (1997). Activation of beta-catenin-Tcf signaling in colon cancer by mutations in beta-catenin or APC. Science *275*, 1787–1790.

Murata, S., Yashiroda, H., Tanaka, K. (2009). Molecular mechanisms of proteasome assembly. Nat. Rev. Mol. Cell Biol. Feb;10 (2):104-15.

Narayan, P., Ehsani, S., Lindquist, S. (2014). Combating neurodegenerative disease with chemical probes and model systems. Nat Chem Biol. Nov;10(11):911-20.

Naszai, M., et al. (2015). Intestinal stem cell proliferation and epithelial homeostasis in the adult Drosophila midgut. Insect Biochem Mol Biol. Dec;67:9-14.

Neumann, M., Sampathu, D.M., Kwong, L.K., et al. (2006). Ubiquitinated TDP-43 in frontotemporal lobar degeneration and amyotrophic lateral sclerosis. Science. 314:130–133.

Nishisho, I., Nakamura, Y., Miyoshi, Y., Miki, Y., Ando, H., Horii, A., Koyama, K., Utsunomiya, J., Baba, S., and Hedge, P. (1991). Mutations of chromosome 5q21 genes in FAP and colorectal cancer patients. Science. *253*, 665–669.

Nusse, R., Clevers, H. (2017). Wnt/β-catenin signaling, disease, and emerging therapeutic modalities. Cell *169*, 985–999.

Nottbohm, A.C., Dothager, R.S., Putt, K.S., Hoyt, M.T., Hergenrother, P.J. (2007). A colorimetric substrate for poly-ADP-ribose polymerase-1, VPARP, and tankyrase-1. Angew Chem Int Ed Engl. 46(12):2066-9.

Ocampo, A., Liu, J., and Barrientos, A. (2013). NAD+ salvage pathway proteins suppress proteotoxicity in yeast models of neurodegeneration by promoting the clearance of misfolded/oligomerized proteins. Hum. Mol. Genet. *22*, 1699–1708.

Ohlstein, B., Spradling, A. (2006). The adult *Drosophila* posterior midgut is maintained by pluripotent stem cells. Nature *439*, 470–474.

Palazzo, L., Thomas, B., et al. (2015). Processing of protein ADP-ribosylation by Nudix hydrolases. Biochem J. Jun 1; 468(2): 293–301.

Pereira, M. E. & Wilk, S. (1990). Phosphorylation of the multicatalytic proteinase complex from bovine pituitaries by a copurifying cAMP-dependent protein kinase. *Arch. Biochem. Biophys.* 283, 68–74 (1990).

Perina, D., Mikoč, A., Ahel, J., Cetković, H., Zaja, R., Ahel, I. (2014). Distribution of protein poly-ADP-ribosylation systems across all domains of life. DNA Repair (Amst). 23:4–16.

Port, F., Chen, H.-M., Lee, T., and Bullock, S.L. (2014). Optimized CRISPR/Cas tools for efficient germline and somatic genome engineering in *Drosophila*. Proc. Natl. Acad. Sci. *111*, E2967–E2976.

Price, J.C., Guan, S., Burlingame, A., Prusiner, S.B., and Ghaemmaghami, S. Analysis of proteome dynamics in the mouse brain. Proc. Natl. Acad. Sci. USA 107, 14508–14513.

Riccio, A.A., McCauley, M., Langelier, M-F., Pascal, J.M. (2016). Tankyrase sterile α motif domain polymerization is required for its role in Wnt signaling. Structure 24:1573–1581.

Rousseau, A., Bertolotti, A. (2018). Regulation of proteasome assembly and activity in health and disease. Nat Rev Mol Cell Biol. Nov;19(11):697-712.

Ruf, A., Mennissier de Murcia, J., de Murcia, G. & Schulz, G. E. (1996). Structure of the catalytic fragment of poly-ADP-ribose polymerase from chicken. *Proc. Natl Acad. Sci. USA* 93, 7481–7485.

Rubinfeld, B., Robbins, P., El-Gamil, M., Albert, I., Porfiri, E., and Polakis, P. (1997). Stabilization of beta-catenin by genetic defects in melanoma cell lines. Science *275*, 1790–1792.

Riffell, J.L., Lord, C.J., and Ashworth, A. (2012). Tankyrase-targeted therapeutics: expanding opportunities in the PARP family. Nature Reviews Drug Discovery. 11; 923–936.

Saito-Diaz, K., Benchabane, H., Tiwari, A., Tian, A., Li, B., Thompson, J.J., Hyde, A.S., Sawyer, L.M., Jodoin, J.N., Santos, E., et al. (2018). APC inhibits ligand-independent Wnt signaling by the clathrin endocytic pathway. Dev. Cell *44*, 566–581.e8.

Salic, A., Lee, E., Mayer, L., and Kirschner, M.W. (2000). Control of β-catenin stability: Reconstitution of the cytoplasmic steps of the Wnt pathway in *Xenopus* egg extracts. Mol. Cell *5*, 523–532.

Satoh, K., Sasajima, H., Nyoumura, K., Yokosawa, H. & Sawada, H. (2001). Assembly of the 26S proteasome is regulated by phosphorylation of the p45/Rpt6 ATPase subunit. *Biochemistry* 40, 314–319.

Savas, J.N., Toyama, B.H., Xu, T., Yates, J.R. 3rd, Hetzer M.W. (2012). Extremely long-lived nuclear pore proteins in the rat brain. Science. Feb 24;335(6071):942.

Seimiya, H., Muramatsu, Y., Smith, S., Tsuruo, T. (2004). Functional subdomain in the ankyrin domain of tankyrase 1 required for poly(ADP-ribosyl)ation of TRF1 and telomere elonga- tion. Mol Cell Biol 24:1944–1955.

Schreiber, V., Dantzer, F., Ame, J.C., de Murcia, G. (2006) Poly(ADP-ribose): novel functions for an old molecule. Nat Rev Mol Cell Biol 7: 517–528.

Sharifi R, Morra R, et al. (2013). Deficiency of terminal ADP-ribose protein glycohydrolase TARG1/C6orf130 in neurodegenerative disease. EMBO J. May 2;32(9):1225-37.

Singh, H.R., et al. (2017). A Poly-ADP-Ribose Trigger Releases the Auto-Inhibition of a Chromatin Remodeling Oncogene. Mol Cell. Dec 7;68(5):860-871.e7.

Slade, D., Dunstan, M., Barkauskaite, E., Weston, R., Lafite, P., Dixon, N., Ahel, M., Leys, D., Ahel, I. (2011). The structure and catalytic mechanism of a poly-ADP-ribose glycohydrolase. Nature. 477:616–620.

Smith, S., Giriat, I., Schmitt, A., de Lange, T. (1998). Tankyrase, a poly(ADP-ribose) polymerase at human telomeres. Science 282:1484–1487.

Song, C., et al. (2014). Control of lipid metabolism by Tachykinin in *Drosophila.* Cell Rep. Oct 9; 9(1): 40–47.

Starcevic, M., Dell'Angelica, E.C. (2004). Identification of snapin and three novel proteins (BLOS1, BLOS2, and BLOS3/reduced pigmentation) as subunits of biogenesis of lysosome-related organelles complex-1 (BLOC-1). The Journal of Biological Chemistry. 279 (27): 28393–401.

Teloni, F., Altmeyer, M. (2016). Readers of poly-ADP-ribose: designed to be fit for purpose. Nucleic Acids Res.44.pp. 993-1006.

Toyama, B.H., Savas, J.N., Park, S.K., Harris, M.S., Ingolia, N.T., Yates, J.R. 3rd, Hetzer, M.W. (2013a). Identification of long-lived proteins reveals exceptional stability of essential cellular structures. Cell. Aug 29;154(5):971-82.

Toyama, B.H., Hetzer, M.W. (2013b) Protein homeostasis: live long, won't prosper. Nat Rev Mol Cell Biol. Jan;14(1):55-61.

Theodosiou, N.A., and Xu, T. (1998). Use of FLP/FRT system to study *Drosophila* development. Methods A Companion to Methods Enzymol. *14*, 355–365.

Tian, A., Benchabane, H., Wang, Z., and Ahmed, Y. (2016). Regulation of stem cell proliferation and cell fate specification by Wingless/Wnt signaling gradients enriched at adult intestinal compartment boundaries. PLoS Genet. *12*.

Ueki, Y., et al. (2007). Increased myeloid cell responses to M-CSF and RANKL cause bone loss and inflammation in SH3BP2 "cherubism" mice. Cell. Jan 12;128(1):71-83.

Verdin, E. (2015). NAD+ in aging, metabolism, and neurodegeneration. Science *350*, 1208–1213.

Vilchez, D., Saez, I., Dillin, A. (2014). The role of protein clearance mechanisms in organismal ageing and age-related diseases. Nat Commun. Dec 8;5:5659.

Vyas, S., and Chang, P. (2014). New PARP targets for cancer therapy. Nat. Rev. Cancer *14*, 502–509.

von Rotz, R.C., Kins, S., Hipfel, R., von der Kammer, H., Nitsch, R.M.(2005). The novel cytosolic RING finger protein dactylidin is up-regulated in brains of patients with Alzheimer's disease. Eur J Neurosci. Mar; 21(5): 1289-98.

Wang, S., Xing, Z., Vosler, P.S., Yin, H., Li, W., Zhang, F., Signore, A.P., Stetler, R.A., Gao, Y., and Chen, J. (2008). Cellular NAD+ replenishment confers marked neuroprotection against ischemic cell death role of enhanced DNA repair. Stroke J. Cereb. Circ. *39*, 2587–2595.

Wang, W., Li, N., Li, X., Tran, M.K., Han, X., Chen, J. (2015). Tankyrase Inhibitors Target YAP by Stabilizing Angiomotin Family Proteins. Cell Rep. Oct 20; 13(3): 524-32.

Wang Y., Kim N.S, Haince J.F., Kang H.C., David K.K., Andrabi S.A., Poirier G.G., Dawson V.L., Dawson T.M. Poly-ADP-ribose (PAR) binding to apoptosis- inducing factor is critical for PAR polymerase-1-dependent cell death (parthanatos). Sci Signal. 2011 Apr 5; 4(167) : ra20.

Wang, Z., Tian, A., Benchabane, H., Tacchelly-Benites, O., Yang, E., Nojima, H., and Ahmed, Y. (2016a). The ADP-ribose polymerase Tankyrase regulates adult intestinal stem cell proliferation during homeostasis in *Drosophila*. Development *143*, 1710–1720.

Wang, H., Lu, B., et al. (2016). Tankyrase inhibitor sensitizes lung cancer to endothelial growth factor receptor (EGFR) inhibition via stabilizing angiomotins and inhibiting YAP signaling. JBC. 291;29,15256-15266.

Wang, Z., Tacchelly-Benites, O., Yang, E., Thorne, C.A., Nojima, H., Lee, E., and Ahmed, Y. (2016b). Wnt/wingless pathway activation is promoted by a critical threshold of Axin maintained by the tumor suppressor APC and the ADP-ribose polymerase Tankyrase. Genetics *203*, 269–281.

Wang, Z., Michaud, G.A., Cheng, Z., Zhang, Y., Hinds, T.R., Fan, E., Cong, F., Xu, W. (2012). Recognition of the iso-ADP-ribose moiety in poly(ADP-ribose) by WWE domains suggests a general mechanism for poly-ADP-ribosylation- dependent ubiquitination. Genes Dev. Feb 1; 26(3): 235-40.

Xie, Y. (2010) Structure, assembly and homeostatic regulation of the 26S proteasome . J. Mol. Cell Biol. Dec;2(6):308-17.

Xu, D., Liu, J., Fu, T., Shan, B., Qian, L., Pan, L., Yuan, J. (2017). USP25 regulates Wnt signaling by controlling the stability of Tankyrases. Genes Dev. May 15;31(10):1024-1035.

Xu, H., Luo, P., Zhao, Y., Zhao, M., Yang, Y., Chen, T., Huo, K., Han, H., Fei, Z. (2013). Iduna protects HT22 cells from hydrogen peroxide-induced oxidative stress through interfering poly-ADP-ribose) polymerase-1-induced cell death (parthanatos). Cell Signal. Apr; 25(4): 1018- 26.

Xu, N., Wang, S.Q., Tan, D., Gao, Y., Lin, G., and Xi, R. (2011). EGFR, Wingless and JAK/STAT signaling cooperatively maintain *Drosophila* intestinal stem cells. Dev. Biol. *354*, 31–43.

Yang, E., Tacchelly-Benites, O., Wang, Z., Randall, M.P., Tian, A., Benchabane, H., Freemantle, S., Pikielny, C., Tolwinski, N.S., Lee, E., et al. (2016). Wnt pathway activation by ADP-ribosylation. Nat. Commun. *7*.

Yang, B.J., et al. (2016). *Arabidopsis* PROTEASOME REGULATOR1 is required for auxin-mediated suppression of proteasome activity and regulates auxin signaling. Nat. Commun. 7: 11388.

Yashiroda, H. et al. (2015). N-terminal alpha7 deletion of the proteasome 20S core particle substitutes for yeast PI31 function. Molecular and cellular biology 35, 141-152.

Ye, P., Chiang, Y.J., Qi, Z., Li, Y., Wang, S., Liu, Y., Li, X., Che, Y.G. (2018). Tankyrases maintain homeostasis of intestinal epithelium by preventing cell death. PLoS Genet. Sep 27;14(9):e1007697.
Ye, J.Z., de Lange, T. (2004). TIN2 is a tankyrase 1 PARP modulator in the TRF1 telomere length control complex. Nat Genet. Jun;36(6):618-23.

Yeh, T.Y., Sbodio, J.I., Tsun, Z.Y., Luo, B., Chi, N.W. (2007) Insulin-stimulated exocytosis of GLUT4 is enhanced by IRAP and its partner tankyrase. Biochem J 402: 279–290.

Yilmaz, O.H., Katajisto, P., et al. (2012). mTORC1 in the Paneth cell niche couples intestinal stem-cell function to calorie intake. Nature. Jun 28;486(7404):490-5.

Zaiss, D.M., Standera, S., Holzhutter, H., Kloetzel, P. & Sijts, A.J. (1999). The proteasome inhibitor PI31 competes with PA28 for binding to 20S

proteasomes. FEBS letters 457, 333-338.

Zeidler, M.P., Bach, E.A., and Perrimon, N. (2000). The roles of the *Drosophila* JAK-STAT pathway. Oncogene *19*, 2598–2606.

Zhang, H., Ryu, D., Wu, Y., Gariani, K., Wang, X., Luan, P., D'Amico, D., Ropelle, E.R., Lutolf, M.P., Aebersold, R., et al. (2016). NAD+ repletion improves mitochondrial and stem cell function and enhances life span in mice. Science aaf2693.

Zhang, Y., Liu, S., Mickanin, C., Feng, Y., Charlat, O., Michaud, G.A., Schirle, M., Shi, X., Hild, M., Bauer, A., et al. (2011). RNF146 is a poly-ADP-ribose-directed E3 ligase that regulates Axin degradation and Wnt signaling. Nat. Cell Biol. 13, 623–629.

Zhang, Y., Wang, J., Ding, M., Yu, Y. (2013). Site-specific characterization of the Asp- and Glu-ADP-ribosylated proteome. Nat Methods. 10:981–984.

Zhong, L., Belote, J.M. (2007). The testis-specific proteasome subunit Prosalpha6T of *D. melanogaster* is required for individualization and nuclear maturation during spermatogenesis. Development 134(19): 3517-3525.

Zhong, L., Ding, Y., Bandyopadhyay, G., et al. (2016). The PARsylation activity of tankyrase in adipose tissue modulates systemic glucose metabolism in mice. Diabetologia. 59: 582.

Zhong, L., Yeh, T.Y., Hao, J., et al. (2015) Nutritional energy stimulates NAD+ production to promote tankyrase-mediated PARsylation in insulinoma cells. PLoS One 10, e0122948.

Zhou, F., Rasmussen, A., Lee, S., and Agaisse, H. (2013). The UPD3 cytokine couples environmental challenge and intestinal stem cell division through modulation of JAK/STAT signaling in the stem cell microenvironment. Dev. Biol. 373, 383–393.

Zhu, X., Xing, R., Tan, R., Dai, R., Tao, Q. (2017). The RNF146 E3 ubiquitin ligase is required for the control of Wnt signaling and body pattern formation in *Xenopus*. Mech Dev. January 1; 147 28-36.

Zoranovic, T., Grmai, L., and Bach, E. (2013). Regulation of proliferation, cell competition, and cellular growth by the *Drosophila* JAK-STAT pathway. Jak-Stat *2*, e25408.